Cell death mechanisms in human endogenous cardiac progenitor cells due to receptor tyrosine kinase inhibitor toxicity

Robert Walmsley

Submitted in accordance with the requirements for the degree of
Doctor of Philosophy

The University of Leeds
School of Biomedical Science

July, 2020

The candidate confirms that the work submitted is his own, except where work which has formed part of jointly-authored publications has been included. The contribution of the candidate and the other authors to this work has been explicitly indicated below. The candidate confirms that appropriate credit has been given within the thesis where reference has been made to the work of others.

Acknowledgements

I would like to thank my supervisor Dr. Andrew J. Smith for welcoming me to his group and providing guidance and support for the last 3.5 years of my PhD. I would also like to thank Professor Derek S. Steele for providing guidance and support and invaluable knowledge in calcium handling. Thank you to all past and present members of the Cellular Cardiology group for their help and support, with a special thank you to Miriam Hurley for always being a good friend and helping with the project. I would also like to thank Dr. Kathleen Wright and Tim Munsey for organising the lab/reagents and being there for anything I needed regarding my experiments and for their practical knowledge. A special thank you to my friend Dr. Eleni Kyriakopoulou for her continued support, project input and weekend and experimental help. Another thank you to my best friends Dr. Christian Sargent, Dr. Chelsea Wood, Dr. David Scully, Jamie Barr, Mitesh Parekh and Amy Doyle for their support and putting up with me talking about my project constantly for the past 3.5 yr. I would also like to give the biggest thanks to my fiancé Elliott Shone and my family for supporting me not only through my PhD but also my whole academic journey. Finally, I would like to thank the University of Leeds for funding and guidance during this project.

Publications

Published

Matthew J. Burke *et.al*. Receptor tyrosine kinase inhibitors cause dysfunction in adult rat cardiac fibroblasts *in vitro*, 2019 *Toxicology in Vitro.*

Andrew J. Smith *et.al.* Poor Recovery From Receptor Tyrosine Kinase Inhibitor Cardiotoxicity is Linked to Toxic Effects on Cardiac Stem Cells, 2018 Circulation.

Submitted

Andrew J. Smith *et.al.* Receptor tyrosine kinase inhibitors negatively impact on the pro-reparative characteristics of human cardiac progenitor cells, 2020. Cardiovascular Research.

Prepared

Robert Walmsley *et.al.* Imatinib-Mesylate induces necroptosis in cardiac progenitor cells.

Robert Walmsley *et al.* Sorafenib-tosylate induces cell death in cardiac progenitor cells through a calcium-dependent mechanism.

Abstract

The development of receptor tyrosine kinase inhibitors as anti-cancer drugs has improved patient prognosis, however they have also been linked to cardiotoxic side-effects. The impact of receptor tyrosine kinase inhibitors on human endogenous cardiac progenitor cells could have long-term impacts on myocardial ability to repair itself after damage. To study these toxic effects on cardiac progenitor cells, we isolated these cells from human right atrial appendage samples by immunomagnetic cell sorting, to obtain c-Kit-positive, CD45-negative cells. Cells were characterised and maintained *in vitro*, then imatinib, sunitinib or sorafenib was applied at concentrations equivalent to peak or trough plasma levels. Impact on cardiac progenitor cells viability and activation of cell death pathway mechanisms were investigated by: viability assay (fluorescein diacetate) and live cell staining to identify apoptotic or alternative cell death pathway activation. Further reverse transcription qPCR analyses of apoptosis, Western blotting, immunocytochemistry and calcium imaging provided a broad screen of underlying mechanisms. The work in this thesis indicates possible therapeutic targets to overcome imatinib-induced cell death through either inhibition of necroptosis or autophagosome formation. Sunitinib increased apoptosis-associated gene expression however did not induce late stage apoptotic cell death. Finally sorafenib-induced toxicity was shown to be through a calcium-dependent mechanism, which provides new insight into the possible use of voltage gated ion channel inhibitors to overcome these adverse events. Overall the project highlights the importance of investigating specific cell death pathways to determine the best therapeutic target and provides new findings into cardiac progenitor cells.

Table of Contents

Contents

List of Tables

List of Figures

Abbreviations

8CPT	8-(4-Chlorophenylthio)adenosine 3',5'-cyclic monophosphate
AO	acidic organelles
ASK1	apoptosis signal-related kinase
BAD	The BCL2 associated agonist of cell death
BAX	Bcl-2-associated X protein
BCA	bicinchoninic acid assay
BCL-2	B-cell lymphoma 2
bFGF	basal fibroblast growth factor
BID	BH3 interacting-domain death agonist
BMP	Bone morphogenetic protein
BSA	bovine serum albumin
cDNA	complementary DNA
CML	chronic myeloid leukaemia
CRD	cysteine-rich domain
DMEM	Dulbecco's Minimum Essential Medium
DMSO	Dimethyl sulfoxide
D-PBS	Dulbecco's Phosphate-Buffered Saline
Dvl	dishevelled
ECM	extracellular matrix
EGF	epidermal growth factor
EPAC	exchange factor directly activated by cAMP
ER	endoplasmic reticulum
ERBB2	Erb-B2 Receptor Tyrosine Kinase 2
ERK	extracellular signal-regulated kinases
ESCs	embryonic stem cells
ESQ	embryonic stem cell-qualified foetal bovine serum
FADD	Fas-associated protein with death domain
FASR	FAS receptor
FDA	Fluorescein diacetate
FGF	fibroblast growth factors
Fluo-4	Fluo-4 AM
Gd^{3+}	gadolinium
GIST	gastrointestinal stromal tumours

GSK-3	glycogen synthase kinase 3
HCC	hepatocellular carcinoma
HF	heart failure
HGF	hepatocyte growth factor
HSCs	hematopoietic stem cells
ICC	immunocytochemistry
IGF	insulin growth factor
IP3R	inositol trisphosphate receptor
JNK	c-Jun N-terminal kinase
KLF4	kruppel like factor 4
LC3	Microtubule-associated protein 1A/1B-light chain 3
LIF	leukaemia inhibitory factor
LVEF	left ventricular ejection fraction
MCU	mitochondrial calcium uniporter
MFI	mean fluorescent intensity
MLKL	Mixed Lineage Kinase Domain Like Pseudokinase
MPTP	mitochondrial permeability transition pore
MSC	Mesenchymal stem cells
Nec-1	Necrostain-1
NNC	NNC 55-0396
NSCs	neural stem cells
Oct4	octamer-binding transcription factor 4
PARP	Poly (ADP-ribose) polymerase
PDGF	platelet-derived growth factor
PDGFR	platelet-derived growth factor receptors
PISCES	The Pilot Investigation of Stem Cells in Stroke study
PLA	proximity ligation assay
PS	phosphatidylserine
RCC	renal cell carcinoma
RCF	relative centrifugal force
RIP	receptor-interacting serine/threonine-protein kinase
ROS	reactive oxygen species
RTKIs	receptor tyrosine kinase inhibitors
RT-qPCR	Reverse transcription quantitative polymerase chain reaction
RYR	Ryanodine receptors

SERCA	sarco/endoplasmic reticulum Ca^{2+}-ATPase
SM	Sunitinib
SOCE	store operated calcium entry
SOX2	SRY (sex-determining region Y)-box 2
ST	Sorafenib
STAT	Janus kinase(JAK)/signal transducer
TAE	Tris-acetate-EDTA
tBID	truncated BH3 interacting-domain death agonist
TBS	tris-buffered saline
TERT	telomerase reverse transcriptase
TGF	Transforming Growth Factor
TMRM	tetramethylthodamine, methyl ester, perchlorate
TNF	Tumour necrosis factor
TNFR	TNF receptor-1
TRADD	tumor necrosis factor receptor type 1-associated death domain protein
TRP	transient receptor potential
TUNEL	terminal deoxynucleotidyl transferase dUTP nick end labelling
VEGF	vascular endothelial growth factor
VEGFR	vascular endothelial growth factor receptor
vWF	von Willebrand factor
Δψm	mitochondrial membrane potential

Chapter 1. Introduction

1.1 Stem Cells

Stem cells have two defining characteristics: their capacity to self-renew and differentiate to produce specialised functional cells. Self-renewal is the division of one stem cell into another stem cell with indistinguishable features, whereas differentiation is the potential for a primitive cell to become a more specialised cell type. Stem cells vary greatly depending on their attributes such as potency, plasticity and ability to self-renew (Cianflone et al., 2019; Faissner, 2020; Phinney and Pittenger, 2017).

Stem cells are present during all stages of life in an organism, from developmental stages through to neonatal and adult growth. During embryonic development, a fertilised egg divides until formation of the morula, a sixteen-cell structure that creates any cell within the organism, including embryonic tissue (placental cells). At four d of development, the cells undergo ‘compaction’ to form the blastocyst. The compaction of the morula creates a group of cells called the inner cell mass, comprised of cells known as embryonic stem cells (ESCs) (Gilbert, 2000). The ESCs are pluripotent meaning they form all three germ layers within the organism: the ectoderm, mesoderm, and endoderm. Embryonic stem cell pluripotency is governed by key transcription factors such as Nanog, octamer-binding transcription factor 4 (Oct-4), and SRY (sex-determining region Y)-box 2 (SOX2), these act as molecular markers for identification of a range of different stem cells (Boyer et al., 2005; Chen et al., 2008).

1.1.1 Somatic Stem cells

Somatic stem cells reside within tissues and organs of an adult organism as undifferentiated cells, defined by the same stem cell properties of self-renewal and differentiation, with differentiation range normally limited to cell types native to the tissue they reside within. Many functioning organs have stem cells, such as the heart (cardiac progenitor cells), brain (neural stem cells, (NSCs)) and bone marrow (mesenchymal stem cells (MSCs)) (Beltrami et al., 2003; Faissner, 2020; Phinney and Pittenger, 2017). Somatic stem cells are generally present in a quiescent state, meaning that they are not active in the cell cycle (Blau et al., 2001). Somatic stem cells range in potency from unipotent to multipotency and can only produce cells within their residing environment, for example, NSCs only produce ectodermal cells (neuronal or glial) (Rammensee et al., 2017), not endodermal or mesoderm cell types. Notably, somatic stem cells differentiate across germ layers if selective pressures are added and this process is known as transdifferentiation (**refer to section 1.1.3**). Somatic stem cells are central to repair mechanisms following tissue damage (Hoffman and Dow, 2016). Before discussing the therapeutic applications of stem cells, it is essential to understand how stem cells self-renew and differentiate.

1.1.2 Self-renewal

Self-renewal occurs either by asymmetrical or symmetrical division: stem cells were previously believed to divide mainly by asymmetric division, in which the stem cell divides into two daughter cells (one stem cell and one progenitor

cell). However, there is evidence that symmetrical division also occurs, especially in mammalian systems (Morrison et al., 1997; Yoo and Kwon, 2015). The ability for a stem cell to self-renew is a vital characteristic, as it replenishes the pool of stem cells available throughout the organism's lifetime. Stem cells divide at different rates; for example, ESCs divide rapidly during development; however, adult hematopoietic stem cells (HSCs) are more quiescent (Pietras et al., 2011).

Differential regulation of signalling pathways are required to control the extent to which a stem cell; these regulations include hedgehog, Wnt, Notch, Bone morphogenetic protein (BMP)/Transforming Growth Factor (TGF)-β and Hippo signalling (Yoo and Kwon, 2015). Wnt signalling controls cell fate decisions during development, self-renewal and regulates intracellular calcium, acting via three pathways: canonical, non-canonical and non-canonical Wnt/calcium pathway. Canonical Wnt signalling is is hallmarked by accumulation of beta-catenin within the cytosol and translocation into the nucleus. When Wnt signalling is not activated, beta-catenin is usually destroyed by the beta-catenin destruction complex which includes proteins such as; axin, glycogen synthase kinase 3 (GSK-3), adenomatosis polyposis coli and protein phosphatase 2A. A downstream protein called dishevelled (Dvl) inhibits the activation of GSK-3; therefore, beta-catenin is not destroyed and accumulates in the cytosol. The survival and accumulation of beta-catenin causes it to translocate to the nucleus, where it acts as a transcriptional co-activator for genes essential for self-renewal such as *CCND1 and* MYC (**Figure 1.1**) (Liu et al., 2005).

Wnt signalling is important for stem cell renewal, Wnt3a (frizzled receptor ligand) has been used to activate the Wnt signalling pathway in HSCs, leading to a 5.8-fold increase in cell number and inhibition of differentiation (Willert et al., 2003). Inhibition of canonical Wnt pathway using a soluble form of the frizzled cysteine-rich domain (CRD), which prevents Wnt ligands from binding to the frizzled receptor and hence blocks receptor activation, this inhibition caused a 4-fold reduction in growth compared to the control (Reya et al., 2003).

1.1.2.1 Stem cell niche role in self renewal

The stem cell niche contains environmental factors that can stimulate cells to enter the cell cycle. The external stimuli include cell-cell interactions, growth factors/cytokines (including interleukins), local conditions (oxygen, glucose, and nitric oxide levels) and epigenetic factors, which all contribute to the regulation of self-renewal (Pennings et al., 2018). The importance of the niche in self-renewal has been shown using haemopoietic stem cells (HSCs), which were co-cultured with osteoblasts *in vitro,* leading to an increase in HSC self-renewal. Osteoblasts express membrane-bound ligands and adhesion receptors that regulate HSCs, including Angiopoietin 1, Jagged 1, and N-cadherin (Jung et al., 2008). Osteoblasts secrete cytokines and growth factors that control the microenvironment for HSCs proliferation such as BMP2,7, TGF-beta, and stromal cell-derived factor -1 (Chen et al., 2012).

The stem cell niche can be mimicked and manipulated during *in vitro* studies using selective factors to control the cells proliferation rates and inhibit their differentiation, keeping them in a primitive stem cell state useful for analysis.

One example of this is using leukaemia inhibitory factor (LIF). Leukaemia inhibitory factor prevented NSC senescence, increased proliferation and maintained long term culturing up to 110 population doublings (Wright et al., 2003). One proposed method of LIF signalling is through the activation of Janus kinase (JAK)/signal transducer and activator of transcription pathway (STAT). The JAK/STAT pathway increases self-renewal and activates AKT, which aids in cell survival by upregulating transcription factors Nanog, octamer-binding transcription factor 4 (Oct4) and SOX2 (**Figure 1.1**) (Graf et al., 2011). The stem cell niche influences signalling pathways, for example, cell-cell interactions are thought to activate the Hippo pathway, which suppresses cell proliferation by phosphorylation, cytoplasmic retention and proteasomal degradation of transcriptional co-activators such as yes-associated protein (Gumbiner and Kim, 2014).

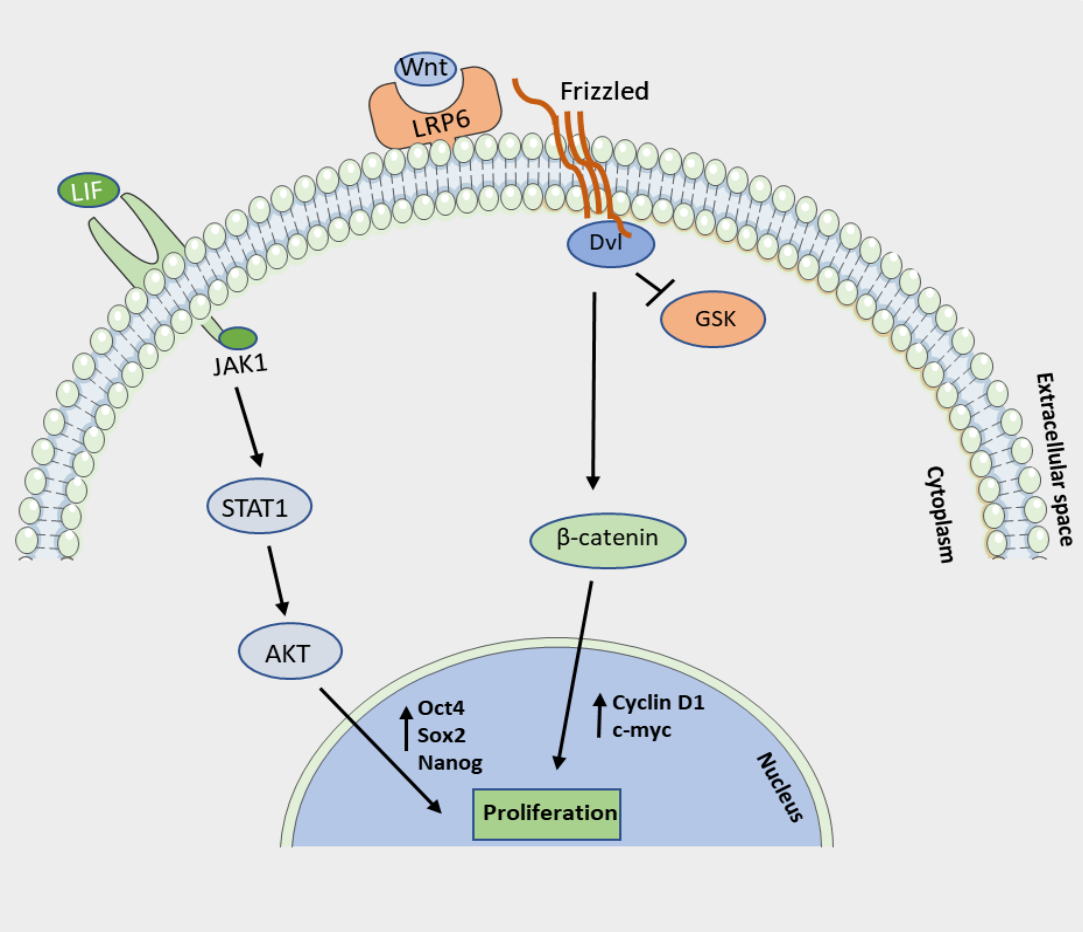

Figure 1. 1. Schematic representation of stem cell renewal. Diagram showing the involvement of Wnt and LIF signalling pathways in cellular proliferation.

1.1.3 Differentiation

Differentiation can be defined as the ability of a stem cell to develop into a more specialised cell type and is subdivided into potency, plasticity, and commitment. The most potent stem cells are known as totipotent: stem cells that can differentiate into any cell type within the organism including extra-embryonic cells (Zakrzewski et al., 2019). Pluripotent stem cells are a less potent cell present during embryonic development, which can differentiate into any cell within the germ layers, excluding embryonic tissue. Multipotent stem cells cannot normally cross germ layers: for example if a cell has committed to becoming mesodermal, it will not be able to differentiate into an ectodermal cell type. Stem cells within adult tissues have lower potency (commonly multipotent) than the totipotent and pluripotent stem cells found in development (Raff, 2003).

An effective way to visualise differentiation and potency is to apply Waddington's Epigenetic Landscape. This concept, first depicted in “An Introduction to Modern Genetics (1939)”, showed the metaphor of an inclined surface with a marble at the top of the hill, representing a cell in early development (pluripotency). This marble moves down the hill, across ridges and valleys (representing the expression of genes that cause the cell to progress down specific fates), with the marble’s movement downhill representing a cell’s journey through developmental stages. As the marble reaches the lowest point of the hill it comes to rest, a representation of cells in adulthood that are senescent and do not differentiate (“An Introduction to Modern Genetics. By C. H. Waddington,” 1939) (**Figure 1.2A**) (Goldberg et al., 2007). Other researchers have adapted this model to explain

dedifferentiation and transdifferentiation (**Figure 1.2B-C**) a form of cellular reprogramming. Dedifferentiation shows the marble moving back up the hill; this represents a cell moving from a mature cell to a progenitor cell. Transdifferentiation is shown by the movement of the marble over a ridge, which is a metaphor for the cell switching germ layers (Takahashi, 2012). The landscape was adapted to illustrate induced pluripotency (Takahashi and Yamanaka, 2015) and used to quantify a prediction of cellular differentiation (Bhattacharya et al., 2011).

One stem cell which has extensive research on their differentiation potential are NSCs, which are multipotent, differentiating into cells within the central nervous system including neurons, astrocytes and oligodendrocytes (Franco et al., 2012). Neural stem cells are present in developing and adult systems and can be characterised with a variety of markers such as Nestin, SOX2 (intracellular markers), ATP-binding cassette superfamily G member 2 and fibroblast growth factors (FGF) 4 (Zhang and Jiao, 2015). The differentiation of NSCs *in vivo* depends on where the progenitor cell migrates to in the brain (subventricular or ventricular zone) (Franco et al., 2012). Once differentiated, characterisation of the cells is important with molecular markers such as β-tubulin+ (neurons), Rip-antigen+ and Oligodendrocyte Marker O4+ (oligodendrocytes) and S100-β+, (astrocytes) showing the need to use different characterisation markers for mature cell types (Carpentier and Palmer, 2009; Franco et al., 2012; Palmer et al., 1999; Song et al., 2002). If NSCs were differentiated into neurons, synaptic formation and functional activity can be assessed with electrophysiology, to ensure the mature cells are functional. *In vitro* differentiation can lead to morphologically similar cells to

those seen *in vivo*, but their functional activity might not reflect a mature cell *in vivo*. Neural stem cell-derived neurons have been shown to function similarly to primary mature neurons, with functional synaptic connections, responses to neurotransmitters and firing action potentials (Song et al., 2002).

Regulation of differentiation relies on pathways similar to self-renewal such as Wnt, Notch, BMP and hedgehog (Wu and Sun, 2006). Within neurogenesis, a small alteration in Notch signalling can change the cells fate. When Notch signalling is active within the NSCs, the cells fate becomes glial in lineage mainly astrocytic and therefore inhibits neuronal or oligodendrocyte formation. Inhibiting Notch induces the cell to commit to a neuronal lineage (Wang et al., 1998). Inhibiting Notch within *Drosophila melanogaster* leads to a fully neurogenic phenotype and therefore the nervous system does not function due to lack of glial cells (Lai, 2004). These findings show the importance of regulation in differentiation.

Although somatic stem cells have a limited range of potency, there is evidence that a cell can change its fate. Specialised cells have been shown to dedifferentiate and reprogram into a different cell type (Jopling et al., 2011). De-differentiation has been demonstrated in studies of the regenerative capabilities of zebrafish. Ventricular resection (20%) of a zebrafish heart triggers the cardiomyocytes to undergo limited dedifferentiation, as shown by the loss of sarcomeric structures and expression of cell cycle regulators (Jopling et al., 2011). These cardiomyocyte progenitors are shown to be proliferative and can create new cardiomyocytes, forming a heart with no morphologically distinguishable difference after repair (Jopling et al., 2010; Poss et al., 2002). If an existing differentiated cell has a low tendency to

proliferate, its ability to dedifferentiate into a more primitive cell type could allow the damaged tissue to regenerate more efficiently, especially when the stem cell pool is low. Cell plasticity also refers to the ability of a cell to move outside of its “normal” differentiation pathway, as seen with transdifferentiation. Transdifferentiation is the ability for the cell to cross lineages, for example if the stem cell committed to a mesodermal lineage becomes a cell with an endodermal lineage: evidence suggests that specific cells with high plasticity can switch between all three germ layers (Jopling et al., 2011).

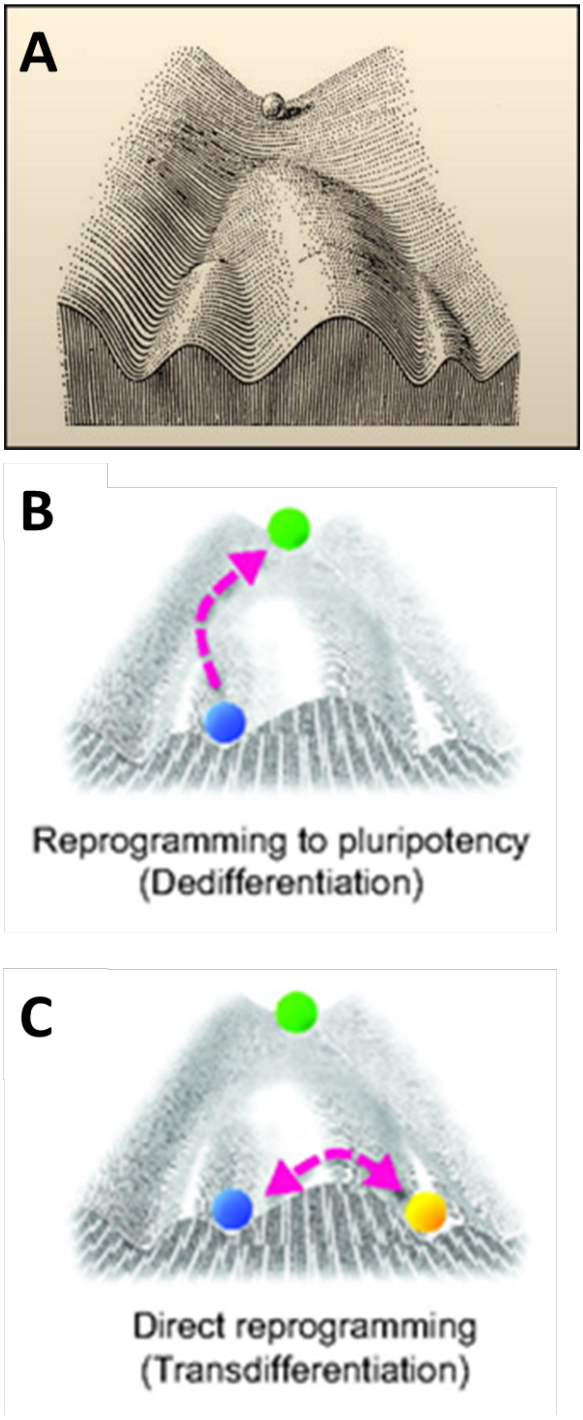

Figure 1. 2. Epigenetic landscape concept created by Waddington in 1957 to represent cellular decisions during development. The cell (represented by a ball) can take different paths leading to different cell fates. **(A)** Figure reprinted from Waddington, 1957. **(B-C)** adaption of the Waddington concept. **(B)** showing a cell on the lower incline (blue) being pushed back up the slope towards a pluripotent nature (green). **(C)** Adaption reflecting the process of transdifferentiation with one cell switching fates (shown by movement over a ridge) (image adapted from Takahashi, 2012).

1.1.4 Role of stem cells in human pathophysiology

Stem cells can have both paracrine protective mechanisms and a regenerative capability within pathophysiology. Wound healing is one model which illustrates the paracrine mechanisms of a stem cell: this is a multifactorial process involving cells, growth factors and the extracellular matrix (ECM) (Gonzalez et al., 2016). One cell type central to the process is the MSC. Mesenchymal stem cells can self-renew and differentiate into mesodermal cells, including chondrocytes, osteoblasts and adipocytes (Shojaei et al., 2019). Wound healing can be broadly separated into three phases: inflammatory, proliferative and remodelling. During the inflammatory phase, MSCs regulate the immune response by suppressing pro-inflammatory cytokines such as tumour necrosis factor (TNF)-α and Interferon-γ. Mesenchymal stem cells increase anti-inflammatory cytokines such as interleukin IL-10 and IL-4 (Aggarwal and Pittenger, 2005). These regulations are important within wound healing to prevent the wound from becoming non-healing and chronic. During the proliferation stage, MSCs secrete several growth factors such as vascular endothelial growth factor (VEGF), platelet-derived growth factor (PDGF) and hepatocyte growth factor (HGF), all of which contribute to the ECM and help to stimulate granulation and epithelialization (Chen et al., 2008; Wang et al., 2004). Mesenchymal stem cells also help to recruit other important cell types for repair, including keratinocytes and fibroblasts. During remodelling, the cells produce TGF-β3 and FGF-7, important for preventing scar formation and organisation of ECM deposition (L. Chen et al., 2008; Shojaei et al., 2019; Wang et al., 2004). Overall MSCs

are central to wound repair within adult systems providing ECM support, anti-inflammatory effects and cellular recruitment within healing wounds.

The regenerative potential of stem cells in skeletal muscle, which normally has periods of regeneration and repair in healthy physiology, relies on a specific stem cell known as satellite cells (Liu et al., 2018). Debates over whether satellite cells are stem cells are ongoing mainly because of their unipotency, as they can only form myoblasts (Boonen and Post, 2008). However, their capacity to self-renew and ability to differentiate *in vivo* gives them the characteristics of a skeletal muscle stem cell (Boonen and Post, 2008). Satellite cells have been shown to become proliferative and differentiate into myoblasts after skeletal muscle damage. These newly-formed myoblasts mature into functional myocytes and repair the skeletal muscle damage (Liu et al., 2018).

1.1.5 Uses of stem cells in regenerative medicine

Stem cells are currently being extensively researched across a range of avenues for therapeutic use in regenerative medicine. Somatic stem cells are being manipulated, transplanted and adapted to regenerate damaged tissue; examples include spinal cord injury, myocardial infarctions, graft-versus-host disease and cancer therapies. Mesenchymal stem cells have been used in clinical studies for multiple reasons including bone and cartilage repair, for their anti-inflammatory effects and spinal cord injury. At least eleven clinical studies have been carried out using MSCs for treatment for graft-versus-host disease, with each trial showing mixed results (Galipeau and Sensébé, 2018).

Mesenchymal stem cells have been shown in previous studies to have anti-inflammatory and anti-microbial effects, which are important for treating patients with steroid-resistant graft-versus-host disease (Meisel et al., 2011).

During spinal cord injury, neuronal connections become lacerated or compressed, causing neuronal dieback,and the formation of a glial scar within the central nervous system. Post-injury, reactive astrocytes undergo morphological changes and extend their processes, causing the formation of a glial scar. Astrocytes within the glial scar also secrete factors that contribute to the ECM, including chondroitin sulfate proteoglycans. Chondroitin sulfate proteoglycans prevent new neuronal connections from forming within the glial scar and therefore prevent the damage from being repaired. Mesenchymal stem cells can bridge this gap between neurons through the glial scar, allowing new neuronal connections, which aid regeneration of the spinal column (Dasari et al., 2014).

Neural stem cells are involved in multiple clinical trials of their use as a therapeutic strategy for neurodegenerative disorders. The Pilot Investigation of Stem Cells in Stroke study (PISCES) was started as a cell-based therapy to treat patients with stroke disabilities. Phase I of this study enrolled 11 patients with disability after ischaemic stroke and administered a range of doses of a NSC cell line (ReNeuron ltd, CTX cells). The trial aimed to evaluate the possible side effects of the CTX cells and to observe any side effects of the implantation protocol. The results showed no adverse effects from the cell therapy and improvements in neurological conditioning compared to pre-baselines before treatment (Alcacer-Pitarch et al., 2012). A continuation trial (PISCES II) showed 4 of 23 patients to have improved upper limb movement

following NSC implantation (Muir et al., 2020). Overall, the study of stem cells highlights the important role they play in the future of regenerative medicine, via their direct repair of lost tissue and also their paracrine protective effects through secretion of pro-survival secretome. One important stem cell found within the heart is the cardiac progenitor cells, these have been shown to be vital for cardiac repair after diffuse injury.

1.2 Endogenous Cardiac Progenitor cells

For many years, it was believed that the heart had no regenerative capability in the cardiomyocyte compartment and identifying progenitor cells in cardiac tissue was thought futile. However, the heart has been shown to have cycling ventricular cardiomyocytes and forms new microvasculature throughout life (Bergmann et al., 2009). It is now widely accepted that the heart possesses endogenous CPCs, cells with the potential to form new cells within the myocardium and contribute to cardiac repair (Ellison et al., 2013). Cardiac progenitor cells demonstrate the defining traits of stem cells, specifically their ability both to self-renew and to differentiate. Cardiac progenitor cells also have paracrine protective effects, able to prolong cardiomyocyte survival after injury (Smith et al., 2018; Kawaguchi et al., 2010). A mechanism for cardiomyocyte protection is an exciting concept that could be exploited therapeutically and provide answers for cardiac repair and drug-induced cardiotoxicity.

1.2.1 Characterisation and isolation of cardiac progenitor cells

The first evidence of CPCs was in 2002, with the suggestion that the human heart could possess an endogenous stem cell population (Quaini et al., 2002). Following this, the human CPC were isolated and manipulated *in vitro* and *in vivo* using characterisation and differentiation techniques (Beltrami et al., 2003). These cells are identified by expression of the receptor tyrosine kinase c-Kit and resistance protein 1, stem cell antigen-1. The cells must be negative for blood lineage markers CD45 and CD31 distinguishing them from mast cells and endothelial cells (Beltrami et al., 2003; Ellison et al., 2013; Vicinanza et al., 2017). These c-Kit$^+$ CPCs are capable of self-renewal and developing into different myocardial cell types including smooth muscle, endothelial cells and to a limited extent cardiomyocytes (Beltrami et al., 2003; Ellison et al., 2013; Smith et al., 2014). Cardiac progenitor cells can make a valuable contribution to cardiac tissue due to their replacement of damaged cells and aiding the recovery of injured cells by release of pro-survival growth factors (Ellison et al., 2013; Kawaguchi et al., 2010). Cardiac progenitor cells are located in the atrium and ventricular apex, although these cells are low in number with around 1 CPC per 10,000 cardiomyocytes (Beltrami et al., 2003). Due to the scarcity of CPCs, an optimised isolation and characterisation protocol was developed, including the use of LIF to inhibit their differentiation, growth factors to maximise proliferation and the use of low oxygen levels to maintain their stem cell state (Smith et al., 2014). Another method for isolation is using cardiosphere-derived cells, this method involves using tissue dissection to create explant medium, the fibroblasts are encouraged to cover the vessel. Once covered, small round phase-bright cells begin to migrate from the

explants (cardiospheres) which can then be collected for selection. These cells are then positively enriched for c-Kit and stem cell antigen-1 to remove any HSCs (Chen et al., 2013).

1.2.2 Cardiac progenitor cells and their role in regeneration of the myocardium

Cardiac progenitor cells are more effective within neonatal hearts, mainly because fewer cells are in a senescent and quiescent state. Comparisons between adult and neonatal CPCs have shown neonatal cells have significantly improved cardiac function (Simpson et al., 2012). Other studies have shown rodent CPCs increased cardiomyocyte differentiation more than that of adult CPCs, possibly due to a reduction in c-Kit expression (Zaruba et al., 2010). However, current research has shown in both *in vivo* and *in vitro* studies, that adult CPCs can be beneficial to myocardial recovery. Cardiac progenitor cells have been shown in a rodent model to be necessary for myocardial regeneration; this was demonstrated by inducing diffuse myocardial injury. Proliferative CPCs were removed (using mitotic agent 5-fluorouracil), this led to severe cardiomyopathy with lowered numbers of cardiomyocytes, compared to the control (without 5-fluorouracil) in which regeneration occurred. The reintroduction of CPCs also leads to the recovery being reversed, showing the important impact CPCs have in the myocardium after damage (Ellison et al., 2013).

These cells have also been shown to have a paracrine protective effect when in co-culture with adult cardiomyocytes, the CPCs were grown on inserts to separate them from the cardiomyocyte population (no direct interactions).

These findings showed reduced caspases 3 activity and improved levels of cardiomyocyte contractility and attachment when co-cultured with CPCs on culturing inserts. The study did not show cardiomyocyte proliferation but did show prolonged cardiomyocyte survival. As these two cell populations had no direct contact this shows the cardiomyocytes protection was due to paracrine mechanisms. These paracrine protective effects are occurring through insulin growth factor receptor and HGF signalling (Kawaguchi et al., 2010). These findings were reinforced in pig hearts with induced acute myocardial infarction, followed by co-administration of HGF and insulin growth factor (IGF). The findings showed the CPCs were activated and encouraged to differentiate by HGF and IGF *in vitro*. Improved cardiac function was observed with increased cardiomyocyte survival, reduced fibrosis and the generation of new myocardium at 21 and 60 d after acute myocardial infarction (Ellison et al., 2011).

1.2.3 Therapeutic strategies for cardiac progenitor cell infusion

Preclinical studies have shown that both intramyocardial and intracoronary injections of CPCs lead to poor graft retention; one study suggests the majority of cells are lost after the first d of engraftment. The study infused 100,000 CPCs, with a retention of approximately 5000 cells after 24 h. Although poor retention of CPCs was seen, the LVEF significantly improved, suggesting that the effects of the cells are possibly due to paracrine protection (Hong et al., 2014; Li et al., 2016). These preclinical studies are important to guide how clinical trials are carried out; for example, the use of intracoronary infusion over intramyocardial and also the need for an increased number of CPCs during engraftment.

There have been two important clinical trials involving the use of CPCs for myocardial infarctions; the SCIPIO trial and CADUCEUS trial. The SCIPIO trial showed promising results, with c-Kit$^+$ CPCs administered via coronary infusion to adult patients with myocardial infarctions causing a 12.3% increase in LVEF and 44% reduction in infarct size at 12 months post-infusion. (Chugh et al., 2012). The CADUCEUS trial also showed positive effects on the myocardium one year after CPC infusion, with reduced scar mass, improved viable tissue and improved contractility, although this trial used a heterogeneous cell population (only around 2% of these cells c-Kit$^+$). However, there were no differences between groups when assessing LVEF. The differences in LVEF seen in these trials could highlight the importance of specifically isolating the c-Kit$^+$, CD34$^-$, CD45$^-$ cell population for infusion (Makkar et al., 2012; Malliaras et al., 2014).

Overall, these two studies highlight the potential for future therapeutic strategies using c-Kit$^+$ CPC infusion after myocardial insult, however improving the consistency of CPC isolations and cellular retention might be required to improve the clinical outcome.

The evidence presented displays the damage caused by RTKIs on cardiomyocytes but raises the question about RTKIs effects on regeneration. Cardiac progenitor cells have been selected as an important source for cardiomyocyte repair. Therefore, understanding how RTKIs impact CPCs could provide answers to why the cardiomyocytes are not being renewed or protected.

1.3 Cell death mechanisms

Having reviewed stem cell literature, it is important to acknowledge cell death mechanisms as these signalling pathways are involved in many cellular responses and disorders, for example, to control cell proliferation, cardiotoxicity and therapeutic strategies (Singh et al., 2019). Cell death signalling can be separated into two broad categories: controlled and non-programmed cell death. Controlled cell death is defined by strict regulatory molecular machinery; this is usually a natural cellular process important for organismal homeostasis (Fuchs and Steller, 2011; Galluzzi et al., 2016; Nagata and Tanaka, 2017). There are many forms of programmed cell death including intrinsic apoptosis, extrinsic apoptosis, autophagy-dependent cell death, mitochondrial-dependent necrosis and necroptosis (Galluzzi et al., 2018).

1.3.1 Apoptosis

1.3.1.1 Extrinsic apoptosis

Apoptosis occurs in multicellular organisms and is controlled by energy-dependent biochemical events; it can be further subcategorised into extrinsic and intrinsic cell death (D'Arcy, 2019). The process has been targeted by therapeutic studies to overcome many pathologies such as cancer, autoimmunity and degenerative diseases (MacFarlane, 2009). Extrinsic apoptosis is characterised by activation of FAS receptor (FASR) and TNF-α receptors. Activation of the FASR by FAS ligand activates Fas-associated protein with death domain (FADD), which binds to the death domain of the

FASR, causing procaspase 8 (inactive) to be cleaved and into activate caspase 8 (Nagata, 2018). Caspase 8 has two routes through which it can drive apoptosis: a) cleavage and activation of procaspase 3 or 7; b) cleavage of the BH3 interacting-domain death agonist (BID) to truncated BID (tBID), which helps the oligomerization of Bcl-2-associated X protein (BAX), this protein causes a pore formation within the mitochondria membrane. In healthy cells, BAX is inhibited by B-cell lymphoma 2 (BCL-2), however during apoptosis BCL-2 is inhibited and therefore prevents inactivation of BAX (Ashe and Berry, 2003). Mitochondrial membrane disruption causes release of cytochrome C, which binds with procaspase 9 and apoptotic protease activating factor 1, forming the apoptosome. The apoptosome is responsible for cleavage of procaspase 9 into activated caspase 9, which directly activates procaspase 3 or 7 (**Figure 1.3**) (Ashe and Berry, 2003). TNF receptor-1 (TNFR) is activated by TNF-α ligand, causing conformational change leading to the release of receptor-interacting serine/threonine-protein kinase (RIP)1 and tumour necrosis factor receptor type 1-associated death domain protein (TRADD). There are three different outcomes which could occur, complex IIa, complex IIb or complex IIc. Complex IIa is similar to FASR signalling whereby procaspase 8 is cleaved leading to the formation of tBID or activation of procaspase 3 or 7 to initiate apoptosis. Complex IIb involves the association of RIP1, RIP3 and FADD (active) causing the induction of RIP1-dependent apoptosis (Sheikh and Huang, 2003). Complex IIc occurs if caspase 8 and FADD are inactive and therefore allowing RIP1 and RIP3 to become activated. RIP1 and RIP3 activation cause the phosphorylation of Mixed Lineage Kinase Domain Like Pseudokinase

(MLKL), a protein which then disrupts the plasma membrane and initiates necroptosis (**Figure 1.4**) (Liu et al., 2019).

1.3.1.2 Intrinsic apoposis

Intrinsic apoptosis is linked to the permeabilization of the outer membrane of the mitochondria, induced by pro-apoptotic proteins such as BAX and jBID. A pro-survival protein known as RAF-1 is activated by RAS, leading to the activation of the extracellular signal-regulated kinases (ERK) pathway. The ERK protein is an essential pathway for cell proliferation and survival. The cell survival protein RAF-1 also has an anti-apoptotic property whereby it inhibits The BCL2 associated agonist of cell death (BAD), which normally inactivates the anti-apoptotic protein BCL-2. Thereby if RAF-1 is inhibited, BAD will no longer be inactive, allowing blocking of BCL-2 signalling and therefore BAX will oligomerize the mitochondria. Another important pro-apoptotic factor is c-Jun N-terminal kinase (JNK), which either cleaves BID to form the variant jBID, or translocates to the nucleus and phosphorylate c-jun. C-jun is a transcription factor that can upregulate pro-apoptotic factors such as p53 and FASR, thereby increasing the apoptosis rate. Failure in cell survival mechanisms also contributes towards apoptosis: Poly (ADP-ribose) polymerase (PARP) is involved with the DNA repair process; it works alongside other repair proteins and in cases of low damage to DNA, can repair breaks by increasing ATP and NAD. In cases of apoptosis-induced cell death, PARP is cleaved by executioner caspases and is unable to repair DNA breaks. In cells with inactive caspases but high amounts of DNA damage, PARP is overexpressed: this causes depletion of NAD+ and ATP, leading to necrotic cell death (Chaitanya et al., 2010).

Finally, calpains are caspase-independent proteases that are activated by increased calcium levels. During cell death initiation, there is a calcium influx, both from surrounding areas and intracellular stores, due to mitochondrial pore formation and endoplasmic reticulum (ER) stress. Once calpains are active, they can directly activate the executioner caspases (**Figure 1.5**) (Momeni, 2011).

Both extrinsic and intrinsic apoptosis are caspase-dependent, the final stage of apoptosis leading to activation of executioner caspase 3 or 7, these proteins are key to initiating cell death through DNA cleavage. Executioner caspases cause DNA fragmentation by inactivating DNA fragmentation factor 45 by proteolytic cleavage, which allows caspase-activated DNase to fragment DNA (Wid, 2000; Wolf et al., 1999).

1.3.2 Necroptosis

For many years necrosis was believed to be an uncontrolled cell process, but new research has demonstrated a controlled version of necrosis, known as necroptosis. Necroptosis occurs if caspase 8 is inhibited and therefore prevents the cell from undergoing apoptosis and leading to this alternative cell death pathway. Inhibited caspase 8 causes activation of RIP1 and RIP3 via phosphorylation and deubiquitination, this activation causes RIP1 to interact with RIP3 through the receptor homology domain, leading to the formation of the necrosome (Xie et al., 2013). The necrosome further activates MLKL via phosphorylation (Dhuriya and Sharma, 2018) (**Figure 1.4, complex IIc**). Although RIP1 is necessary for endogenous necroptosis, previous reports

have shown that RIP3 overexpression activates MLKL independent of RIP1 (Dondelinger et al., 2013). Once activated, MLKL translocates and affects the cell in one of two ways: a) it causes the recruitment of sodium and calcium channels or b) it interacts with phosphatidylinositol phosphate and causes pore formation in the plasma membrane and thus loss of plasma membrane integrity (Cai et al., 2014). Necroptosis induces a similar phenotype to necrosis, with the end-stage cell death causing membrane rupture (Taylor et al., 2008).

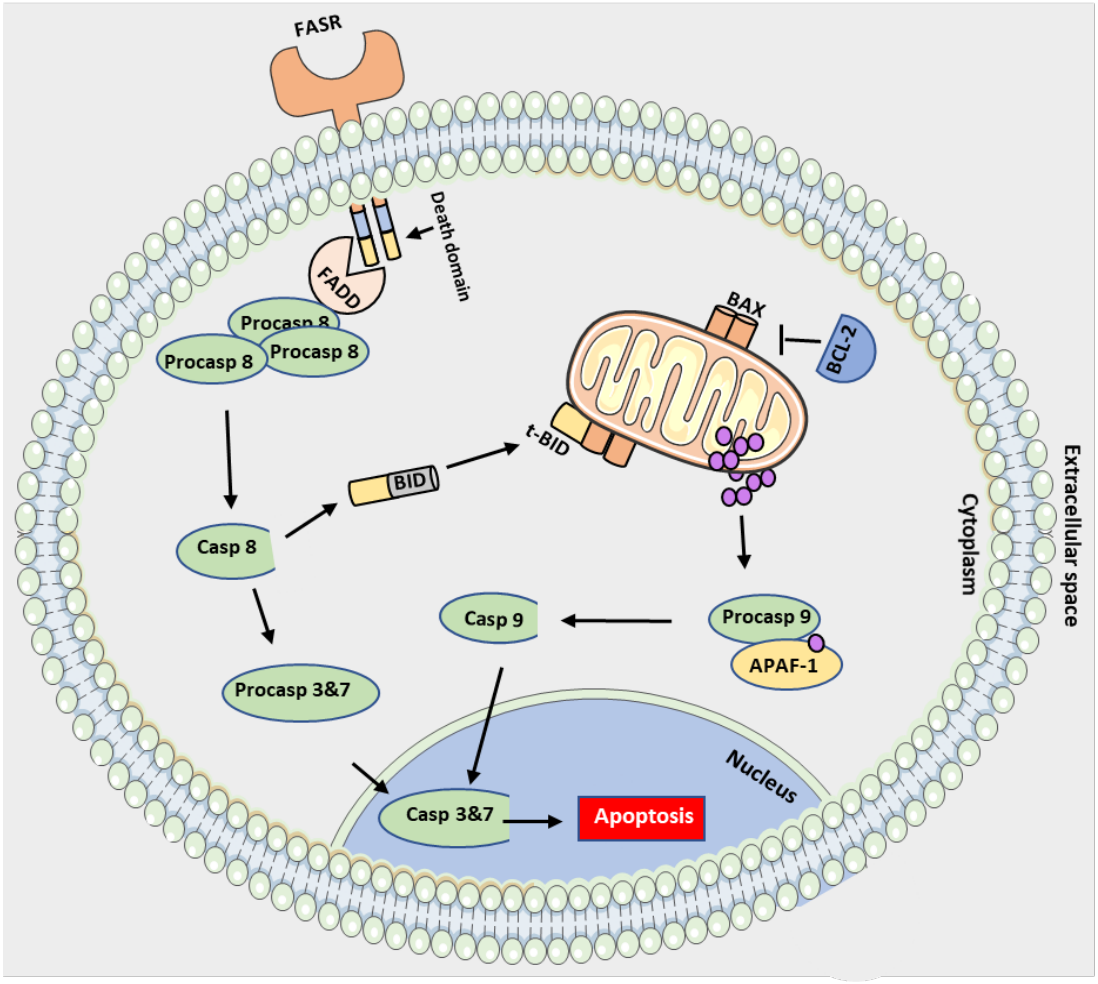

Figure 1. 3. Schematic representation of extrinsic apoptosis induced by FASR activation.

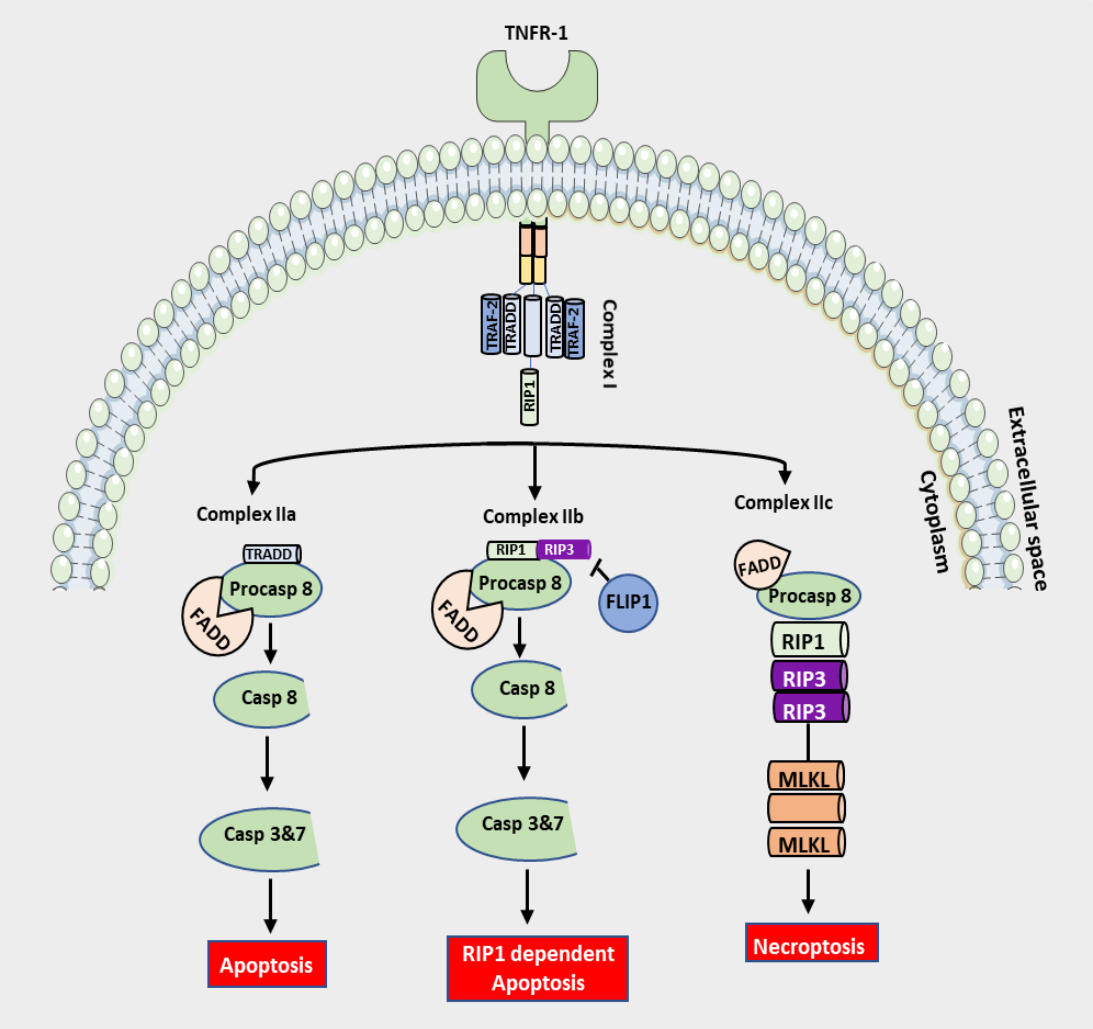

Figure 1. 4. Schematic representation of extrinsic apoptosis and necroptosis induced by TNFR activation.

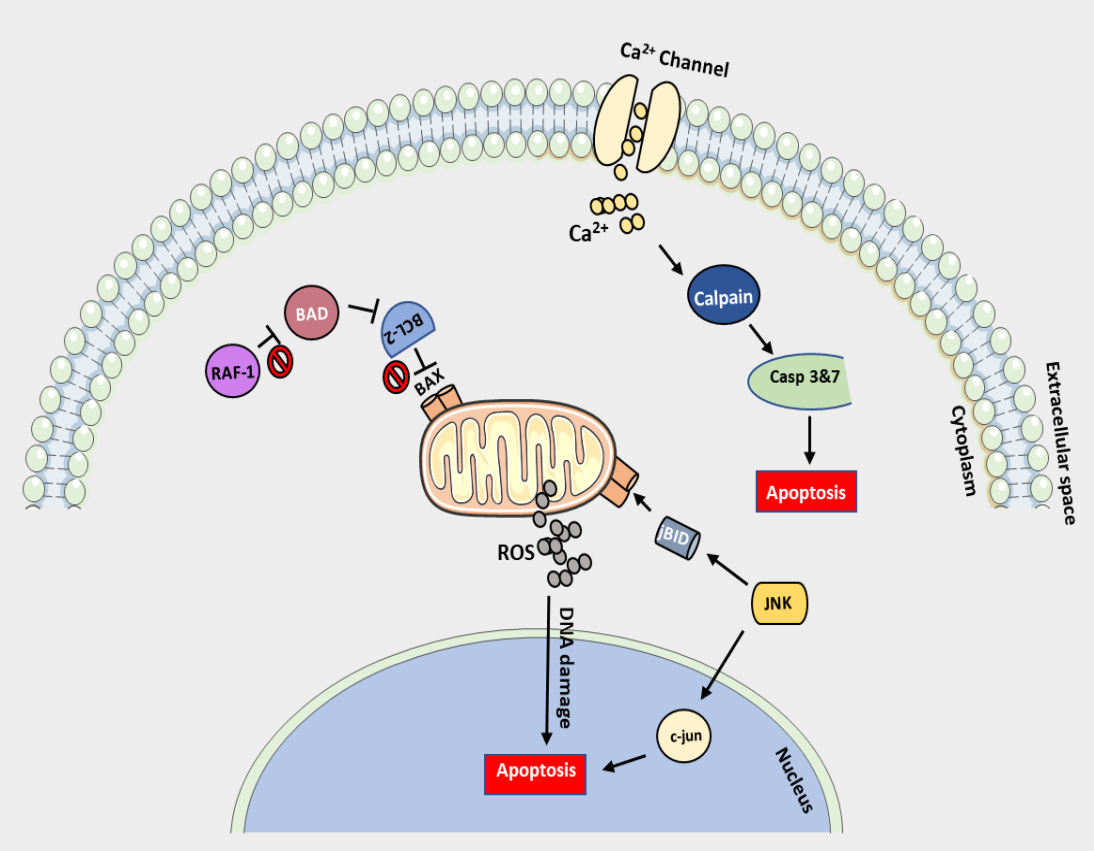

Figure 1. 5. Schematic representation of intrinsic apoptosis.

1.3.3 Necrosis

Necrosis is fast and uncontrolled, it is caused by physical disassembly of the cell and is normally identified by a drop in ATP, which can be triggered by multiple factors such as radiation, heat, toxins and oxygen depletion (Adigun et al., 2020). Necrosis presents a challenge as specific proteins do not control it and therefore it has no targets for identification. The gold standard for identifying necrosis is by investigating the absence of controlled cell death markers, e.g. caspase activity (Krysko et al., 2008). Necrosis is a relatively fast process and therefore cells lose their membrane integrity early in the cell death pathway, which can be identified with carbocyanine monomer nucleic acid stains such as ToPro-3 (Xie et al., 2015). Necrotic cell morphology varies depending on the cell type and trigger for cell death: common findings include dilation of organelles, dissociation of ribosomes from the Golgi apparatus and chromatin condensation (Ziegler and Groscurth, 2004).

1.3.4 Calcium-mediated cell death

Calcium is an important s messenger for many cellular processes; therefore maintaining a constant internal calcium concentration is vital for cell survival (Cerella et al., 2010). Calcium concentrations in the cell cytosol and mitochondrial matrix are approximately 100-500 nM; this is around 10,000 times lower than the extracellular calcium concentration. The ER and sarcoplasmic reticulum calcium concentration in contrast has been estimated to be between 0.1-1 mM; these differing calcium levels are tightly regulated by various proteins (Hajnóczky et al., 2003).

Cellular stresses and insults can alter calcium homeostasis, which worsens cell damage. Calcium has been shown to influence different cell death pathways, including apoptosis, necroptosis and through ER or mitochondrial stresses. Calcium released from the ER is transmitted to the mitochondria, under low calcium release from the ER the mitochondria can sequester the calcium in a cell survival response. However, if the calcium release from the ER exceeds mitochondrial capacity, the calcium will activate the opening of the mitochondrial permeability transition pore (MPTP) (Halestrap, 2009). Opening of the MPTP causes release of calcium and cytochrome C into the cytosol; as previously mentioned, which is important for the induction of extrinsic apoptosis (Orrenius et al., 2003). This process is also regulated by a positive feedback loop whereby the secreted cytochrome C influences transcriptional factors to upregulate inositol trisphosphate receptor (IP3R), causing further release of calcium from the ER (Boehning et al., 2003). Alongside cytochrome C release, other apoptotic factors also influence calcium transport: anti-apoptotic factor BCL-2 limits the release of calcium from the ER (and subsequent mitochondrial uptake). BCL-2 has been shown to either directly affect IP3R channels by reducing the probability of pore opening or through reducing the free calcium within the ER (Foyouzi-Youssefi et al., 2000; Pinton et al., 2000). Pro-apoptotic factors increase the sensitivity of mitochondria to calcium uptake (BAD and tBID) or to calcium release from the ER (BAX) (Csordás et al., 2002; Roy et al., 2014; Scorrano et al., 2003).

1.4 Receptor tyrosine kinases contribution to in cancer

Cancer is estimated to affect 2.5 million people in the United Kingdom, with general chemotherapy treatments having a wide range of side effects (Maddams et al., 2012; Pearce et al., 2017). Cancer therapies have been developing towards targeted therapies, focusing on proteins or genes specific to a tumour. One such set of proteins are tyrosine kinases, which regulate activity by adding phosphate groups to tyrosine residues on the target protein using ATP (Arora and Scholar, 2005). Tyrosine kinases are vital for major biological processes such as differentiation, growth, apoptosis and cell survival within normal cells (Arora and Scholar, 2005; Paul and Mukhopadhyay, 2004). While tyrosine kinases are tightly regulated in normal cells, mutations can induce kinase overexpression, leading to phosphorylation of multiple substrates, proliferation and activation of cell survival mechanisms. The overexpression of cell survival and proliferation can lead to uncontrolled cell growth and therefore development of cancer cells. Mutations in these tyrosine kinases, created an area of interest to identify treatments for many different cancer types (Paul and Mukhopadhyay, 2004).

Receptor tyrosine kinases are membrane receptors that recognise and interact with growth factors, cytokines and hormonal substrates, initiating proliferation pathways. These RTKs all share common structural features including extracellular domain for ligand binding, a transmembrane domain and an intracellular region. The intracellular region contains the kinase domain, this contains two lobes the n-lobe important for binding and positioning of ATP and the c-lobe which contains the tyrosine activation loop, the phosphorylation state of these tyrosine residues regulates the RTK activity

(Schlessinger, 2000). It has been shown that mutations and overexpression of RTKs can cause cancer by increasing proliferation, cell survival and aid in metastasis. One study showed 11% of patients with GIST expressed a mutation in exon 11 for c-Kit, this mutation is within the juxta-membrane and allows for ligand-independent activation. Activation of an RTK without a ligand removes one of the regulatory controls for kinase activity and leads to permanent activation. Another well studied tyrosine kinase mutation in cancer can be found in chronic myeloid leukaemia (CML) where translocation of chromosomes 9 and 22 leads to the fusion protein BCR-ABL. Similarly, with c-Kit mutation in GIST, the tyrosine kinase BCR-ABL is continuously active and causes an increase in downstream pathways such as JAK/STAT and MAPK; increasing cell survival and proliferation.

Receptor tyrosine kinases also play an important role in hypervascular tumours, these are associated with an increased vascular network, making them difficult to remove via surgery. In RCC the inactivation of the *von Hippel-Lindau* gene leads to the dysfunction of the hypoxia response genes including increase expression of VEGF (Choueiri et al., 2006). Downstream signalling of VEGFR increases angiogenesis, such as the activation of RAF leading to an increase in endothelial proliferation, MAPK activation increasing endothelial cell migration and AKT phosphorylation leading to increase in endothelial cell survival and vascular permeability. These all contribute to the hypervascular state of RCCs and is why VEGFR therapies are currently the best strategy for patients. Various studies, including clinical trials, have researched receptor tyrosine kinase inhibitors (RTKIs): these drugs block RTK autophosphorylation

and therefore prevent uncontrolled proliferation by binding to their intracellular domain (Schlessinger, 2000).

1.5 Receptor tyrosine kinase inhibitors

Receptor tyrosine kinase inhibitors function by blocking RTKs on cells such as vascular endothelial growth factor receptors (VEGFRs), platelet-derived growth factor receptors alpha and beta (PDGFR-α and -β), c-Kit and Erb-B2 Receptor Tyrosine Kinase 2 (ERBB2) (Bono et al., 2013; Shi et al., 2016). By blocking these receptors, RTKIs prevent downstream signalling cascades which increase angiogenesis (VEGFR), cellular migration (PDGFR) and proliferation (c-Kit) (Bikfalvi, 2004; H. Shi et al., 2016; Yu et al., 2001). Due to the ubiquitous and diverse nature of RTKs, numerous drugs have been developed with different affinities for specific receptors, including imatinib (IM) (c-Kit), trastuzumab (ERBB2), sunitinib (SM) and sorafenib (ST) (VEGFR) (Force et al., 2007). Receptor tyrosine kinase inhibitors were designed as a more targeted cancer therapy than commonly-used chemotherapeutics such as doxorubicin, which can cause high levels of cardiotoxicity (Orphanos et al., 2009). The survival rate for a range of cancers including gastrointestinal stromal tumours (GISTs), renal cell carcinoma (RCC) and breast cancers have been improved by RTKI treatment (Demetri et al., 2006; Motzer et al., 2009a). While RTKIs are efficient anti-oncogenic agents, recent studies have shown that these inhibitors can also cause cardiotoxicity (Orphanos et al., 2009).

1.5.1 Mechanisms of action and clinical cardiotoxicity

Receptor tyrosine kinase inhibitors are designed to target different RTKs and therefore have different mechanisms of action. Clinical cardiotoxicity can be manifested in various ways depending on the impact of the drug on the patient, including a decline in left ventricular ejection fraction (LVEF), signs of heart failure (HF), abnormal electrocardiogram readings and enzyme levels (Chung et al., 2013). Detailed baseline assessments should be taken from each patient, including risk factors, cardiac disease history, cardiac medication history and previous chemotherapy before starting a new treatment (Chung et al., 2013). Three different RTKIs will be discussed these are IM, SM and ST, these were chosen as suitable candidates because of their slight variation in RTK targets, use in different cancer treatments and extent of previous reports on cardiotoxicity.

1.5.2 Imatinib Mesylate

Imatinib mesylate is primarily used to treat patients with chronic myeloid leukaemia (CML) and GISTs, normally prescribed at between 400-600 mg/d. The drug was developed due to the discovery of the fusion protein BCR-ABL complex, which is common in CML (Iqbal, 2014). The fusion protein is hyperactivated, leading to sustained phosphorylation of substrates which contribute to cell survival and eventually CML. Imatinib was designed to inhibit the phosphorylation effect of the BCR-ABL fusion protein by blocking its ATP binding domain, meaning the substrate will remain inactive and subsequent cell survival signals will not be initiated (Chen et al., 2008). This blockage of the BCR-ABL fusion protein makes it an extremely effective targeted therapy

for CML, with an average 10 yr survival rate of 81% (Hochhaus et al., 2017; Capdeville et al., 2002).

Preclinical study of IM, including a 26-week repeat dose rat study, 13-week dog study and 39-week study in monkeys, showed no adverse cardiac observations (Sacha, 2014). However, post-approval clinical research has identified signs of cardiotoxicity caused by IM treatment (Atallah et al., 2007a; Kerkelä et al., 2006a; Ran et al., 2012). Clinical investigations into IM-induced cardiovascular effects have been carried out, with Kerkelä et al. (2006) reporting data from 10 patients who developed HF after IM treatment (400-800 mg/d). Further studies have also identified a possible link between IM and cardiotoxicity: Atallah et al. (2007) reviewed cardiac events from patient clinical trials using IM, and of 1276 patients, 22 (1.7%) showed signs of HF. Ran (2012) evaluated the risk of IM in elderly patients with CML, with one patient developing a decrease in LVEF four d post IM treatment (400 mg/d) but who recovered once IM treatment was withdrawn (Ran et al., 2012). The Kerkelä and Atallah studies have both been criticised, as a high percentage of the subjects who acquired HF had pre-existing conditions that increase HF risk, including diabetes, hypertension and coronary artery disease (Mellor et al., 2011).

1.5.3 Sunitinib Malate

Sunitinib malate is an RTKI used to treat RCC and IM-resistant GISTs, with the clinical dose ranging between 12-50 mg/d. Sunitinib malate is a more potent therapy for cancer treatment, as it targets multiple RTKs such as c-Kit, VEGFRs and PDGFRs. It was approved for the treatment of advanced RCC

in 2006 by the US food and drug administration and provided an option for patients who have IM-resistant disease (Coppin, 2008). By blocking phosphorylation of VEGFRs (2, 3), it prevents angiogenesis which is vital for tumour expansion. Without new vasculature, cancer cells cannot receive the signals needed for survival and thereby restricting their ability to metastasise (Coppin, 2008). Sunitinib may also have off-target effects by inhibiting molecules such as ribosomal s6 kinase, an important anti-apoptotic factor that normally blocks effects of BAD a pro-apoptotic factor. With the inhibition of ribosomal s6 kinase, BAD can inhibit the anti-apoptotic factor BCL-2. BCL-2 is vital for preventing apoptosis and works directly on inhibiting BAX and hence leads to the induction of apoptosis (Chen Ming Hui et al., 2008). This pro-apoptotic effect of SM is important for cancer therapies, helping to diminish cancer cell numbers, but could also be the basis of its cardiotoxic effects.

Pre-approval evaluation of SM caused a wide range of adverse cardiovascular effects. Sunitinib caused a reduction in the LVEF of primates in preclinical assessments (“GIST | SUTENT® (sunitinib malate) | Safety Info). Cardiotoxicity induced by SM has also been recorded in clinical studies: one single-arm, blinded study showed dose-dependent QT prolongation in patients with advanced solid tumours (Bello et al., 2009). Prolongation of QT can lead to life-threatening ventricular arrhythmias such as *torsades de pointes* and consequent cardiac arrest (Yap and Camm, 2003). However, none of the patients’ interval prolongation values was deemed severe (>500 ms) (Bello et al., 2009). Another clinical study, in which patients were given the approved dose (50 mg daily) illustrated the cardiotoxic effects of SM (Chu et al., 2007):

11% of patients developed adverse cardiac events; of these patients, 20% had a decline in LVEF below normal limits, 47% were hypertensive (>150/100mm Hg) and showed signs of HF (Chu et al., 2007).

1.5.4 Sorafenib Tosylate

Sorafenib tosylate is used to treat conditions such as RCC and melanoma, normally prescribed at 400 mg/d. In common with SM, ST inhibits the activation of VEGFRs (2, 3), PDGFRs and c-Kit, therefore preventing metastasis and tumour survival (Force et al., 2007). Sorafenib has been proposed to have somewhat different off-target effects to SM, mediated via inhibition of proto-oncogene serine/threonine-protein kinase RAF-1, a well-known pro-survival kinase that activates the ERK pathway. Inhibiting RAF-1, thus blocks ERK activation and prevents cell survival mechanisms, as appropriate for an anti-oncogenic agent. Sorafenib has also been suggested to be pro-apoptotic: by blocking RAF-1, it prevents the blockage of the pro-apoptotic factor apoptosis signal-regulating kinase 1 (ASK-1) (Lee and Kim, 2018). The protein ASK-1 activates JNK and therefore, apoptosis (Ichijo et al., 1997). These pro-apoptotic and anti-survival mechanisms make ST an effective therapeutic strategy for RCC and melanoma treatments.

Preclinical safety assessment of ST in rats showed signs of cardiac tissue autolysis, inflammation and degeneration (“Drug Approval Package: Nexavar (Sorafenib) NDA #021923,” n.d., p. 021923). A trial involving canines also raised concerns, with one animal showing signs of cardiac congestion and elevated creatine kinase levels, indicating myocardial damage (“Drug Approval Package: Nexavar (Sorafenib) NDA #021923,” n.d., p. 021923).

Based on the preclinical findings and knowledge about RTKI drugs and cardiotoxicity, the pharmacology review of the preclinical package stated that ST carried a high potential for cardiotoxicity ("Drug Approval Package: Nexavar (Sorafenib)).

Cardiac ischaemia or infarction was reported in 3% of ST-treated patients in a randomised, double-blind clinical trial, compared to 1% of patients in the placebo group (Escudier et al., 2009). In a study of patients with RCC treated with either SM or ST (Schmidinger et al., 2008), 33.8% of patients experienced cardiac events (events defined as: increased creatine kinase, arrhythmias, left ventricular dysfunction or acute coronary syndrome) (Schmidinger et al., 2008). The patients were placed on appropriate treatment and the symptoms found to be reversible (Schmidinger et al., 2008).

Overall the published clinical and pre-clinical data demonstrate the cardiotoxic effects caused by RTKIs. However, to better understand the underlying mechanisms, it is important to review the literature describing the direct effects of RTKIs on cardiomyocytes.

1.6 Receptor tyrosine kinase inhibitor-induced cellular damage

1.6.1. Cardiomyocyte damage due to receptor tyrosine kinase inhibitors

Cardiomyocytes contribute the bulk of cardiac muscle and provide its vital contractile function; their damage leads to weakening of the heart muscle, cardiomyopathy, arrhythmias and HF (Woodcock and Matkovich, 2005).

Reviewing the effects of RTKIs on cardiomyocytes is therefore a key step for understanding how RTKIs cause cardiotoxicity.

In vitro experiments using myocardial biopsies from IM-treated patients, with no previous history of coronary artery disease, were analysed using electron microscopy, which showed the mitochondria to have membranous whorls in the cardiomyocytes (Scheinfeld and Schienfeld, 2006), a feature previously linked to toxin-induced myopathies (Khan, 1995). Additional changes were seen in the mitochondria, with variation in size, shape and a lack of cristae, and in the cytosol, where scattered lipid droplets, vacuoles and glycogen accumulation were observed (Scheinfeld and Schienfeld, 2006). These results could be indicating a necrotic cell death mechanism, which was represented by the formation of lipid droplets and vacuoles.

IM-induced Cardiotoxic effects have also been demonstrated using mouse models, in which healthy mice were given a range of doses of IM, electron micrographs showed results similar to those seen in the patient myocardial biopsies (Kerkelä et al., 2006a). Another comparable feature was that cardiomyocytes showed mitochondrial abnormalities (pleomorphism and increased number of mitochondria). The highest IM dose was associated with an increase in calcium opening of the MPTP, which would lead to the release of cell death proteins (Kerkelä et al., 2006a). Further myocardial abnormalities have been reported in rat models using IM, including cytoplasmic vacuolisation and myofibrillar loss (Herman et al., 2011). This study found evidence supporting three different mechanisms for cardiomyocyte toxicity within rat hearts: apoptosis, necrosis and autophagy (Herman et al., 2011), evidence for each of these pathways having been demonstrated in previous research

(Kerkelä et al., 2006; Kyrylkova et al., 2012; Wolf et al., 2010; F. Zhao et al., 2010). Kerkela *et al*. (2006) showed expression of several apoptotic markers after isolated cardiomyocytes were exposed to 5 μM of IM (Kerkelä et al., 2006a), with an additional study associating cardiomyocyte necrosis with high doses of IM (Wolf et al., 2010). Other researchers could have identified a switch between apoptosis and necrosis after cardiomyocytes were treated with IM (F. Zhao et al., 2010).

Kerkelä *et al.* (2009) analysed endomyocardial biopsies from patients with RCC who developed decompensated systolic HF after SM treatment (37.5 mg/d), identifying several alterations in cardiomyocyte mitochondrial structure using transmission electron microscopy including expanded mitochondria with deficient or absent cristae. Further analysis of cardiomyocytes from two patients with IM-resistant GISTs, who developed HF after being treated with SM, identified cardiomyocyte hypertrophy and abnormal mitochondrial structures (effaced and swollen cristae) (Kerkela et al., 2009b).

Cultured rat cardiomyocytes treated with SM, may undergo apoptosis (Kerkela et al., 2009b). Although apoptosis had been demonstrated in rat cardiomyocytes and patient models, the mouse model showed no signs of cardiomyocyte apoptosis (Chu et al., 2007; Kerkela et al., 2009b). The study looked at using α-adrenergic agent phenylephrine to mimic an increase in blood pressure. Phenylephrine increased cardiomyocyte apoptosis 7-fold, as indicated by terminal deoxynucleotidyl transferase dUTP nick end labelling (TUNEL) staining (Chu et al., 2007), suggesting a possible link between SM-

induced cardiomyocyte apoptosis and high blood pressure. Sunitinib has also been shown to cause a significant loss of mitochondrial membrane potential (Δψm) cardiomyocytes, this reduction in Δψm has been associated with the generation of ROS and programmed cell death (Zamzami et al., 1995). Cardiomyocyte energetics were also impaired with a significant reduction in ATP during treatment with SM (Kerkela et al., 2009b).

In contrast, Zhao *et al.* (2010) identified cell death by autophagy rather than apoptosis in H9c2 rat cardiac myoblasts exposed to SM (Y. Zhao et al., 2010)., with cells dying in a dose-dependent manner when exposed to a range of SM concentrations (2.5-20 μM). Treating H9c2 cells with SM and a caspase inhibitor (zVAD-fmk), to investigate the role of apoptosis in SM-induced cell death, showed no effect on H9c2 cell survival, indicating that apoptosis was not the mechanism of cell death (Y. Zhao et al., 2010). The study also showed the induction of autophagy, with acridine orange fluorescent staining and identification of autophagosome changes after SM treatment, s (Y. Zhao et al., 2010).

Sorafenib has been demonstrated to increase reactive oxygen species (ROS) production in human cardiomyocytes (Kawabata et al., 2015). One suggested mechanism for this is that ST treatment reduces stanniocalcin 1 expression, which normally facilitates a reduction in ROS production (Kawabata et al., 2015; Liu et al., 2012). Sorafenib toxicity was demonstrated in isolated adult feline left ventricular myocytes exposed to ST (0.5 μM-50 μM) (Duran et al., 2014). Although lower concentrations (0.5–5 μM) had no apparent effect on cardiomyocyte survival, higher concentrations of ST treatment (10-50 μM),

reduced myocyte number after only 12 h. Western blot analysis of caspase 3 and TUNEL staining showed no signs of apoptosis; it was therefore concluded that ST-induced cardiomyocyte necrosis, which is believed to be the cause of reduced myocardial mass, with surviving cardiomyocytes consequently undergoing pathological hypertrophy. These findings are consistent with the evidence of ST increasing individual cardiomyocyte size but reducing overall heart weight (Duran et al., 2014).

Rat H9c2 cells have been used to show ST toxicity, including analysis of mitochondrial function (Will et al., 2008). Sorafenib caused a 4 fold-lower IC50 dose in galactose media (10.1 μM) compared to glucose (44.7 μM), suggesting damage to mitochondrial metabolism (Will et al., 2008). Further to this, ST inhibited complexes II, III, V at doses of 3-5 μM, and higher concentrations complexes I and IV of the electron transport chain (Will et al., 2008). This inhibition of the electron transport chain would reduce the amount of ATP produced within the cell, both caspase inhibition and ATP deficiency are a strong indication of necrotic cell death. These studies show that RTKIs have adverse effects on cardiomyocytes, findings that raise the question of whether the drugs affect other cell types within the myocardium, including cardiac progenitor cells.

1.6.2. Possible cardiac progenitor cell damage due to receptor tyrosine kinase inhibitor targets

As mentioned previously the main identifier of the CPCs is c-Kit, this RTK is a primary target for all three RTKIs studied in this project. Therefore, it is important to theorise the possible impacts c-Kit inhibition could have on the CPCs. It has previously been shown that mice with lowered expression of c-

Kit have accelerated ageing and reduced myocardial repair than those with normal expression (Marino et al., 2019). One reason for this could be due to the dependency that the CPCs have on c-Kit, previous findings have shown that these cells benefit from c-Kit activation leading to increased survival, migration and reduced cell death (Vajravelu et al., 2015). Therefore, it is fair to assume these RTKs might have a negative impact on the CPC population. Another important target for the SM and ST is the VEGFRs, these receptors and its agonist VEGF have been shown to be important for CPC signalling. Three different VEGF-A subtypes prompted CPC adhesion through VEGFR and PKC-α signalling. The *in vivo* administration of VEGF-A promoted the engraftment of CPCs in damaged hearts and reduced infarct size and fibrosis (Tang et al., 2015). Other studies have also shown VEGF to be important for the translocation of CPCs to the site of damage (He et al., 2016). The RTKIs of this study also inhibit the PDGFRs, however, our previous work has shown little/no expression of these receptors and therefore the impact of their inhibition on CPCs is thought to be minimal. Therefore it is again theorised that inhibiting these RTKs will impair the CPC function through reduced cell proliferation, attachment and migration.

1.7 Aims and objectives

Taken together, previous research has revealed the importance of investigating RTKI induced cardiotoxicity, with a focus around exploiting CPCs. This project aims to characterise the cell death pathways in CPCs after exposure to IM, SM and ST. The long-term aim would be to identify possible targets for inhibition of specific cell death pathways in CPCs without changing

the RTKI chemotherapy actions and therefore help protect cardiomyocytes. It is hypothesised that all three RTKIs will be toxic to the CPCs. It is also theorised that IM and SM will induce apoptosis whereas ST will induce an alternative cell death pathway.

Thus, the specific objectives of this study are:

1. To prove CPCs have stem cell properties and express RTKI targets
2. To map the cell death pathway induced by IM
3. To determine the cell death pathways induced by SM
4. To identify the cell death pathways induced by ST
5. To determine targets for possible cell death inhibition for each treatment

Chapter 2. Materials and Methods

2.1 Materials

Collagenase type II (Lorne laboratories)

0.22 µm and 100 µm filters (Millipore)

Fetal Bovine Serum (ThermoFisher)

Optiprep™ solution (Sigma)

MACs kit (Miltenyi biotec)

CD117+ and CD45+ beads (Miltenyi biotec)

Minimum Essential Medium-F12 HAMS (DMEM, Sigma),

Insulin-Transferrin-Selenium (Life Technolgoies)

LIF (Millipore),

Epidermal growth factor (EGF) (Peprotech)

Basal fibroblast growth factor (bFGF) (Peprotech)

Neurobasal medium (Life Technologies)

Glutamax (Sigma)

B27 supplement (Life Technolgoies)

N2 supplement (Life Technolgoies).

Embryonic stem cell-qualified foetal bovine serum (ESQ, ThermoFisher), penicillin-streptomycin (Life Technologies).

Fungizone (Invitrogen)

Gentmicin (Sigma)

25 cm^2 and 75 cm^2 flask

CellStart (Sigma)

Dulbecco's phosphate-buffered saline (D-PBS)

Dimethyl sulfoxide (DMSO).

15 ml and 50 ml sterile conical tubes

Accutase (Sigma)

CryoVials (ThermoFisher

Mr. Frosty™ container (ThermoFisher)

Haemocytometer chamber (Nanoentek)

96 well plates (Sigma)

Dexamethasone (Sigma)

Ascorbic acid (Sigma)

Oxytocin acetate (Sigma O6379),

beta-glycerol phosphate (Sigma),

TGF-beta (Peprotech)

RNeasy RNA isolation kits (Qiagen):

1% β-mercaptoethanol (Sigma)

Fluorescein diacetate (Sigma)

QIAshredder (Qiagen),

SYBR green

Tris-acetate-EDTA (TAE) buffer (Millipore).

SYBR safe (Biorad)

DNA ladder (Biorad).

Hoechst

tetramethylthodamine, methyl ester, perchlorate (ThermoFisher)

ybrant™ FAM caspase 3/7 dye (Invitrogen)

ToPro-3 (Invitrogen)

CellCarrier-96 Ultra Microplate (Perkin Elmer)

bovine serum albumin (Sigma A9418

annexin binding buffer (BioLegend),

annexin V pacific blue (BioLegend).

Acridine orange (ThermoFisher)

confocal microscopy (Zeiss LSM880).

ROS/Superoxide Detection Assay Kit (Abcam, ab139476)

DMF

Thapsigargin

black 96 well clear bottomed plates (Santa Cruz)

Fluo-4 AM (Fluo-4) (ThermoFisher)

calcium free hanks buffer (Gibco)

10 mM HEPES solution (ThermoFisher Scientific),

calcium containing hanks buffer (Gibco)

RIPA buffer (Sigma)

Pierce™ Rapid Gold bicinchoninic acid assay Protein Assay Kit (ThermoFisher)

4x laemmli sample buffer (BioRad)

4-20% polyacrylamide precast gel (BioRad)

1x running buffer (10x Tris-Glycine-*SDS* PAGE *Buffer,* National Diagnostics)

Trans-Blot Turbo Transfer Pack (BioRad) and semi-dry Turbo blotter (BioRad)

Milk powder (Sigma)

Prolong gold (ThermoFisher Scientific)
The Duolink kit was used (Sigma)
goat serum (ThermoFisher, cat.no.10000C)

Cytoflex S flow cytometer (Beckmans)

ImageJ software (NIH)

EVOS (ThermoFisher)

Flexstation 3 (Molecular devices),

G:Box Chemi XT4 (Syngene).

Nanodrop 1000 spectrophotometer (ThermoFisher)
Operetta platform (Perkin Elmer).

Columbus™ software (Perkin Elmer)

2.1.2 Antibodies

Host	Target	Company	Dilution	Applications	Catalogue numbers
Rabbit	MAP1LC3B	Novus	1:4000	Western blotting	NB100-2220SS
Rabbit	MAP1LC3B	Cusabio	1:200	ICC, PLA	CSB-PA887936LA01HU
Mouse	LAMP2	Novus	1:200, 1:100, 1:1000	ICC, PLA, Western blotting	NBP2-22217SS
Rabbit	p-MLKL	Abcam	1:1000	Western blotting	ab187091
Rabbit	total MLKL	Genetex	1:1000	Western blotting	GTX107538S
Rabbit	beta-actin	Cell signalling	1:2000	Western blotting	4970S
Rabbit	SQSTM1 (p62)	ProSci Inc.	1:1000	Western blotting	PSI-5449
Rabbit	Smooth muscle actin	Sigma	1:100	ICC	A2547
Mouse	vWf	Dako	1:200	ICC	A0082
Mouse	BAX	Santa Cruz	1:400	Western blotting	sc-7480
Mouse	Calpain 1	Santa Cruz	1:1000	Western blotting	sc-271313
Mouse	Calpain 2	Santa Cruz	1:1000	Western blotting	sc-373966
Rabbit	ERK	Cell signalling	1:1000	Western blotting	4695
Rabbit	p-ERK	Cell signalling	1:1000	Western blotting	9101
Rabbit	AKT	Cell signalling	1:1000	Western blotting	9272
Rabbit	p-AKT (Ser473)	Cell signalling	1:1000	Western blotting	9271
Mouse	FAS	Santa Cruz	1:1000	Western blotting	sc-8009
Mouse	c-Kit	Santa Cruz	1:1000	ICC	sc-365504
Mouse	RIP1	R&D systems	1:200	ICC	MAB3585-SP
Rabbit	PARP	Cell signalling	1:200	Western blotting	9542
Mouse	RyR2	ThermoFisher	1:200	ICC	MA3-916
Rabbit	RyR2	Sigma	1:200	ICC	HPA020028
Mouse	SERCA	Abcam	1:200	ICC	AB2861
Rabbit	IP3R	ThermoFisher	1:200	ICC	PA1-901
Rabbit	RyR3	Abcam	1:200	ICC	AB9082

Mouse	Pan-RyR	ThermoFisher	1:200	ICC	MA3-925
Rabbit	Alexa 488 (2º)	Invitrogen	1:200	ICC	A11008
Rabbit	Alexa 647 (2º)	Invitrogen	1:200	ICC	A11001
Mouse	Alexa 488 (2º)	Invitrogen	1:200	ICC	A21235
Mouse	Alexa 647 (2º)	Invitrogen	1:200	ICC	A21244

Table 2. 1. List of primary and sary antibodies. List of primary antibodies including host species, target, company, dilution and application.

2.1.3 Primer pairs

Gene target	Forward sequence	Reverse sequence	Product (bp)	mRNA accession number
ACTB	GCCTCGCCTTTGCCGA	CTCGTCGCCCACATAGGAAT	221	NM_001101.3
TNF-α	TAGCCCATGTTGTAGCAAACCC	GGACCTGGGAGTAGATGAGGT	150	NM_000594.3
CAPNS1	CAATGTCCGCTTCGGCTCTA	TGCGACTCACTGCGCC	182	NM_001749.3
PARP	AGCGTGTTTCTAGGTCGTGG	CATCAAACATGGGCGACTGC	194	NM_001618.3
BAX	TAACATGGAGCTGCAGAGGATG	GGGACATCAGTCGCTTCAGTG	299	NM_001291428.1
RIP1	CTGCTCGTCAAGTGTGGGA	CCGAGGTCTGCGATCTTAATGT	702	NM_003804.4
RIP3	TTACCTGCACGACCAGAACC	TGCTGCTCTTGAGCTGAGAC	548	NM_006871.3
MLKL	GTCCGGTACAGTCAGCAGAG	CTTCAAATTTTCCATGCCTTCGC	206	NM_152649.3
BCL-2	CATGTGTGTGGAGAGCGTCA	AGTTCCACAAAGGCATCCAG	171	NM_000633.2
BID	CTGGGAAACTGTTGAGTGGCT	CGTTGTTGACCTCACAGTCCAT	278	NM_197966.2
Calpain	CAATGTCCGCTTCGGCTCTA	TGCGACTCACTGCGCC	182	NM_001749.3
Caspase 8	AGCCCTCTGAATTTGCTAGTC	AATATAATCCGCTCCACCCTTTCC	208	NM_001080125.1
Caspase 9	GCTGTTCAGGCCCCATATGAT	AGAGCACCGACATCACCAAA	327	NM_001229.4
FAS	CCCGACCCAGAATACCAAG	CCCAAGTTAGATCTGGATCCTTCC	166	NM_000043.5
JNK	GCTCTCCAACACCCGTACAT	CACTGCTGCACCTAAAGGAGA	170	NM_001278547.1

PARP	AGCGTGTTTCTAGG TCGTGG	CATCAAACATGGG CGACTGC	194	NM_001618.3
RAF-1	CCTGGCTCCTCAG GTTTAAG	AGGCCAGTCATG CAAGCTCAT	285	NM_002880.3
EPAC	TCTACTCACCCAAG AGGAGCC	CCAGCCCACCTT CATGTTTCT	220	NM_001098531.2
IP3R	TCGGTTGGAGGTC TGCATTC	GCAGCTCCAAAC AAACTGCT	169	NM_033397.3
L-type calcium channel	TCCGAGGTGGGAG CGTA	CGATGTCCCCGA TGTGAAGA	174	NM_199460.3
MCU	CGCCGTTTCCAGTT GAGAGAT	AGGAAGCGATCC TCTGGTGT	191	NM_138357.2
Na-Ca exchanger	GAGTTTGGCGACG ACGAGA	TCCCCATCCCCTT GATTGAGT	155	NM_015063.2
RYR2	AGCCAGTGTCATCC ACCAAC	TTGTGATGCCAAC TGATGAAATCCCC	178	NM_001035.2

Table 2. 2 Sequences for forward and reverse primer pairs. Table includes primer name, forward and reverse sequence, expected product size and accession number. All purchased from sigma.

2.2. Methods

2.2.1 Mammalian cell culture

All reagents were purchased from Life Technologies unless otherwise stated and were sterilized through a 0.22 μm filter. Cells were incubated at 37°C, 5% CO2 and 1% O2 unless otherwise stated.

2.2.1 Human cardiac progenitor cell isolation

Adult CPCs were isolated from right atrial myocardial tissue obtained during routine cardiac surgery; tissue samples were donated by Mr. Prakash Punjabi (Hammersmith Hospital), Mr. David O'Regan and Mr. Sotiris Papaspyros (Leeds General Infirmary). Atrial tissue was used over ventricular due to technical and health consideration for the patients under operation, also all tissue was surgical waste making it easier to acquire, finally age was not an

excluding factor for this project. Right atrial samples were weighed and dissected into 0.5-1 mm^3 pieces, these pieces were placed into a conical flask and subjected to digestion with 0.3 mg/ml collagenase type II (Lorne laboratories). The first tissue digestion was for 5 min at 37°C. Following this the collagenase cell solution was passed through a 100 µm filter into a 50 ml tube before addition of quenching medium (1:1, DMEM and 10% FBS). The tissue fragments were then placed back into the conical flask and the process was repeated for 7-9 digestion cycles of 3 min each at 37°C; each digest supernatant was passed through a 100 µm filter and quenching medium was added to the isolated cell suspension. After digestion, all collected cells were strained through a 40 µm filter. The collected cells were centrifuged at 400 *g* for 10 min to isolate the smaller cell population. The supernatant was then removed and the cell pellet resuspend in 8 ml of medium. Optiprep™ solution was used to remove excess debris including a bottom layer of 36% Optiprep (density 1.12 g/ml) and top layer of 16% Optiprep density (density 1.06 g/ml) (Sigma) diluted in DMEM with 10% FBS, followed by the cell solution which was then pelleted by centrifugation (no break/acceleration 800 *g* for 20 min). Three cell isolates were used throughout the project (collected from three separate atrial biopsies), named PP006, SP006 and DOR006.

The cells then underwent magnetic bead separation according to the manufacturer's guidelines (Miltenyi biotec), in order to negatively enrich (remove) CD45-positive cells, then positively enrich (select for) the CD117/c-Kit-positive cell population. After selection, cells were re-suspended in growth medium and plated onto one well of a 6 well plate coated with CellStart (Sigma), at a density of 1000-10,000 cells/well depending on biopsy sample

size. Cells were cultured in a humidified tissue culture incubator at 37°C, 5% CO_2, 1% O_2 and passaged on reaching 70-80% confluency. The CPCs were grown in lowered oxygen concentration (1%) compared to “normal” hyperoxic cell culture conditions (21%), as previous reports showed lowered oxygen concentration aids stem cell proliferation and inhibit differentiation (Mohyeldin et al., 2010). The lowered oxygen concentration was also used to mimic *in vivo* conditions, oxygen levels in the human body differ greatly based on the location ranging from 0.3% in the mucosal layer of the large intestine up to 14% in the epithelial cells of the lungs (Mas-Bargues et al., 2019). The CPCs are primarily found deep within the apex of the heart surrounded by a large number of other cardiac cell types and therefore it is believed that they are within a naturally oxygen-deprived environment between 1-2% (van Oorschot et al., 2011). The isolation procedure used magnetic bead separation over FACs due to the relatively low number of cells obtained ensuring minimum cell loss.

2.2.2 Human cardiac progenitor cell growth medium

Cardiac progenitor cell growth medium was prepared by mixing two separately-prepared solutions. The first solution contained: Dulbecco’s Minimum Essential Medium-F12 HAMS (DMEM, Sigma), Insulin-Transferrin-Selenium (1% vol/vol), LIF (10 ng/ml, Millipore), epidermal growth factor (EGF) (20 ng/ml, Peprotech), basal fibroblast growth factor (bFGF) (10 ng/ml, Peprotech). The s solution contained: Neurobasal medium, Glutamax (2% vol/vol, Sigma), B27 supplement (2% vol/vol), N2 supplement (1% vol/vol). After both solutions were made, 45% of each were added into a final mix,

followed by embryonic stem cell-qualified foetal bovine serum (ESQ, 10% vol/vol), penicillin-streptomycin (1% vol/vol) gentamycin (0.1% vol/vol) and Fungizone (0.1% vol/vol). The growth factors or cytokines in the medium act to inhibit stem cell differentiation (LIF) or aid proliferation (EGF and bFGF).

2.2.3 Maintenance of cells, thawing, passaging and freezing

A 25cm^2 flask was coated with CellStart (Sigma) solution (1:50 in Dulbecco's phosphate-buffered saline (D-PBS)) and incubated at 37°C for 1-2 h. The CPC Cryovial (TheroFisher) was removed from liquid nitrogen storage and immediately transferred to a water bath (37°C). The vial was defrosted until only partially thawed, to limit toxicity from warmed dimethyl sulfoxide (DMSO). Cells were then transferred into a 15 ml sterile conical tube containing 10 ml of passaging medium (DMEM and 10% foetal calf serum), then centrifuged at 300 *g* for 5 min, supernatant was removed and the cell pellet re-suspended in 7 ml of growth medium and seeded in a 25 cm^2 flask.

Cells were passaged upon reaching 80% confluency, to prevent cell-cell contact inhibition and consequent differentiation. Cells were rinsed with D-PBS containing antibiotics (1% penicillin-streptomycin, 0.1% Fungizone and 0.1% gentamicin) to remove any traces of growth medium. Then Accutase (Sigma) solution was applied to the cells and incubated for 5-7 min until cells had detached (checked microscopically), after which the cell suspension was aspirated and passaging medium (containing 10% foetal bovine serum) added to neutralise the enzymatic action of Accutase. The cell suspension was then centrifuged at 300 *g* for 5 min, supernatant aspirated and the pellet re-suspended in growth medium (**refer to table 2.1 for solution volumes**). Re-

suspended cells were either added to vessels to maintain the cell isolates or counted for use in further experiments. These cells were identified to be proliferative and viable throughout passages 0-18, however, due to reduced stem cell gene expression and morphological changes suggesting cell arrest after P18 these cells were excluded from experiments.

If frozen cell stocks were required, cells were detached and pelleted as described above and the necessary volume of freezing medium was prepared: 1 ml per vial (70% growth medium; 20% ESQ-FCS; 10% DMSO). Cell pellets were resuspended in freezing medium and transferred to CryoVials (ThermoFisher), stored in a Mr. Frosty™ container (ThermoFisher) to allow gradual freezing at -80°C for 48 h, before transfer to a liquid nitrogen cell bank for long-term storage.

Vessel	Coating	PBS wash	Accutase	Passage medium	Growth medium
T25cm flask	2 ml	2 ml	2 ml	6 ml	7 ml
T75cm flash	5 ml	5 ml	5 ml	15 ml	20 ml
10cm dish	4 ml	4 ml	4 ml	12 ml	10 ml
6 well plate (per well)	1 ml	1 ml	1 ml	6 ml	2 ml

Table 2. 3. Vessel volumes required for cell maintenance including coating, PBS washes, Accutase, passage medium and growth medium.

2.2.4 Cell counting

Standard cell counting methods were used: 10 µl of cell suspension was pipetted into a disposable haemocytometer chamber (Nanoentek), cells were

visualised under a microscope and counted manually. The four corner grids of a haemocytometer were counted and the average taken: this gave the number of cells in 0.1 µl of solution, which was then multiplied to determine cell density per µl. These values were used to calculate the volume of cell suspension required for each experiment, using the following equation: Volume of cell suspension required (µl) = number of cells desired (cell number)/actual cell density (cell number/µl).

2.2.5 Clonogenicity assay

Cells were pelleted, resuspended and counted as previously described. The cell solution was diluted in growth medium to a final density of 10 cells/ml, allowing 1 cell to be added to each well of a 96 well plate (100 µl per well). Cells were allowed to attach for 4-5 h and then assessed by microscopy to identify wells containing a single cell. Cells were then maintained for 6 d, with images taken on d 1, 2, 3, 4 and 6 for wells containing a single clonal colony. This process was repeated for cells at multiple passage numbers (4, 10, 18 and 21) to confirm retention of clonogenicity across passages.

2.2.6 Differentiation of CPCs

The CPCs were differentiated into either endothelial cells or smooth muscle cells to confirm the cells were multipotent. To form endothelial cells, CPCs were grown on coverslips (5000 cells/coverslip) and allowed to adhere overnight in normal CPC growth medium. The medium was then changed to CPC growth medium without LIF and with lowered ESQ concentration (2%): this slowed cell proliferation and encouraged the cells to differentiate along the

endothelial lineage. To differentiate CPCs into smooth muscle cells, the CPC growth medium was replaced with differentiation medium; alpha modified MEM (Sigma M0894), 2% ESQ (Invitrogen), 1 μM dexamethasone (Sigma), 50 μg/ml ascorbic acid (Sigma), 100 nM oxytocin acetate (Sigma O6379), 10 mM beta-glycerol phosphate (Sigma), 1% penicillin/streptomycin (Sigma), 0.1% gentamicin (Sigma), 0.1% Fungizone (Invitrogen) and 5ng/ml TGF-beta (Peprotech) for 14 d; medium was replenished every 3 d.

2.2.7 Cell treatments

For the following assays, the RTKIs were added at either 'peak' concentrations for 24 h or 'trough' concentrations for 7 d: these were based around clinically-comparable data for each drug, which were assessed for IM using patient peak and trough plasma levels (Demetri et al., 2009; Leveque and Maloisel, 2005). The peak concentration refers to C_{max} which is the maximum concentration of the drug in the plasma before the s dose (~10 μM). The trough concentration refers to the C_{min}, the lowest level of drug in the plasma after admission, the trough levels were used to investigate the effects of low drug concentration over a longer period (~5 μM). For SM and ST the standard daily doses were taken to be clinically-comparable, which were: 75 mg/d for SM (equates to ~2 μM) and 600 mg/d for ST (~10 μM), IM daily dose is also 600 mg/d. This study focuses on the higher end of the recommended doses as shown in previous studies (Burke et al., 2019; Rodríguez-Hernández et al., 2020; Sandhu et al., 2017; Smith Andrew J et al., 2018). For some experiments it was important to investigate dose dependent effects, therefore the cells were treated with a

range of drug concentrations (x10 higher or lower than the clinical comparable concentration).

2.3 Cell viability assay using Fluorescein diacetate hydrolysis

Fluorescein diacetate (FDA) is a non-polar, non-fluorescent compound used to measure cell viability. Healthy cells contain active non-specific esterases, which cleave the acetate groups from FDA, leaving the polar fluorescent bioproduct fluorescein, with comparatively poor membrane permeability: this is retained intracellularly and thus marks a viable cell.

The FDA assay was performed as previously described (Smith et al., 2009). 5,000-20,000 CPCs were plated into each well of a 96 well plate and treated with RTKIs or other conditions in growth medium for 24-72 h depending on the experiment. After treatment, medium was removed and replaced with 5 µg/ml FDA (in 1% ethanol, 9% PBS and 90% DMEM-F12), incubated for 10 min at 37°C. Fluorescence readings were taken using a Varioskan Flash plate-reader (v.4.00.53) at excitation/emission of 485 nm/520 nm. Cell viability was calculated as treated groups/untreated groups x100 (%).

2.4 Quantitative reverse transcription PCR

2.4.1 Sample preparation

Reverse transcription quantitative polymerase chain reaction (RT-qPCR) is the process of converting RNA into complementary DNA (cDNA) for quantification of gene expression. To collect an RNA sample >100 ng/µl, cells were plated onto 100 mm dishes at 250,000 cells per dish, treatments were added at

clinically-comparable concentrations for both peak (24 h) and trough concentrations (7 d). Once the cells were pelleted, they were resuspended in 1 ml of D-PBS (with antibiotics) and centrifuged at 211 RCF, 4°C for 5 min. The D-PBS was removed, and cells stored at -80°C until required.

2.4.2 Total RNA isolation

Total RNA was isolated using RNeasy RNA isolation kits (Qiagen): the cells were homogenised in RLT buffer with 1% β-mercaptoethanol (Sigma) and added to a QIAshredder (Qiagen), spun at 14,000 relative centrifugal force (RCF) for 2 min. An equal volume of molecular grade ethanol (70%) was added to the lysate and mixed. The resultant solution was placed into a RNeasy Mini spin column and centrifuged at 9391 RCF for 15 s, with flow through discarded. The RNA was then isolated using the Qiagen RNeasy mini kit to ensure optimal RNA yield. The purity of the RNA sample was tested using a Nanodrop 1000 spectrophotometer (ThermoFisher). The purity of RNA was assessed by the ratio of absorbance at 260 nm and 280 nm; RNA samples with an absorbance reading of above 1.9-2.1 were accepted. A s ratio absorbance of 260 nm and 230 nm was also considered as a s measure of purity with values of >1.7 accepted. Samples with values below these limits were rejected, as this indicated phenol or protein contamination.

2.4.3 cDNA synthesis

Isolated RNA was used as a template to create cDNA with the iScript cDNA synthesis kit (Biorad), per reaction (100 µl of cDNA): dNTP reaction mix (1:5), reverse transcriptase (1:20) and 2000 ng of RNA (remaining volume was made

with molecular biology-grade water). The complete mixture was prepared in 200 µl tubes (Thermofisher), then placed in a CFX96 thermocycler (Biorad) for cDNA synthesis: 25ºC for 5 min (allowing dNTPs bind to 3' RNA strand); 42ºC for 30 min (for optimal reverse transcriptase enzyme activity to attach dNTPs); finally the mixture was heated to 85ºC to prevent any additional enzyme activity and the sample was cooled to 4ºC pending collection.

2.4.4 Primer design and preparation

Messenger RNA sequences for all primers were obtained from the NCBI nucleotide database and ran through Primer BLAST software (NCBI). All primer sequences were ordered from Sigma and reconstituted in molecular biology grade water (maintained as 100 µM stock solutions at -80ºC). (**Refer to Table 2.1**). The 100 µM stocks were diluted with molecular biology grade water before use in experiments (5 µM).

2.4.5 PCR reaction

For each well of a 96-well PCR plate, a total volume of 20 µl was added (plate maintained on ice during loading): 10 µl SYBR green, 1.2 µl of each of the forward and reverse primers (5 µM stock), 5.6 µl molecular biology grade water, followed by 2 µl cDNA. Each primer pair would bind to the complementary structures on the cDNA, the fluorescent compound SYBR green bound to any double stranded DNA present within the mix, thus identifying the presence of the target sequence (primer + cDNA strand).

Samples were heated to 95ºC for 5 min to denature cDNA double strands. Following this, 95°C for 10 s and then lowered to 60ºC for 30 s for primer

binding and then 72ºC for 30 s to allow the SYBR green binding. This process was repeated for 40 cycles. After completion of the PCR process, a melt curve was generated: the plate was heated from 65ºC to 95ºC, in increments of 0.5ºC for 5 s each. The melt curve was used to indicate the presence of one amplicon after the RT-qPCR assay; one single peak represents one specific amplicon. Data were analysed using CTX manager software and transferred to Excel for statistical analyses.

2.4.6 Agarose gel electrophoresis

After RT-qPCR, samples were assessed on a 2% agarose gel, to confirm the size of reaction products and confirm that only one product was formed. Firstly, 1.6 g of agarose (Appleton) was added to 80 ml 1x Tris-acetate-EDTA (TAE) buffer (Millipore). The solution was heated until the agarose was fully dissolved, and the solution left to cool to room temperature. Once cooled, 5 µl of SYBR safe (Biorad) was added to the solution, which was then placed into a gel tank with a 10 well-forming comb for 30 min to set at room temperature. Following this, 10 µl of each RT-qPCR product was mixed with 7x DNA loading dye and loaded to wells alongside a DNA ladder (Biorad). The RT-qPCR products were separated by electrophoresis at 100 V for 1 h at room temperature. The DNA products were visualised using an automated developer (G-box, Syngene).

2.5 Live cell imaging

2.5.1 Automated High Content Microscopy and Analysis

The high content image analysis was performed to identify whether the cells were undergoing apoptosis or necrosis. Four different dyes with different

emission wavelengths were used. Hoechst (455 nm) allowed identification of the cell nuclei, a cell permeable cationic dye called tetramethylthodamine, methyl ester, perchlorate (TMRM, 575 nm) was used to identify the cells cytoplasm/ Δψm. A key identifier of apoptosis Vybrant™ FAM caspase 3/7 dye (Invitrogen) (488 nm) was used, a dye which produces a fluorescent by-product when it interacts with the active site of either caspase 3 or 7 (executioner caspases). ToPro-3 (661 nm) is a dye which has a high affinity for nucleic acids in DNA and only enters the nucleus once there is a loss of cell membrane integrity. First, cells were added to a CellCarrier-96 Ultra Microplate (Perkin Elmer), 5000 cells/well. Fam/Cas dye (1:150) was added and incubated for 1 h and washed with apoptosis wash buffer (Life Technologies V35118, diluted 1:10). Hoechst 1:200, ToPro-3 1:1000 and TMRM 1:100,000 (Invitrogen) was added and incubated for 10 min, then replaced with growth medium (without indicators) and analysed by an operetta platform (Perkin Elmer). The results were interpreted using the Columbus™ software.

2.5.2 Flow cytometry

Cells were grown in culture depending on the experimental design and were then pelleted via centrifugation at 300 *g* for 5 min and then re-suspended in D-PBS; the cells were then pelleted at 300 *g* for 5 min. Finally, cells were re-suspended in incubation buffer, D-PBS (Ca^{2+} and Mg^{2+} free, Invitrogen 14190-136); 2.5 g bovine serum albumin (Sigma A9418); 1% Penicillin/Streptomycin (Invitrogen 15140-122); 0.1% Fungizone (Invitrogen 15290-018); 0.1% Gentamicin (Sigma G1397). The cells were analysed using the Cytoflex S flow

cytometer (Beckmans). First the unstained sample was used to set the experimental parameters using a forward and side scatter dot plot to identify the cell population. Once identified the population was gated for viable cells, ensuring dead cells and duplicated cells were excluded from the analysis. The correct emission filters were selected depending on the dye used.

2.5.2.1 Mitochondrial membrane potential analysis

In order to evaluate the effect of RTKIs on the Δψm, flow cytometry was used to analyse the retention of TMRM. Cells were seeded onto 100 mm dishes until 80% confluent; TMRM (1:300,000) was added for 10 min and the cells were then washed with PBS before detaching using Accutase. Flow cytometry procedure was then followed (**refer to Chapter 2.4.2.**), a 561 nm/585 nm filter was used to detect the TMRM signal. Following this, the relative Δψm was calculated using the TMRM fluorescence intensity of treated cells relative to untreated cells.

2.5.2.2 Apoptosis assay

Annexin V was used to detect the presence of apoptosis. In healthy cells a protein known as phosphatidylserine (PS) is transported to the inner leaflet of the cell membrane. When cells become apoptotic the cell membranes phospholipids lose their asymmetry causing the exposure of PS on the outer leaflet of the membrane; acting as a death signal to surrounding phagocytes. This process has been exploited for apoptosis detection; Annexins are ubiquitous proteins that can bind PS. Therefore, when cells become apoptotic, annexin proteins which have been labelled with a known fluorochrome (Pacific

Blue) can bind to PS and release emitted light which can be detected, whereas in healthy cells annexin cannot bind to PS as it is on the inner membrane and therefore no signal is detected **(Figure 2.1)** (Lecoeur et al., 1997)**.**

Cells were seeded onto 100 mm dishes (300,000 cells/dish) incubated overnight. Cells were detached using Accutase and pelleted, cells were then washed with 1 ml of 1x annexin binding buffer (BioLegend), centrifuged at 300 *g* for 10 min. The pellets were then resuspended in 100 µl of 1x annexin binding buffer, followed by 10 µl of annexin V pacific blue (BioLegend). The solution was mixed and incubated on a rotator for 15 min at room temperature in the dark. Following this 1 ml of annexin binding buffer was added and the solution was centrifuged at 300 *g* for 10 min. The buffer was then aspirated and 500 µl of fresh binding buffer was added. Signal was detected using flow cytometry (405 nm emission) and analyzed using Cytoexpert.

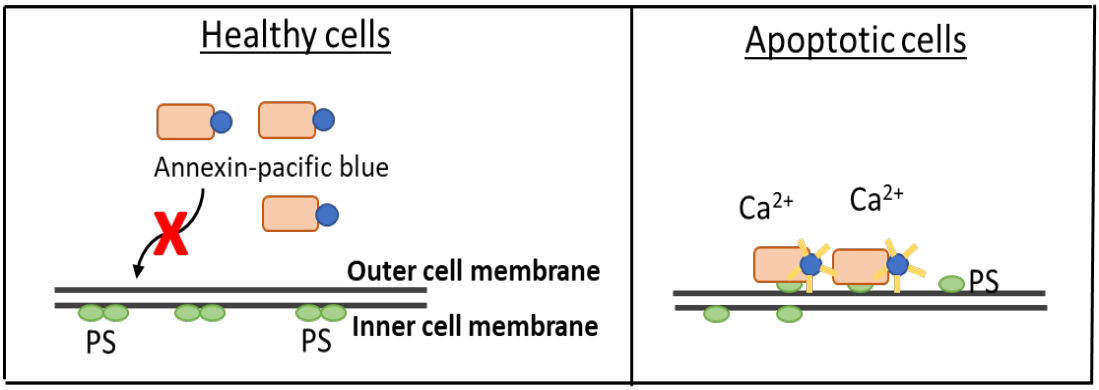

Figure 2. 1. Schematic representation of Annexin V binding. Healthy cells show no exposure of PS on their outer membranes and therefore annexin cannot bind and no signal is release. In apoptotic cells PS is translocated to the outer membrane where annexin conjugated to pacific blue can bind and release emitted light which can be detected.

2.5.3 Detection of acidic organelle

To determine the role of autophagy in IM-induced cell death, acridine orange was used to identify increased acidic properties within the cell, indicating the presence of increased lysosomal content. Acridine orange is permeable to cells: once inside, the dye is sequestered and protonated within lysosomes, with the low pH causing the dye to emit red fluorescence, which can be detected by standard fluorescent microscopy. Cells were plated onto a 12 well plate and allowed to reach 80% confluence. Following this, 5 μM acridine orange was added to cells and incubated 37ºC for 30 min. Cells were then washed once with PBS and imaged using confocal microscopy (Zeiss LSM880). ImageJ was used to threshold images, “isodata” was selected from default threshold settings; and the number of positive cells were counted manually.

2.5.4 Total reactive oxygen species and superoxide detection

Total ROS (hydrogen peroxide, peroxynitrite, hydroxyl radicals, nitric oxide, and peroxy radical) and superoxides (includes hypochlorous acid and nitric oxide) were both detected to ensure accurate representation of RTKI-induced oxidative stress. Cells were seeded onto a black 96 well plate at a density of 10,000 cells/well and incubated overnight. Following this, peak concentrations of each RTKI treatment were added to the cells for 24, 48 and 72 h. ROS/Superoxide Detection Assay Kit (Abcam, ab139476) was used; the oxidative stress detection reagent (green) was reconstituted in 60 μl of anhydrous DMF to create a stock solution of 5 mM. The superoxide detection

reagent (red) was also reconstituted in 60 µl of DMF, to create a 5 mM stock solution. The 1x wash buffer was made by dissolving the contents of the packet provided in 1 L of deionized water. The 2x ROS and superoxide detection mix was prepared as followed; 20 ml of growth medium and 8 µl of each dye, gently mixed to make a 1:2500 diluted staining solution which was then added to each well and incubated 37ºC for 1 h. The detection mix was then discarded and washed with 1x wash buffer. The cells were imaged using an EVOS microscope (GFP and Texas red filters were used). ImageJ was used to threshold images, which were then manually counted.

2.5.5 Calcium imaging

Thapsigargin (Badrilla) was used to initiate the store-operated calcium entry (SOCE) pathway. Thapsigargin works by noncompetitively inhibiting the sarco/endoplasmic reticulum Ca^{2+}-ATPase (SERCA) protein. SERCA is the main calcium channel controlling the influx of calcium from the cytosol into the ER. Blocking SERCA caused a depletion of the internal stores and activated the SOCE pathway. Alongside thapsigargin, cells were grown in a calcium-free environment, thereby further depleting intracellular calcium concentrations. Following this, calcium was reintroduced with or without RTKIs at varying concentrations and the time taken for calcium to recover was recorded.

Cells were seeded into a black 96 well clear bottomed plates (Santa Cruz), 20,000 cells/well, then incubated overnight. Fluo-4 AM (Fluo-4) (ThermoFisher) was used as a calcium indicator; 5 µM was added to each well, incubated 37ºC for 1 h. During the incubation the pre-treatment plate was

prepared; all conditions were diluted in calcium free hanks buffer (Gibco) with 10 mM HEPES solution (ThermoFisher Scientific), pH 7.5. The positive control was hanks buffer plus 5 µM thapsigargin, negative control was hanks buffer only and RTKIs were diluted in hanks buffer. After the fluo-4 incubation the pre-treatment solutions were applied to the cells for 30 min and incubated at 37°C. Next, the compound plate solutions were prepared. These solutions were the same as the pre-treatment plate minus thapsigargin and with calcium containing hanks buffer (Gibco) with 10 mM HEPES, pH 7.5. The fluo-4 signal was measured using the Flexstation 3 (Molecular devices), the program used was as follows; 1. Flex, 2. Wavelength: excitation; 488/emission: 525, cut off 520, 3. Time set to 200 s, interval of 1.52 s, 4. Compound plate transfer 200 µl total volume, pipette height 200 µl, pipette volume 50 µl transfer time of 30 s. The results were analysed using Excel and data were normalized against the base signal (accounting for dye loading). The following equation was used to determine calcium response; calcium response = average base signal before stimulation – maximum signal produced. This equation was applied to all treatments and then normalized against the control.

2.6 Protein biochemistry

Cells were plated onto 100 mm dishes and treated with RTKIs or co-treated as mentioned in the results sections. After treatment, cells were lysed; 100 µl of premade RIPA buffer (Sigma) was added to each dish, the sample was then left on ice for 5 min. Following this, the samples were centrifuged at 10,000 RCF for 10 min and the supernatant was transferred to new tubes.

2.6.1 Bicinchoninic acid assay

After the protein samples were purified, a bicinchoninic acid assay was used to determine the concentration of the protein samples. Bovine serum albumin was serially diluted to a concentration of 2 mg/ml, 1.6 mg/ml, 1.2 mg/ml, 1.2 mg/ml, 0.8 mg/ml, 0.4 mg/ml and 0 mg/ml into a 96 well plate; by diluting BSA standard (ThermoFisher) in Molecular Biology grade water. Cardiac progenitor cell protein samples were added neat; all samples were added in triplicates. Pierce™ Rapid Gold bicinchoninic acid assay Protein Assay Kit (ThermoFisher) was mixed as per manufactures instructions and 200 µl was added to each protein sample, mixed and incubated at room temperature for 5 min. Samples were measured using Flexstation for 480 nm absorbance, standard curves were generated using Excel and the linear equation was used to calculate the unknown protein concentrations (**Figure 2.2**).

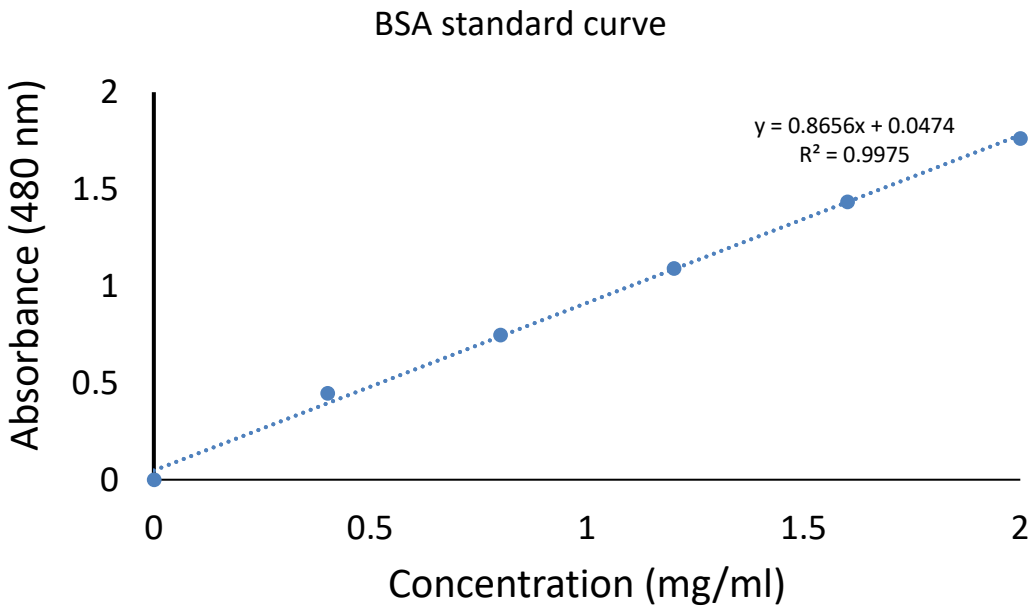

Figure 2. 2. Representative BSA standard curve. Graph depicting a range of BSA (0-2 mg/ml) and their respective absorbance (480 nm), linear equation and R^2 value.

2.6.2 Western blot

Following this, dependent on the protein of interest, 10 µg-50 µg of sample protein was mixed with 4x laemmli sample buffer (BioRad) containing β-mercaptoethanol (1:20). The samples were then boiled at 95°C for 5 min before being centrifuged at 10,000 RCF for 1 min. The samples were then loaded into a 4-20% polyacrylamide precast gel (BioRad) and separated by electrophoresis using 1x running buffer (10x Tris-Glycine-*SDS* PAGE *Buffer,* National Diagnostics) for approximately 1 h 20 min at 120 V. The gel was then transferred using Trans-Blot Turbo Transfer Pack (BioRad) and semi-dry Turbo blotter (BioRad) for 30 min using pre-set standard protocol for all molecular weight proteins (25V). During the transfer stage 10x tris-buffered saline (TBS)-tween wash buffer was prepared (**Table 2.3**). After transfer the membranes were blocked in 5% blocking buffer (1x wash buffer with 5% milk powder or BSA) for 1 h at room temperature on a shaking platform. Primary antibodies were prepared in 5% blocking solution (TBS-tween plus 5% milk powder or BSA); rabbit anti-human Microtubule-associated protein 1A/1B-light chain 3 (LC3) (Novus) 1:4000, rabbit anti-human p62 (*ProSci* Inc) 1:1000, mouse anti-human Lysosome-associated membrane protein 2 (LAMP-2) (Novus) 1:1000, rabbit anti-human p-MLKL (Abcam) 1:1000, rabbit anti-human total-MLKL 1:1000 (Genetex), mouse anti-human BAX (Santa Cruz) 1:400, mouse anti-calpain and calpain 2 (Santa Cruz) 1:1000, rabbit anti-human ERK, p-ERK (Cell Signalling) 1:1000, rabbit anti-human AKT, p-AKT (Cell Signalling) 1:1000 and rabbit anti-human beta-actin (cell signalling) 1:2000, membranes were placed into primary antibodies and incubated overnight at 4°C (**Table 2.4**). This was followed by three 10 min TBS-tween washes before

exposure to sary antibodies (anti-rabbit (cell signalling), anti-mouse (cell signalling) 1:1000) in blocking buffer for 1 h room temperature. The blots were developed using West Pico plus (Thermofisher) and imaged on imaging workstation G:Box Chemi XT4 (Syngene).

10x TBS stock (10x wash buffer)	
Tris base	60.6 g
Sodium Chloride	87.7 g
1x wash buffer (2L)	
10xTBS	200 ml
Tween-20	2 ml
pH	7.5

Table 2. 4. Recipes for 1L of 10x TBS stock and 1X wash buffer (2 L).

2.6.3 Quantification of Western blots

Western blot images were analysed by densitometry with ImageJ software. The band of interest was drawn around using the rectangle tool and the signal intensity was determined by the “measure” function. This rectangle was then moved over to the next band of interest ensuring that the box remained the same size, this was continued until all band intensities were measured. These readings were copied to Excel and the treated data were normalised against the control.

2.7 Immunocytochemistry

For immunocytochemistry (ICC) staining, cells were fixed using 2% paraformaldehyde for 10 min room temperature, 4 x 10-min washes D-PBS room temperature. Followed by permeabilization with 0.1% triton x100 in PBS for 10 min, room temperature. Cells were then blocked with 0.05% Triton x100, goat/donkey serum and D-PBS for 1-h room temperature, followed by primary antibody staining overnight 4°C in a humified chamber. Following this, the cells were washed 3 x 20-min with D-PBS, followed by sary antibody 1:200 either 488 or 555 or 647 for 2 h room temperature. The cells were then washed 3 x 20 min with PBS (0.1%), DAPI stained 1:1000 for 14 min, followed by 3 x 10-min washes. Cells grown on coverslips were then mounted using prolong gold (ThermoFisher Scientific) onto coated slides.

2.7.1 Proximity ligation assay

The proximity ligation assay (PLA), allows visualisation of two proteins that are within 40 nm of each other and therefore indicates higher probability of direct binding. The Duolink kit was used (Sigma DUO92002, DUO92004, DUO92008), the procedure involves targeting two proteins of interest with primary antibodies from different species and with sary antibodies modified to carry oligonucleotide DNA sequences with opposite charges. Following this corresponding DNA sequences were added which hybridize to the PLA probes on the saries (only if the two probes are in close contact). Ligase was applied which ligates the DNA sequence into a circular template, this is then amplified by DNA polymerase; up to 1000-fold through rolling-circle amplification.

Fluorescently labelled oligonucleotides hybridise to the amplified sequences allowing visualisation of the target proteins as a single spot (Söderberg et al., 2006). The cells were cultured on 8 well glass chamber slides (ThermoFisher 155409) and treated with 10 µM IM for 24 or 48 h, or 400 nM rapamycin (Cell guidance systems) for 4 h.

Cells were fixed with 2% paraformaldehyde for 10 min at room temperature, then permeabilized with 0.1% Triton X-100 and blocked in goat serum (ThermoFisher, cat.no.10000C) for 1 h at room temperature. Cells were then incubated with primary antibodies: mouse anti-human LAMP2 (Novus) 1:200 and rabbit anti-human MAP1LC3B Antibody (CSB- Cusabio, cat.no. PA887936LA01HU) 1:200, overnight 4°C. For sary incubation, PLA (+) and PLA (-) probes were incubated for 1 h in a humidified incubator. For each treatment (40 µl); 8 µl of PLA (+) and 8 µl of PLA (-) were added in 24 µl of blocking buffer and placed onto the treatment wells. The cells were then washed with PLA wash buffer A and incubated with ligation reaction mix (40 µl); 8 µl of ligation buffer, 1 µl ligase in 31 µl of dH_2O for 30 min in a humidified chamber. The cells were washed 3 times with PLA wash buffer A and incubated with the amplification reaction mix; 8 µl amplification buffer; 0.5 µl DNA polymerase in 31.5 µl of dH_2O for 100 min in a humidified incubator at 30°C. Finally, cells were washed 3 times with PLA wash buffer A and 0.01% wash buffer B for 10 min. The results were visualised using an Airyscan confocal microscope (Zeiss LSM880) at x60 magnification. Following the acquisition, PLA punctum staining was manually counted for each condition.

2.8 Statistical analyses

Statistical analysis was performed on data collected from three or more biological replicates. Data are presented in bar or line graphs as the mean of

all repetitions; the error bars are represented by the standard error of the mean (S.E.M). Data normality was tested using the Shapiro-Wilk Test (SPSS). One-way ANOVA (SPSS) was used for comparison of mean data between groups for all data which were normally distributed, followed by *post hoc* Tukey test for comparison within groups (SPSS). All other data were compared using Two-tailed, unpaired Student's *t*-test (Excel).

Chapter 3. Characterisation of human cardiac progenitor cells

3.1 Introduction

The first stage of the project was to characterise that the cells are a homogenous population and have been correctly isolated. Cardiac progenitor cells are isolated by positive enrichment for c-Kit and negative enrichment for CD45, these are the minimum criteria as outlined in previous research (Vicinanza et al., 2017). Enrichment for c-Kit alone obtains a heterogenous population of cells, including mast and endothelial cells (Ellison et al., 2011; Vicinanza et al., 2017)

There has been much controversy around whether CPCs are indeed stem cells, the main reason for this is the conflicting evidence over whether they make a major contribution to the formation of new cardiomyocytes in the adult heart Jesty et al., 2012; Liu et al., 2016; Sultana et al., 2015; van Berlo et al., 2014). However, other research has shown that correctly isolated CPCs can differentiate into new cardiomyocytes after myocardial damage (Pfister Otmar et al., 2005; Smith et al., 2014) and are sufficient for cardiac regeneration following diffuse injury (Ellison et al., 2013; Pfister Otmar et al., 2005; Smith et al., 2014). A previous study had shown that the CPCs become increasingly senescent with age (increased senescence-associated β-galactosidase and DNA damage marker (γH2AX-positive) and shortened telomerase length), although CPC numbers were unaffected by age (Lewis-McDougall et al., 2019). Therefore, future cell therapies involving CPCs could investigate strategies for removing these senescent cells before transplantation. Current

research is investigating the use of CPCs for vascular and smooth muscle repair, there is also increased evidence that CPCs contribute to the myocardial extracellular matrix by the release of paracrine cytokines and growth factors (Jiang and Xu, 2019; Ott et al., 2007). Two important growth factors have been identified as HGF and IGF-1 which have been shown to aid in pig myocardial regeneration (Ellison et al., 2011).

Given the relatively recent discovery of CPCs and with the majority of CPC research primarily focused on their potential to generate cardiomyocytes, there is still relatively known about their primitive state, including how these cells can transport calcium into and out of the cell. This chapter will therefore investigate the proteins involved in calcium handling within the native CPC population. One indication is based on mouse neonatal ventricular precursor cells shown to express both L and T type calcium channels. Although mouse neonatal ventricular cells are different from human adult CPCs, they are both an example of an immature cardiac progenitor cell (Hotchkiss et al., 2014; Linask and Linask, 2010). A s study of CPC calcium handling identified regulation by IP3R and 26% of the cell population had oscillating calcium activity; however this study only selected cells for c-Kit expression, so did not precisely select the CPC population (Ferreira-Martins João et al., 2009). It is important to determine which receptors are expressed by the CPCs before carrying out further work, as RTKIs vary in potency and affinity for target receptors (e.g. IM targets PDGFR over VEGFR) (O'Sullivan et al., 2007; Yıldırım et al., 2016). Overall this chapter aims to further the understanding of the CPC field, confirming the cells have stem cell properties and calcium handling proteins.

3.2 Results

3.2.1 Cardiac progenitor cells express stem cell factors

To confirm CPC population purity, cells were stained by ICC for c-Kit expression. The cells showed diffuse staining for c-Kit across multiple passages (4, 10, 18 and 21), on the cell membrane and filopodia, however the majority of the staining was cytoplasmic. The staining was most prominent at passage 4, however all passages show positive staining compared to negative controls (**Figure 3.1**).

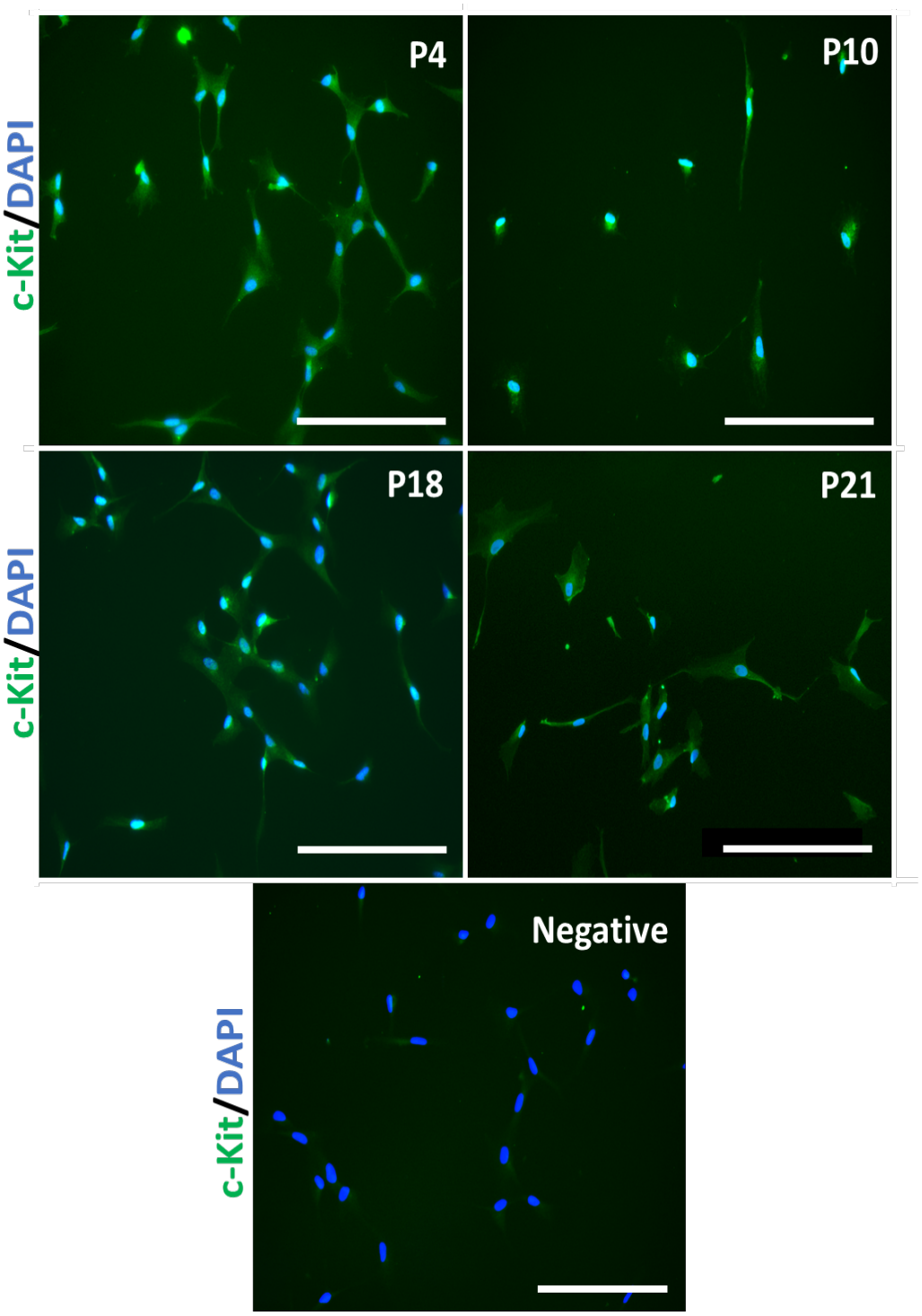

Figure 3. 1. c-Kit staining of CPCs. Micrographs of c-Kit and DAPI staining in CPCs (passages 4, 10, 18 and 21). Cells showed positive c-Kit staining (green) with DAPI stained nuclei (blue) in all samples**.** The negative control is CPCs stained without primary antibody (negative)**.** Scale bar=200 µm.

Reverse transcription qPCR was used to confirm CPC expression of stem cell genes. Expression levels in all passages were normalised against the earliest passage (passage 4) for comparison; c-Kit gene expression indicated the opposite finding to staining intensity, with increased c-Kit gene expression over passages 4 to 18, however this was significantly reduced at passage 21 ($p<0.05$). Relative normalised expression for kruppel like factor 4 (KLF4) was increased at passage 10 and 18 and a significant reduction was observed at passage 21 *vs.* passage 4 ($p<0.05$). Nanog, Oct4, SOX2 showed an increase in expression in passage 10, with no difference at passage 18 and reduced expression at passage 21 ($p<0.05$). Telomerase Reverse Transcriptase (TERT) showed a significant reduction at passage 18 and 21 *vs.* passage 4 (**Figure 3.2A**). To confirm a single gene product was generated by each primer pair, the RT-qPCR products were analysed on an agarose gel. One product was identified for β-Actin, SOX2, Nanog, Oct4, KLF4 and TERT; however, two products were seen for c-Kit expression, one band of around 200 kb and the s of around 150 kb. These two different c-Kit transcripts correlate with the different cell isolates used, with higher expression of 200 kb band in DOR006 samples (passages 4 and 10) and the 150kb band visually stronger in PP006 samples (passages 18 and 21) (**Figure 3.2B**).

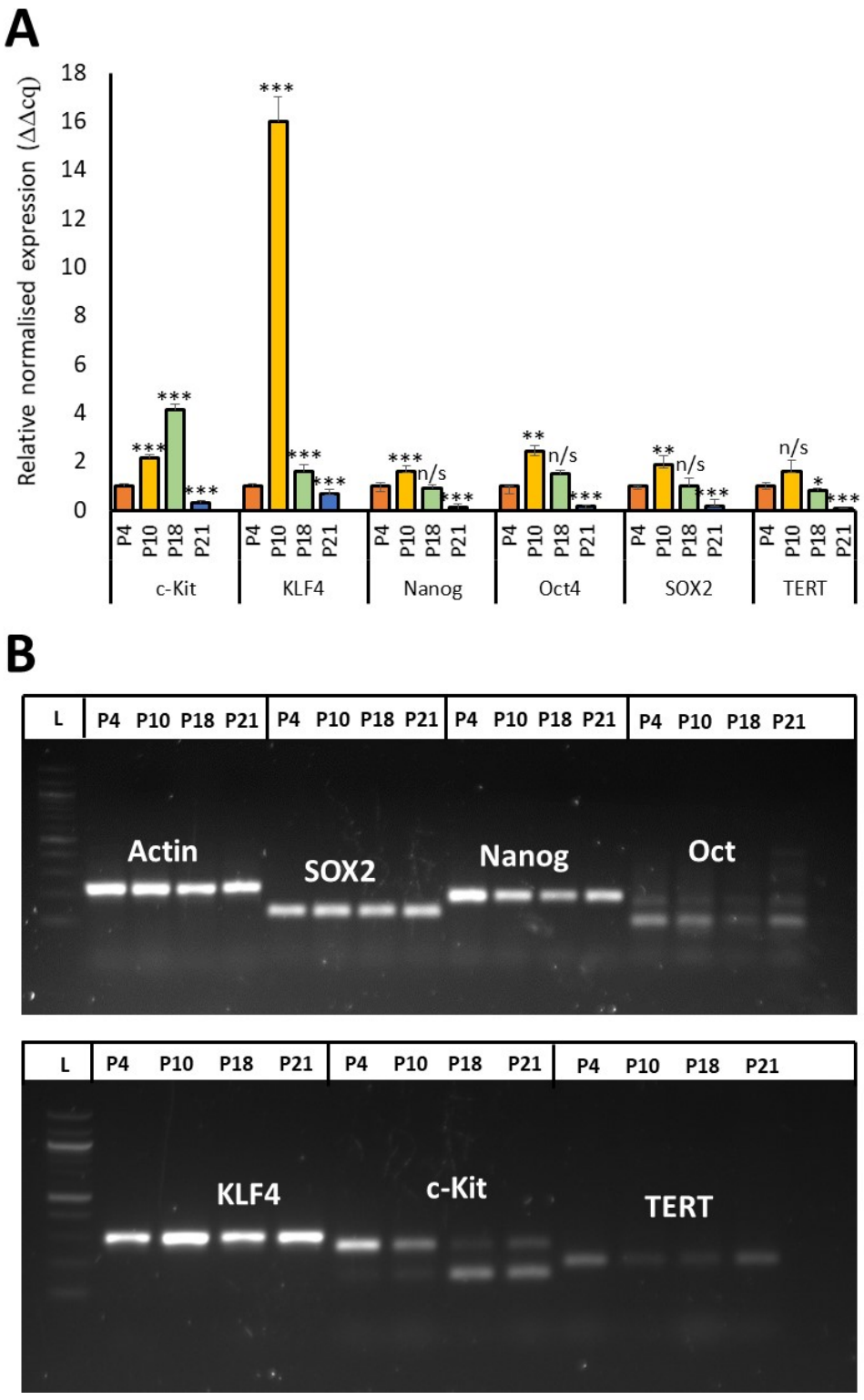

Figure 3. 2. Confirming stem cell gene expression in CPCs. **(A)** Relative normalised gene expression of c-Kit, KLF4, Nanog, Oct4, SOX2 and TERT expression over passage 4, 10, 18 and 21. **(B)** DNA agarose gels showing single products for Actin, SOX2, Nanog, Oct4, KLF4 and TERT and two products for c-Kit. n=3, *t*-test.

3.2.2 Cardiac progenitor cell clonogenicity

One important characteristic of a stem cell is the ability to self-renew, forming clonal copies of itself: therefore to determined whether CPCs could divide by symmetric division. Cells were first plated at a density of a single cell in each well of a 96-well plate, thus ensuring that any cell colony generated would be clonal. Cells were maintained in culture for one week and images recorded on d 1, 2, 3, 4 and 6 to assess rates of division; this process was repeated for CPCs from passages 4, 10, 18 and 21. Cells (DOR006, passage 4) were grown *in vitro* and images recorded. The images showed 1 cell after 1 d growth, 2 cells after 2 d, with a continued cell growth up until d 6. Cells were small and round before attachment, following attachment cells have a smooth, flatter appearance with cellular extensions (**Figure 3.3A**). Cells from passages 4 and 10 showed comparable morphological characteristics and growth patterns (**Figure 3.3B**).

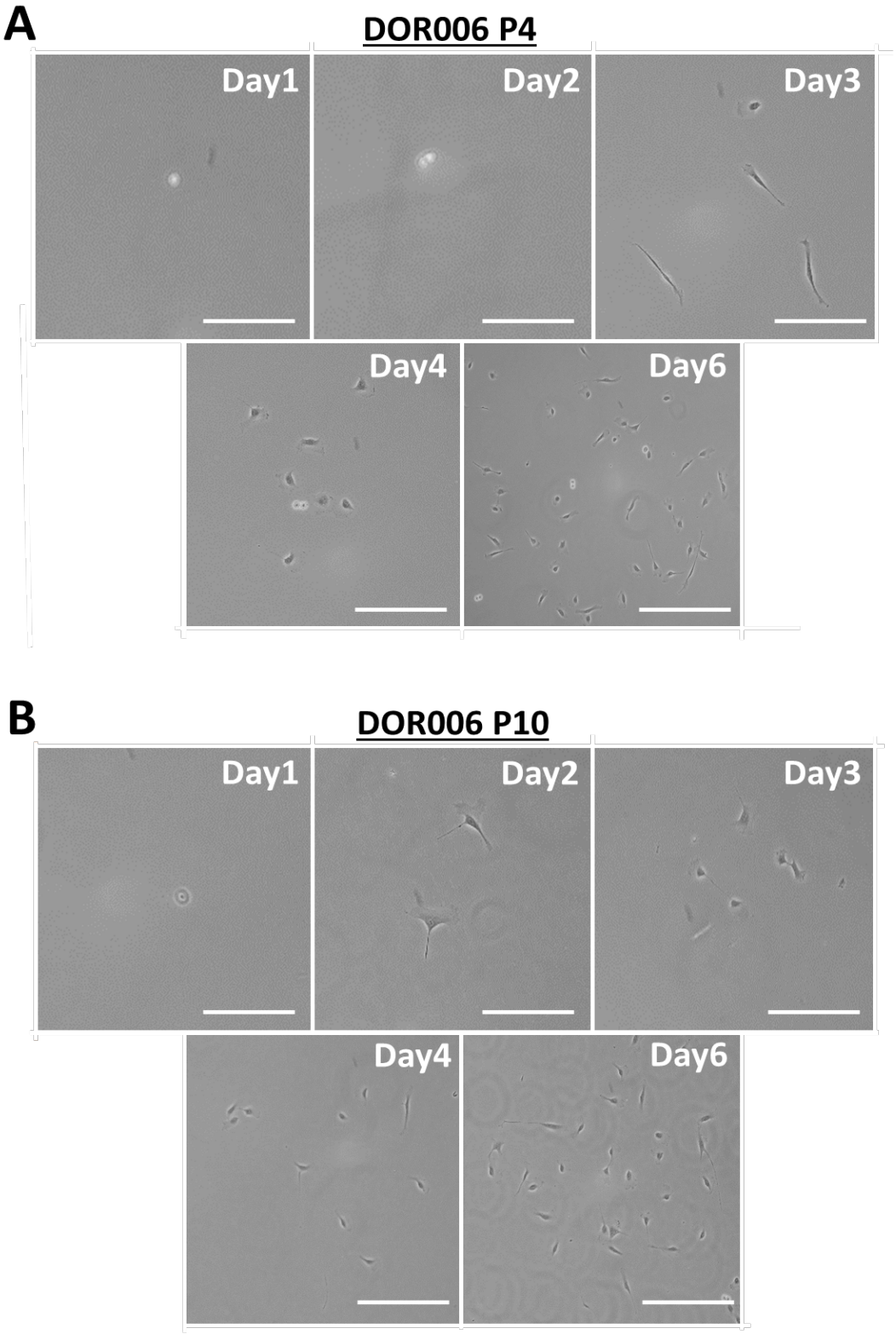

Figure 3. 3.CPC clonogenicity at passage 4 and 10. (A) Images of CPC clonal colony (cell line DOR006) passage 4 over 6 d *in vitro*. **(B)** Images of CPC clonal colony (cell line DOR006) passage 10 over 6 d *in vitro* . All cells double every ~24 h and grow over 6 d. Scale bar=100 µm.

The same procedure was used to determine self-renewal of cell line PP006 at passages 18 and 21. The images showed single cells at d 1, which doubled consistently over the following d. Cells showed a comparable phenotype to DOR006, with a small round shape before attachment, and following attachment a smooth, flatter appearance with cellular extensions, at passages 18 and 21 (**Figure 3.4**).

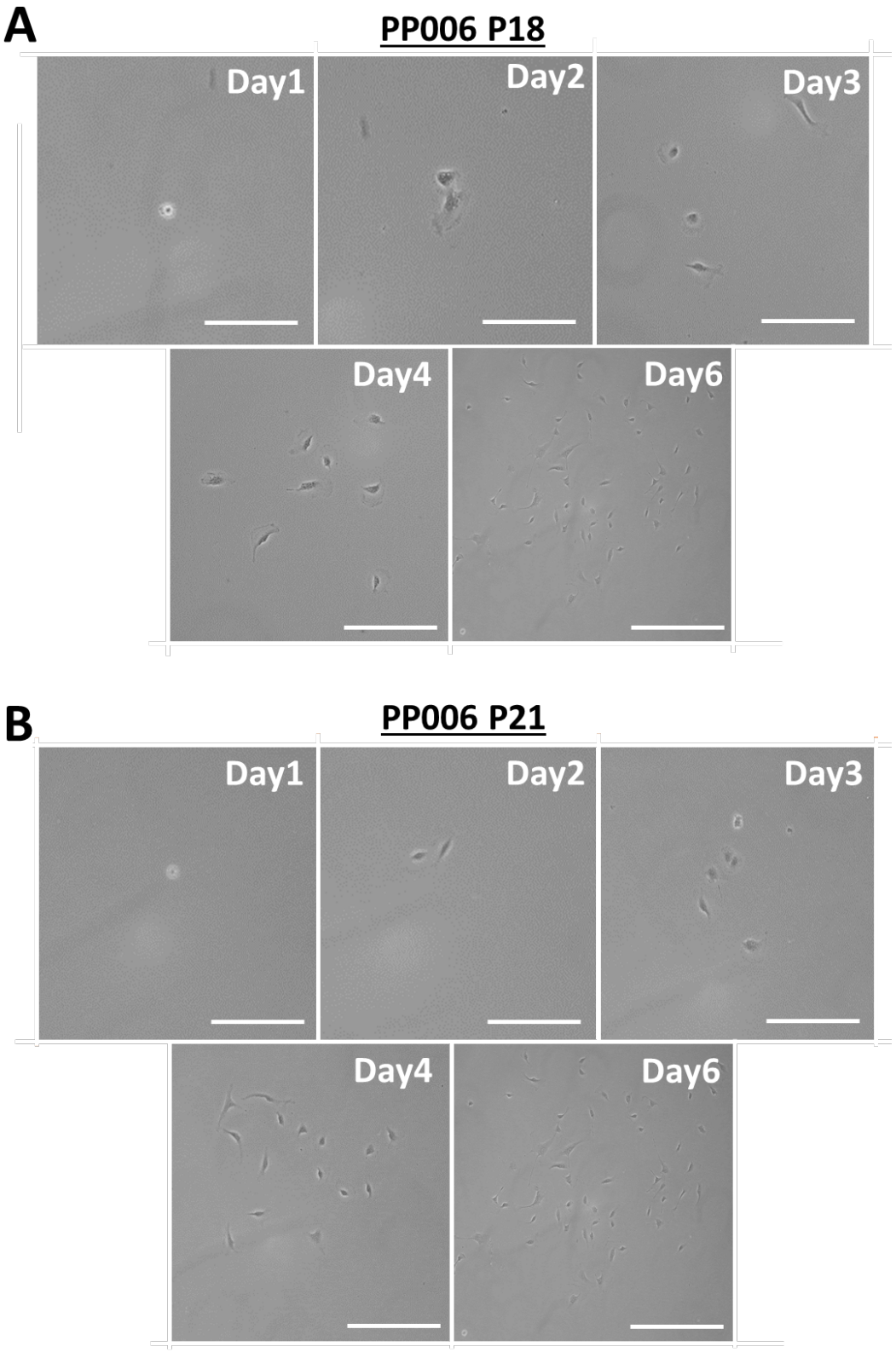

Figure 3. 4. CPC clonogenicity at passage 18 and 21. (A) Images of CPC clonal colony (cell line PP006) passage 18 over 6 d *in vitro*. **(B)** Images of CPC clonal colony (cell line PP006) passage 21 over 6 d *in vitro* . All cells double every ~24 h and grow over 6 d. Scale bar=100 µm.

3.2.3 Cardiac progenitor cells can differentiate into endothelial and smooth muscle cells

Having confirmed the CPCs actively expressed stem cell genes and could self-renew, the next step was to confirm their ability to differentiate into the lineages of endothelial and smooth muscle cells, as identified in multiple prior studies (Ellison et al., 2013; Smith et al., 2014; Vicinanza et al., 2017). Cells were differentiated, stained by ICC for the marker of a mature endothelial cells von Willebrand factor (vWF), then imaged using confocal microscopy. The images showed positive vWF staining in passages 4,10 and 18, however this decreased at passage 21. The vWF staining was mainly cytoplasmic, with staining on the cellular extension. Although cells from passage 21 had visually weaker staining than the other passages, the staining was nonetheless stronger than in the negative control (**Figure 3.5**). Cells were differentiated into smooth muscle cells for 14 d *in vitro*, after which cells were stained for smooth muscle actin. Staining was consistent across all passages, with a distinct striated phenotype consistent with the smooth muscle cell phenotype. Differentiated cells had a larger surface area than undifferentiated CPCs, with a width of ~100 μm compared to 5-10 μm for undifferentiated cells. No staining was seen in the negative control (**Figure 3.6**).

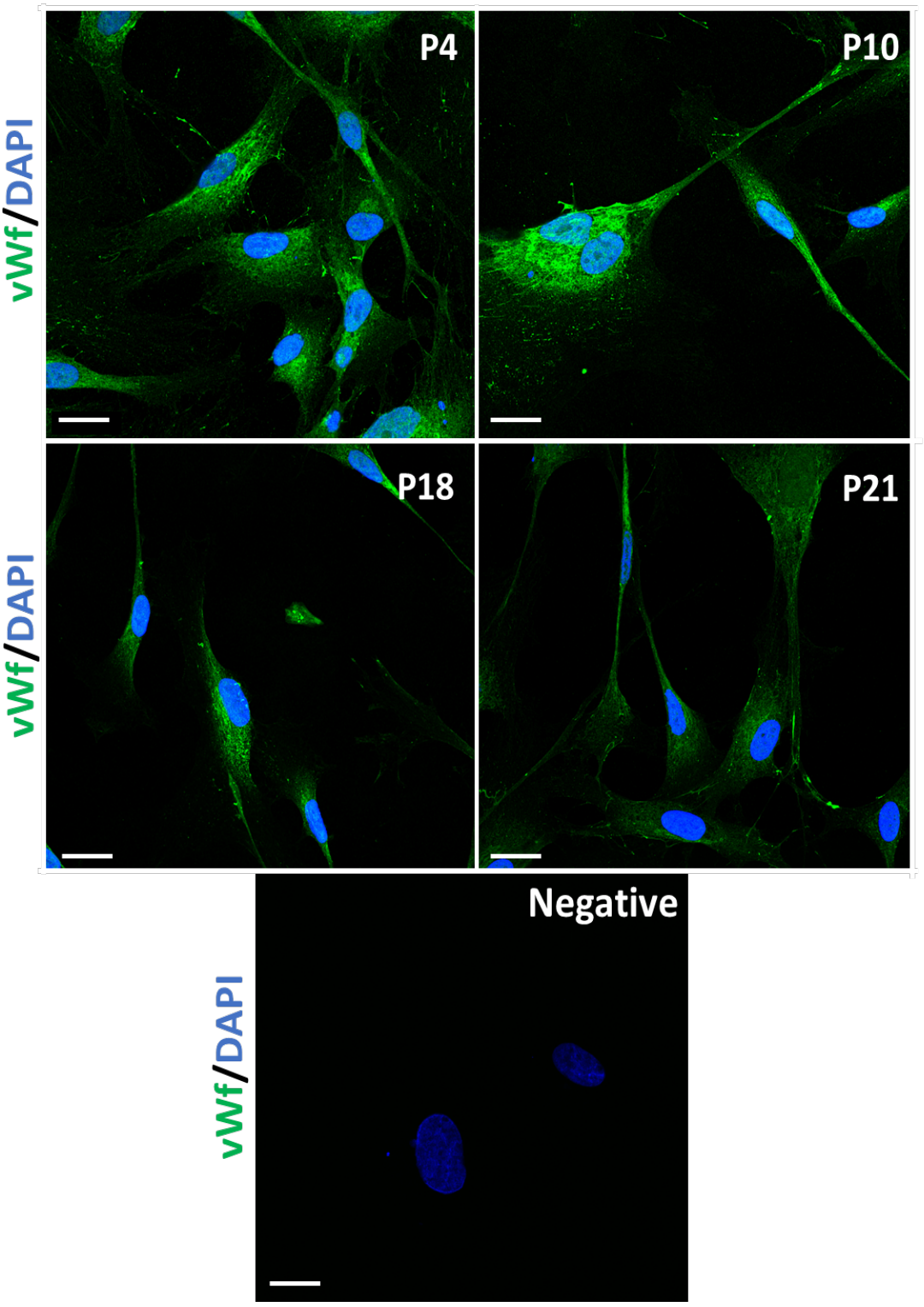

Figure 3. 5. CPCs differentiate into endothelial cells. Micrographs of vWF and DAPI staining in CPCs differentiated to endothelial cells across multiple passages. Cells show positive vWF staining (green) with DAPI-stained nuclei (blue) across all passages. The negative control is CPCs stained without primary antibody (negative) shows no vWf stainin but DAPI staining. Scale bar=20 μm.

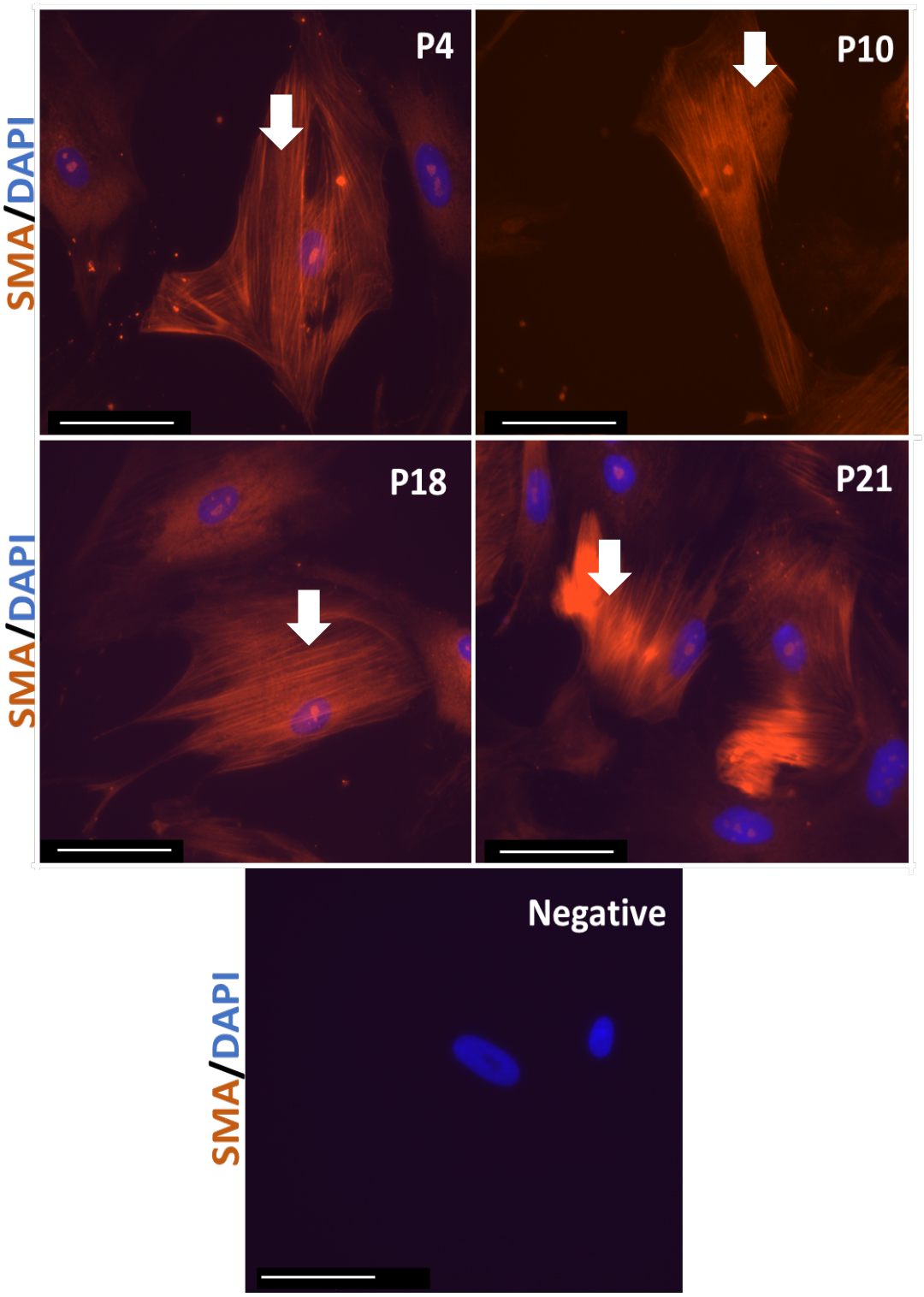

Figure 3. 8. CPCs differentiate into smooth muscle cells. Micrographs of smooth muscle actin and DAPI staining in CPCs differentiated to smooth muscle cells across multiple passages. Cells show positive smooth staining (orange) with DAPI-stained nuclei (blue) across passages. The cells have typical smooth muscle cell staining with striated patterns (arrows). The negative control is CPCs stained without primary antibody (negative) shows no SMA staining but DAPI staining. Scale bar=75 μm.

3.2.4 Cardiac progenitor cell expression of calcium-linked genes and proteins

Calcium is a key compound in cell death pathways, hence we characterised which calcium-handling genes and proteins were present in CPCs. First, RT-qPCR was used to determine which calcium-handling genes were expressed in CPCs, these data showed relative gene expression of $2.96x10^{-4} \pm 1.33x10^{-5}$ for exchange factor directly activated by cAMP (EPAC) expression, $2.87x10^{-4} \pm 8.043x10^{-6}$ IP3R type 1, $7.93x10^{-5} \pm 2.31x10^{-6}$, mitochondrial calcium uniporter (MCU), $7.52x10^{-5} \pm 7.76x10^{-6}$ Na-Ca exchanger, $6.33x10^{-5} \pm 2.09x10^{-6}$ ryanodine receptors (RyR) 2. Whereas, the L type calcium gene (CAV1.2) showed a lower relative gene expression of $6.00x10^{-6} \pm 8.44x10^{-6}$. To confirm one product was being formed a DNA gel was performed, EPAC, IP3R type 1, MCU, Na-Ca exchanger and RYR2 all showed a single product, CAV1.2 showed no signs of a product. Actin was used as a housekeeper gene and showed a cycle threshold number of 15.14 and one single product on the DNA gel (**Figure 3.7**).

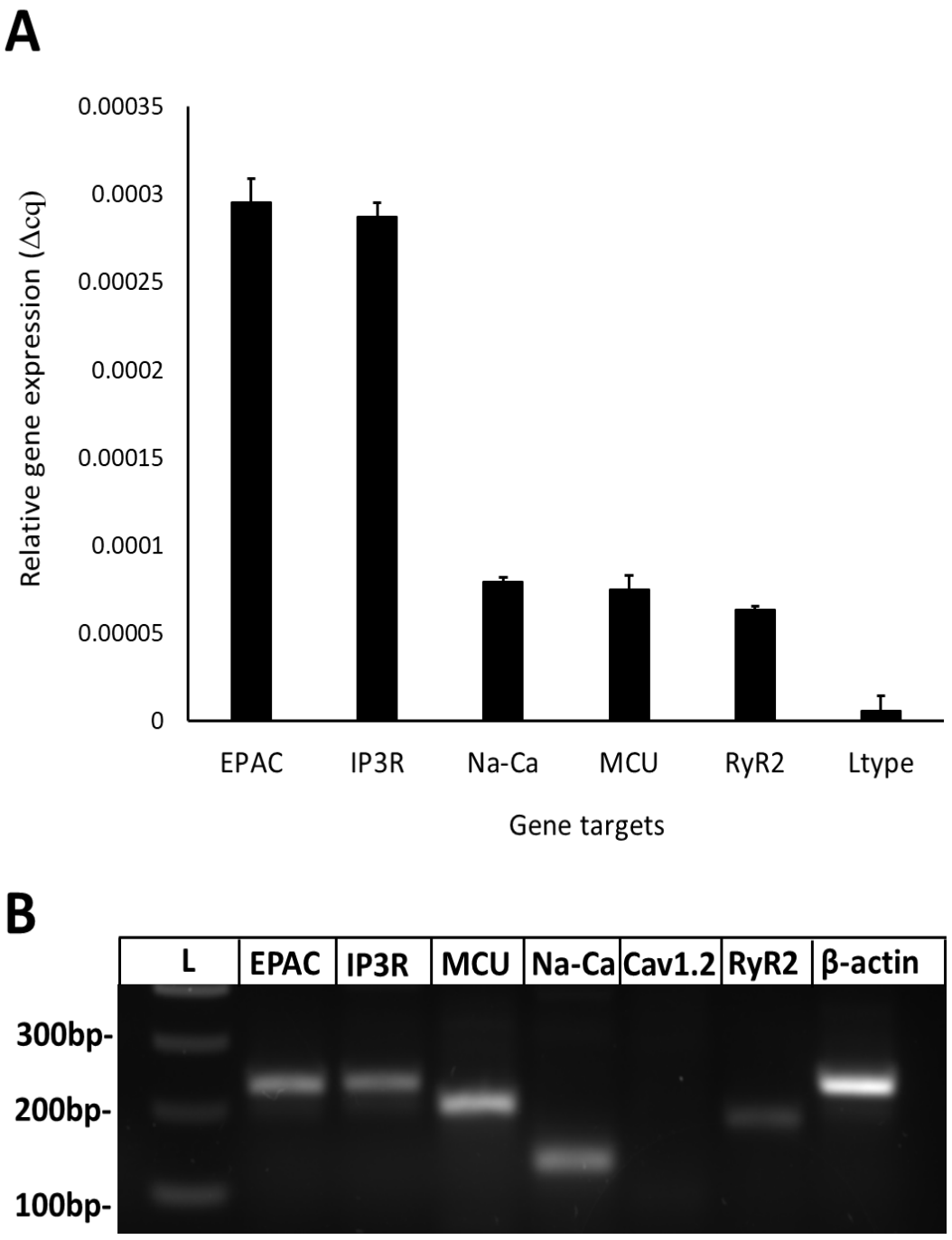

Figure 3. 11. CPC gene expression for calcium proteins. (A) Average Cq (cycle threshold) value for each calcium gene expression; EPAC, IP3R type 1, MCU, Na-Ca exchanger (Na-Ca), L-type (Cav1.2), RyR2 and β-actin (Actin). The cycle number ranges from 26-33 cq. **(B)** DNA agarose gels showing single products for EPAC, IP3R, MCU, Na-Ca, Cav1.2, RyR2 and Actin. All products are between 100-300 base pairs. n=3.

To confirm that these genes were also actively expressed at the protein level, ICC staining was performed for different subsets of RyR (pan RyR, RyR 2 and RyR 3), IP3R type 1 and SERCA. There was no staining for pan RyR, which stains both RyR1 and RyR2: this was confirmed with single RyR2 staining which also showed low staining intensity. RyR3 had visually dense staining, with a diffuse staining pattern throughout the cell cytoplasm. IP3R type 1 also had a diffuse staining pattern within the cell cytoplasm. The cells also expressed SERCA protein, which also was diffuse within the cell. Both negative controls showed no staining in either channel (488 and 555 nm) (**Figure 3.8**).

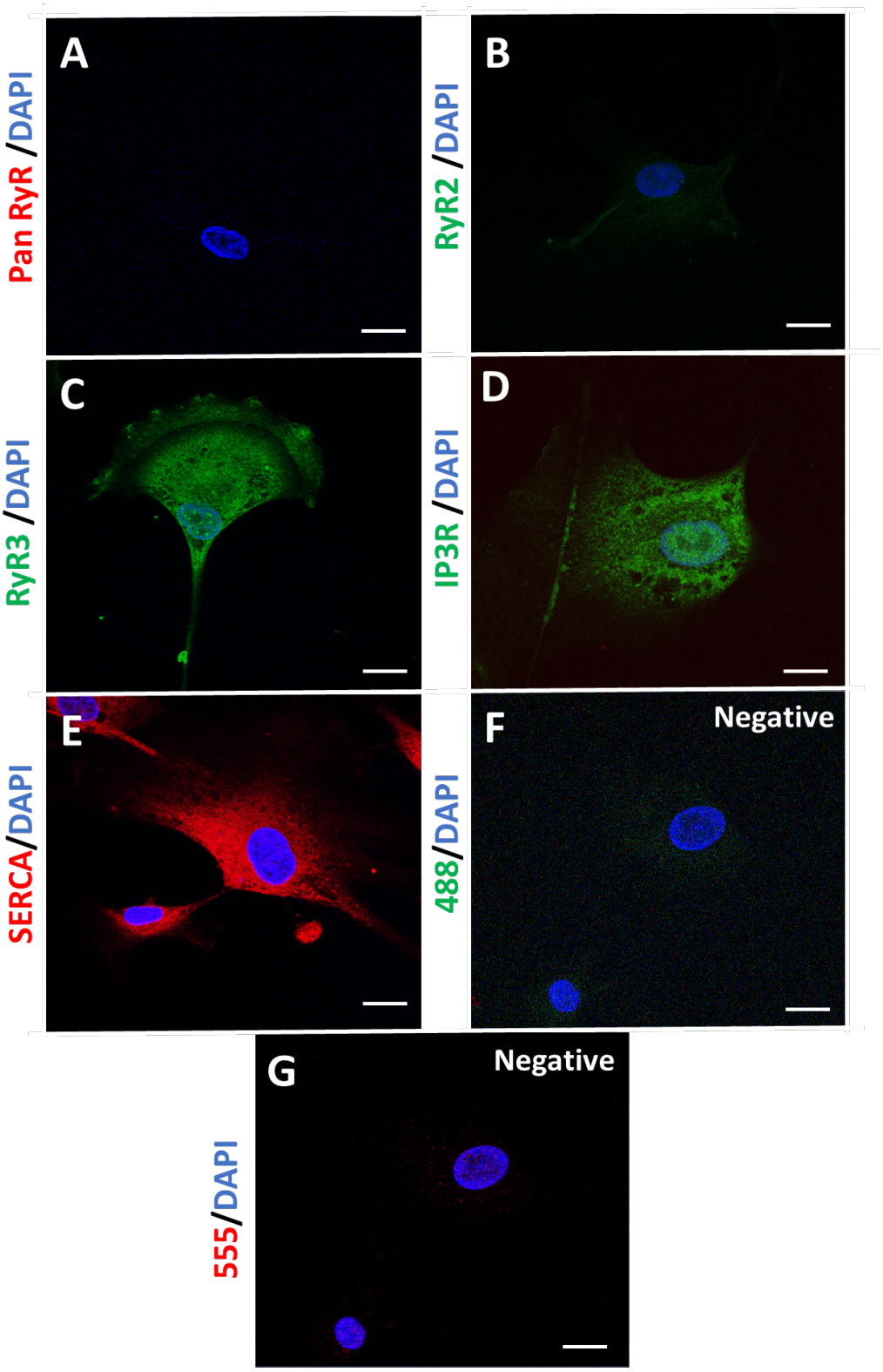

Figure 3. 12. CPCs express calcium handling protein. . Micrographs of **(A)** Pan RyR, **(B)** RyR2, **(C)** RyR3, **(D)** IP3R, **(E)** SERCA and DAPI staining in CPCs. Cells showed no staining for Pan RyR or RyR2, **(F-G)** The negative control is CPCs stained without primary antibody (negative). Scale bar=20 µm.

3.2.5 Cardiac progenitor cell expression of VEGFR targets for receptor tyrosine kinase inhibitors

With CPC stem-like phenotype and calcium handling characterised, we next examined known inhibitory target receptors of RTKIs, with select targets chosen including VEGFR1, VEGFR2, VEGFR3. The CPCs had staining for all three VEGFRs, with the visually weakest staining for VEGFR1 and strongest VEGFR3. The VEGFR1 staining was granular and mainly located on the cell membrane, as expected. The VEGFR2 staining was also granular and located on the cell membrane, with more diffuse staining in the cytoplasm; in contrast VEGFR3 stained primarily the cytoplasm, with expression on the cell membrane. Negative controls showed no staining (488 nm) (**Figure 3.9**).

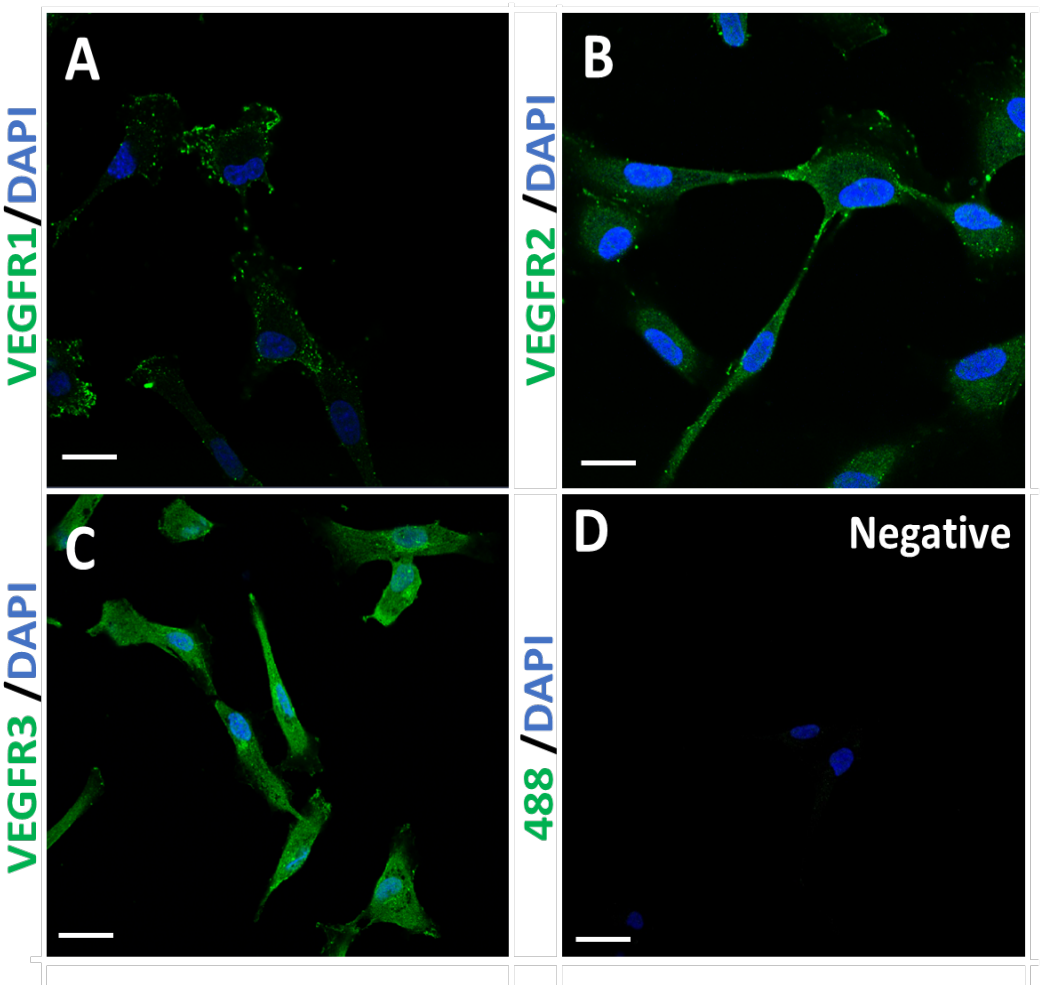

Figure 3. 13. Expression of RTKI known targets in CPCs. Micrographs of **(A)** VEGFR1, **(B)** VEGFR2, **(C)** VEGFR3, **(D)** The negative control is CPCs stained without primary antibody (negative). Scale bar=20 µm.

3.3 Discussion

3.3.1 Stem cell properties of cardiac progenitor cells

With current controversy of whether CPCs are indeed stem cells, the first experimental objective of this project was to characterise the CPC stem cell phenotype, confirming the expression of stem cell genes and CPC ability to self-renew or differentiate (Bollini et al., 2011; Cao et al., 2012; Tang et al., 2018). The CPCs were shown to express c-Kit by positive ICC staining, confirming the purity of the isolated cell population. The c-Kit receptor is not only a CPC surface marker, but also plays an important role in stem cell proliferation and renewal (Lennartsson and Rönnstrand, 2012). These c-Kit data are somewhat limited as ICC staining is only semi-quantifiable, therefore future work could involve a more quantifiable method such as flow cytometry or Western blotting to more accurately compare expression levels across passages.

The expression of specific genes also clarifies the stem cell status of CPCs, with specific genes associated with stem cell proliferation (c-Kit, KLF4, TERT) and multipotency (Nanog, KLF4, Oct4, SOX2). Gene expression showed the presence of each stem cell gene in CPCs, with fluctuations in expression across passages, these differences have been shown in HSCs and MSCs (Dooner et al., 2008; Lian et al., 2016). Expression of these ‘stemness’-related genes were lower in passage 21 CPCs, therefore cells after passage 18 were not used for experiments.

With CPC expression of stem cell genes confirmed, the next step was to investigate if this translated into cell function: a clonogenicity assay was used

to assess CPC self-renewal potential. Cardiac progenitor cell proliferation has been shown in previous studies; confirming one of their stem cell traits (Cottage et al., 2010; Linke et al., 2005; Mouquet Frédéric et al., 2005; Takamiya et al., 2011).

Cardiac progenitor cells have been previously shown to form three cell types from the myocardium; cardiomyocytes, smooth muscle cells and endothelial cells (Ellison et al., 2013; Lewis-McDougall et al., 2019). However, with the previously-mentioned debate concerning whether CPCs can form cardiomyocytes and how effectively such cardiomyocytes can mature, this work's primary focus is on CPC formation of endothelial and smooth muscle cells, which are abilities not in dispute. Our data confirmed previous reports that CPCs can produce both endothelial cells and smooth muscle cells (Ellison et al., 2013; Smith et al., 2014; Vicinanza et al., 2017). The CPCs are here shown to be able to form endothelial and smooth muscle cells across multiple passages without any distinct differences, excepting weaker vWF staining in endothelial cells derived from CPCs at passage 21.

3.3.2 Calcium flux and handling in cardiac progenitor cells

There is limited research evaluating calcium handling within CPCs in their undifferentiated state (Pfister Otmar et al., 2005). The expression data for calcium-handling genes in our project suggested that the CPCs were regulated by RyR3, IP3R type 1, Na-Ca exchanger, MCU and possible contribution from RyR2; with no gene expression of L type calcium channel (Cav1.2). These findings were confirmed through protein expression, which showed positive staining for RyR3 and not RyR1 or RyR2, which have also

been shown in other heterogenous CPC populations (Ellison et al., 2007; Ferreira-Martins João et al., 2009). These results suggest a more immature calcium handling system than that of cardiomyocytes, similar to neonatal cells, HEK cells and NSCs (Chung et al., 2016; Rossi et al., 2002; Yang et al., 2001). The staining for IP3R type 1 and SERCA confirmed this theory. These findings suggest a mechanism whereby calcium would enter the cell through voltage-gated ion channels or transient receptor potential (TRP) channels on the membrane, the increased internal calcium then causing influx of calcium into the ER through the SERCA protein. Once required, internal stores would release their calcium through IP3R type 1 or RyR3, which would increase cytoplasmic calcium levels for internal processes such as cell proliferation. Calcium would leave the cell through Na-Ca exchanger, to maintain equilibrium (**Figure 3.10**). These findings have been previously shown in c-Kit+ cells (heterogenous population), which showed IP3R and SERCA protein expression and a lack of RyR2 protein expression (Ferreira-Martins João et al., 2009). This pathway will become important when assessing the involvement of calcium-controlled cell death in CPCs after RTKIs exposure.

These experiments have limitations, in that the ICC and RT-qPCR data only showed the expression of these calcium handling proteins or genes and does not indicate whether these proteins are functional and important for the CPCs maintenance. Further experiments, including inhibition or stimulation of each protein, could provide evidence of their importance to CPC signalling, for example by use of caffeine to open the RyR receptor (Kong et al., 2008). Limited data were available for assessment of membrane calcium proteins such as TRP channels, voltage-gated ion channels or receptor operated

channels. However, data in Chapter 6 will assess the involvement of voltage-gated ion channels on RTKI-induced cell death, which indicate that voltage-gated ion channels play an important role in CPC maintenance. Another limitation to our study was the use of cav 1.2, this encodes for only one subunit of the L type calcium channel meaning that other L type calcium genes could be expressed. There are also no reliable L type calcium channel antibodies currently available for protein expression confirmation.

3.3.3 Cardiac progenitor cells express known receptor trysoine kinase inhibitor targets

Before investigating the cell death pathways involved in RTKI-induced cell death in CPCs, it was important to confirm that the CPCs expressed RTKI targets. The data previously mentioned showed the expression of c-Kit; following this, CPCs were stained for VEGFR1 , VEGFR2, VEGFR3: these data showed expression of all three proteins. Although the RTKI target proteins were expressed, the highest expression was VEGFR3. The VEGFR ligand known as VEGFA has been previously shown to improve CPC engraftment, improve angiogenesis and performance of the left ventricle: therefore inhibition of these pathways would lead to negative effects on the CPC population (Tang et al., 2015). Imatinibs primary targets are PDGFR-α and VEGFR1 and therefore fewer effects might be seen with IM than SM or ST; which block a broader range of subclasses of VEGFR (1-3) and PDGFR (α-β) (Papaetis and Syrigos, 2009; Pardanani and Tefferi, 2004; Wilhelm et al., 2008) . These experiments have limitations as the techniques used are only semi-quantifiable, this means that the exact amount of each protein cannot be determined and therefore only assumptions can be made regarding the main receptor used by the cells. The experiments also do not show if the

CPCs rely on VEGFR for a functional role, therefore future experiments using VEGFR inhibitors should be planned.

3.3.4 Conclusions

Overall these data provide evidence that CPCs are stem cells, confirming the presence of the two defining abilities of a stem cell: to self-renew and to differentiate. The CPCs were shown to be clonogenic and multipotent, differentiating into two distinct cell lineages. The CPCs also expressed ‘stemness’ genes including Nanog, Oct4, SOX2, TERT and KLF4, which are all essential for proliferation and differentiation. There was no downregulation in ‘stemness’ gene expression across passages 4-18, however passage 21 cells were deemed unsuitable, due to reductions in stem cell gene expression and differentiation potential. Further CPC characterisation identified distinct calcium handling apparatus, similar to other immature cell types, involving RyR3, IP3R and SERCA. Finally, the cells showed expression of RTKI targets, including VEGFRs 1, 2 and 3.

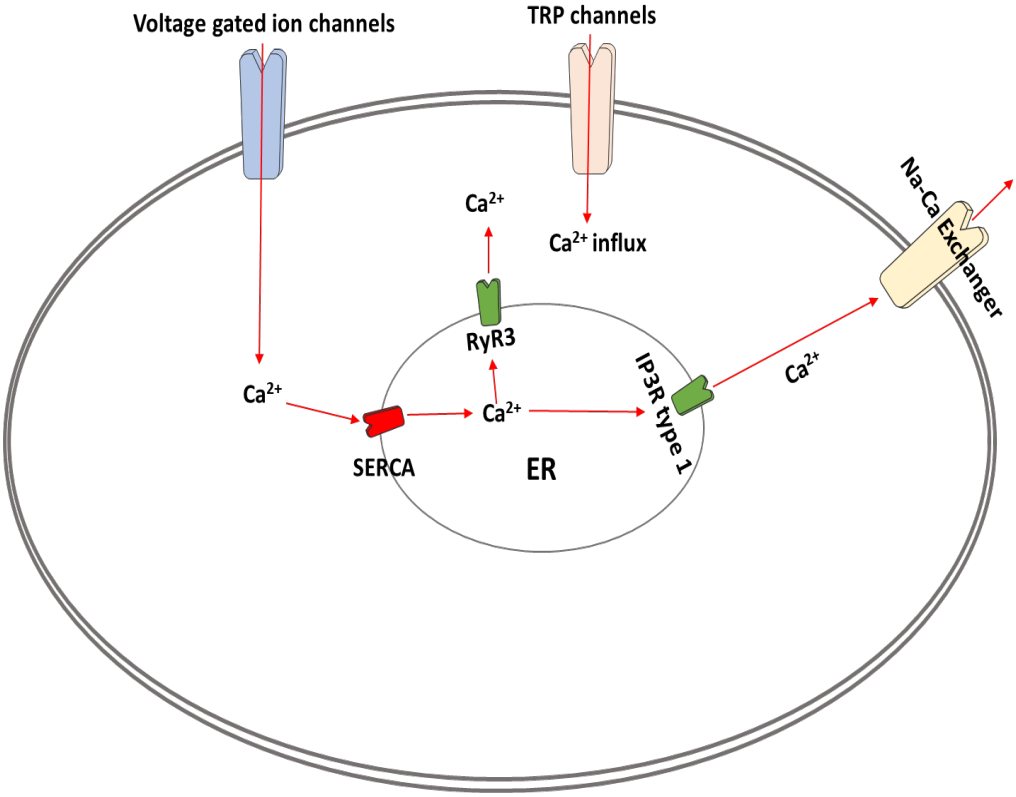

Figure 3. 16. Schematic representation of a proposed model for CPC calcium handling. Calcium enters the cell through voltage-gated ion channels or TRP channels, with an increase in cytoplasmic calcium causing calcium influx into the ER through SERCA channels. When required, calcium leaves the ER through RyR3 or IP3R type 1 and is utilised for internal processes. Finally, calcium would leave the cell through the Na-Ca exchanger. Calcium movement represented by arrows.

Chapter 4. Investigating imatinib induced toxicity in CPCs

4.1 Introduction

Imatinib is an RTKI currently used to treat patients with CML and GISTs (Peng et al., 2005) and is a non-selective inhibitor of receptor tyrosine kinases such as c-Kit, PDGFR, intercellular Abl and chimeric fusion protein BCR-Abl (Buchdunger et al., 2000; Druker et al., 1996; Heinrich et al., 2000). The survival of patients presenting with CML has vastly improved since the introduction of IM (Kantarjian et al., 2012).

Although IM has demonstrated great benefits to patients, with reduced side-effect profile and improved survival, it has been linked to adverse side-effects such as cardiotoxicity in some patients; especially within the ageing population (Xu et al., 2009). Cardiotoxicity induced by IM was reported during treatment of ten patients, with LVEF reduced in these patients below 50% of baseline (Kerkelä et al., 2006b). However, a subsequent study of 1276 cases showed adverse cardiac events after IM treatment were rare: 22 patients suffered congestive heart failure, with age and pre-existing cardiac conditions being contributory factors (Atallah et al., 2007b). Other studies showed an association of IM with cardiac hypertrophy and heart failure in patients treated for GISTs, along with elevated levels of natriuretic peptide precursor B, a predictive marker for future cardiovascular events (Park et al., 2006). Further evidence of potential adverse effects of IM was found in cardiomyocytes *in vitro*, with IM leading to altered calcium transients, cardiomyocyte hypertrophy, mitochondrial dysfunction and cell death (Barr et al., 2014; Fernández et al.,

2007; Herman et al., 2011). Our previous study (Burke et al., 2019) identified the effects of IM on adult cardiac fibroblasts, with significant impact on viability and proliferation. The study also showed changes to the expression of growth factors and cytokines (TGF-β1; PDGF; IL6; IL1β), indicating that further investigation of mechanisms of IM-induced cardiotoxicity was required.

To fully understand how RTKIs cause adverse effects on the myocardium, it is important to investigate their cellular implications. Apoptosis is a tightly-regulated process defined by the activation of pro-apoptotic factors such as executioner caspases 3 and 7, which eventually lead to DNA fragmentation and cell death (Slee et al., 2001). There is now strong evidence of an alternative cell death pathway independent of apoptosis, called necroptosis (programmed necrosis). This is a version of necrosis regulated by the expression of activated proteins: RIP1, RIP3 and MLKL (Linkermann and Green, 2014; Murphy et al., 2013; Vanlangenakker et al., 2011).

Another relevant process is autophagy, as this has previously been linked to cell death, including the leakage of pro-cell death signals from lysosomes (Guicciardi et al., 2004). However, other studies have shown autophagy to be an initiator of other cell death pathways such as apoptosis, rather than a direct cause of death (Kroemer and Jäättelä, 2005; Mazure and Pouysségur, 2010). Understanding the involvement of autophagy in IM-induced cell death could be of great clinical significance, as studies have suggested that autophagy is a possible cause for IM resistance in cancer patients (Carew et al., 2008).

The aim of the work in this chapter was to identify the cell death pathways involved in IM-induced toxicity in human endogenous CPCs, with the hope of finding a mechanism to overcome this adverse side effect.

4.2 Results

4.2.1 Imatinib causes reduced cardiac progenitor cell viability

It has been previously documented that RTKIs cause damage to cardiomyocytes *in vitro*, however limited research is available on CPCs; therefore this study first established whether RTKIs cause cell death within the CPC population. This study will evaluate the effects of both peak concentration (IM 10 μM) of these drugs over 24 h which is the rough estimate for how long it would take for the drug to reach its peak concentration (equivalent to the maximum drug concentration within patients plasma). The study will also investigate the effects of the trough concentrations (IM 5 μM) over 7 d to establish long term effects of low doses (the lowest concentration of drug recorded in patient plasma). The study also investigated the dose dependent effects of the drugs by assessing x10 higher or lower concentration than that of the clinically comparable concentration. Cells were grown *in vitro* and exposed to a range of concentrations: for 24 h at peak concentration and 7 d at trough concentration, with viability then measured by FDA assay (**Figure 4.1**). Cell viability was reduced by 28.0 ± 2.7% after cells were treated for 24 h with 10 μM IM and by 35.0 ± 3.6% after 100 μM exposure for 24 h, relative to the control (n=5, $p<0.05$. **Figure 4.1A**). The same analysis of viability post-IM was applied to trough concentrations (0.5 μM, 5 μM and 50 μM) of IM over 7 d. The results showed reduced cell viability when compared to the control: 5 μM IM reduced viability by 28.0 ± 2.3% and 50 μM IM by 79.1 ± 3.8%; 0.05 μM and 0.5 μM IM did not affect CPC viability (**Figure 4.1B)**.

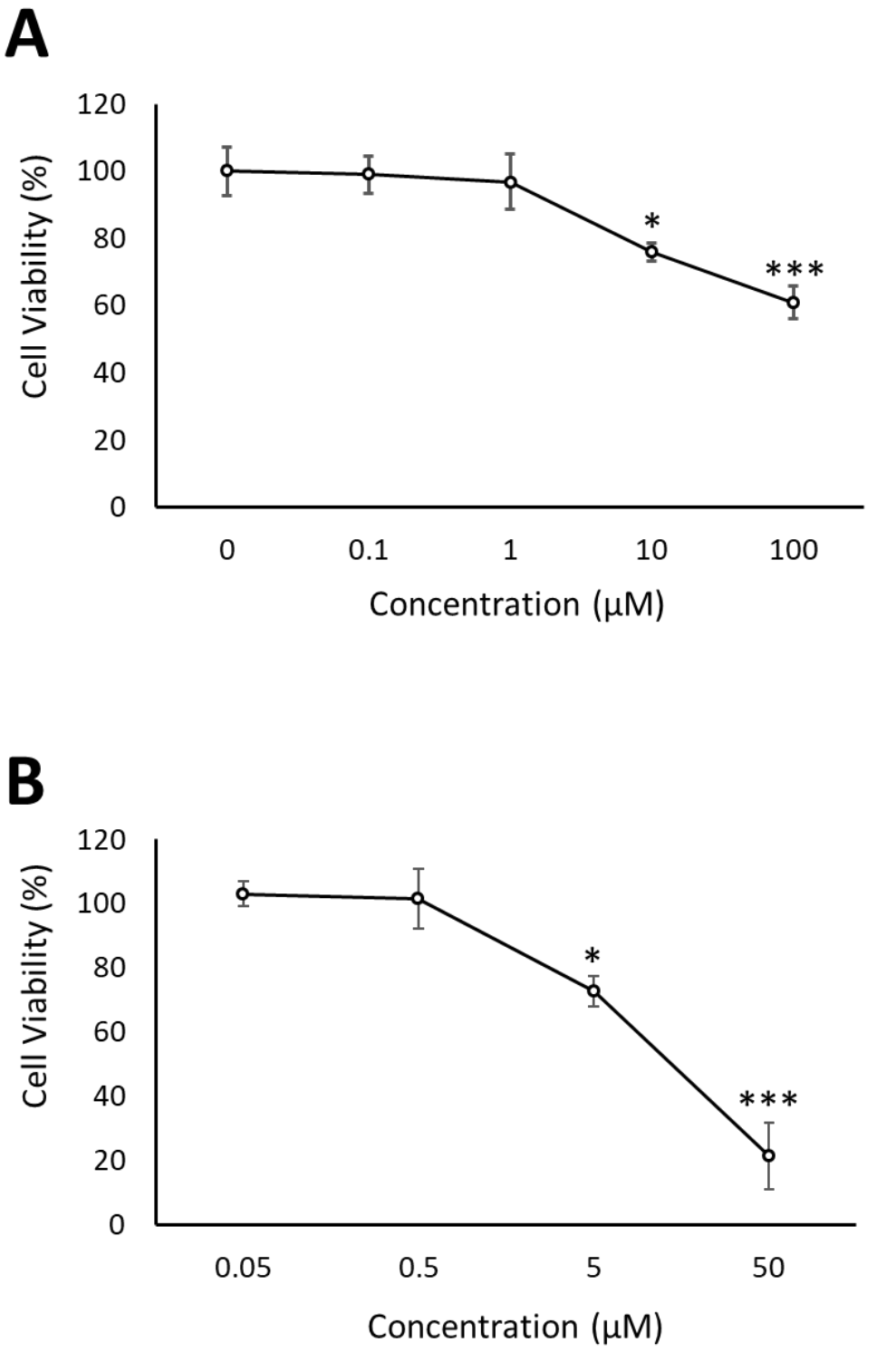

Figure 4. 1. Changes in cell viability after IM exposure. CPCs were treated with a range of IM concentrations and cell viability assayed by FDA. **(A)** Cells treated with 0.1, 1, 10 or 100 µM IM for 24 h before assessment of viability **(B)** Cells treated with 0.05-50 µM IM for 7 d. Data are mean±SEM, n=8; *p<0.05, **p<0.01, ***p<0.001, ANOVA with *post hoc* Tukey's test.

4.2.2 Imatinib does not trigger cardiac progenitor apoptosis

Next, the study investigated the mechanism of IM-induced toxicity, to determine whether the cell death was via apoptosis or an alternative pathway. Live cells were stained after IM treatment for 24 h and 7 d with TMRM, ToPro-3 Vybrant ® FAM Caspase-3 and -7 , and DAPI (Mioulane et al., 2012). Caspases -3 and -7 are both executioner caspases and are a standard marker for identifying the presence of apoptosis (Mioulane et al., 2012; van Heerde et al., 2000). The dye TMRM was used as a cytoplasmic marker (mitochondria sequester TMRM and in healthy cells shows a cellular outline), and DAPI was used to identify the cell's nucleus. Finally, ToPro-3 was used to identify late-stage cell death, as it enters cells only in the presence of increased cell membrane permeability (**details in Chapter 2.1**).

After treatment with 10 µM or 100 µM IM for 24 h, no signs of increased caspase-3/7 activity were seen in either IM-treated or control cells (**Figure 4.2A)**. However, ToPro-3 was identified within the nuclei of CPCs after treatment with 10 µM and 100 µM IM (**Figure 4.2A**). Quantification showed a significant increase of 13.6 ±1.5% of cells being positive for ToPro-3 after 100 µM IM (n=4, $p<0.05$). Although 10 µM IM caused no significant effect, there was a 6.4 ± 1.2% fluctuation in nuclear ToPro-3 expression (n=4, $p>0.05$, **Figure 4.2B**). Staining intensity of TMRM was reduced in CPCs after 10 µM IM treatment by 15 ± 2.5% and at the higher concentration of 100 µM IM by 35.0 ± 4.2% compared to the control (n=4, $p<0.05$) (**Figure 4.2C**).

A

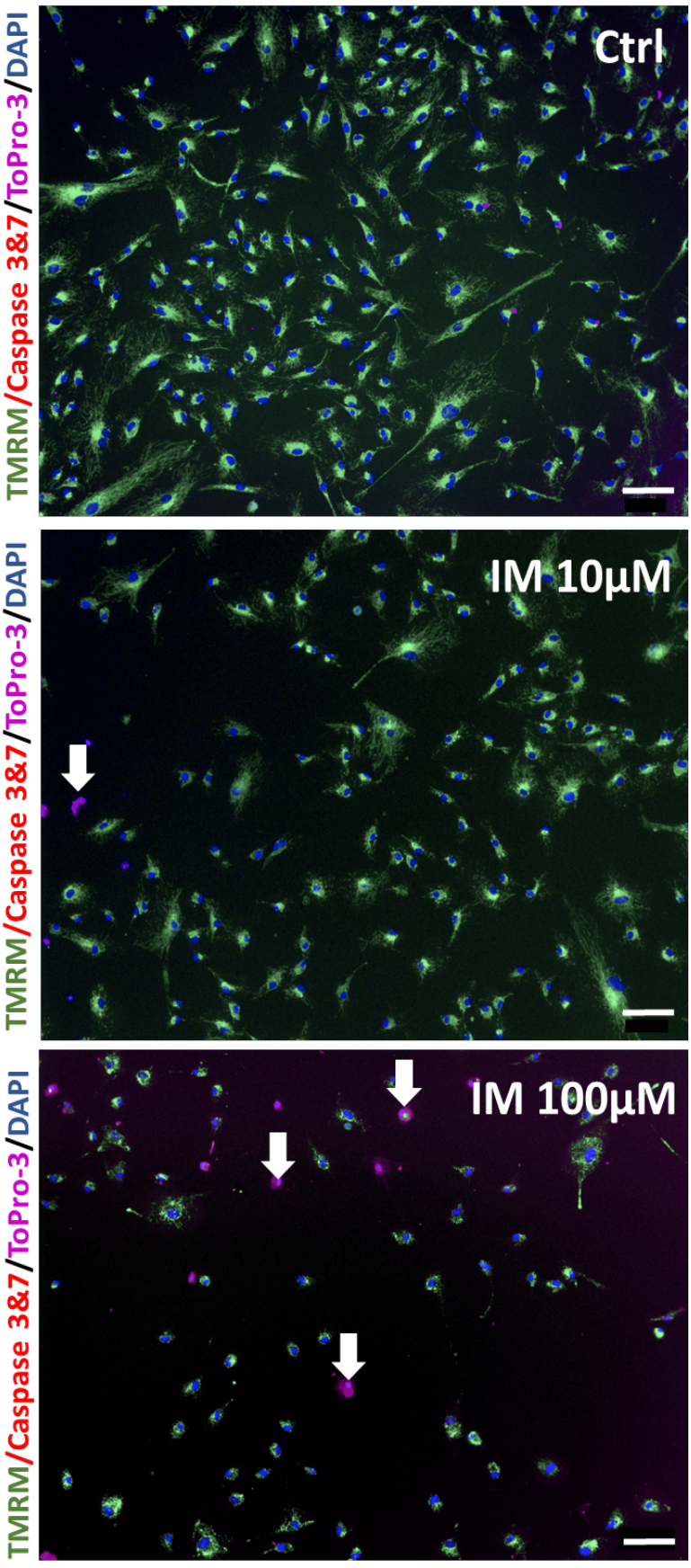
TMRM/Caspase 3&7/ToPro-3/DAPI
Ctrl
TMRM/Caspase 3&7/ToPro-3/DAPI
IM 10µM
TMRM/Caspase 3&7/ToPro-3/DAPI
IM 100µM

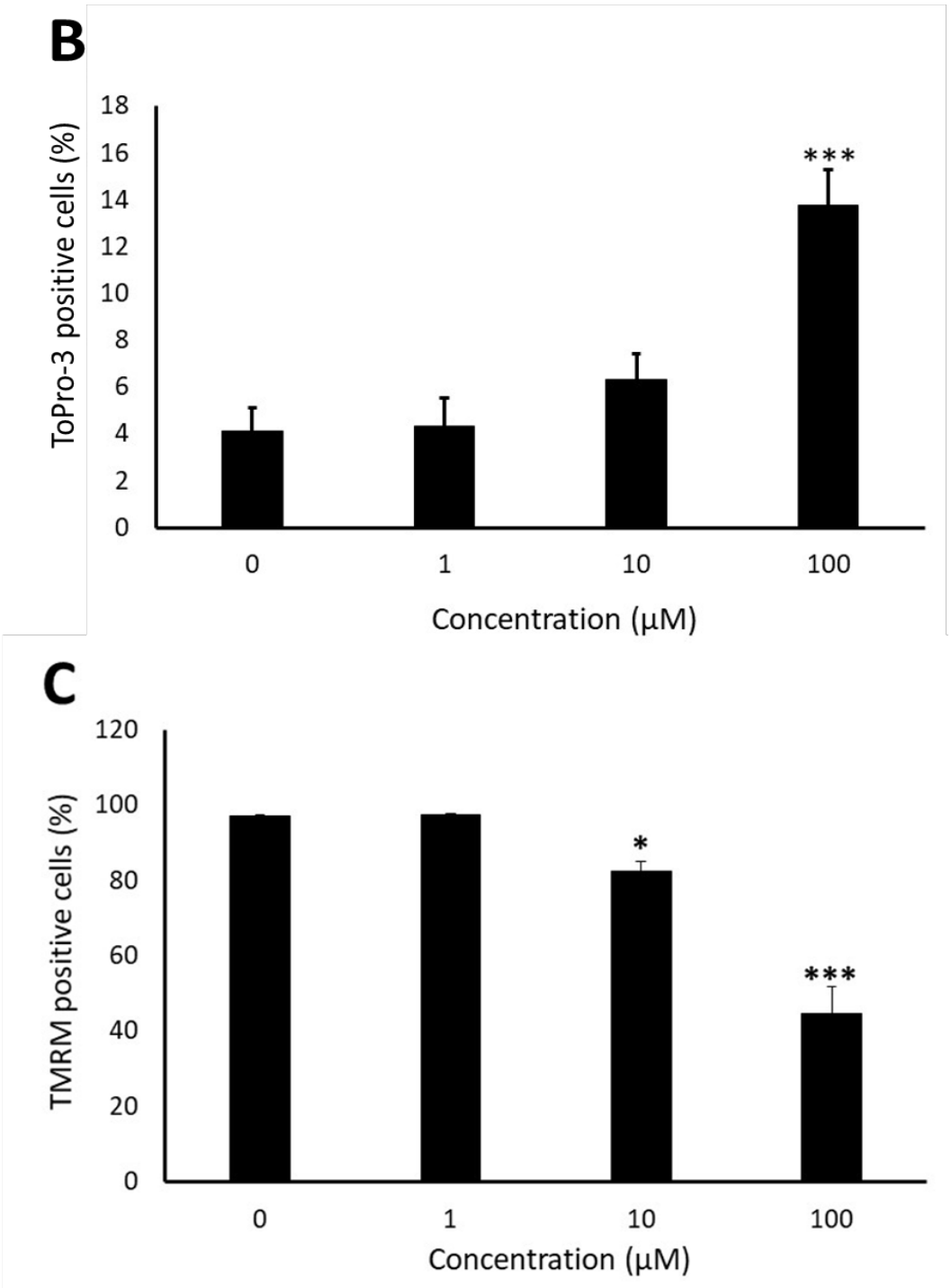

Figure 4. 2. Identifying the activation of executioner caspases and presence of ToPro-3 in CPCs after IM 24 h treatment. (A) Images of untreated cells and cells treated with 10 µM or 100 µM IM and stained for TMRM (dark green), ToPro-3 (magenta), and caspase 3/7 (red). Control cells and IM-treated cells showed no caspase 3 and 7 activation. Imatinib treated cells showed ToPro-3 staining (arrows). **(B)** Quantification of ToPro-3 positive cells after 0-100 µM IM treatment. **(C)** Quantification of TMRM staining after 1, 10 and 100 µM IM treatment *vs.* untreated control cells (0 µM). Data are mean±SEM, n=4, *p<0.05, ***p<0.001, scale bar=100 µM, ANOVA with *post hoc* Tukey's test.

To overcome the limitations of semi-quantifiable ICC data, flow cytometry was used to verify these TMRM findings. Cells were grown *in vitro* and treated as previously mentioned, then stained with TMRM. Application of IM caused a left shift (reduction) in fluorescent intensity in a dose-dependent manner (**Figure 4.3**). Cardiac progenitor cells treated with 10 μM IM reduced the TMRM events by 26.4 ± 6.5%, 20 μM IM reduced the events by 38.9 ± 6.3% and 50 μM IM treatment by 61.8 ± 6.8% and finally FCCP (positive control) which decouples the mitochondria can be seen to have reduced the events by 96.4 ± 12.5% within the gated region (**Figure 4.3A**). These data were reinforced by the changes in mean fluorescent intensity (MFI) of TMRM with a reduced average fluorescence to 74.6 ± 6.5% after 10 μM IM treatment to 49.2 ± 6.8% after 50 μM IM *vs.* 96.5 ± 6.2% in control cells (n=6, $p<0.05$) (**Figure 4.3B**).

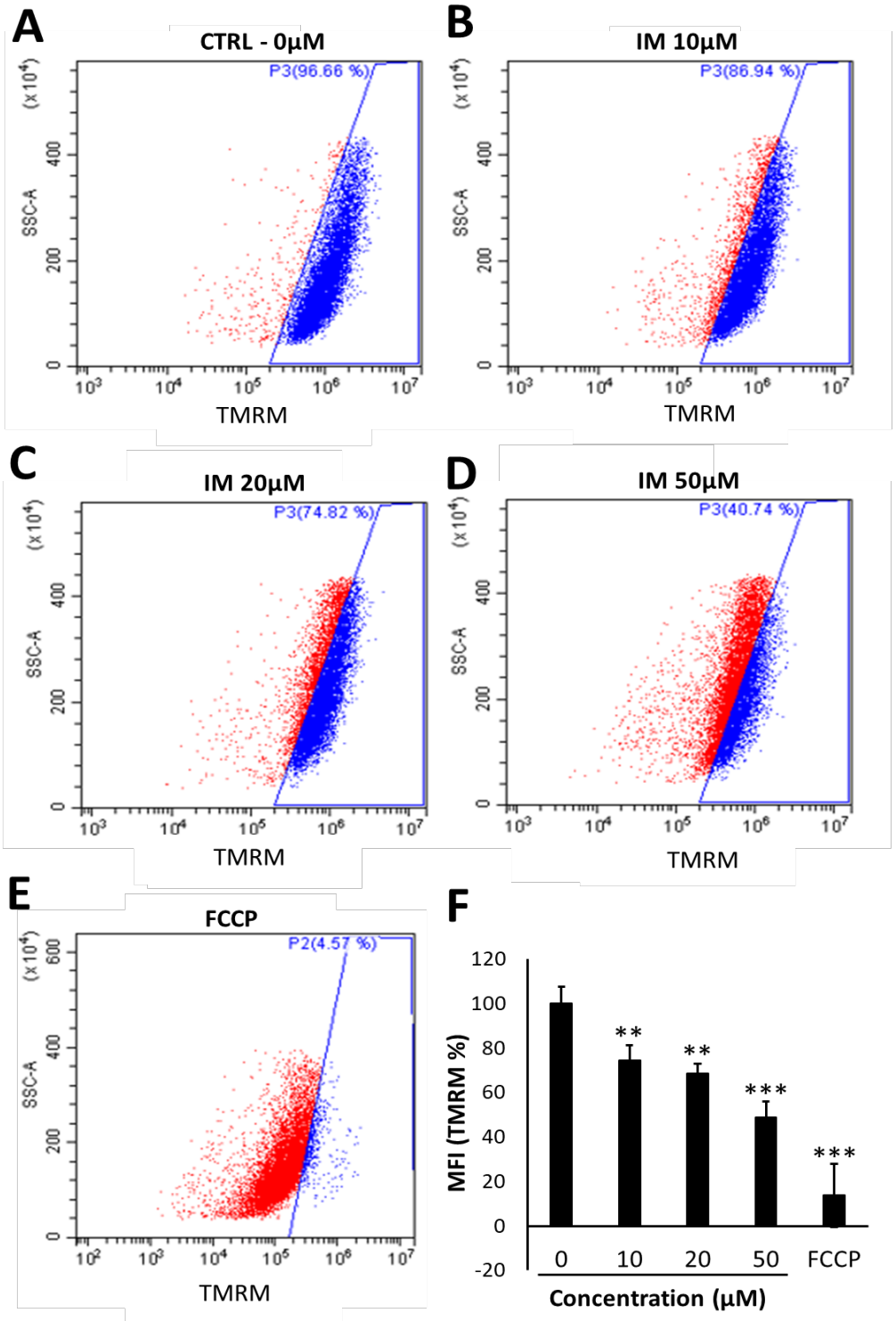

Figure 4. 3. Changes in CPC Δψm after IM exposure. **(A-E)** Intensity of TMRM fluorescence following application of IM or FCCP **(A)** untreated control 0 µM **(B)** 10 µM **(C)** 20 µM **(D)** 50 µM **(E)** 10 µM FCCP. Viable cells with "normal" TMRM signal have been gated in blue, any cells with reduced fluorescence are shown in red. Cells treated with 10 µM IM, 20 µM IM, 50 µM IM and positive control 10 µM FCCP all showed cells with left shift in intensity (red). **(F)** Quantification of TMRM MFI normalised against control cells (100 %). Data are mean±SEM, n=6, **p<0.01, ***p<0.001, ANOVA with *post hoc* Tukey's test.

Further examination of both apoptosis and necroptosis gene expression were investigated. These genes included caspase 8, TNF-α, BAX, RIP1, RIP3 and MLKL. RT-qPCR was used to detect changes in gene expression after exposure to 10 μM IM for 24 h. The largest relative gene expression was PARP, followed by; MLKL, caspase 8, RIP3, RIP1, calpain and TNF-α in both the control and IM-treated samples (**Figure 4.4A**). There was no significant change in gene expression of either apoptotic (BAX, caspase 8, PARP, calpain and TNF-α) or necroptosis associated genes (RIP1, RIP3 and MLKL). The ΔΔcq gene expression was greatest for caspase 8 (1.6 ± 0.5 fold), TNF-α (1.6 ± 0.2 fold) and RIP3 (1.4 ± 0.0 fold) (n=3, p>0.05) (**Figure 4.4B**).

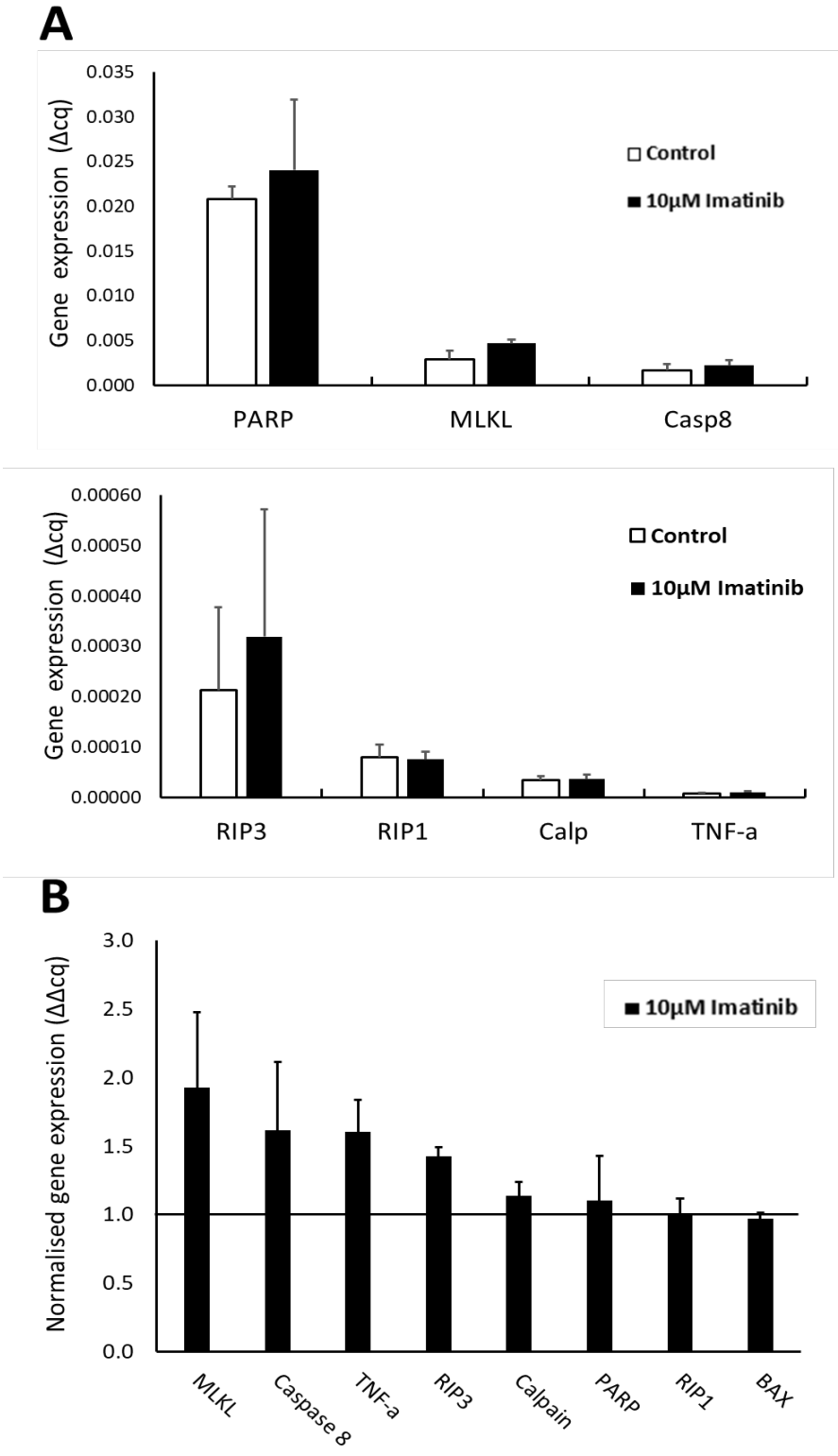

Figure 4. 4. Changes in gene expression in CPCs after exposure to 10 µM IM for 24 h(A) Gene expression (relative to β-actin) in control (white) and IM-treated (black) samples, for a range of cell death-associated genes. **(B)** Changes in gene expression over control (control = 1.0; dashed line); negative values represent reduced gene expression. Data are **(A)** Δcq±SEM or **(B)** ΔΔcq±SEM, n=3, *t*-test.

4.2.3 Treatment of cardiac progenitor cells with imatinib for 7 d did not cause apoptosis

Live-cell staining showed no activation of caspase-3 and -7; however it showed an increase in ToPro-3 staining, cells treated with 5 μM IM had 10.3 ± 1.5% of cells positive for ToPro-3 and 50 μM IM 52.3 ± 18.3% relative to with 1.3 ± 0.5% of untreated cells (n=4, p<0.05) (**Figure 4.5A-B)**. There was no significant change in apoptosis-associated genes such as calpain 1.3 ± 0.0 fold, PARP 1.2 ± 0.3 fold, caspase 8 1.1 ± 0.6 fold and TNF-alpha 0.9 ± 0.2 fold (n=3, p>0.05). There were no changes seen in necroptosis-associated genes; RIP1 1.2 ± 0.0 fold, RIP3 1.1 ± 0.5 fold and MLKL 0.9 ± 0.2 fold (n=3, p>0.05) (**Figure 4.5C**).

A

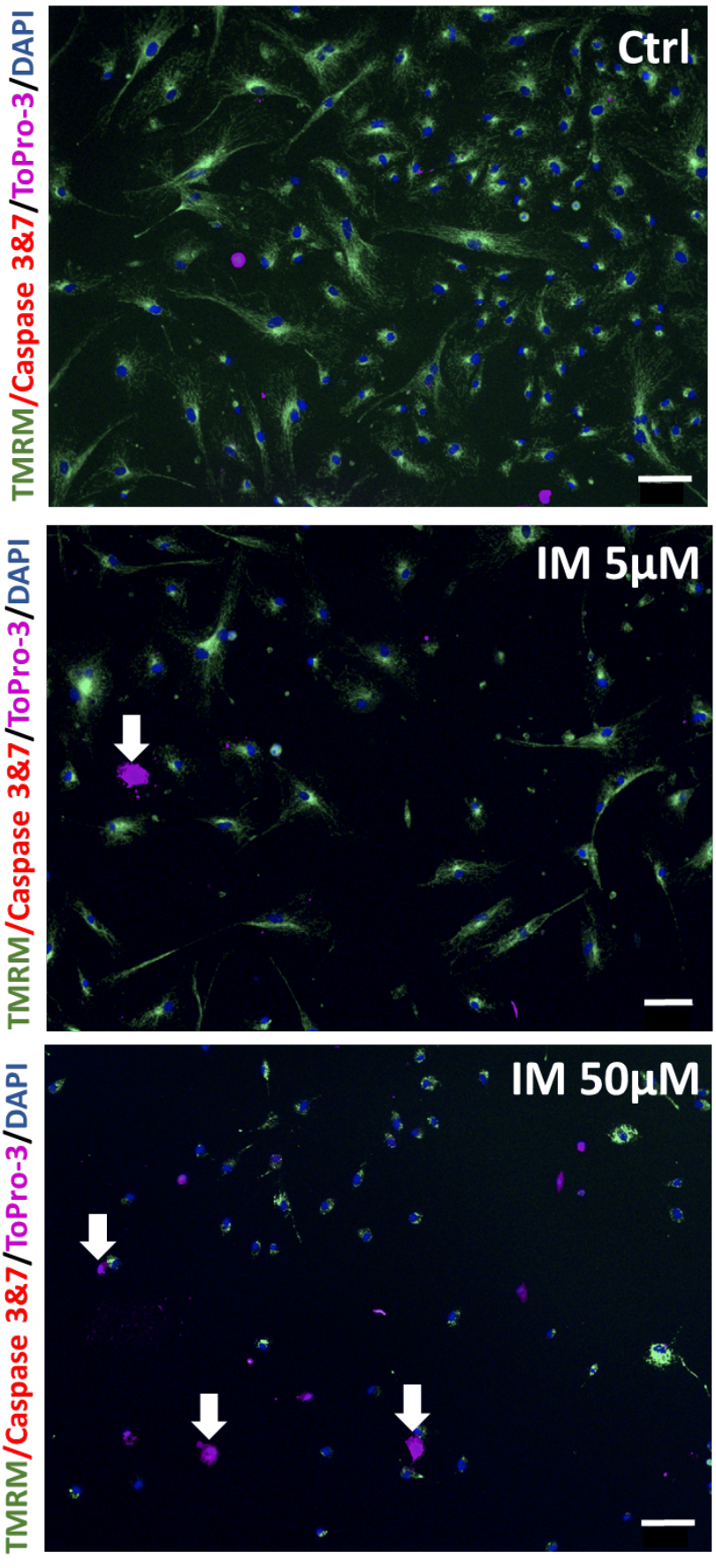
TMRM/Caspase 3&7/ToPro-3/DAPI
Ctrl
TMRM/Caspase 3&7/ToPro-3/DAPI
IM 5µM
TMRM/Caspase 3&7/ToPro-3/DAPI
IM 50µM

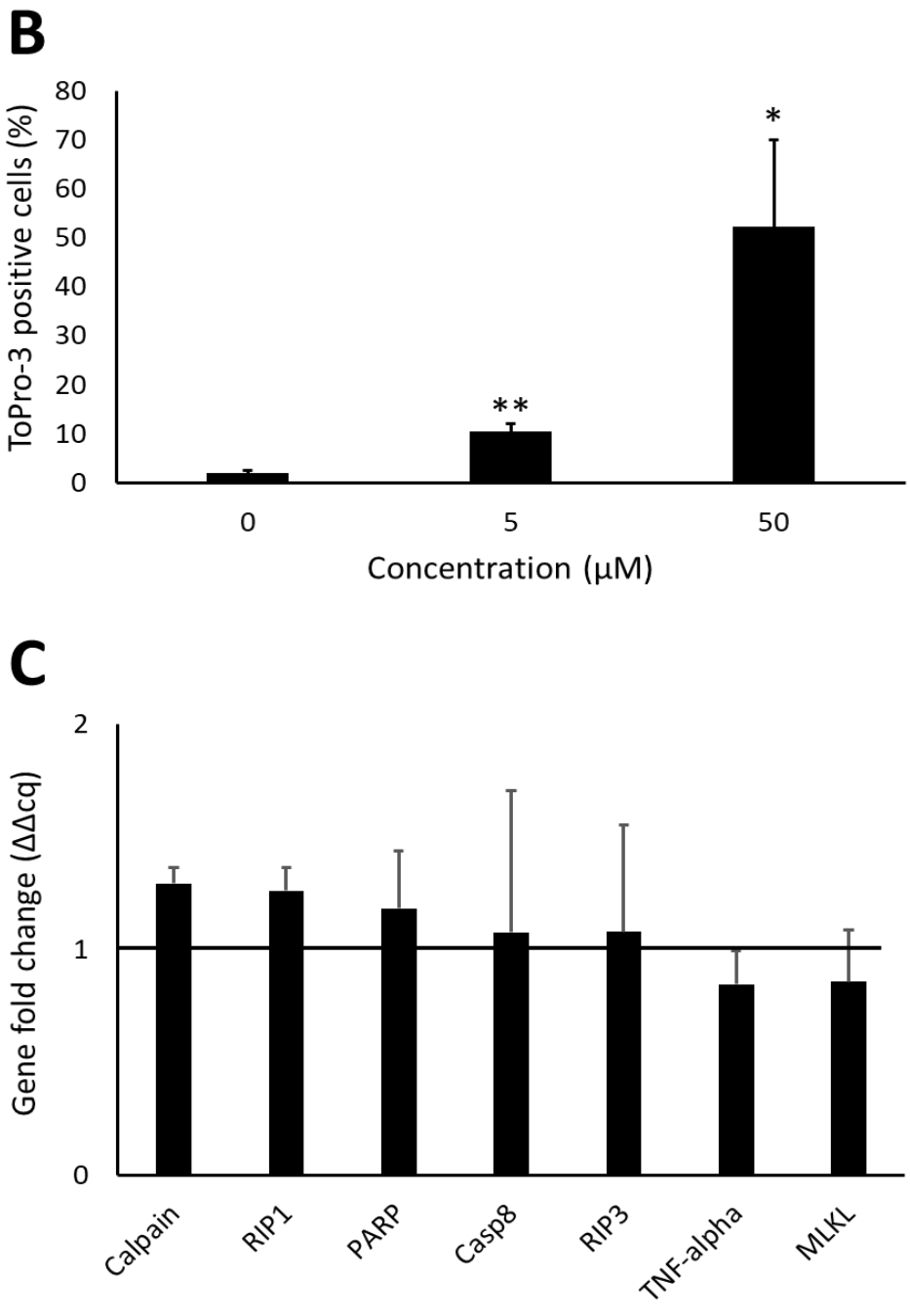

Figure 4. 5. Identifying the activation of executioner caspases, ToPro-3 and changes in gene expression in CPCs after IM 7 d treatment. (A) Cells treated with 0 µM, 5 µM or 50 µM IM stained for TMRM (dark green), ToPro-3 (magenta), and caspase 3/7 (red). Control cells and IM-treated cells showed no caspase 3 and 7 activation. Imatinib treated cells showed ToPro-3 staining (arrows). **(B)** Quantification of ToPro-3 positive cells after 0-100 µM IM treatment. **(C)** Changes in gene expression in CPCs after IM 7 d treatment *vs.* control (control = 1.0; solid line); negative values represent reduced gene expression Data are mean±SEM, n=4, *p<0.05, **p<0.01, ANOVA with *post hoc* Tukey's test.

4.2.4 Imatinib 48 h treatment impairs CPCs autophagic flux

To determine the role of autophagy in IM-induced cell death, acridine orange was used to identify whether the drug increased acidic properties within the cell (acidic organelles (AO)). The cells showed a significant increase in the number of AOs after being exposed to 10 μM IM for 24 h, 48 h and 72 h (**Figure 4.6A-D**). Quantification of acridine orange showed increased staining after CPCs were exposed to 10 μM IM for 24 h with 55.0 ± 6.4% of cells being positive, after 48 h 60.0 ± 5.7% and IM 72 h 73.0 ± 3.1% relative to 9.0 ± 3.0% in untreated control cells (**Figure 4.6E**). To examine this further, Western blotting was used to assess any changes in total protein expression of the specific lysosomal marker LAMP2. Cardiac progenitor cells showed an increased LAMP2 protein expression after 10 μM IM and showed a 2.4 ± 0.3 foldchange relative to untreated control cells (1.0 ± 0.0) (**Figure 4.2.6F**).

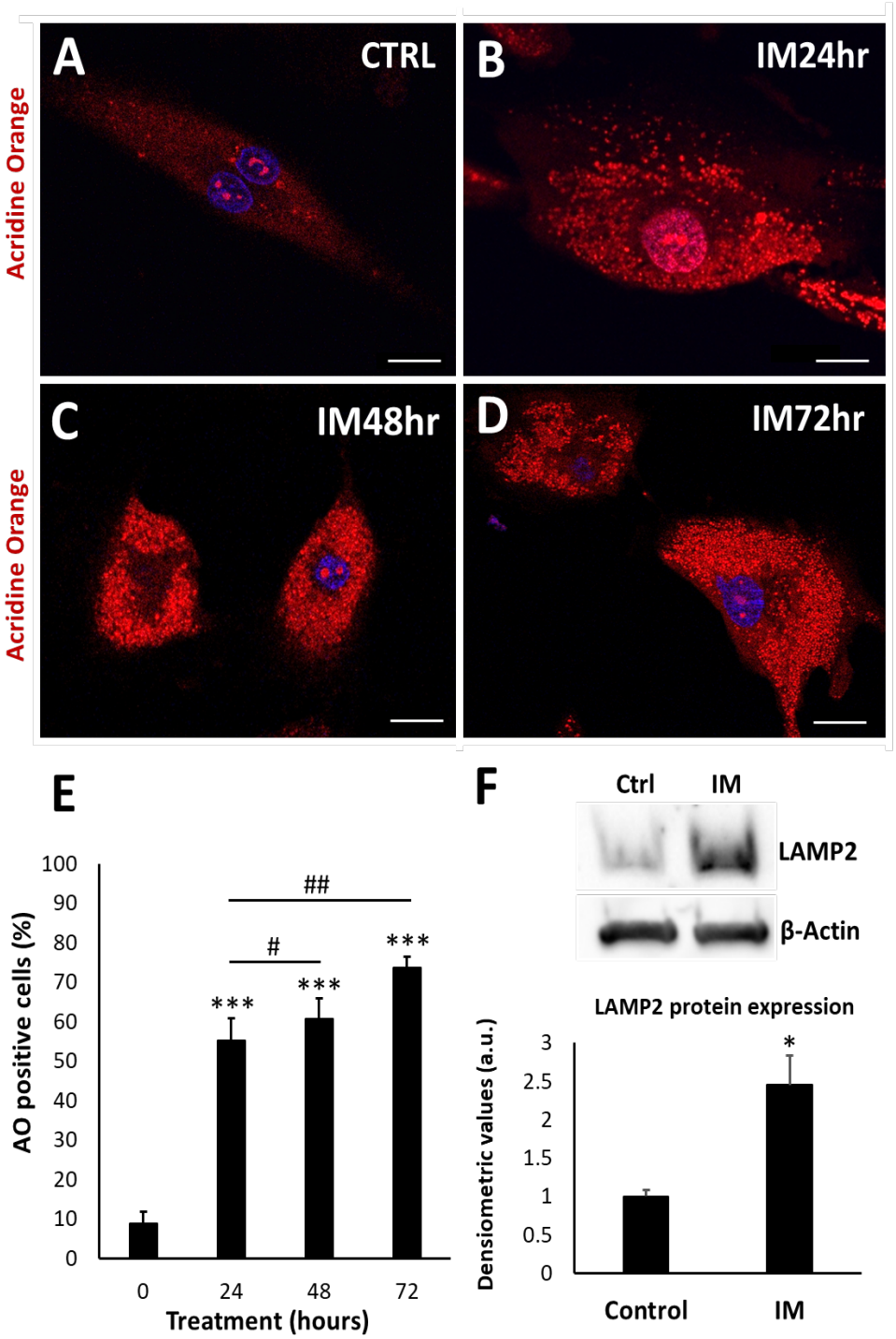

Figure 4. 6. IM-induces accumulation of acidic vesicle organelles. Representative images of CPCs stained with acridine orange; staining represents AOs (arrows). **(A)** Control cells, 10 μM IM for **(A)** 24 **(C)** 48 and **(D)** 72 h treatment. **(E)** Quantification of the acridine orange staining in CPCs IM-treated (10 μM) relative to control. Data are mean±SEM, n=5. ***p<0.001 *vs.* control, #p<0.05, ###p<0.001 *vs.* IM 24 h treatment, ANOVA with *post hoc* Tukey's test**. (F)** Representative image of LAMP2 Western blot, control and 10 μM IM treatment (24 h), β-actin was used as a loading control. Densitometric quantification of |Western blot for LAMP2, corrected for β-actin and normalised against control. Data are mean±SEM, n=3, *p<0.05, *t*-test.

Having identified that IM increased the AOs and lysosome formation, it was important to evaluate the autophagic flux. The autophagic flux is best defined as how well the autophagosomes can fuse with the lysosomes to remove unwanted proteins such as p62 (Kroemer and Jäättelä, 2005). To measure the autophagic flux, western blotting was used to analyse the involvement of autophagosome marker LC3II and the removal of p62 protein. A lysosomal inhibitor known as bafilomycin A1 (bafilomycin) was used to prevent proteins from being degraded by the acidic properties of the lysosomes. Therefore, if the cell had a functional autophagic flux, there would be an increase in protein levels after bafilomycin inhibition. Western blot analysis of IM 24 h treatment showed a 2.7 ± 1.3, 1.9 ± 0.0 fold increase in LC3II and p62 respectively, which further increased with bafilomycin; 3.4 ± 0.3, 3.9 ± 0.8 fold. However, IM-48 h showed a 2.6 ± 0.2, 2.7 ± 0.3-foldchange of LC3II and p62, which showed no significant increase with bafilomycin treatment; 2.7 ± 0.1, 2.6 ± 0.0 fold when compared to the control (1.0 ± 0.0) (**Figure 4.7A-B**).

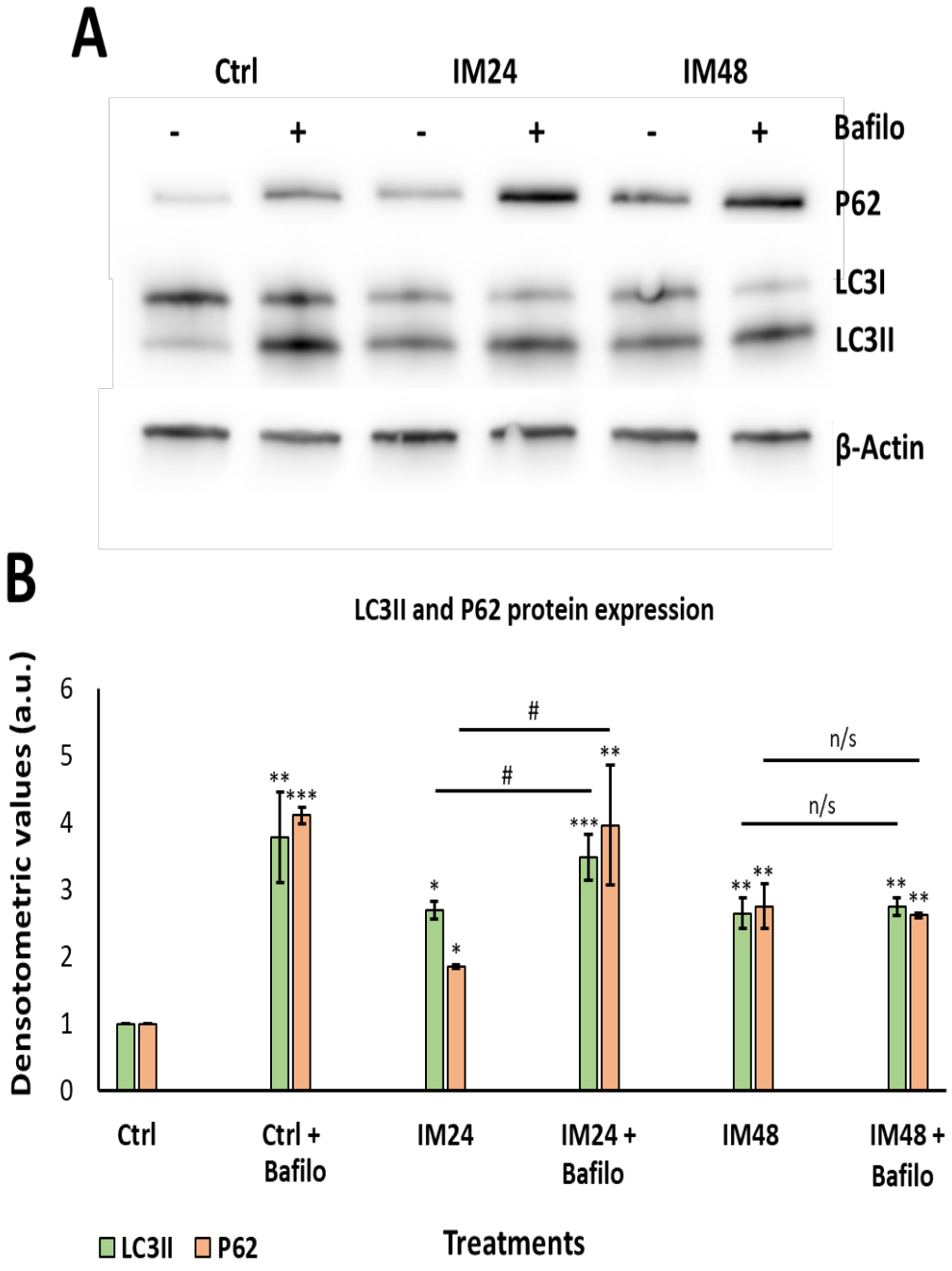

Figure 4. 7. Investigating CPC autophagic flux after IM treatment. (A) Representative Western blot for P62, LC3I and LC3II for control lysates, 10 μM IM 24 h and IM 48 h treatment with/without bafilomycin treatment (represented by – or + symbol). β-actin was used as a loading control **(B)** Densiometric quantification of Western blots for P62 (orange) and LC3II (green) after IM 24 h, IM 48 h treatment, +/- bafilomycin (bafilo) *vs.* control. Data are mean±SEM, n=5. *p<0.05, **p<0.01, ***p<0.001 *vs.* control, #p<0.01 *vs.* IM 24 h treatment, n/s refers to not significant, ANOVA with *post hoc* Tukey's test.

To determine the specific positioning of autophagosomes and lysosomes, ICC staining was used for LC3II and LAMP2 (DAPI for nuclear staining); to identify whether the autophagosomes are colocalised with the lysosomes. Micrographs showed dense staining of both LC3II and LAMP2 proteins within all samples (**Figure 4.8A**). Further quantification confirmed Western blot findings with a 10.0 ± 3.5% increase in LC3/LAMP2 association after IM exposure for 24 h, which is decreased after 48 h of IM treatment to 5.0 ± 2.%. The positive control of rapamycin showed a 40.0 ± 2.6% increase in LC3/LAMP2 association. However, opposite findings were seen for LAMP2/LC3II association which decreased after 24 h IM treatment to 5.0 ± 3.2%, IM 48 h 19.0 ± 4.6 % and rapamycin 32.0 ± 1.3%. These results could be due to staining pattern and density of LAMP2 compared to LC3II, with more LC3II staining than LAMP2 stain (**Figure 4.8B**).

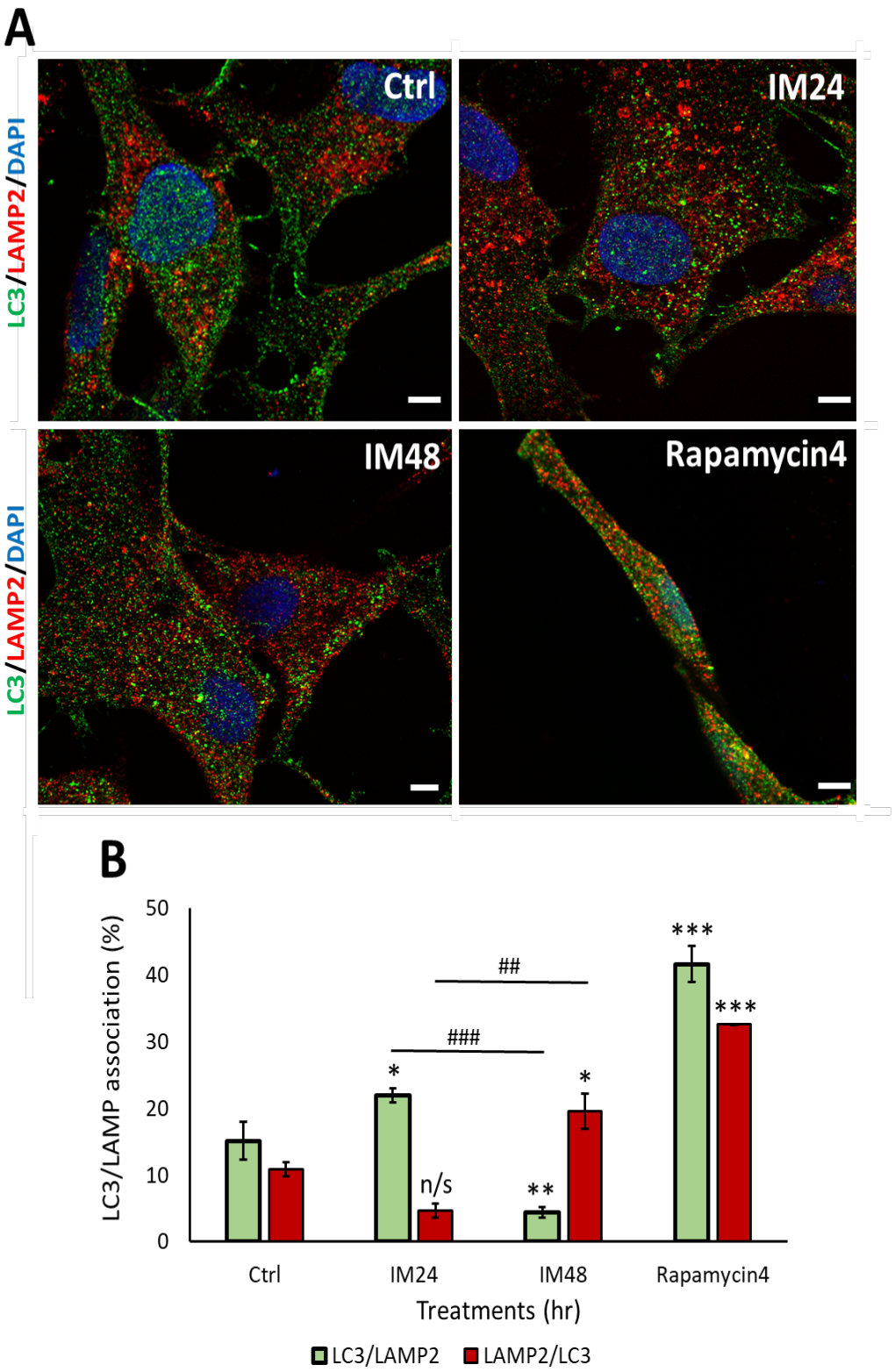

Figure 4. 8. LC3 and LAMP2 association using airyscan imaging. **(A)** Representative images of LAMP2/LC3 staining showing the expression of both proteins in untreated cells, IM 24 h, and IM 48 h treated cells and rapamycin treated cells. **(B)** Colocalisation analysis using Image j platform, quantification of the association between LC3/LAMP2 (green) and LAMP2/LC3 (red) after IM 24 h, 48 h treatment or rapamycin 4 h treatment. Data are mean±SEM, n=3, *p<0.05, **p<0.01, ***p<0.01 *vs.* the control. Scale bar=40 µm, ANOVA with *post hoc* Tukey's test.

There are limitations with standard ICC staining, including the density of each stain and nonspecific background, which could interfere with the results. An alternative method to study proximity of two proteins is the PLA assay based on this principle; the signal is only generated when two proteins are within 40 nm distance of each other suggesting physical association (**see Chapter 2.6.1**). The cells were treated with IM for 24 or 48 h and then fixed and stained for LC3II and LAMP2. Cells were also treated with rapamycin for 4 h as a positive control for autophagy. There was an increase in PLA puncta when comparing control cells to IM 24 h treated cells. However, there was a reduction in red puncta when examining cells treated with IM for 48 h and increased puncta in rapamycin-treated cells relative to untreated control cells. (**Figure 4.9A-D**). These findings were reinforced by quantification of PLA puncta per cell with 32.1 ± 3.7 red puncta after IM treatment for 24 h ($p<0.05$), there was a significant reduction in the number of PLA puncta after IM 48 h treatment to 2.7 ± 0.7 ($p<0.05$). Cardiac progenitor cells treated with rapamycin showed a significant increase in PLA puncta staining with 103.1 ± 7.4 per cell, relative to the untreated cells with 11.3 ± 2.1 puncta per cell ($p<0.05$) (**Figure 4.9E**).

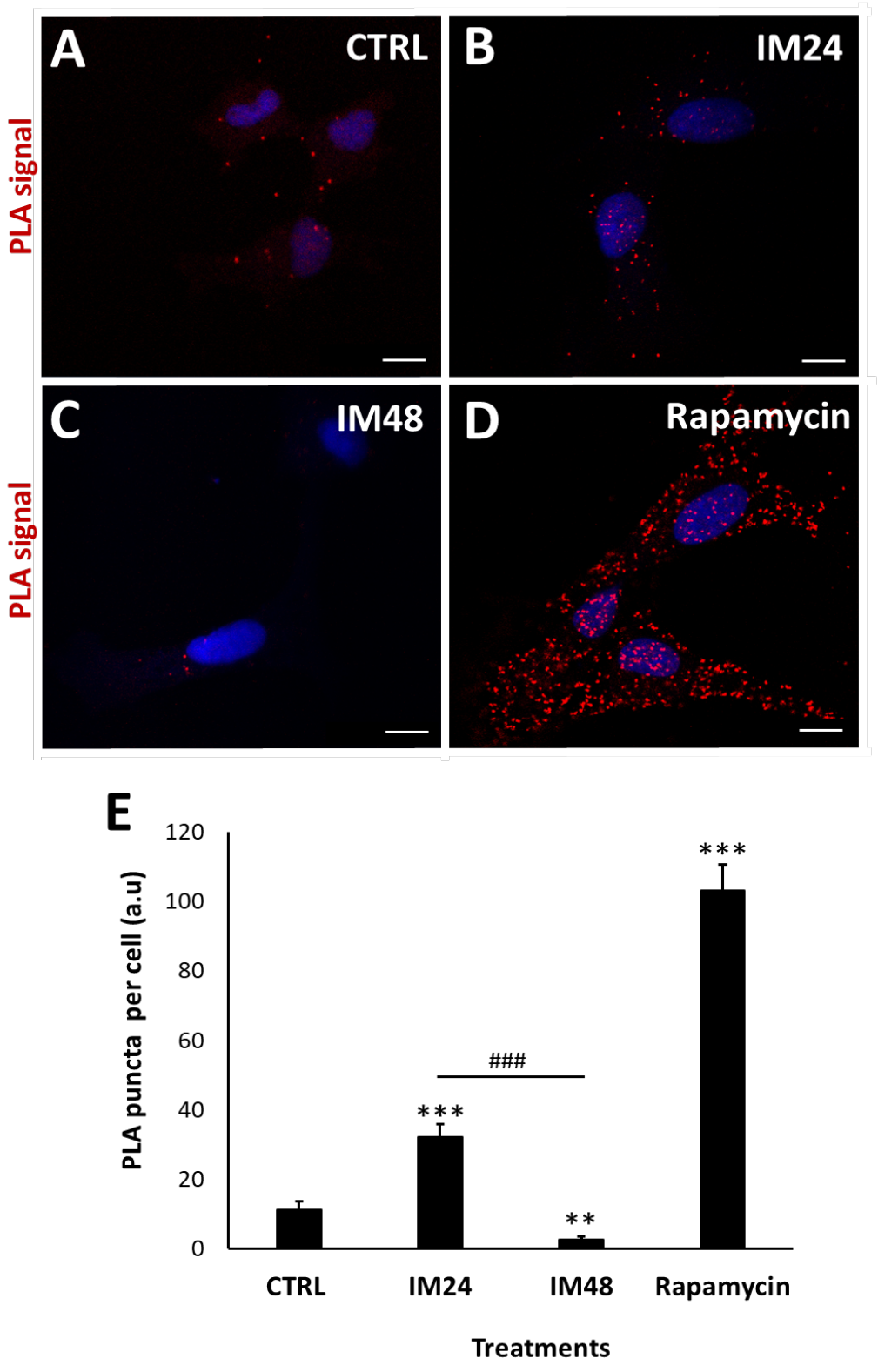

Figure 4. 9. IM reduces the proximity between LC3II and LAMP in CPCs. (A-D) PLA representative images of control cells showing low PLA signal, IM 24 h increased signal, IM 48h reduced signal and rapamycin high PLA red puncta (arrows). **(E)** Quantification of PLA puncta after IM 24 h, IM 48 h and rapamycin treatment for 4 h. Data are mean±SEM, n=10 **p<0.05, ***p<0.001 *vs.* control, ###p<0.001 *vs.* IM 24 h treatment, Scale bar=10 µm, *t*-test.

4.2.5 Autophagic impairment is not the main contributor to cell death

Once it was determined that IM was impairing the autophagic flux in CPCs, it was important to see whether this was contributing to cell death. Therefore, to examine this, an autophagosome inhibitor was used (wortmannin); this prevents the initial formation of autophagosomes and is an upstream autophagy inhibitor. Western blots were carried out to confirm that wortmannin was preventing the formation of autophagosomes by analysing the LC3II expression (**Figure 4.10A**). Densitometry values of LC3II levels showed a decrease in LC3II expression when IM was co-treated with wortmannin for 24 h, with no reduction at 48 h (n=1) (**Figure 4.10B**). Following this, a cell viability test was performed, IM 24 h treatment showed a 15.5 ± 1.5% reduction in viability; cells co-treated with IM and wortmannin for 24 h reduced viability by only 9.1 ± 3.7% (n=3, $p>0.05$) compared to the control. There was no significant difference between control and IM co-treated with wortmannin for 24 h. However, there was also no significant difference between IM 24h treatment only compared to IM co-treated with wortmannin for 24 h (**Figure 4.10C**).

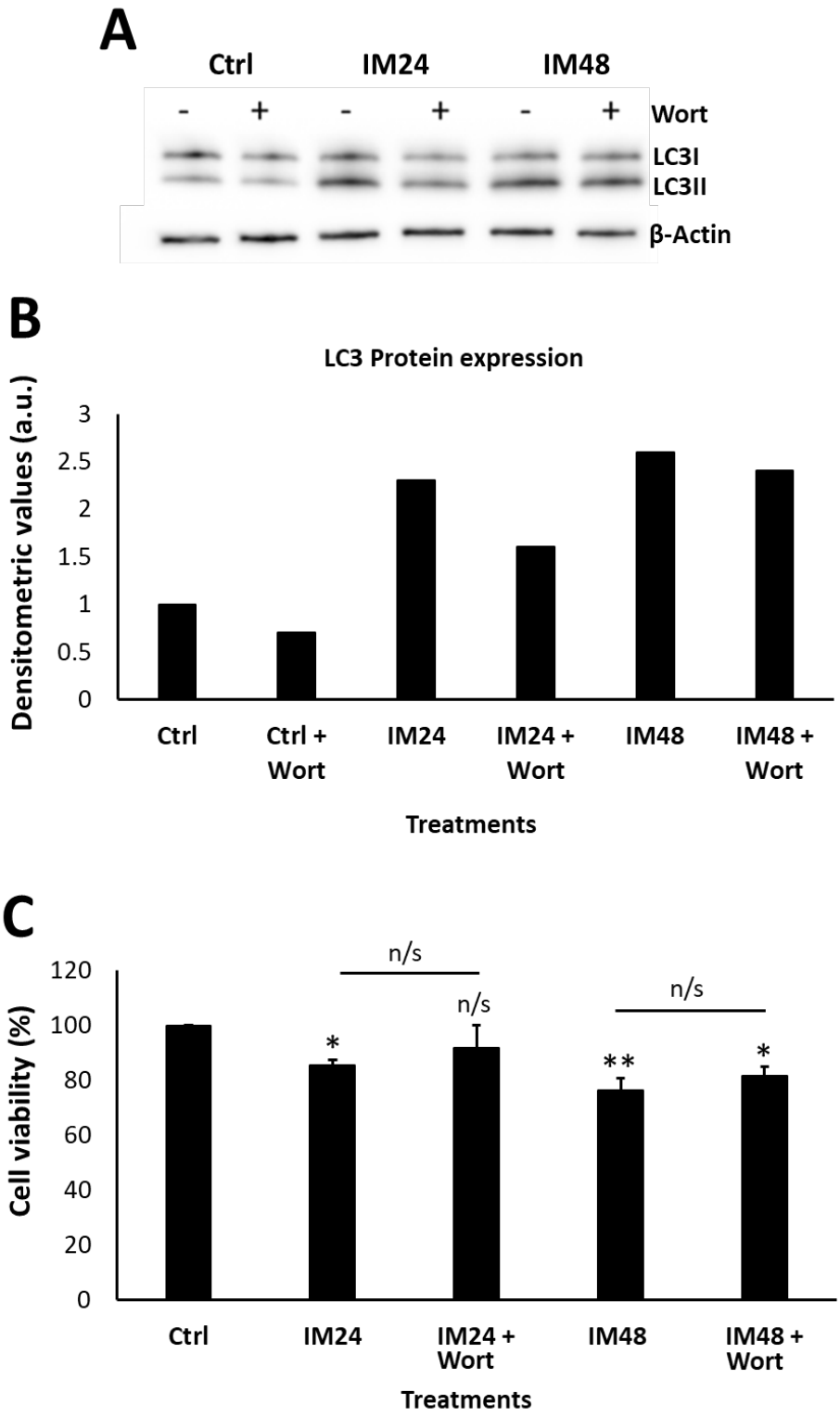

Figure 4. 10. IM-induces cell death and is partially recovered by autophagosome inhibition. (A) Western blot image and densitometric values shown for LC3II expression after IM treatment for 24 or 48 h with/without wortmannin (wort). Data are means, n=1. **(B)** Cell viability analysis of IM 24 h treatment, IM 24 h co-treated with wort, IM 48 h treatment and IM 48 h co-treated with wort, data are mean±SEM, n=3. *p<0.05, **p<0.01 *vs.* control, n/s=not significant *vs.*IM24 or IM48. ANOVA with *post hoc* Tukey's test.

4.2.6 Imatinib-induces necroptotic cell death within cardiac progenitor cells, which is reversed by RIP1 inhibition

As IM was inducing cell death but not through apoptosis and only a partial contribution from autophagy, it was important to investigate other pathways, including necroptosis. Necroptosis can be defined by the activation of specific proteins such as MLKL, RIP1 and RIP3. Western blotting revealed an increase in total MLKL and phosphorylated MLKL after IM-treatment *vs.* control (**Figure 4.11A**). Densitometry of the activated protein (total protein/phosphorylated protein) confirmed this with an 8.5 ± 2.5 fold increase after IM treatment, and the positive control showed a 26.4 ± 0.5 fold increase when compared to the control (n=3, $p<0.05$) (**Figure 4.11A**). Necrostain-1 (nec-1) was used to inhibit RIP1 an upstream necroptosis initiator, following nec-1 inhibition cell viability was measured. These data demonstrated that IM 24h treatment showed 22.6 ± 2.5% reduction (n=4, $p<0.05$) in viability whereas IM 24h co-treated with nec-1 showed a 12.1 ± 3.2% reduction in viability (n=4, $p>0.05$) relative to the untreated control cells (**Figure 4.11C**).

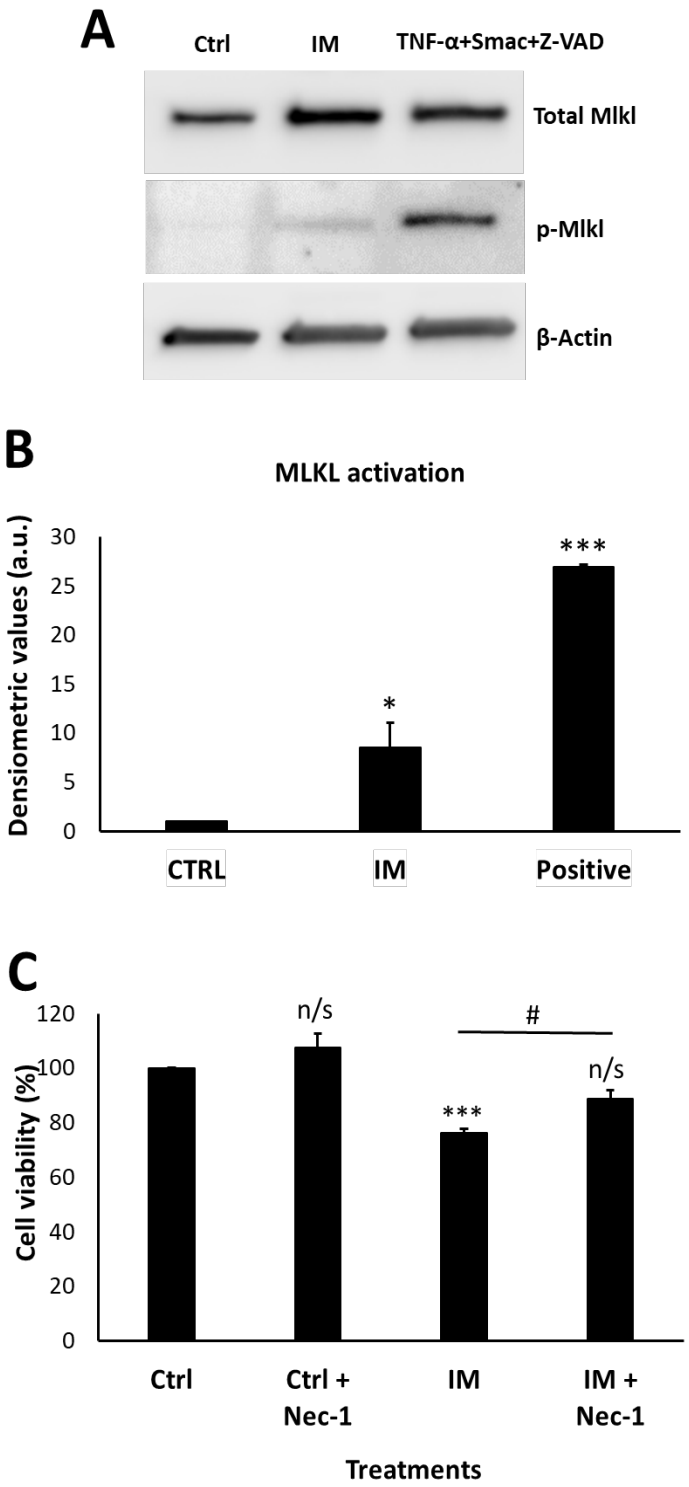

Figure 4. 11. IM-induces necroptotic cell death and is rescued by RIP1 inhibition. **(A)** Western blot representative image showing expression of total MLKL and p-MLKL after IM 24 h treatment and positive control (TNF-α, SMAC mimetic and Z-VAD). **(B)** Densitometric values showed MLKL activation after IM treatment and positive control treatment. Data are mean±SEM, n=3, *t*-test. **(C)** Cell viability analysis of nec-1 inhibition; control cells, control cells treated with nec-1, IM alone and IM co-treated with nec-1. Data are mean±SEM, n=4. *p<0.05, ***p<0.001, *n*/s=not significant *vs.* control, #p<0.05 vs. IM 24 h, ANOVA with *post hoc* Tukey's test.

4.2.7 Imatinib increased calcium reuptake after store operated calcium inhibition

Another key signalling molecule involved in cell death is calcium, which can act as a s messenger and activate various cell death pathways. To identify whether calcium was involved in IM-induced cell death, various experiments were done, including investigating SOCE and chelating calcium to investigate its impact on cell viability. Firstly, thapsigargin was used to deplete the CPCs internal stores (by inhibiting SERCA), to examine the reuptake of calcium after IM treatment. Alongside thapsigargin, a low external calcium concentration was applied to the cells; ensuring the internal source of calcium was depleted. This reduction in store calcium concentration is normally recovered by a process known as SOCE. To test whether IM increased or decreased the calcium reuptake; a calcium-sensitive dye known as fluo-4 was used.

The cells were pre-treated in a calcium-free environment with thapsigargin (negative control did not contain thapsigargin) with or without 1,10 or 100 μM IM for 30 min. The Fluo-4 signal was then measured at 1.52-s intervals over 30 s before addition of calcium with or without different concentrations of IM. The calcium was then measured for a further 170 s, and the values were then normalised against the basal calcium to remove variability from dye loading. All basal calcium levels remained stable until stimulation with the addition of calcium with or without IM (30 s), the negative control remained relatively flat even after the addition of calcium with peak stimulation reaching 1.0 ± 0.0. The positive control cells (IM0) showed a peak fluorescence of 1.5 ± 0.0, 1 μM IM of 1.6 ± 0.8, 10 μM IM of 1.6 ± 0.0 and 100 μM IM of 1.7 ± 0.1 (**Figure 4.12A**). The calcium response shown cells treated with 1 μM IM to have a 1.2 ± 0.1,

10 μM IM 1.4 ± 0.0 and 100 μM IM 1.3 ± 0.1 fold increase *vs.* control cells (1.0 ± 0.0) (n=5, $p<0.05$) (**Figure 4.12B**).

As there was a small increase in calcium reuptake, it was important to analyse whether calcium impacted on cell viability. The use of EGTA to chelate calcium is well documented, with a stoichiometry of 1:1. Cells were grown in medium with or without IM and with or without 1 mM of EGTA, for 24 h followed by measurement of viability using the FDA assay. There was a significant reduction in viability to 74.0 ± 7.4% after 10 μM IM treatment *vs.* control cells. There was a significant reduction in cell viability when 10 μM IM was co-treated with EGTA; 70.4 ± 4.3% (n=3, $p<0.05$) *vs.* control cells (100 ± 0.0 %) (**Figure 4.12C**). There was no significant difference between IM-alone *vs.* IM co-treated with EGTA (n=3, $p>0.05$)

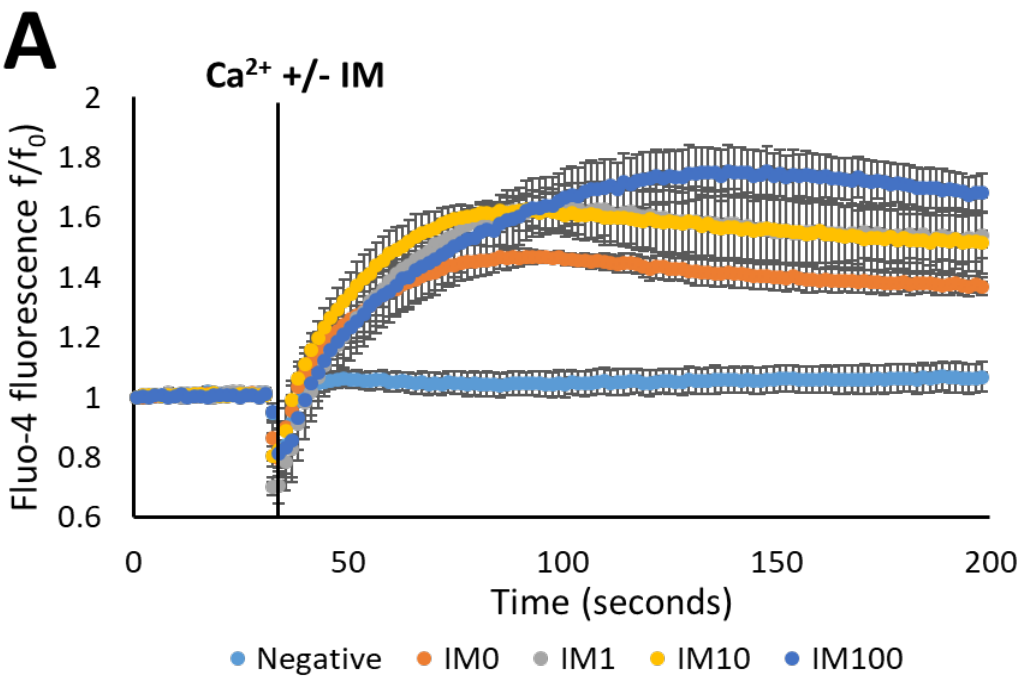
A
Ca2+ +/- IM
Fluo-4 fluorescence f/f0
2
1.8
1.6
1.4
1.2
1
0.8
0.6
0
50
100
150
200
Time (seconds)
Negative
IM0
IM1
IM10
IM100

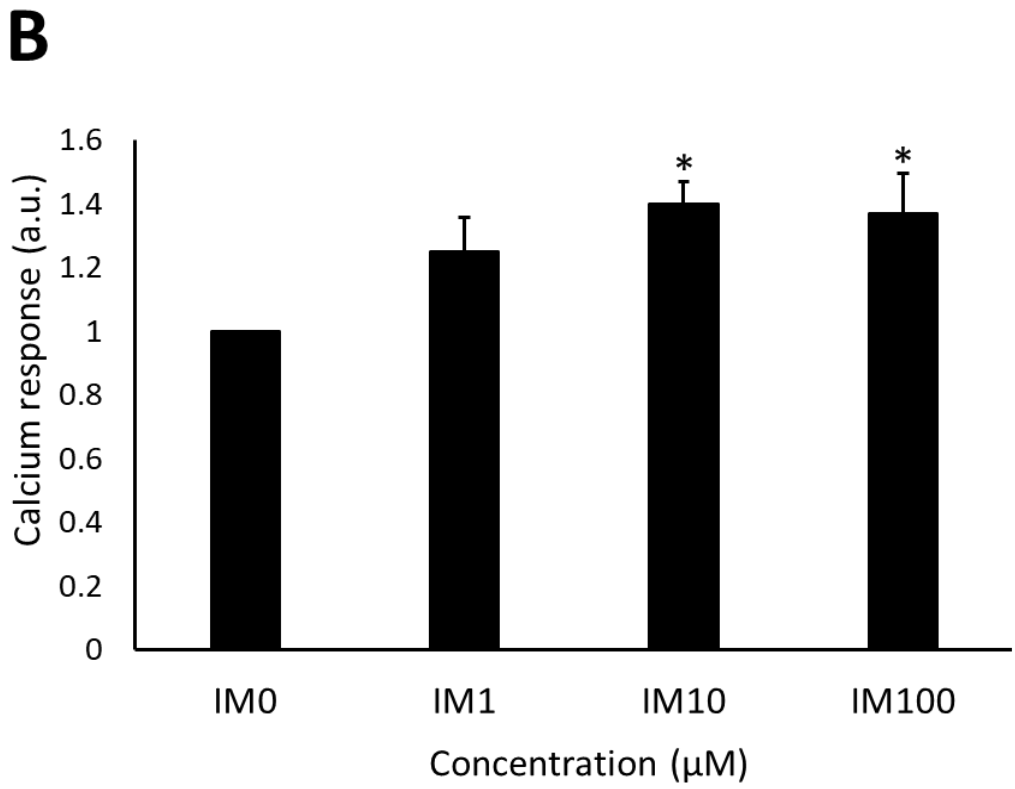
B
Calcium response (a.u.)
1.6
1.4
1.2
1
0.8
0.6
0.4
0.2
0
*
*
IM0
IM1
IM10
IM100
Concentration (µM)

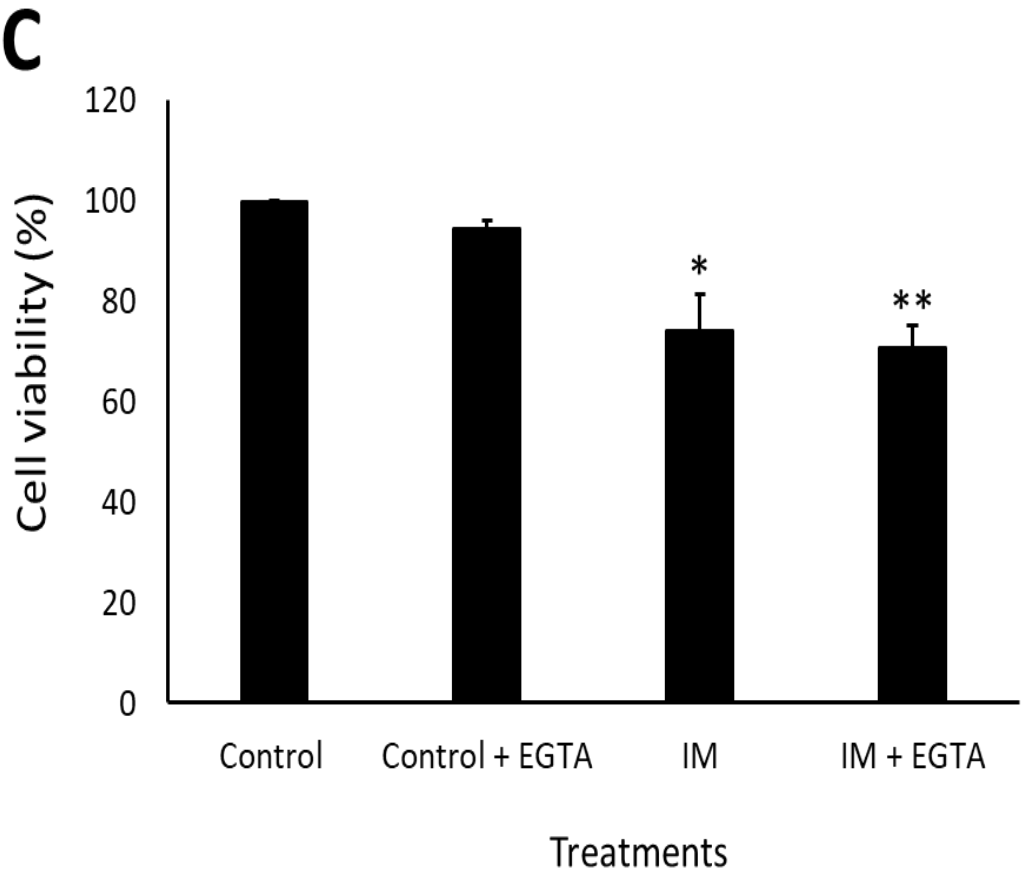

Figure. 4. 12 C**alcium exchange in CPCs after IM treatment**. **(A)** Time course assay of calcium signalling after thapsigargin pre-treatment, +/-1 µM, 10 µM and 100 µM IM, each data point represents 1.52 s. After 30 s of imaging the different concentrations of IM were injected with calcium. Negative control are cells without thapsigargin pre-treatment. Data are mean±SEM, n=5. **(B)** Quantification of calcium response (peak signal-mean baseline signal) for 1, 10, 100 µM IM treatment. Data are mean±SEM, n=5 *p<0.05. ANOVA with *post hoc* Tukey's test. **(C)** Cell viability measured using FDA assay, cells were either untreated (control), treated with 1 mM EGTA, 10 µM IM alone or 10 µM IM co-treated with 1 mM EGTA for 24 h followed by detection of viable cells. Data are mean±SEM, n=3, *p<0.05, **p<0.01, ANOVA with *post hoc* Tukey's test.

4.2.8 Imatinib increased superoxide formation in cardiac progenitor cells but did not increase total ROS

Oxidative damage can cause multiple cellular complications such as reduced mitochondrial function and initiation of cell death pathways (de Arriba et al., 2013). To give an accurate and detailed investigation into ROS it was important to evaluate both total ROS (hydrogen peroxide, peroxynitrite, hydroxyl radicals, nitric oxide, and peroxy radical) and superoxides (includes hypochlorous acid and nitric oxide). Cells were grown *in vitro* and exposed to 10 μM IM for 24,48, and 72 h followed by cell staining for total ROS and superoxides and imaged using fluorescent microscopy. There was an increase in red superoxide signal after IM treatment for all time points; however, there was no change in total ROS production as indicated by the lack of green staining (**Figure 4.13A**). Semi-quantification of the superoxide staining showed increased staining to 22.0 ± 2.5 cells after IM 24 h treatment and subsequently increased further to 30.0 ± 4.3 after 48 h; relative to the untreated control cells of 3.0 ± 1.3 cells positive for superoxide's (p<0.05). Cells treated with IM for 72 h showed superoxide level of 31.0 ± 3.7 cells compared to the control (n=4, p<0.05); there was no significant difference between 48 h and 72 h treatment (n=4, p>0.05) (**Figure 4.13B**).

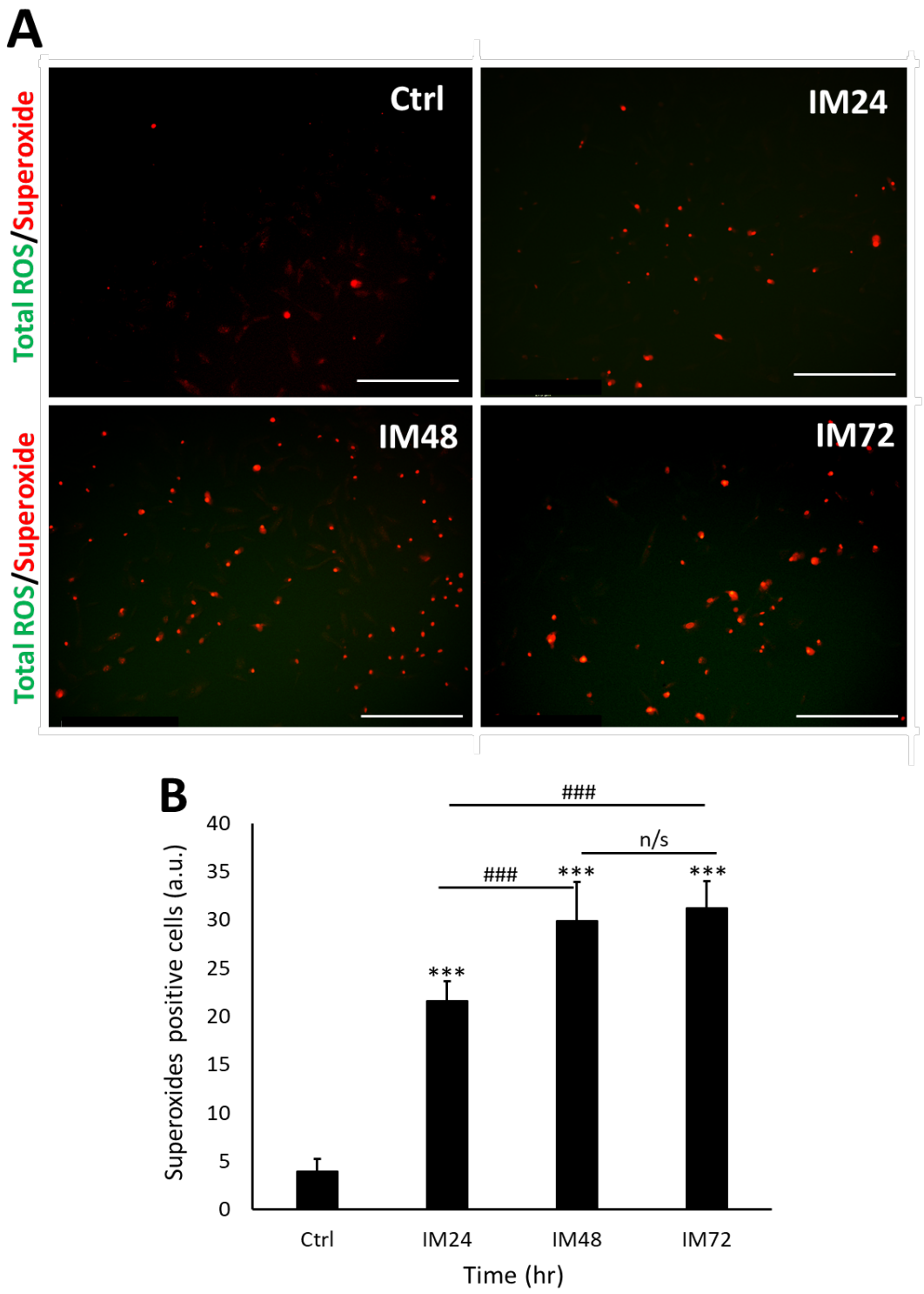

Figure 4. 13. Total ROS and superoxide signalling in CPCs after IM treatment. **(A)** Representative images of total ROS (Green) and superoxide's (Red) after 10 μM IM treatment for 24,48 and 72 h. No total ROS detected (green), superoxide detected **(B)** Semi-quantification of superoxide positive cells after IM treatment (24,48 and 72 h). Data are mean±SEM, n=4, ***p<0.001 *vs.* control, ###p<0.001 *vs.* IM 24 h treatment, n/s refers to not significant, scale bar=275 μm, ANOVA with *post hoc* Tukey's test.

4.3 Discussion

4.3.1 Imatinib-induced cardiac progenitor cell death and reduced mitochondrial membrane potential independent to apoptosis

This study demonstrated that IM could impact the CPC population. Only a few previous studies have fully investigated the cell death pathways induced by IM (Kerkelä et al., 2006b; Moehring et al., 2005; Okada et al., 2004); with an even smaller number addressing the effects on CPCs (Savi et al., 2018; Vajravelu et al., 2015). Imatinib reduced CPC numbers via a reduction in cell viability, but independent of apoptosis. This is different to findings in other cell types with previous reports showing an increase in caspase 3, BAX, cytochrome C and TUNEL positive cells in cardiomyocytes and cancer cell lines (Kerkelä et al., 2006b; Savi et al., 2018). The present study did not find evidence of activated caspase 3 and 7 or an increase in apoptosis-associated gene expression. However, there was an increase in ToPro-3 fluorescence at the higher dose of IM treatment, consistent with membrane damage and cell death. Further investigation of IM's effects on the Δψm confirmed previous findings in cardiomyocytes and CML cells; that IM caused a reduction in membrane potential (Kerkelä et al., 2006b; Kim et al., 2004; Yu et al., 2012). One reason for this could be the leakage of lysosomal content such as zinc during autophagy, as previously shown (Li et al., 2017a). Therefore, it was important to analyse the contribution of autophagy in IM-induced cell death.

There was a limitation with our study as caspase 3 and 7 are known to be time-sensitive with a short life span of activation (Walsh et al., 2008). Therefore, this current study could have missed changes in apoptosis for example lack of increased ToPro-3 at 10 μM IM treatment alongside no activation of caspase

3 and 7 could indicate an early stage cell death; whereby the caspases are still inactive. Further experiments might be of value to assess the involvement of caspase activity at later time points, for example 48 or 72 h. The same limitation could apply to changes in gene expression; however, these data do confirm that 24 h of IM treatment does not induce apoptosis cell death.

4.3.2 Imatinib impairs the autophagic flux

Autophagy is a normal cell cycle process used to removed unwanted proteins from the cell, however, during times of stress and injury can lead to cell death (Dikic and Elazar, 2018). Imatinib increased the number of AOs within CPCs, and these were accompanied by an increase in expression of the lysosomal structural protein LAMP2; this has been shown in a previous study, suggesting that IM-induced autophagy was due to the inhibition of c-Abl rather than c-Kit or PDGF (Mancini et al., 2014). Here, the autophagic flux was shown to be impaired at 48 h, although IM increased the number of autophagosomes and lysosomes, their ability to fuse were impaired.

It has previously been documented that IM is being sequestered by the lysosomes because of IM's weak basic properties; meaning it is attracted to the acidic nature of the lysosomes (Burger et al., 2015; Chapuy et al., 2009). There are three pathways suggested for how IM passes through the lysosomal membrane: autophagocytosis, passive diffusion or transporter-mediated accumulation (Kaufmann and Krise, 2007). It Is theorised that the accumulation of IM in the lysosomes contributed to the impairment of the autophagic flux. However, when autophagy was blocked by an upstream

inhibitor, which prevents the formation of autophagosomes, there was no significant change in cell viability when compared to IM 24 h treatment alone. Although there was no significant change compared to IM 24 h, there was an increase in cell viability to a level no longer significantly different from that of untreated cells. The inhibition of autophagosome formation could, therefore, be considered as a potential therapeutic target to aid in the protection of CPCs, although existing data are contradictory. One previous study showed that inhibiting upstream autophagy using 3-methyladenine or Atg5 inhibition impaired the chemotherapeutic effect of IM in a range of cancer cell lines (Shingu et al., 2009). In apparent contradiction, other reports using K562R cells have shown 3-methyladenine improved IM-induced cancer cell death (Chen et al., 2018). Therefore, further work is required to understand fully whether wortmannin could be used to protect the CPCs and keep the chemotherapy action of IM. Another potential action is blocking downstream autophagy using bafilomycin which has previously been shown to increase the chemotherapy action of IM; however, may not be translational to our study due to the accumulation of unwanted proteins which could lead to increased cell death.

4.3.3 Imatinib-induced cell death via necroptosis

Due to the impairment of the autophagic flux and an increase in p62 protein, our study investigated the involvement of necroptosis cell death in IM-induced toxicity. A previous study by Goodall *et.al.* showed the presence of p62 protein to be vital for the phosphorylation of MLKL and if p62 was removed the cell death pathway would switch to apoptotic cell death (Goodall et al., 2016). Our

current study had shown the absence of key apoptotic markers after IM treatment; the expression of phosphorylated MLKL was therefore measured to determine whether IM was inducing cell death through necroptosis.

Our study showed an increase in MLKL activation compared to untreated cells. This cell death pathway has yet to be identified within IM-induced cardiotoxicity or within previous cancer cell research, which elude to IM-induced toxicity to be through apoptotic cell death (Belloc et al., 2007; Juurikivi et al., 2005; Kerkelä et al., 2006b; Savi et al., 2018), although one study was unable to identify apoptosis in cardiomyocytes (Barr et al., 2014). As the viability of CPCs were rescued using a RIP1 inhibitor (nec-1), this could provide a vital therapeutic target to protect CPCs from damage and in turn, protect cardiomyocytes. Further experiments would be needed to confirm nec-1 does not affect the chemotherapy action of IM, although previous cancer studies show cell death through apoptosis and not necroptosis; this could be due to the lack of investigation into necroptosis cell death. Further detailed experiments would include investigation into RIP1 activity and co-immunoprecipitation experiments for autophagy proteins and necroptosis proteins.

4.3.4 Imatinib stimulates store operated calcium entry independent of calcium chelation

Calcium is a key s messenger involved in cellular processes, including cell survival, cell death and cell motility (Clapham, 2007). It was important to see if the cell death mechanisms involved in CPCs exposure to IM were linked to calcium signalling. Imatinib has previously been documented to influence

calcium signalling within neonatal rat ventricular myocytes with an increase in peak systolic calcium transients and sarcoplasmic reticulum uptake (Barr et al., 2014). Calcium has also been shown to directly interact with necroptosis through an increase in cytoplasmic calcium, ER stress and calcium overload; leading to ROS production and activation of calcium-calmodulin kinase II (Nathan, 2003; Nomura et al., 2014; Zhu et al., 2018). We, therefore, looked at how IM affected the SOCE in CPCs; these data suggest that IM can increase the calcium reuptake after store depletion (through thapsigargin inhibition). One theory for how calcium can influence cell death is because high internal calcium can cause the internal stores to overload causing ER stress, which has been documented in cardiomyocytes (Kerkelä et al., 2006b; Zhu et al., 2018, p. 3). However, our study showed that after chelating calcium by 1 mM (using EGTA), there was no change to cell viability; demonstrating that IM-induced cell death appears to be independent to calcium in CPCs.

These experiments did have limitations; the SOCE was designed to see how calcium would respond after direct IM application for 30-40 min. Therefore, these data are not directly translational to the 24 h time point. Our study attempted to investigate the changes in CPC calcium levels over 24 h of IM treatment, however, due to toxicity of fluo-4 and fura-2-AM over prolonged periods, these experiments were not reliable. These experiments found cells treated with IM and incubated with calcium dye underwent cell death at a quicker rate than cells which were incubated with IM alone (data not shown). Therefore, to overcome this, cell viability was assessed at 24 h after cells were treated with IM and co-treated with EGTA; the theory behind this was a lowered calcium concentration would protect the cells from ER overload.

These data indicated towards CPCs being able to induce calcium reuptake as an acute response to IM and also lowered experimental calcium was not an optimal method for protection of the CPC population.

4.3.5 Imatinib increased superoxide levels but not total ROS production

Reactive oxygen species involvement in necroptosis has previously been documented in numerous studies (Kim et al., 2007; Shindo et al., 2013; Vanlangenakker et al., 2011). One study suggests a link between ROS and the stability of RIP1 and RIP3 interactions. In contrast, other research suggests that ROS scavengers are unable to protect against necroptosis cell death in HT-29 colorectal carcinoma cells. One current theory is that ROS might be required for necroptosis which is dependent on RIP3 activation through its upstream interactions with RIP1, whereas RIP3 oligomerisation independent of RIP1 does not require ROS (Schenk and Fulda, 2015). These studies did not distinguish between total ROS and superoxide's. One study has shown that the suppression of mitochondrial superoxides through antioxidants had reduced RIP signalling (Huang et al., 2013). Therefore, it was important for this current study to analyse the involvement of both total ROS and superoxides in IM-induced cell death.

The current ICC approach showed no signs of total ROS production; however there was an increase in superoxides after 24 h of IM exposure; which was further increased after 48 h before plateauing. One theory for this could be due to the damage or impairment to the Δψm (Echtay et al., 2002; Skulachev, 1996). The impaired mitochondria cause the release of superoxides and

therefore cause an increase in the interaction between RIP1 and RIP3 as previously described. Overall the current superoxide study is limited as the experimental design involved a low sensitivity technique of fluorescent imaging and manual counting; further experiments would be needed to confirm these findings. Experiments could include the use of antioxidants such as mitoTEMPO or antioxidant superoxide dismutase to see if the superoxide expression is reversible. Following this, an immunoprecipitation assay involving RIP1 and RIP3 could help explore whether the superoxide production is linked to the necroptosis cell death. If antioxidants helped the viability of these cells by interfering with ripoptosome formation, this should be an easy and simple method to implement into clinical studies to help with IM-induced side effects.

4.3.6 Trough concentrations of imatinib are toxic to cardiac progenitor cells and do not initiate apoptosis

Finally, it was important that this study addressed the long-term implications of IM by assessing the toxicity of trough concentrations over a 7-d period. As shown in the data IM caused a significant reduction in CPC viability after 5 μM IM exposure for 7 d, which was reinforced by live-cell staining for ToPro-3. The ToPro-3 staining was significantly increased in CPCs after IM exposure and had increased ToPro-3 positive cells compared to the peak concentration. The staining showed no evidence of apoptosis shown by an absence of staining for caspase 3 and caspase 7 activity. These trough data seem to indicate a similar cell death pathway as the peak concentration. The changes in gene expression also showed no significant increase in either apoptosis-associated

genes or necroptosis genes, consistent with the peak concentration. However, the limiting factor for the trough concentration study was the limited data, with no experiments assessing the involvement of necroptosis or autophagy. Therefore, future work suggested would be to investigate the involvement of necroptosis through protein assays, with following on assays for autophagic flux and ROS/superoxide contributions. These data do reinforce that even a low dose of IM over an extended period of time can be toxic to CPCs.

4.3.7 Conclusions

In summary, our study demonstrated a range of impacts caused by clinically used cardiotoxic drug IM on human CPCs. These data suggest a possible mechanism of cell death in CPCs; starting with IM being sequestered by the lysosomes causing an impaired autophagic flux. This impaired flux is likely to release ions such as zinc which can impair the Δψm. This impaired membrane potential will lead to the production of superoxides, helping to form the ripoptosome. Another contributing factor toward the ripoptosome formation is the accumulation of p62 within the cell's cytosol, released from autophagosomes due to impaired autophagic flux. All these factors eventually lead to cell death through necroptosis (**Figure 4.3.1**). Therefore, our study identified two possible targets to overcome IM-induced toxicity on CPCs through either the inhibition of upstream autophagy or via the inhibition of necroptosis.

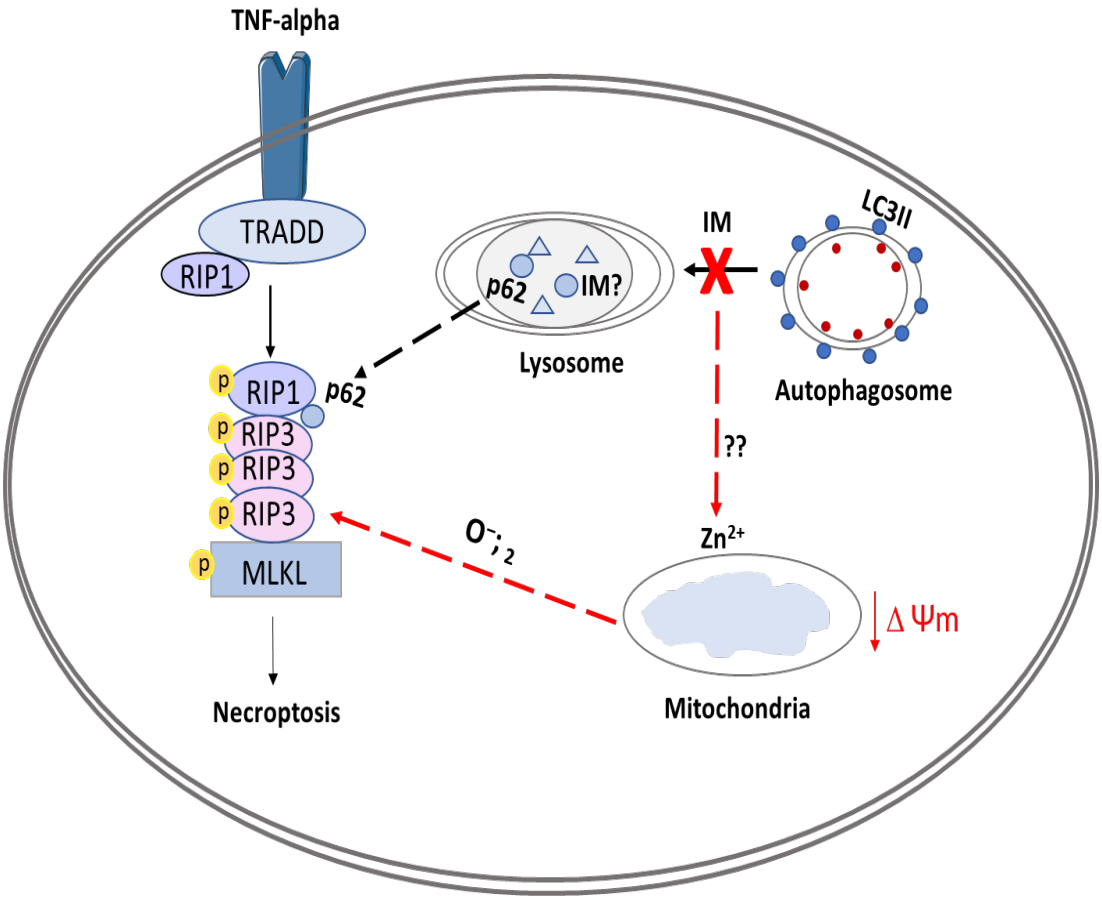

Figure 4. 14. Schematic overview of proposed model for IM-induced cell death in CPCs. The figure shows IM being sequestered by the lysosomes, causing an impaired autophagic flux. This abnormal flux causes the release of zinc ions which affect the Δψm leading to production of superoxides ($O^{-}_{;2}$);these superoxide ions can help form the ripoptosome. The ripoptosome formation is also aided by leakage of p62 proteins from lysosomes and autophagosomes. Finally, the ripoptosome formation causes the activation/phosphorylation of MLKL and initiates necroptosis cell death.

Chapter 5. Sunitinib induced cardiac progenitor cell death

5.1 Introduction

Sunitinib is used to treat patients with GISTs, RCC and pancreatic neuroendocrine tumours. Sunitinib is a non-selective inhibitor of targets such as VEGFR 1-3, PDGFR α and β and *c*olony stimulating factor 1(Chu et al., 2007).

The survival of patients presenting with IM-resistant GISTs has vastly improved since the introduction of SM, with one study showing that SM treatment led to a significant increase in the median progression-free survival, compared to patients treated with interferon alfa (Motzer et al., 2007). A separate study assessing the impact of SM on GIST patients showed a tumour progression time of 27.3 weeks in patients receiving SM, compared to 6.4 weeks in those in the placebo group (Demetri et al., 2006).

Clinical studies have shown SM-induced cardiac effects: one single-arm, blinded study showed dose-dependent QT prolongation involving patients with advanced solid tumours (Bello et al., 2009). A phase 3 randomised trial examined SM-treated patients with metastatic RCC against patients treated with interferon alfa-2a: 10% of the SM group demonstrated a reduction in LVEF below the normal range, with 0.2% of patients experiencing a grade 3 decline in LVEF (LVEF of 20% to 39%) (Motzer et al., 2009b). Patients with GISTs treated by SM also showed signs of cardiotoxicity, with a decline in LVEF seen in 11% of treated patients, compared to 3% in the placebo group (Chu et al., 2007). A meta-analysis has been used to evaluate the risk of HF development in patients taking SM therapy for RCC; this study excluded

patients with a history of cardiac events and evaluated a total of 6935 patients from both randomised and non-randomised studies (Richards et al., 2011).

Previous findings in our research group have confirmed similar results at the cellular level, in both cardiac fibroblasts and cardiac progenitor cells. Sunitinib is toxic to both cardiac fibroblasts and CPCs at the clinically-comparable concentrations shown by reduced cell viability (Burke et al., 2019; Smith et al., 2018). The key findings were that SM caused reduced proliferation and reduced expression of IL1B in adult rat fibroblasts (Burke et al., 2019). In CPCs, SM caused a decline in cell survival proteins such as AKT and p63 and HGF. Sunitinib was delivered into a rodent model for 9 d *in vivo,* impairing cardiac function (68%) relative to both baseline (83%) and control (84%) (Smith et al., 2018) . These findings highlight the importance of assessing the toxicity of SM to the different cell types found within the myocardium.

This chapter aims to identify the cell death pathways involved in SM-induced toxicity in human CPCs, to provide further knowledge to the field.

5.2 Results

5.2.1 Sunitinib-induces cell death within cardiac progenitor cells at both peak and trough concentration

Cardiac progenitor cell viability was reduced by 26.5 ± 6.6% after 2 μM SM treatment and was also declined by 69.6 ± 4.4% after 20 μM SM for 24 h *vs.* control 100 ± 9.5% (n=8, $p<0.05$, **Figure 5.1A**). Cells treated with trough concentrations of SM for 7 d showed a reduced cell viability by 32.0 ± 12.3% after 0.5 μM treatment and further declined by 72.3 ± 11.3% after 5 μM treatment *vs.* control 100 ± 5.8% (n=8, $p<0.05$, **Figure 5.1B**). There were no significant effects seen below the peak and trough clinically-comparable concentrations.

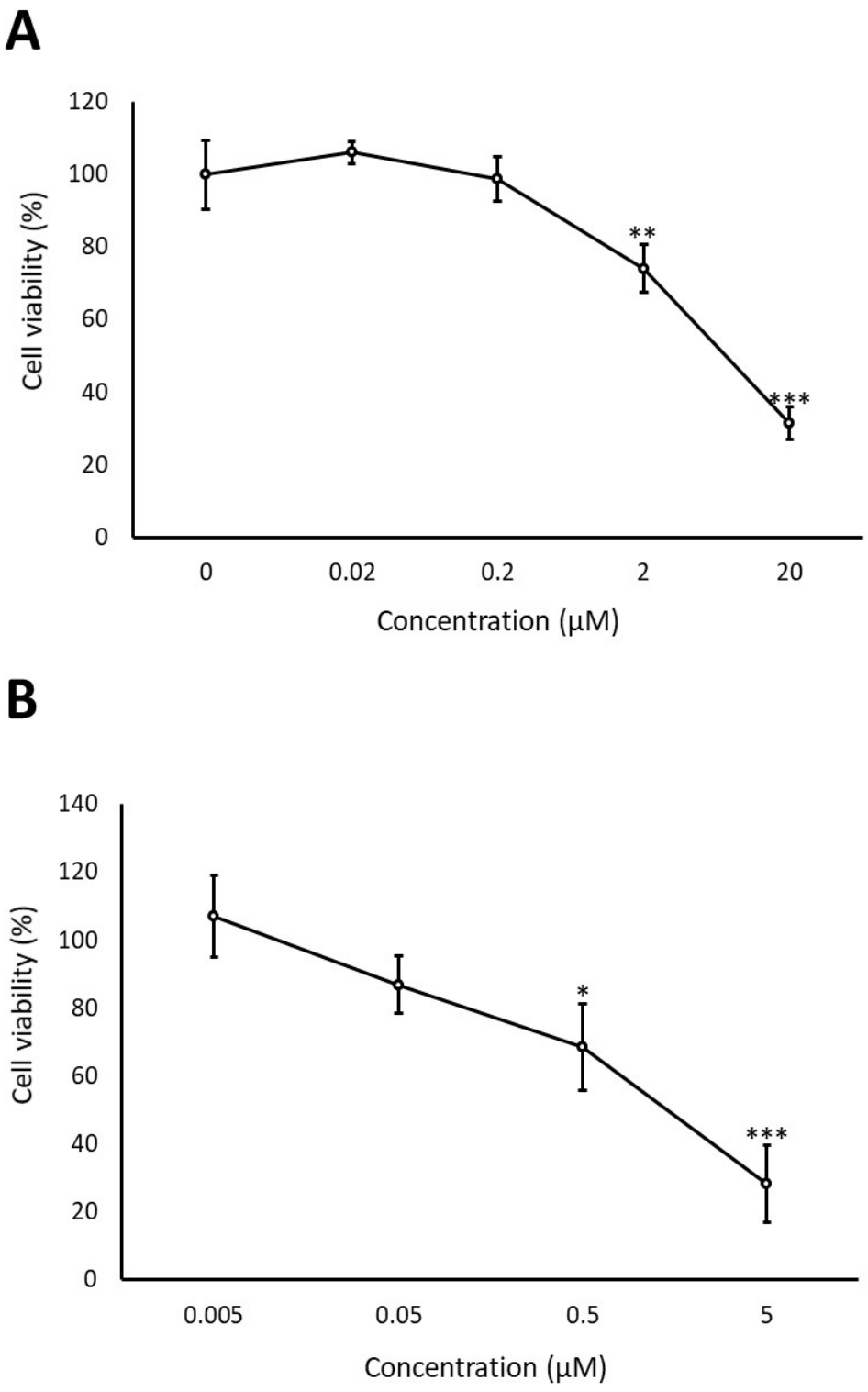

Figure 5. 1. Changes in cell viability after SM exposure. CPCs were treated with a range of SM concentrations and cell viability. **(A)** Cells treated with 0.02, 0.2, 2 or 20 µM SM for 24 h before assessment of viability **(B)** Cells treated with 0.005,0.05,0.5 or 5 µM IM for 7 d. Data are mean±SEM, n=8; *p<0.05, **p<0.01, ***p<0.001, ANOVA with *post hoc* Tukey's test.

5.2.2 Assessment of caspase activity in cardiac progenitor cells after sunitinib exposure

The same procedures were applied as previously discussed in Chapter 4.2.2, to identify the involvement of apoptosis within SM-induced cell death; including live-cell staining and high content image analysis to determine the presence of activated caspase 3/7, ToPro-3 and TMRM. Sunitinib showed an increase in activated caspase 3/7, within the cytoplasm (red); the images also showed visually reduced staining for TMRM with increased concentration of SM (n=4, **Figure 5.2A**). The treatment increased the presence of staining of ToPro-3 from 2.5 ± 0.3% (control) to 4 ± 0.8% (2 μM) and 14 ± 2% (20 μM) ($p<0.05$, **Figure 5.2B**). Quantification of caspase activity reinforced the increase in activation from 0.0 ± 0.0 (control), to 1.2% ± 0.2 (2 μM) and 23% ± 2.5% (20 μM) of SM treatment ($p<0.05$, **Figure 5.2C**).

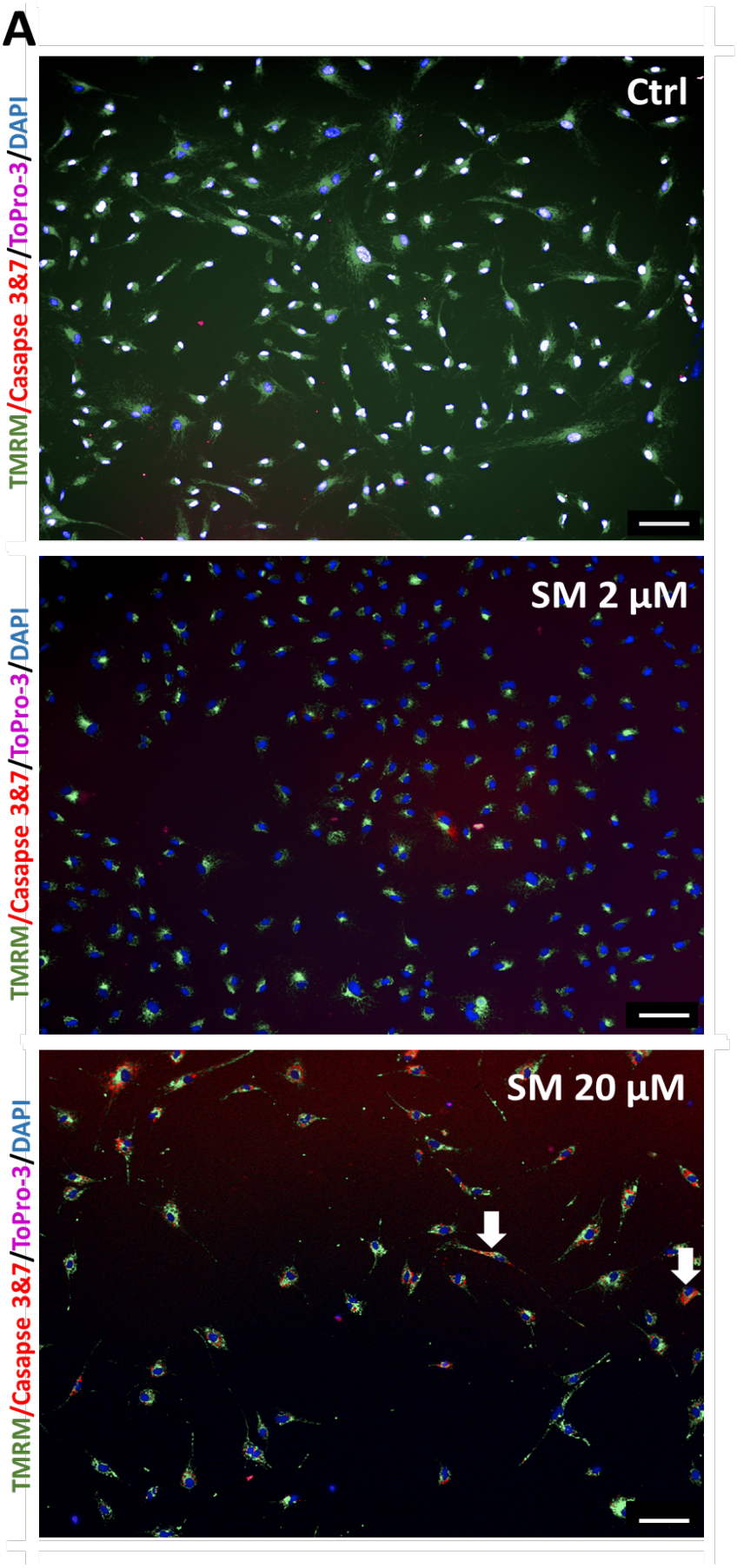
A
TMRM/Casapse 3&7/ToPro-3/DAPI
Ctrl
TMRM/Casapse 3&7/ToPro-3/DAPI
SM 2 µM
TMRM/Casapse 3&7/ToPro-3/DAPI
SM 20 µM

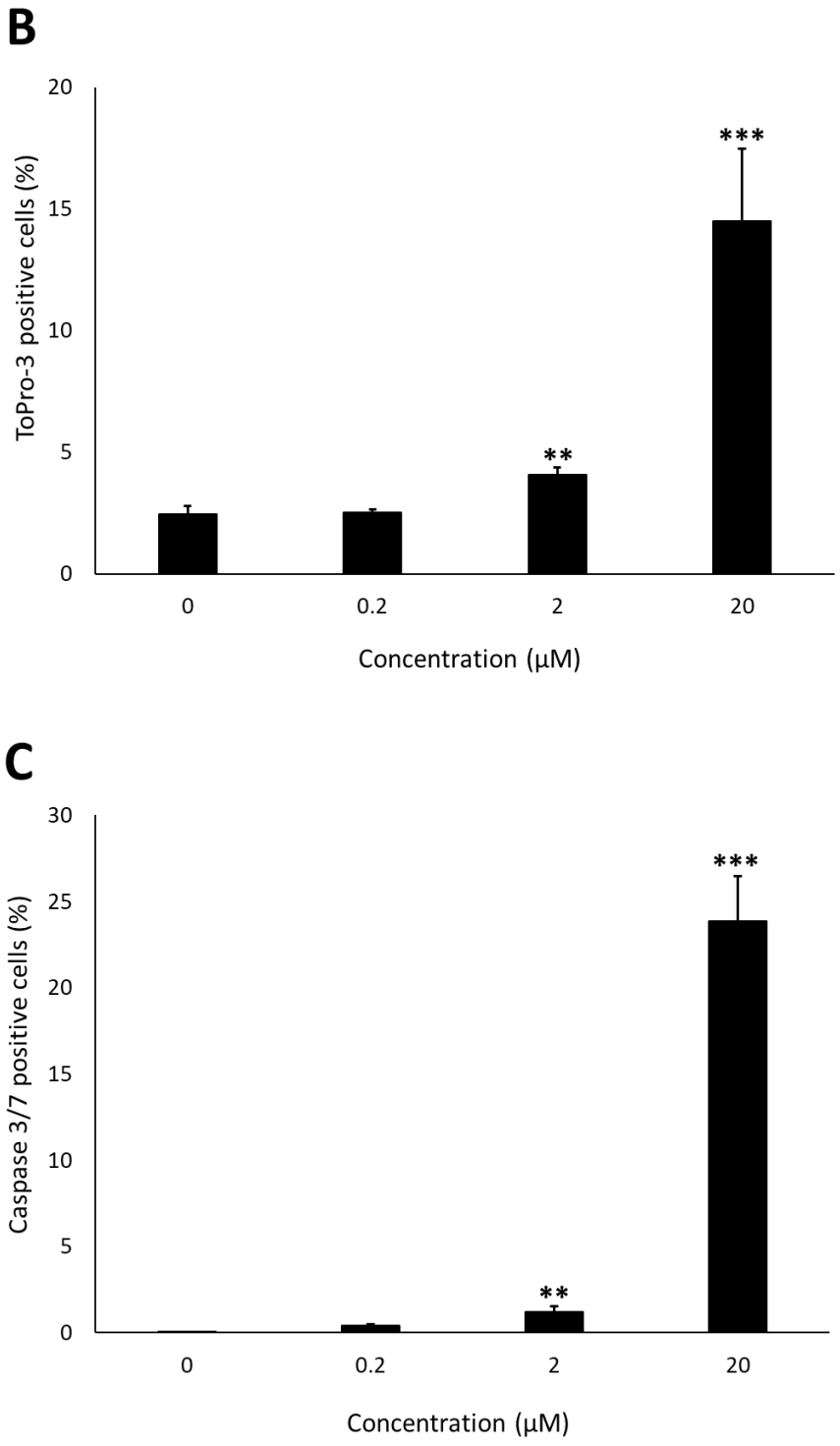

Figure 5. 2. Identifying the activation of executioner caspases and presence of ToPro-3 in CPCs after SM 24 h treatment. (A) Images of untreated cells and cells treated with 2 µM or 20 µM SM and stained for TMRM (dark green), ToPro-3 (magenta), and caspase 3/7 (red). Control cells showed no caspase 3 and 7 activation, however red signal was seen in CPCs treated with 2 µM and 20 µM SM. SM treated cells showed low ToPro-3 staining **(B)** Quantification of ToPro-3 positive cells after 0-20 µM SM treatment. **(C)** Quantification of caspase staining after 0.2, 2 and 20 µM SM treatment *vs.* untreated control cells (0 µM). Data are mean±SEM, n=4, *p<0.05, ***p<0.001, scale bar=100 µM, ANOVA with *post hoc* Tukey's test.

Following this, cells were incubated with a general caspase inhibitor (Z-VAD-FMK) which inhibits a range of caspase activity including caspase 3 and caspase 7. Two methods were applied: cells were either pre-treated for 1 h or co-treated over 24 h with/without 20 μM Z-VAD-FMK and with or without SM (2 μM). Both methods showed no improvement in viability after caspase inhibition, with pre-treatment viability ranging from 86.5 ± 6.9% of cells treated with 2 μM SM only, to 89.1 ± 3.7% when SM treated cells were pre-treated with Z-VAD-FMK. Cells treated with 20 μM SM only showed reduced viability to 67.5 ± 1.2%, which was unchanged with Z-VAD-FMK pre-treatment to 70.1 ± 0.7% (n=3, $p>0.05$, **Figure 5.3A**).

There was also no effect on CPC viability when SM was co-treated with 20 μM Z-VAD-FMK; 0 2 μM SM reduced viability to 88.5 ± 6.9%, when the cells were co-treated this remained unchanged at 83.2 ± 3.7%. There was no significant difference between cells treated with 20 μM SM only (58.2 ± 1.1%) and cells treated with 20 μM SM plus Z-VAD-FMK (51.3 ± 6.5%). The control cells showed no reduction in viability when either pre-treated or co-treated with Z-VAD-FMK (n=3, $p<0.05$, **Figure 5.3B)**.

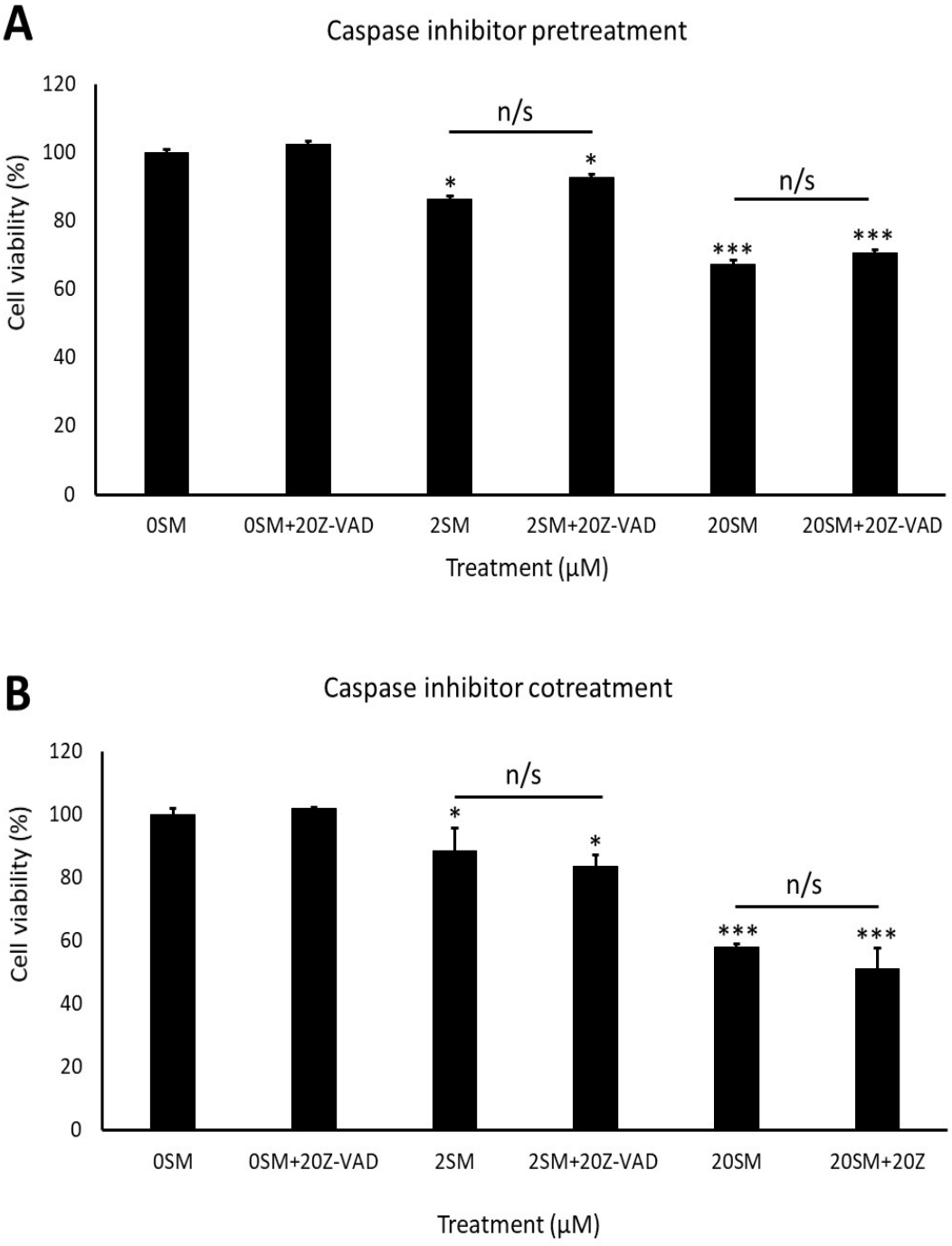

Figure 5. 3. SM-induced cell death was not rescued by general caspase inhibition. (A) Cell viability analysis of cells pre-treated with 20 µM caspase inhibitor Z-VAD-FMK (inhibitor) for 1 h; ctrl cells, ctrl cell pre-treated with inhibitor, 2 µM SM alone, 2 µM SM pre-treated with inhibitor, 20 µM alone and 20 µM SM pre-treated with inhibitor **(B)** Cell viability analysis of cells treated with 20 µM inhibitor for 24 h; ctrl cells, ctrl cells treated with inhibitor, 2 µM SM alone, 2 µM SM co-treated with inhibitor, 20 µM SM alone and 20 µM SM co-treated with inhibitor. Data are mean±SEM, n=4. *p<0.05, ***p<0.001, n/s=not significant, ANOVA with post hoc Tukey's test.

5.2.3 Sunitinib caused high autofluorescence in multiple channels

Cells were treated with 2, 5 and 20 μM SM and analysed using flow cytometry for excitation/emission; 488/525 nm, 561/610 nm, 561/585 nm and 405/450 nm to determine whether SM caused an increased fluorescence in CPCs.

CPCs treated with 2, 5 or 50 μM SM caused an increased fluorescence in the 488/525 nm channel and caused a right shift in intensity (red) compared to the untreated cells (green), with no difference identified between each SM concentration. The untreated cells were gated as negative control (low fluorescence), cells treated with 2,5 or 20 μM SM caused right shift in intensity, whereby 99% of cells had an increased fluorescence *vs.* untreated cells (**Figure 5.4A**). CPCs treated with SM had an increase in fluorescence detected with a 561/610 nm channel. The untreated cells were gated for baseline fluorescence, 2 μM SM caused a 1% increase, 5 μM SM caused 4% increase and 20 μM SM caused 88% of cells to have increased fluorescence (**Figure 5.4B**).

Cells treated with SM caused no change in fluorescence when detected with a 561/585 channel; all events were detected at the same intensity as the untreated cells (grey), and no right shift was detected after cells treated with SM (red) (**Figure 5.5A**). There was also no change detected with the 405/450 channel, control events (blue) and no right shift seen when cells treated with SM (red) (**Figure 5.5B**).

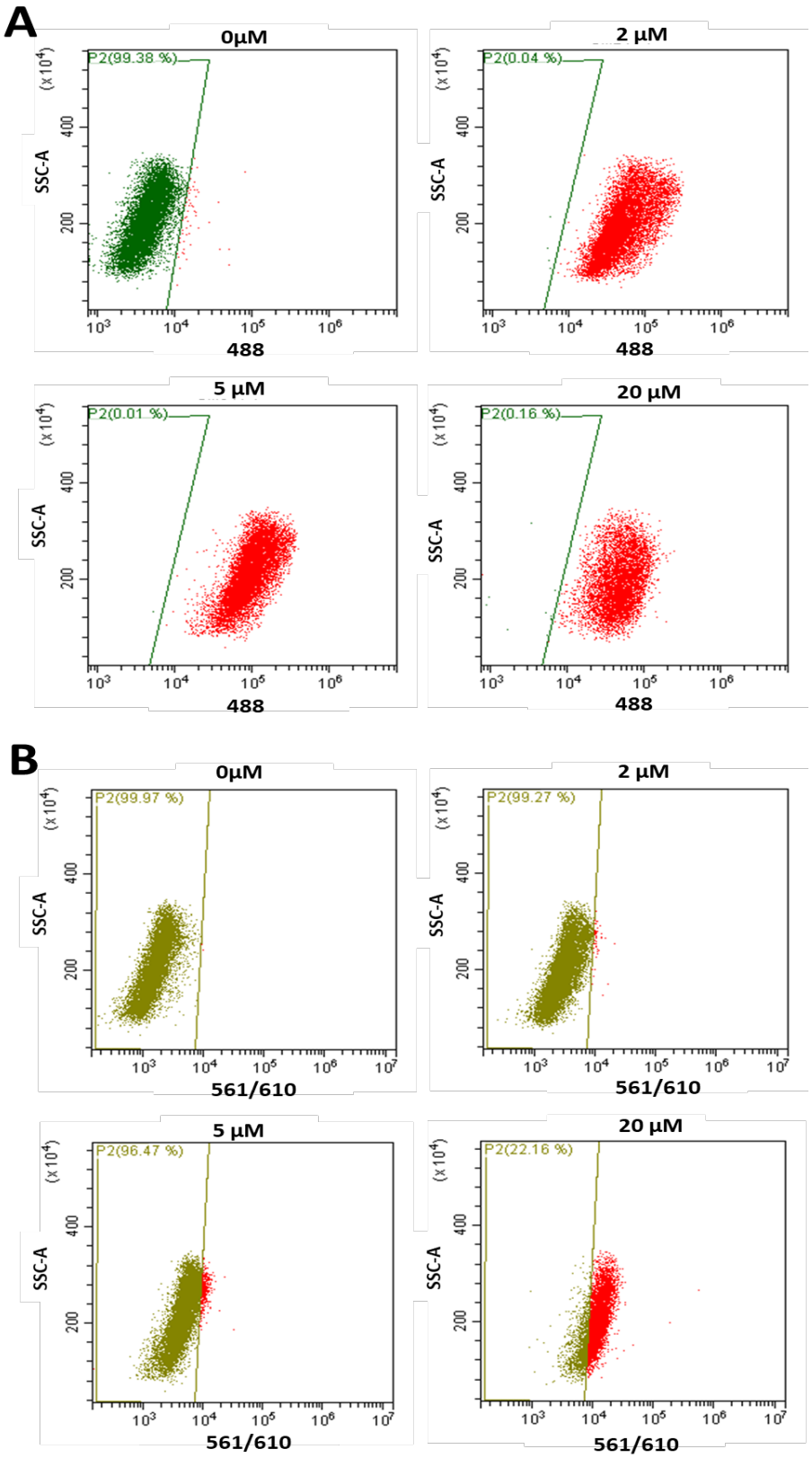

Figure 5. 4. SM autofluorescence assessed by flow cytometry (A) Ctrl cells were gated as a marker of background florescence (green), 2 µM, 5 µM and 20 µM SM showed right shift in 488 nm florescent intensity **(B)** Ctrl cells were gated as a marker of background florescence (yellow), 5 µM and 20 µM SM showed right shift in 561/610 nm florescent intensity.

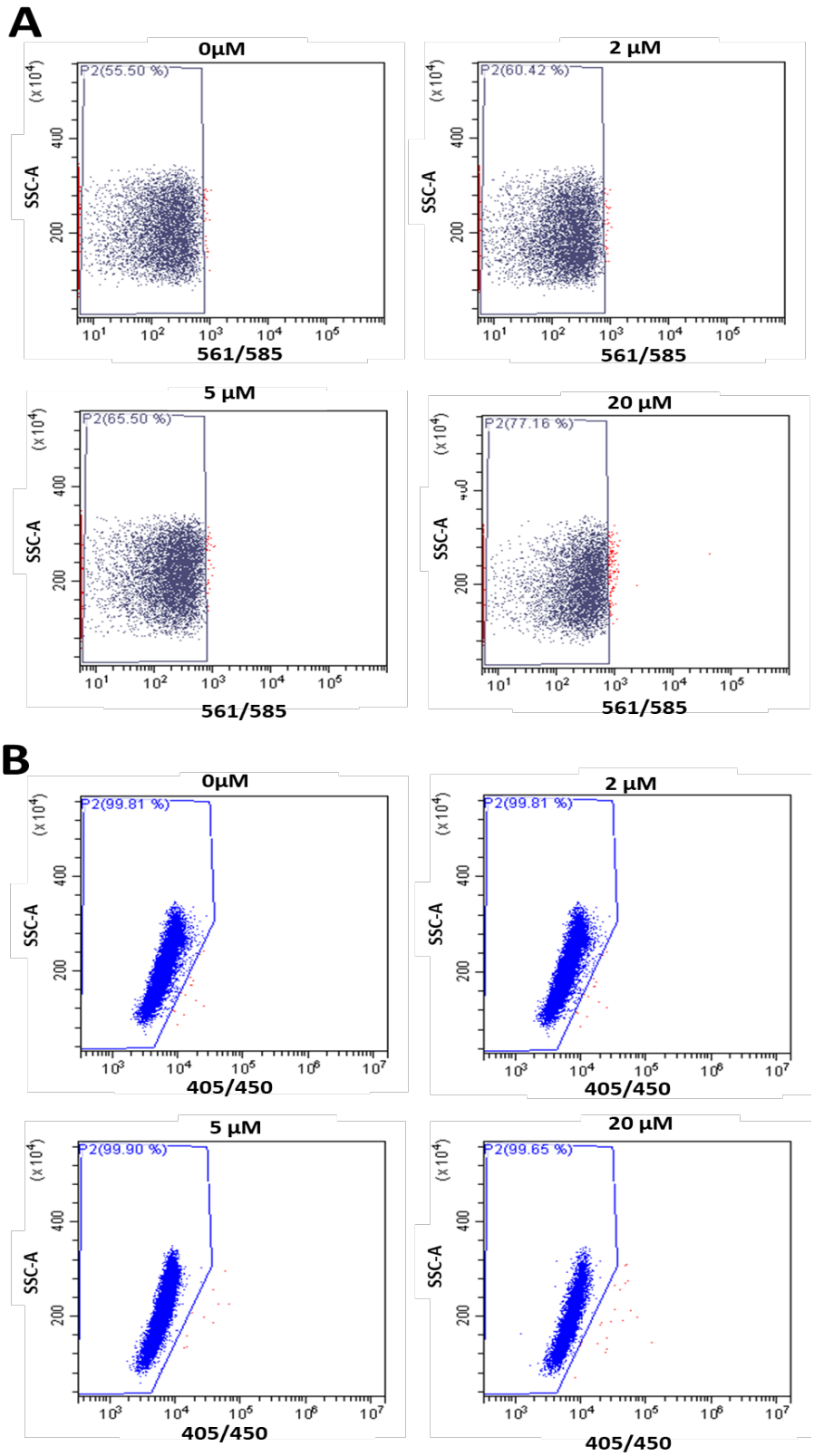

Figure 5. 5. SM autofluorescence assessed by flow cytometry (A) Ctrl cells were gated as a marker of background florescence (grey), 2 µM, 5 µM and 20 µM SM showed no right shift in 561/585 nm channel. **(B)** Ctrl cells were gated as a marker of background florescence (blue), 5 µM and 20 µM SM showed no right shift in 405/450 nm channel.

Confocal microscopy was also used to detect any changes in fluorescence caused by SM using excitation 405 nm, 488 nm, 555 nm and 647 nm. There was low background fluorescence detected in the 405 nm channel, high fluorescence was seen with the 488 nm and 555 nm channel, no fluorescence was detected using a 647 nm laser (**Figure 5.6A**).

These data showed an increase in fluorescence when cells were treated with SM in the 488 nm and 555 nm channels. We next confirmed that this property of SM had not interfered with our cell viability analyses, as fluorescein was excited with a 488 nm laser. Cells were treated with SM (2, 5 or 20 μM), followed by direct detection of SM fluorescence; no difference in fluorescence was seen relative to SM-untreated controls ($n=3$, $p>0.05$, **Figure 5.6B**).

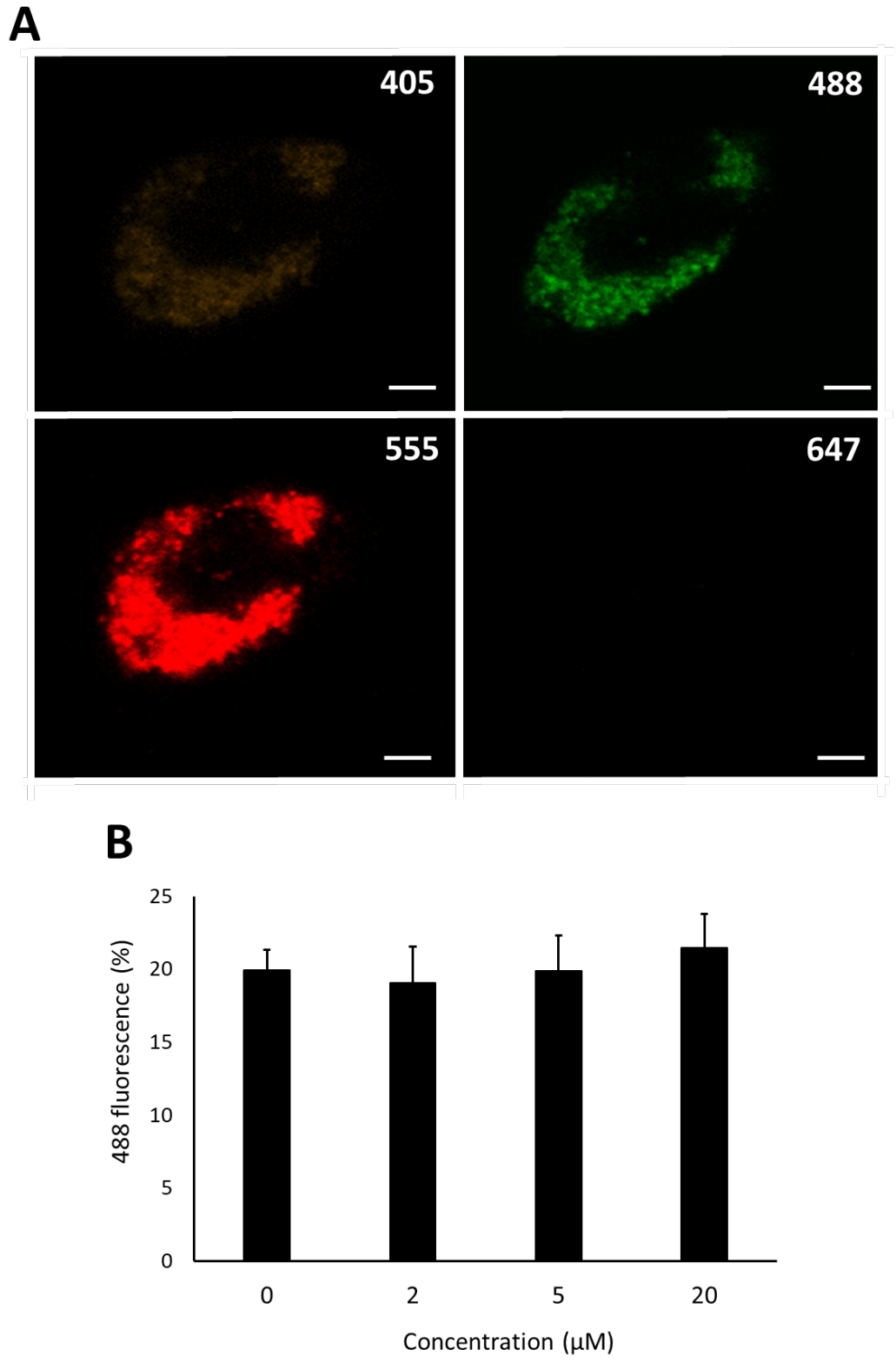

Figure 5. 6. SM autofluorescence assessed by florescent microscopy and plate reader (A) 20 µM SM treated cells imaged with 405 nm, 488 nm, 555 and 647 filter. Signal seen in 405 nm, 488 nm and 555 nm channel **(B)** Cells were treated with 2 µM, 5 µM and 20 µM SM and imaged using Virkon plate reader with 488 nm laser, no differences were seen when compared to control cells (0 µM). n=3, Data are mean±SEM. $p>0.05$, ANOVA with *post hoc* Tukey's test.

5.2.4 Sunitinib exposure increased expression of genes and proteins associated with apoptosis in CPCs

Although the staining of activated caspase 3 and 7 appeared to be a false positive result, due to the autofluorescent properties of SM; it was important to rule out genes and proteins associated with apoptotic cell death. Real time RT-qPCR was used to detect changes in apoptosis-associated gene expression, to investigate the possible apoptotic pathway involved in SM-induced cell death after CPCs were exposed to 2 μM SM for 24 h. Analysis of relative gene expression data showed that the largest gene products were PARP followed by; FAS, JNK, RAF-1, BAX, caspase 8, caspase 9, BCL-2, calpain, BID and TNF-alpha for cells treated with 2 μM SM (n=3, **Figure 5.7A**). The overall increases in foldchange seen after 2 μM SM treatment for 24 h: calpain (3.1 ± 0.73), FAS (2.3 ± 0.8), BAX (1.9 ± 0.2) and BCL-2 (downregulation of 3.5 ± 0.0) *vs.* control (1.0 ± 0.0) (n=3, $p<0.05$, **Figure 5.7B**).

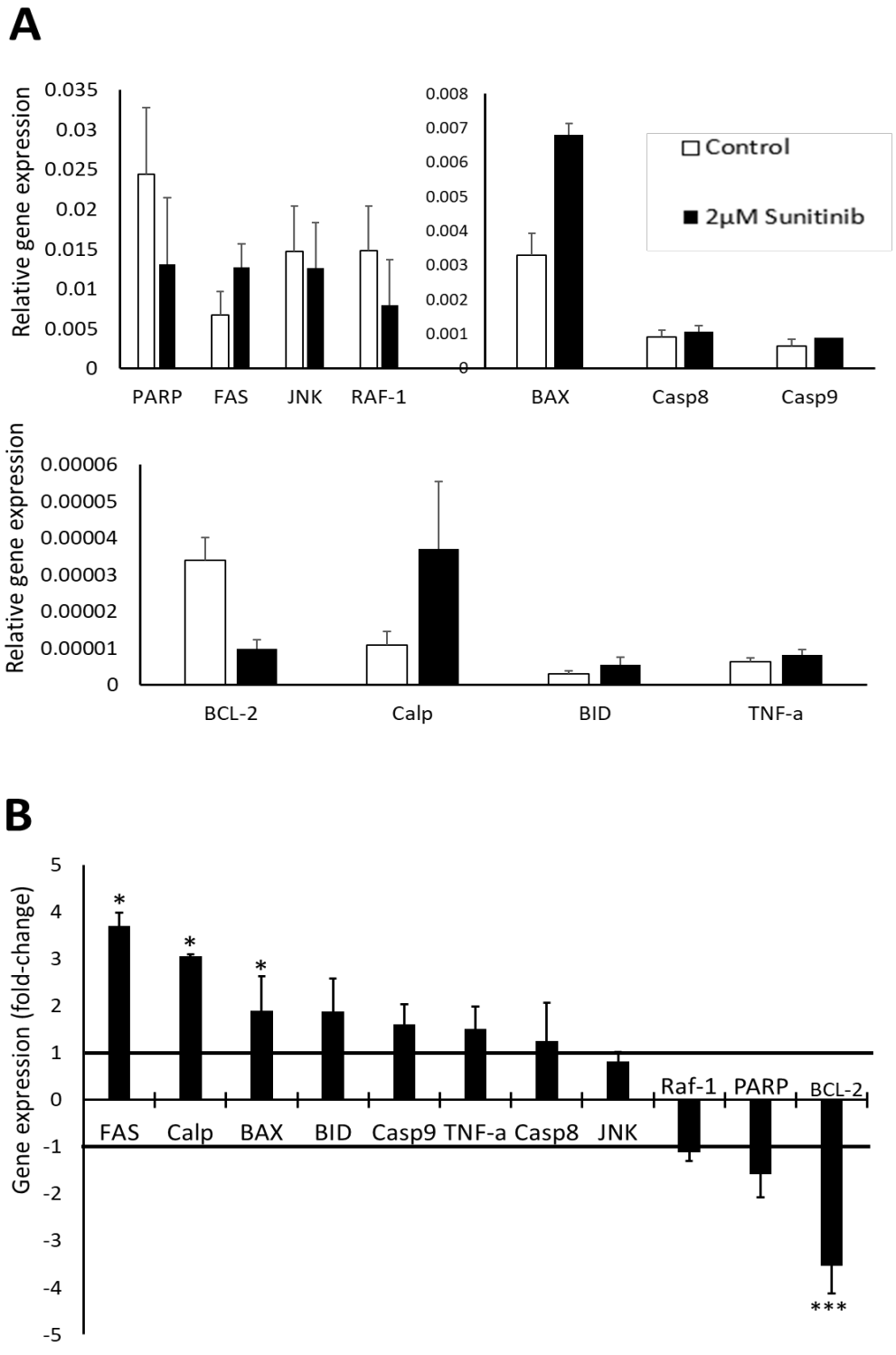

Figure 5. 7. Changes in gene expression in CPCs after exposure to 10 µM SM for 24 h. **(A)** Gene expression (relative to β-actin) in control (white) and SM-treated (black) samples, for a range of cell death-associated genes. **(B)** Changes in gene expression over control (control = +1.0 and -1.0; solid line); negative values represent reduced gene expression. Data are **(A)** Δcq±SEM or **(B)** ΔΔcq±SEM, n=3, *t*-test.

It was important to confirm that changes in gene expression after 2 μM SM treatment for 24 h translated to protein expression; therefore, changes in apoptosis-associated proteins were investigated by Western blotting. Cells treated with SM visually increased protein expression of calpain 1, FASR and BAX *vs.* control cells (**Figure 5.8A**). Densitometry values reinforced these differences with calpain-1 showing the greatest increase in protein expression with a 2.5 ± 0.5-fold increase ($n=3$, $p<0.05$); however, calpain-2 showed no significant change (1.4 ± 0.2 relative to control) ($n=3$, $p>0.05$). The FAS receptor was also increased by 2.1 ± 0.2-fold and BAX 2.1 ± 0.2-fold increase *vs.* control (1.0 ± 0.0) ($n=3$, $p<0.05$, **Figure 5.8B**).

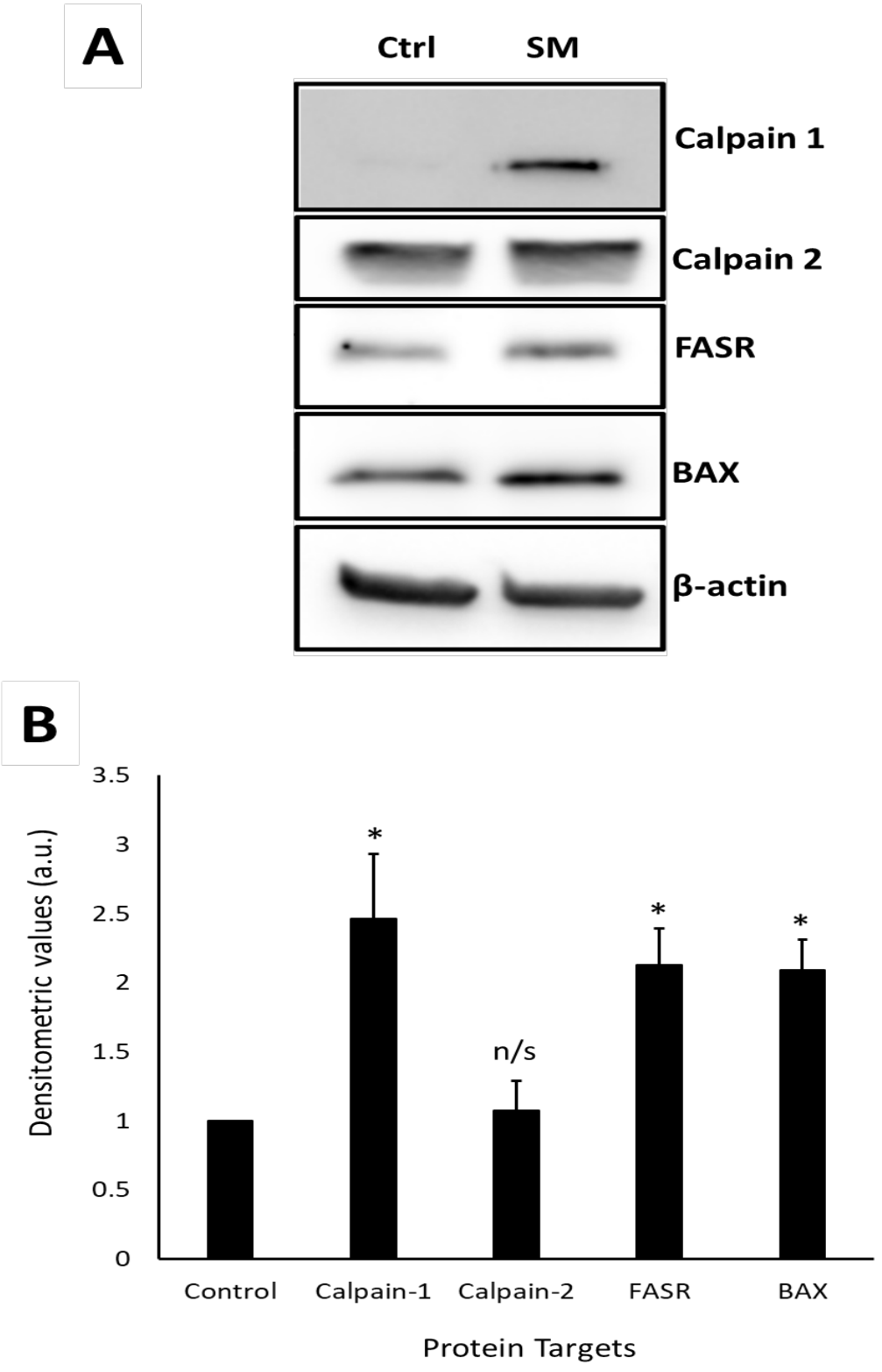

Figure 5. 8. SM increased apoptosis-associated proteins. **(A)** Western blot representative images showing expression of calpain 1, calpain 2, FASR, BAX and loading control β-actin after SM 24 h treatment **(B)** Densitometric values showed increased expression of calpain 1, FASR and BAX *vs.* control. Data are mean±SEM, n=3, *t*-test, *p<0.05, ***p<0.001, n/s=not significant *vs.* control.

After determining an increase in apoptosis-associated proteins, cells were stained using annexin V to replace the previous caspase activity assay which overlapped with SM fluorescence. Cells were treated with SM for 24 h, the cells were then isolated and stained for annexin and analysed using flow cytometry. There was no difference in the scatter graphs, there was no right shift in intensity. However, there was a right shift in intensity when cells were treated with staurosporine (a known apoptosis inducer), with ~50% of cells positive for annexin staining when compared to untreated cells (**Figure 5.9A**).

These data were reinforced by annexin V quantification: 2 μM SM caused a 1.1 ± 0.0, 5 μM 1.3 ± 0.0 and 10 μM 1.5 ± 0.1, but no significant difference seen relative to control ($p>0.05$). Staurosporine-treated positive controls showed a 5.0 ± 0.9-fold increase in annexin relative to control ($n=6$, $p<0.05$, **Figure 5.9B**).

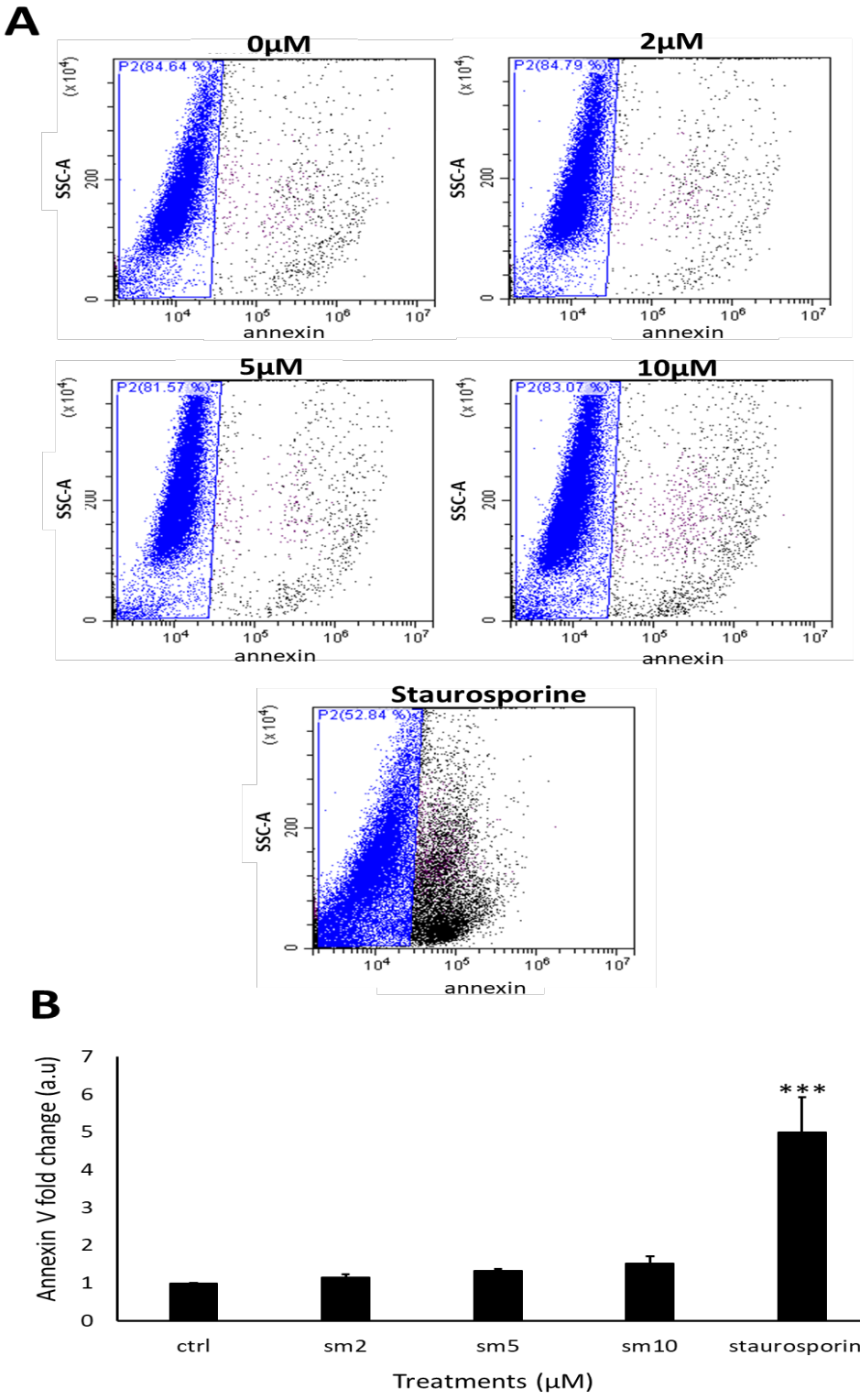

Figure 5. 9. Annexin V staining intensity after SM treatment for 24 h. **(A)** Intensity of annexin V-pacific blue fluorescence following application of SM or Staurosporine, untreated control 0 µM, 2 µM, 5 µM, 10 µM, 10 µM Staurosporine. Viable cells with low signal have been gated in blue, any cells with positive annexin V staining show a right shift in intensity (black). **(B)** Quantification of annexin V MFI, for ctrl cells, 2 µM, 5 µM, 20 µM SM and positive control 10 µM Staurosporine, normalised against control cells (1.0 fold). Data are mean±SEM, n=6, ***p<0.001, ANOVA with *post hoc* Tukey's test.

5.2.5 Sunitinib caused an impaired the mitochondrial membrane potential but was not sequestered by the mitochondria

Cells were maintained *in vitro* and live stained with TMRM to determine SM effects on the Δψm. The untreated cells were gated to determine baseline fluorescence, the fluorescent intensity is left-shifted by SM application, in a dose-dependent manner (**Figure 5.10A**). These data are reinforced by changes in MFI of TMRM: fluorescence was reduced by 2 μM SM treatment to 87.5 ± 1.7% and by 20 μM SM to 53.6 ± 4.4% relative to untreated control (100.0 ± 1.2%) (n=6, $p<0.05$, **Figure 5.10B**).

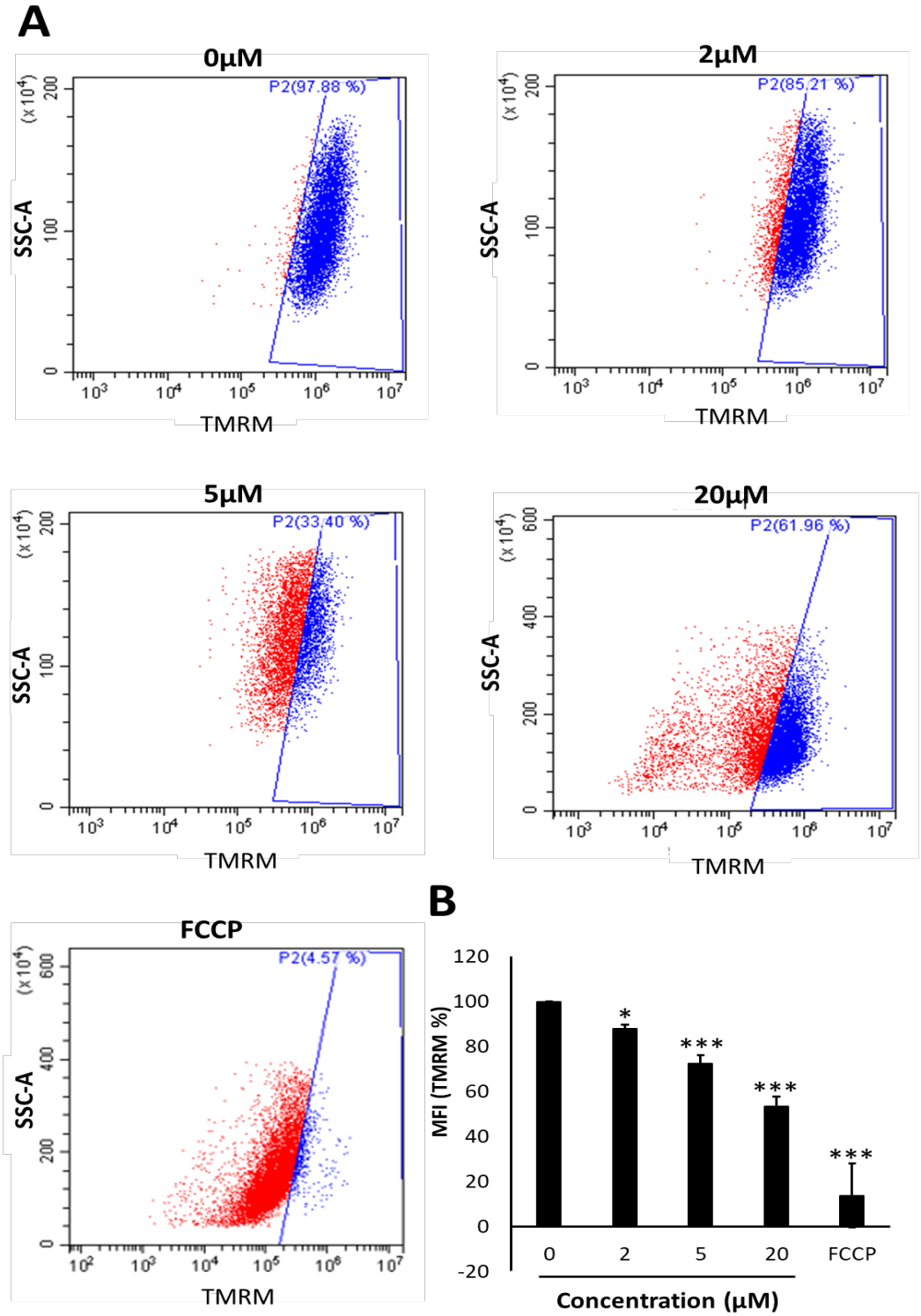

Figure 5. 10. Changes in CPC Δψm after SM exposure. Intensity of TMRM fluorescence following application of SM or FCCP **(A)** untreated control 0 µM,2 µM, 5 µM. 20 µM and 10 µM FCCP. Viable cells with "normal" TMRM signal has been gated in blue, any cells with reduced fluorescence are shown in red. Cells treated with 2 µM SM, 5 µM SM, 20 µM SM and positive control 10 µM FCCP all showed cells with left shift in intensity (red). **(B)** Quantification of TMRM MFI normalised against control cells (100 %). Data are mean±SEM, n=6, **p<0.01, ***p<0.001, ANOVA with *post hoc* Tukey's test.

Confocal microscopy was used to identify any SM sequestration by the mitochondria, as a potential cause of impaired membrane potential. Cells were treated with 10 μM SM for 24 h, followed by TMRM staining as per the previous protocol. Control cells showed positive staining for TMRM (red) and no SM signal (green) (**Figure 5.11A**), while SM-treated cells have both SM signal within the cytoplasm and TMRM staining, the TMRM staining showed no overlap with SM (**Figure 5.11B**). These images were processed using Image J automated threshold settings (isodata) to remove background and nonspecific staining, which confirmed that there was visually no overlap of SM and TMRM (yellow) (**Figure 5.11C**).

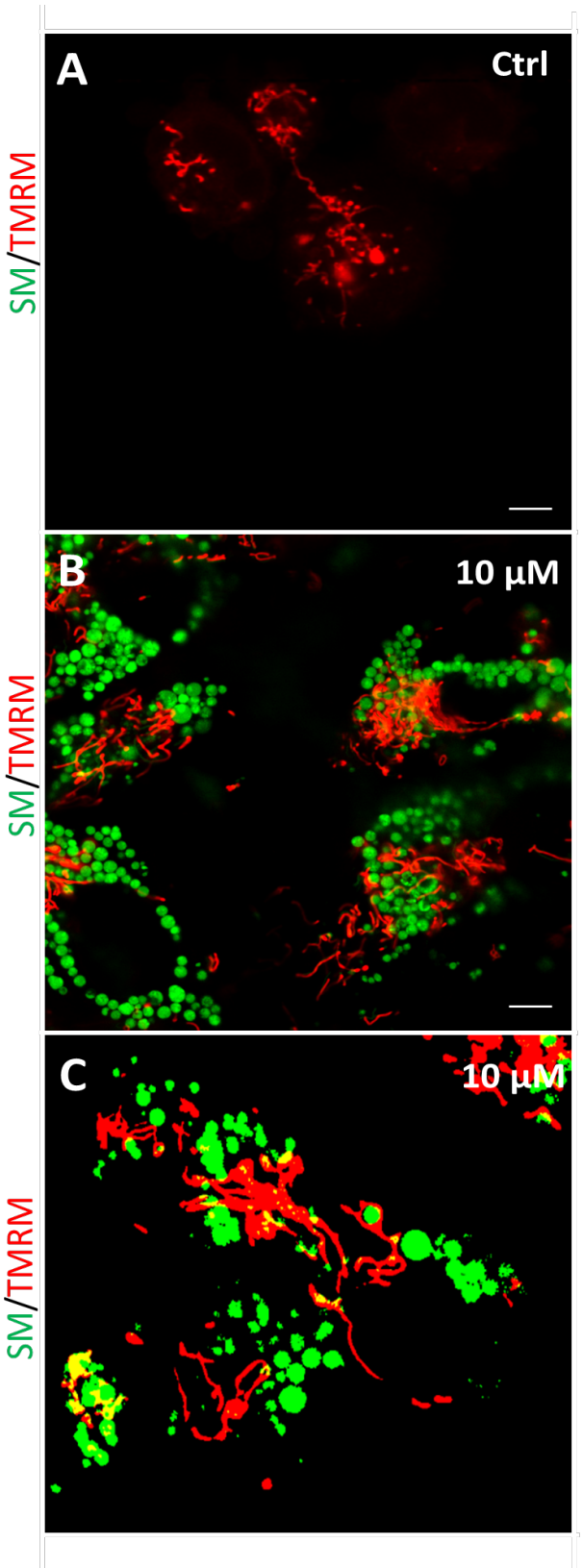

Figure 5. 11. **Cells treated with SM and stained for TMRM**. **(A)** Representative images of SM/TMRM staining showing no SM signal (green) and TMRM staining (red) in untreated cells. **(B)** Cells treated with 10 µM SM shown green signal and TMRM with visually limited co-localisation (yellow). **(C)** Processed image threshold using Image J (isodata) reinforces limited co-localisation between SM and TMRM, scale bar=5 µm.

5.2.6 Sunitinib sequestered by lysosomes and autophagosomes but did not increase lysosomal content

Cells were treated with SM 2, 5 and 10 μM SM for 24 h followed by staining for LAMP2, to determine whether lysosomes sequestered SM. Control cells have positive staining for LAMP2 (red) which is distributed throughout the cytoplasm but the absence of SM signal (green). Cells treated with 2, 5 and 10 μM SM led to increased SM signal, LAMP2 staining remained consistent across doses. Sunitinib and LAMP2 association can be seen to increase with increasing dose of SM, as shown by signal overlap (yellow) (**Figure 5.12A**).

Sunitinib and LAMP2 association were determined using coloc-2 analysis; control cells showed 0.0 ± 0.0 association, 2 μM SM caused 17.5 ± 4.0 in SM/LAMP2 signal (green/red) and 33.3 ± 5.2 LAMP2/SM (red/green) association. The association between SM/LAMP2 was increased after 5 μM treatment to 28.6 ± 6.3 SM/LAMP2 and 47.7 ± 6.8 LAMP2/SM signal. The SM/LAMP2 signal was further increased after 10 μM to 71.3 ± 7.1; however, LAMP2/SM association was decreased to 22.2 ± 1.0 ($n=3$, $p<0.05$, **Figure 5.12B**).

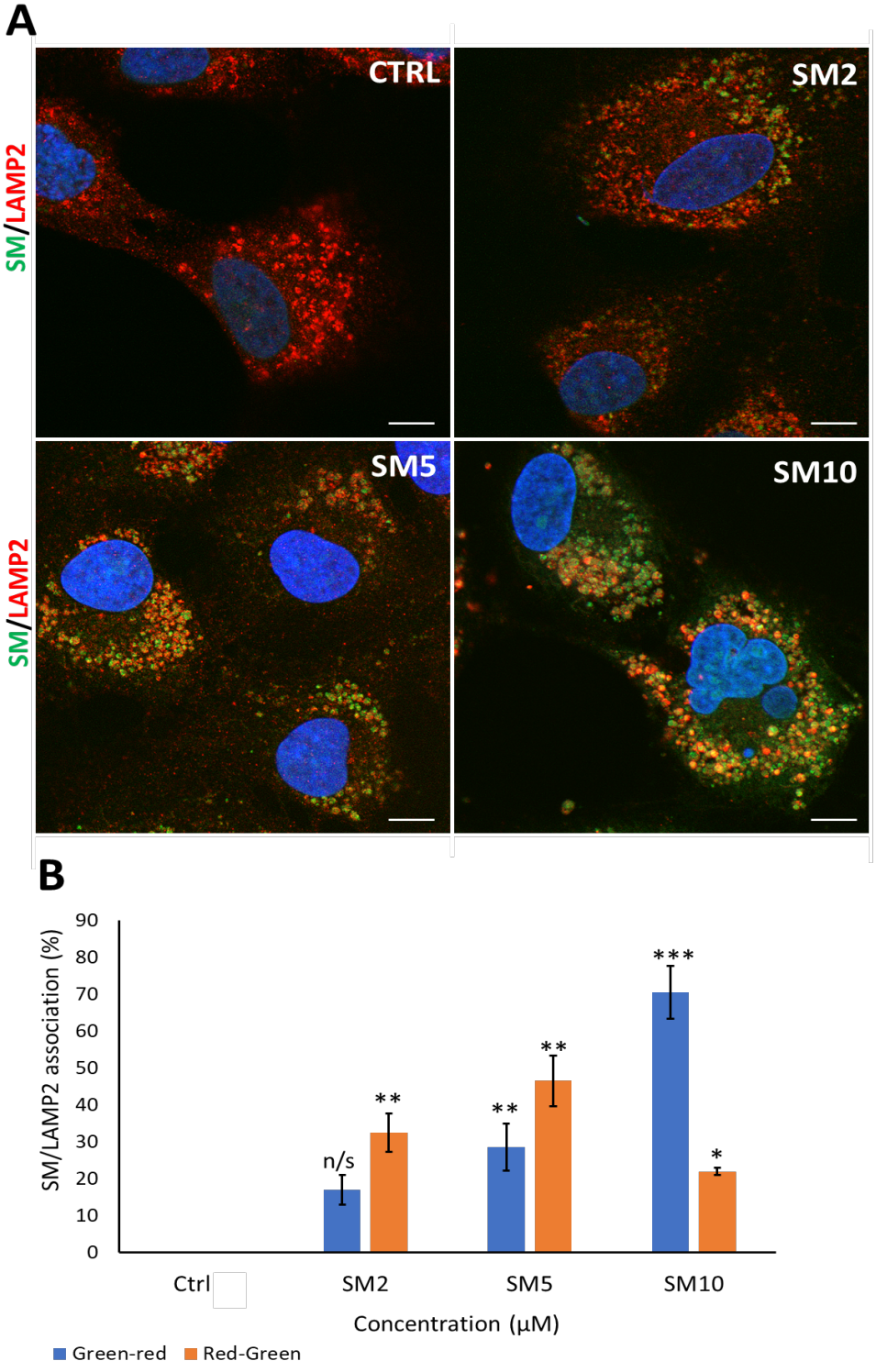

Figure 5. 12. Cells treated with SM and stained for LAMP2. **(A)** Representative images of internalised SM expresion (green) and LAMP2 (red) staining showing no SM signal (green) and LAMP2 staining (red) in untreated cells. 2 µM, 5 µM and 10 µM SM treated cells showed expression of both SM and LAMP2 with increased colocalisation with increased concentration (yellow) **(B)** Colocalisation analysis using Image j platform, quantification of the association between SM/LAMP2 (blue) and LAMP2/SM (orange) after 2-20 µM SM treatment. Data are mean±SEM, n=3, *p<0.05, **p<0.01, ***p<0.01 *vs.* the control. Scale bar=5 µm, ANOVA with *post hoc* Tukey's test.

Following this, the involvement of autophagosomes were investigated by staining SM treated cells with LC3II. Control cells can be seen to have visually weak staining for LC3II (red) and the absence of SM signal (green). Cells treated with 2, 5 and 10 μM SM caused an increase in SM signal, LC3II staining was visually clearer in SM treated cells across all doses. SM and LC3II association were increased as shown by signal overlap (yellow) (**Figure 5.13A**). Sunitinib and LC3II association showed control cells to have 0.0 ± 0.0 association, 2 μM SM caused 44.1 ± 0.1 in SM/LC3II signal (green/red) and 39.5 ± 0.1 LC3II/SM (red/green) association. The association between SM/LC3II was increased after 5 μM treatment to 54.4 ± 0.0 SM/LC3II and 59.3 ± 0.0 LC3II/SM signal. The SM/LC3II signal was further increased after 10 μM SM treatment to 72.2 ± 0.0 however, LC3II/SM association was decreased to 44.3 ± 0.0 ($n=3$, $p<0.05$, **Figure 5.13B**) Although both lysosomes and autophagosomes sequestered SM, SM did not increase AOs Cells were treated with 2 μM SM for 24, 48 and 72 h, followed by acridine orange staining. The signal seen in all samples was low, with no difference in acridine orange staining between control and treated cells (**Figure 5.14 A-D**).

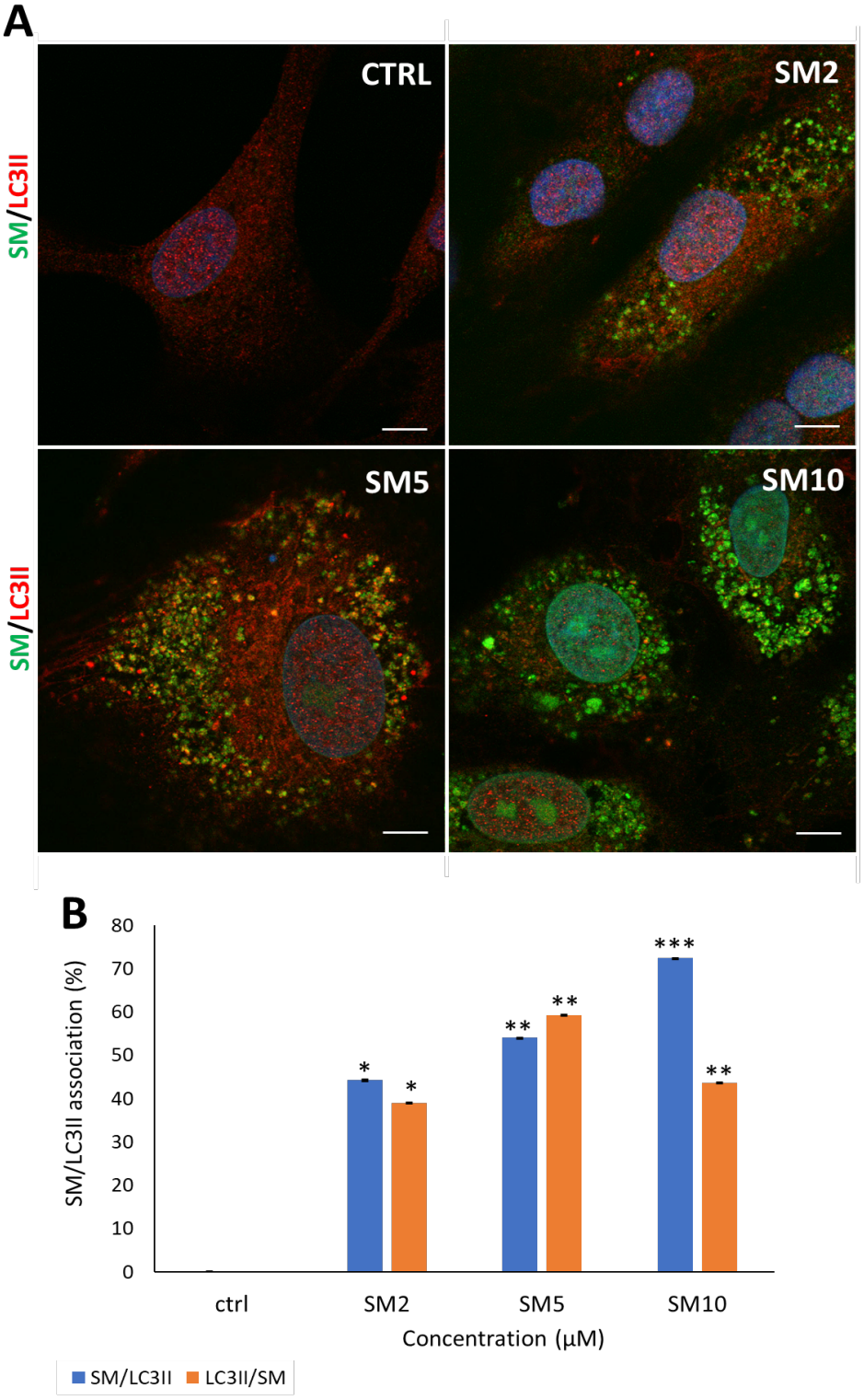

Figure 5. 13. Cells treated with SM and stained for LC3II. **(A)** Representative images of internalised SM expression (green) and LC3II (red) staining showing no SM signal (green) and LC3II staining (red) in untreated cells. 2 µM, 5 µM and 10 µM SM treated cells showed expression of both SM and LC3II with increased colocalisation with increased concentration (yellow) **(B)** Colocalisation analysis using Image j platform, quantification of the association between SM/LC3II (blue) and LC3II/SM (orange) after 2-20 µM SM treatment. Data are mean±SEM, n=3, *p<0.05, **p<0.01, ***p<0.01 *vs.* the control. Scale bar=5 µm, ANOVA with *post hoc* Tukey's test.

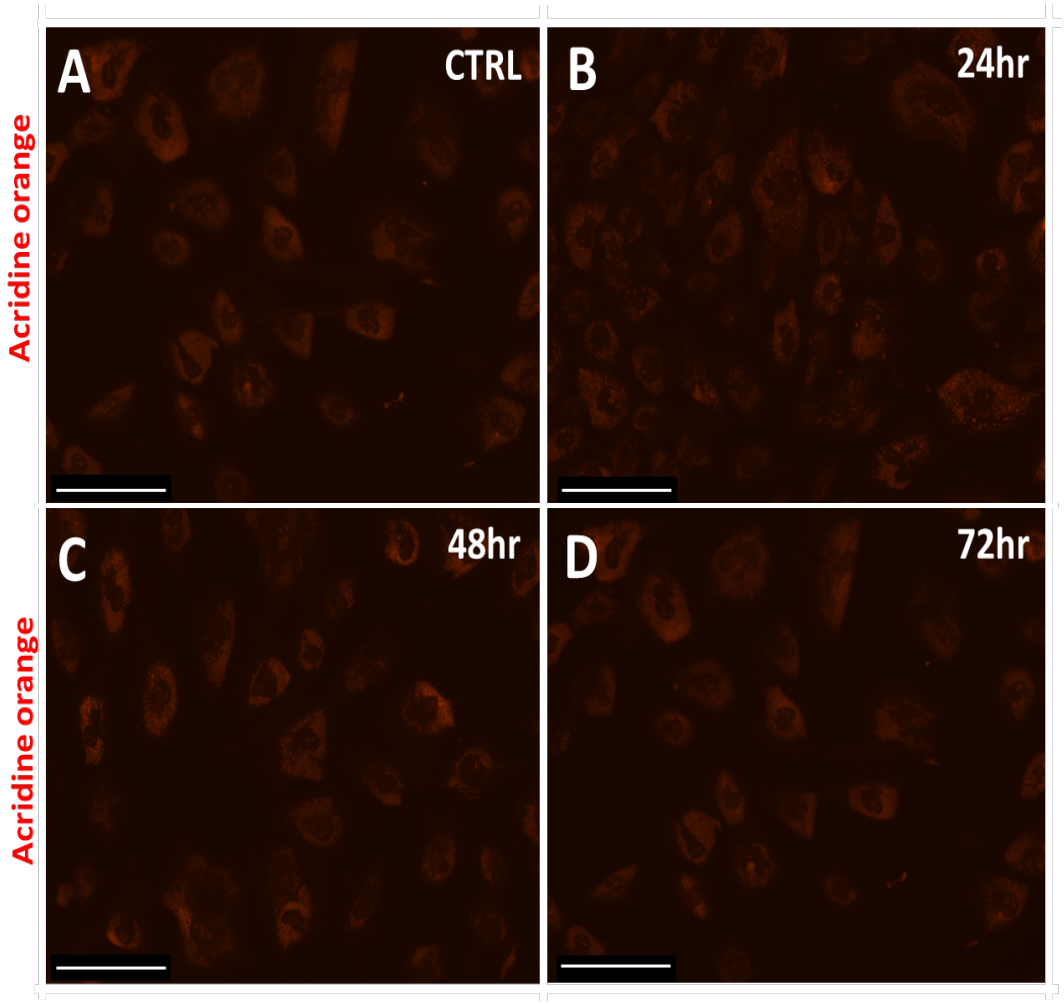

Figure 5. 14. SM did not induce accumulation of acidic vesicle organelles. Representative images of CPCs stained with acridine orange; staining represents AOs in **(A)** untreated control cells and cells treated with 2 μM SM for **(B)** 24 **(C)** 48 and **(D)** 72 h. Scale bar=275 μm.

5.2.7 Sunitinib did not affect calcium reuptake after store operated calcium inhibition, and cell viability is not rescued by calcium chelation

To identify whether calcium was involved in SM-induced cell death, SOCE was investigated and whether chelating calcium helped cell viability as previously discussed in Chapter 4.2.6. Firstly, to examine whether SM effected CPCs ability to recover calcium after depletion of the internal stores by using thapsigargin to inhibit SERCA. The basal calcium remained stable until stimulation with the addition of calcium with or without SM (30 s), the negative control remained relatively flat even after the addition of calcium **(Figure 5.15A**). The maximum change in fluorescence showed 0.2 μM SM; 1.0 ± 0.1-fold increase, 2 μM SM; 1.0 ± 0.1 and 20 μM SM; 0.9 ± 0.1 when normalised against the control (n=5, **Figure 5.15B**).

Although there was no change in calcium reuptake after SOCE inhibition, to confirm calcium was not involved in the death pathway, calcium was chelated with 1 mM EGTA to investigate whether low calcium can rescue CPC viability. There was no significant reduction in cell viability in the control cells with 1 mM of EGTA, however there was a significant reduction in viability to 75.3 ± 1.6% after 2 μM SM treatment and when cells were treated with both SM and EGTA to 77.5 ± 6.2% *vs.* control cells (100 ± 0.0%) ($p<0.05$). There was no significant difference between SM only and SM co-treated with EGTA (n=3, $p>0.05$, **Figure 5.15C**).

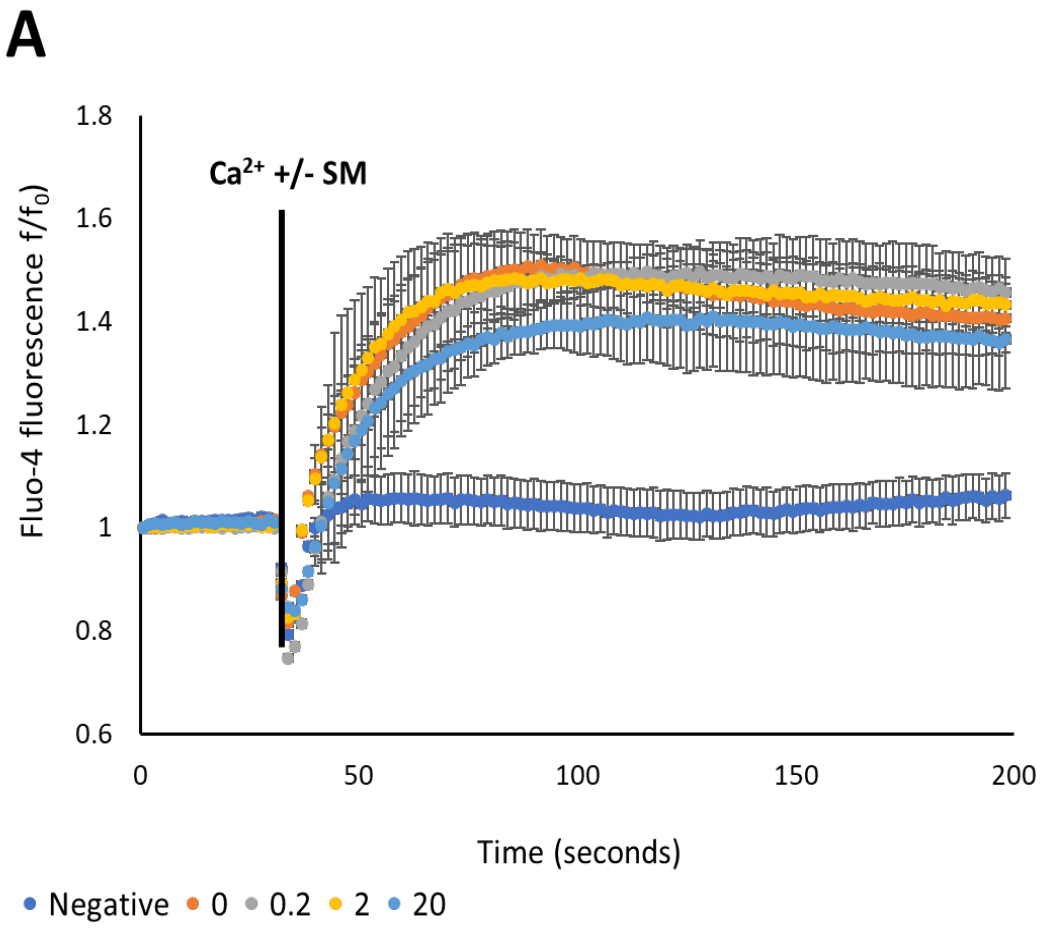
A
Ca2+ +/- SM
Fluo-4 fluorescence f/f0
1.8
1.6
1.4
1.2
1
0.8
0.6
0
50
100
150
200
Time (seconds)
Negative
0
0.2
2
20

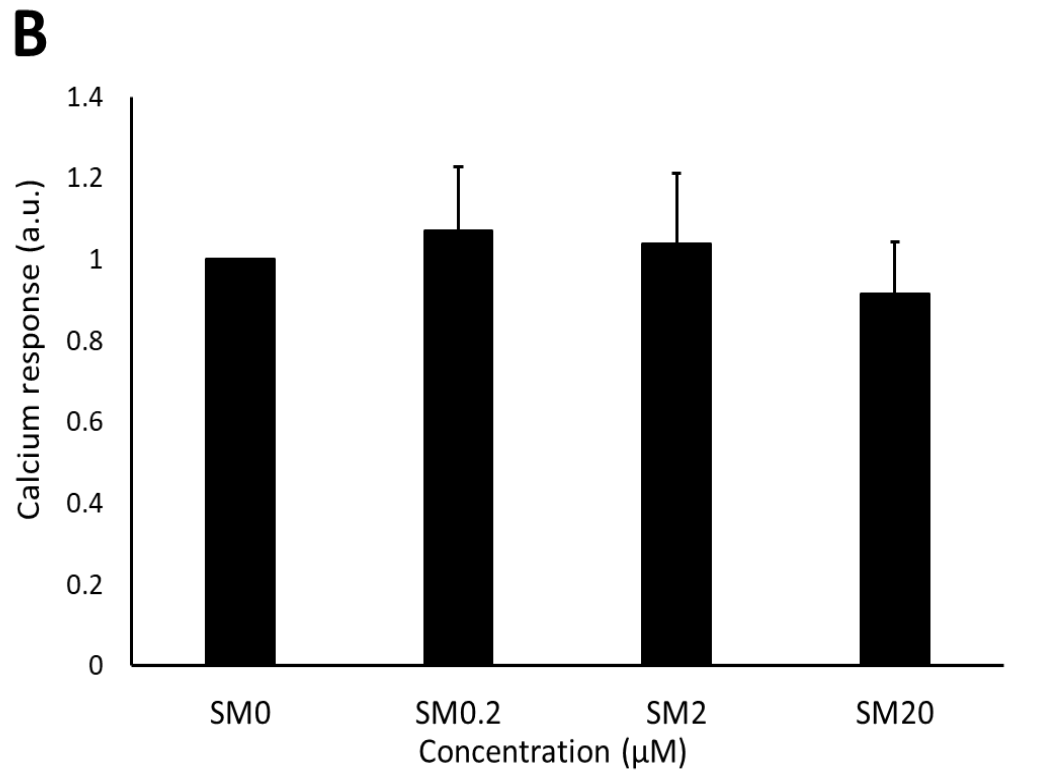
B
Calcium response (a.u.)
1.4
1.2
1
0.8
0.6
0.4
0.2
0
SM0
SM0.2
SM2
SM20
Concentration (µM)

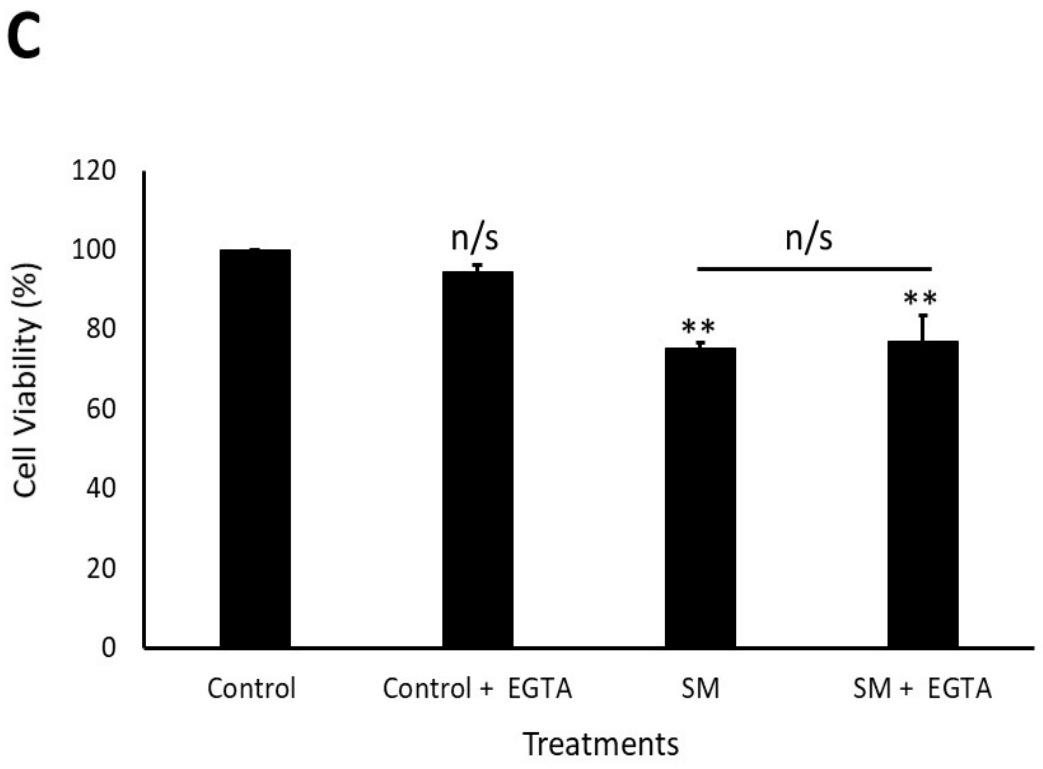

Figure 5. 15. Ca^{2+} exchange in CPCs after SM treatment. **(A)** Time course assay of Ca^{2+} signalling after thapsigargin pre-treatment, +/-0.2 µM, 2 µM and 20 µM SM, each data point represents 1.52 s. After 30 s of imaging the different concentrations of SM were injected with Ca^{2+}. Negative control are cells without thapsigargin pre-treatment. Data are mean±SEM, n=5. **(B)** Quantification of Ca^{2+} response (peak signal-mean baseline signal) for 0.2, 2, 20 µM SM treatment. Data are mean±SEM, n=5 *p<0.05. ANOVA with *post hoc* Tukey's test. **(C)** Cell viability measured using FDA assay, cells were either untreated (control), treated with 1 mM EGTA, 2 µM SM alone or 2 µM SM co-treated with 1 mM EGTA for 24 h followed by detection of viable cells. Data are mean±SEM, n=3, **p<0.01, n/s=not significant, ANOVA with *post hoc* Tukey's test.

5.2.8 Investigation into whether sunitinib-induces necroptosis

Having excluded apoptosis due to the inability for CPCs to recover after caspase inhibition, an alternative pathway was investigated. Gene expression was examined to determine whether RIP1, RIP3 and MLKL were increased after 2 μM SM treatment. The gene expression foldchange were; RIP1; 1.00 ± 0.10, MLKL; 1.29 ± 0.6 and RIP3; 1.42 ± 0.64. There was no significant difference between control cells and SM treated cells (n=3, $p>0.05$, **Figure 5.16A**). A limited investigation into SM-induced necroptosis showed a fluctuation in MLKL protein activation, with a 1.45-fold increase in activity, relative to a 7.99-foldchange in the positive control (n=1, **Figure 5.16B**).

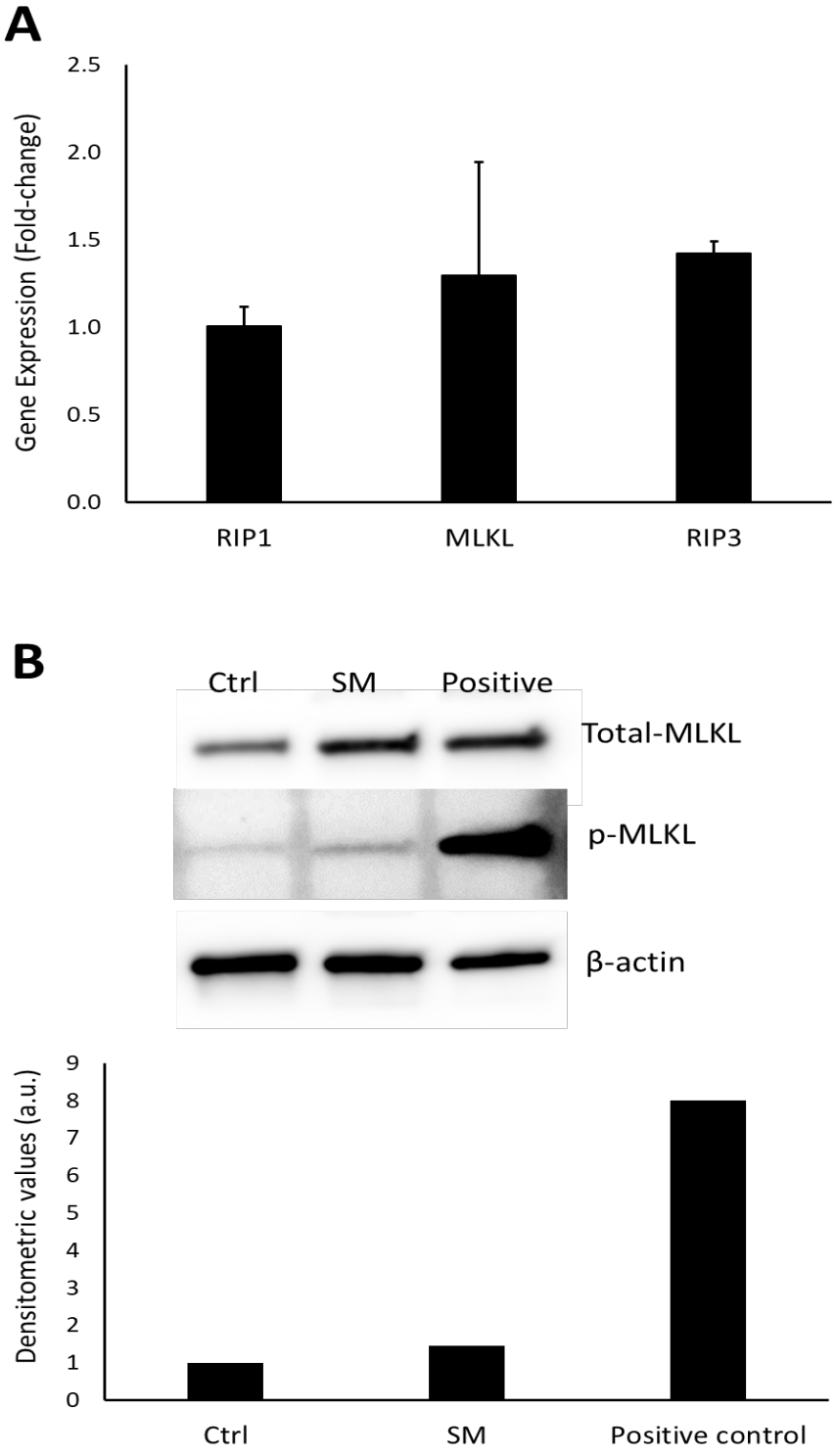

Figure 5. 16. SM 24 h treatment did not increase expression of necroptosis associate genes or protein. **(A)** Relative normalised gene expression for RIP1,MLKL and RIP after 2 μM SM treatment *vs.* control (1), data are ΔΔcq±SEM, n=3, *t*-test. **(B)** Western blot representative image showing expression of total MLKL and p-MLKL after SM 24 h treatment and positive control (TNF-α, SMAC mimetic and Z-VAD). Densitometric values showed MLKL activation after SM treatment and positive control treatment, n=1.

5.2.9 Treatment of cardiac progenitor cells with sunitinib for 7 d did not induce apoptosis

Live-cell staining showed no activation of caspase-3 and -7 or SM autofluorescence; however it showed an increase in ToPro-3 staining, cells treated with 0.5 μM SM had 3.8 ± 0.3 % of cells positive for ToPro-3 and 5 μM SM 16.8 ± 6.3% relative to with 1.8 ± 0.5% of untreated cells (n=4, $p<0.05$, **Figure 5.17A-B)**. There was no significant difference in foldchange for apoptotic genes; BAX, caspase 8, PARP, calpain and TNF-α or necroptosis associated genes; RIP1, RIP3 and MLKL. The gene expression fluctuations were greatest for TNF-α; 2.3 ± 1.7, RIP1; 1.6 ± 0.2, MLKL; 1.4 ± 0.6 and RIP3; 1.2 ± 0.1 foldchange *vs.* control (1.0 ± 0.0) (n=3, p>0.05, **Figure 5.17C**).

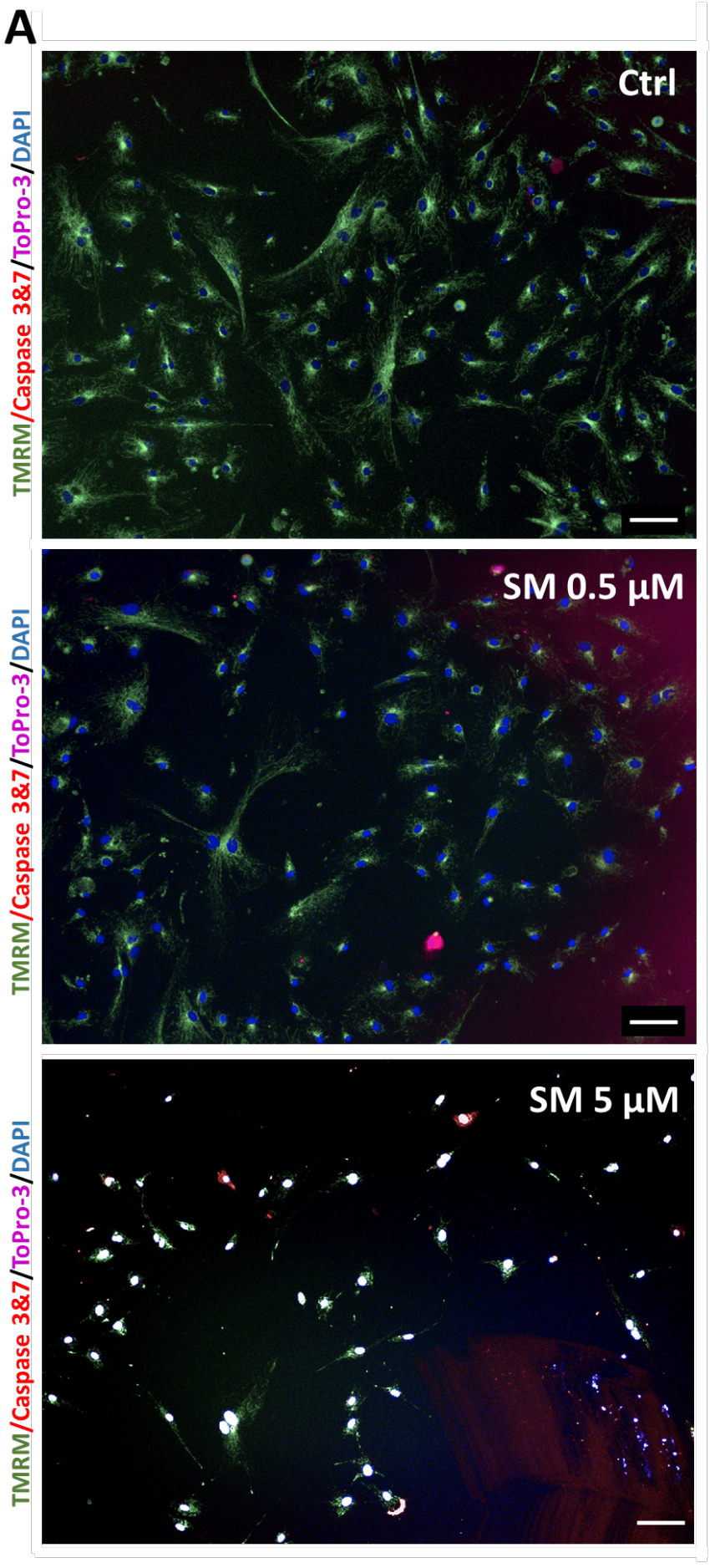
A
TMRM/Caspase 3&7/ToPro-3/DAPI
Ctrl
TMRM/Caspase 3&7/ToPro-3/DAPI
SM 0.5 µM
TMRM/Caspase 3&7/ToPro-3/DAPI
SM 5 µM

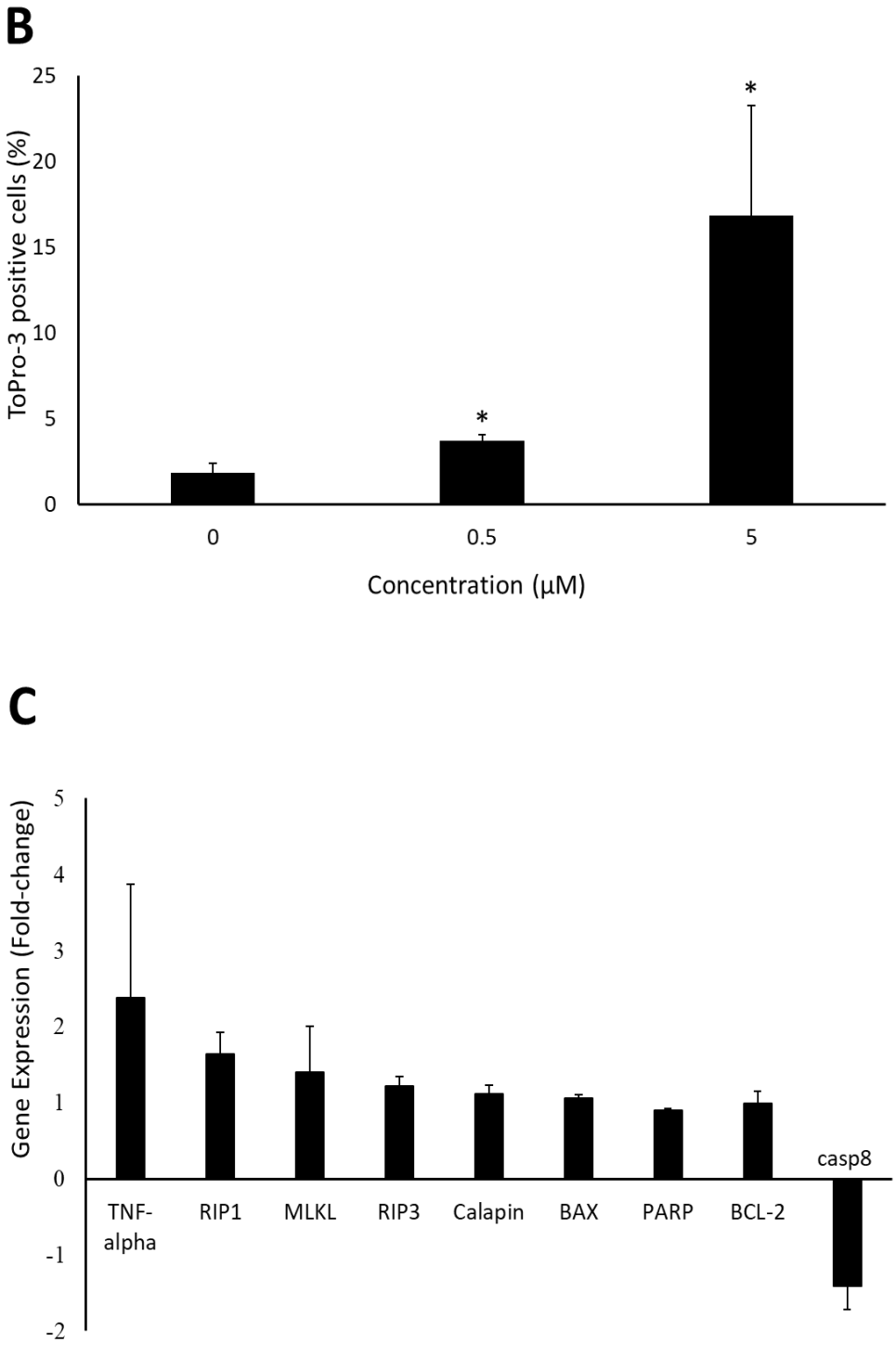

Figure 5. 17. **Identifying the activation of executioner caspases, ToPro-3 and changes in gene expression in CPCs after SM 7 d treatment. (A)** Cells treated with 0 µM, 0.5 µM or 5 µM SM stained for TMRM (dark green), ToPro-3 (magenta), and caspase 3/7 (red). SM treated cells caused no caspase -3 -7 activation. Sunitinib treated cells showed ToPro-3 staining. **(B)** Quantification of ToPro-3 positive cells after 0-5 µM SM treatment. Data are mean±SEM, n=4, *p<0.05, ***p<0.001, ANOVA with *post hoc* Tukey's test. **(C)** Changes in gene expression in CPCs after 0.5 µM SM 7 d treatment *vs.* control (control = 1.0); negative values represent reduced gene expression, Data are ΔΔcq±SEM, p>0.05, *t*-test.

5.3 Discussion

5.3.1 Sunitinib reduced cardiac progenitor cell viability but does not induce apoptosis

Sunitinib treatment showed a decline in cell viability at 2 μM, highlighting the toxic effects of the RTKIs on CPCs. Previously sunitinib has been shown to reduce cell viability within H9C2 cells, cardiac fibroblasts and CPCs (Abrams et al., 2003; Burke et al., 2019; Smith et al., 2018; McMullen et al., 2019).

Although this experiment identified apparent activation of caspase 3 and 7, this is believed to be a false positive, as the toxicity was irreversible with general caspase inhibitor and no annexin V staining was visualised. The false-positive caspase staining was theorised to be due to SM autofluorescence in the 488 nm channel. Although few studies have discussed the fluorescence of SM, research has exploited the autofluorescent properties of SM to assess the relationship between SM and autophagy (Ellegaard et al., 2013; Gotink et al., 2011; Nowak-Sliwinska et al., 2015). However, other studies have shown detection of assays using the excitation of 488 nm and 555 nm which excites SM, suggesting that the fluorescence of SM is still relatively unknown (Chu et al., 2007; Kerkela et al., 2009a; Y. Zhao et al., 2010). These autofluorescence data also aided further experimental design, by avoiding SM concentrations above 10 μM and utilising fluorescence excitation/emission channels of 405/450 nm and 561/585 nm. To identify definitively whether SM-induces apoptosis in CPCs, alternative methods were utilised.

5.3.2 Sunitinib increased apoptosis-associated gene and protein expression but did not induce the final stages of apoptosis

Cardiac progenitor cells treated with SM were tested for changes in gene expression, including apoptosis-specific genes (caspase 9, BAX and BCL-2). The largest change in gene expression was calpain these encode for a protein which are a family of proteases which have shown links to apoptosis aiding in activation of caspase 7 and BAX oligomerisation (Momeni, 2011). There was also upregulated expression of FASR, a well-known death receptor containing an intracellular domain known to initiate apoptosis-induced cell death. The pro-apoptotic factor BAX was also upregulated known to disrupt the mitochondria and the formation of the apoptosome (Micheau and Tschopp, 2003). The protein and gene expression suggest a possible mechanism of: FASR activation, causing cleavage of caspase 8, which cleaves BID in turn, helping to oligomerize the mitochondria, leading to calcium release into the cytoplasm and thereby calpain activation.

Notably, our study findings do not correspond to other results in this chapter, such as SM toxicity affecting CPCs even after general caspase inhibition and the lack of SM-associated annexin V staining. The explanation for increased apoptotic gene and protein expression could be due to: a) SM inability to induce apoptosis fully, b) SM-inducing an early apoptotic pathway that does not induce caspase activation within the time periods examined or c) apoptosis-associated proteins playing an unknown role in an alternative cell death pathway, such as necroptosis (Karch et al., 2015; Shi and Kehrl, 2019). Although some previous studies showed SM-induced apoptosis, other studies have shown the absence of caspase 3 activity in breast cancer cells, human

peripheral T cells and cardiomyocytes, some of these studies used fluorescent channels known to excite SM autofluorescence: therefore definitive conclusions cannot be drawn (Ellegaard et al., 2013; Kerkela et al., 2009a; Mioulane et al., 2012; Shiraishi et al., 1986; Xin et al., 2009; Y. Zhao et al., 2010). Previously, SM has also been shown to induce lysosomal associated cell death (Ellegaard et al., 2013): therefore our study also investigated the involvement of autophagic organelles in SM-induced cell death in CPCs.

5.3.3 Autophagy organelles and not the mitochondria sequestered sunitinib

Sunitinib was shown to reduce Δψm, we therefore investigated whether this was due to SM sequestration by the mitochondria. However, these data showed that mitochondria did not sequester SM, and therefore, the reduction in membrane potential is most likely an indirect action. Previous studies have shown evidence to support that SM caused a disruption in Δψm in rat cardiomyocytes (Chu et al., 2007; Kerkela et al., 2009a; Will et al., 2008). One indirect method for SM-induced reduction of Δψm could be due to increase ROS production. Sunitinib has previously been shown to increase oxidative stress in adult cardiac fibroblasts (McMullen et al., 2018).

To determine whether SM-induced mitochondrial impairment was due to autophagy (**see Chapter 4.3.1**), the autofluorescent property of SM was exploited to determine if the autophagic organelles internalised the drug: these data showed that SM was associated with both lysosomes and autophagosomes. Sunitinib might be interfering with the autophagic flux,

which in turn would cause mitochondrial impairment, as previously discussed in Chapter 4.3.1 (Li et al., 2017b). Other studies have demonstrated that lysosomes sequester SM in both ovarian cancer cells and endothelial cells. Sequestering of SM was demonstrated to have a protective effect in both of these cell types, whereas lysosome rupturing using light was shown to release SM, causing additional cytotoxic effects (Nowak-Sliwinska et al., 2015). The sequestering of SM has also been linked to increased SM-resistance in tumour resistant cells (Gotink et al., 2011).

However, in our study SM did not show an increase in AOs, which was seen by IM-induced autophagy, meaning that SM does not increase the lysosomal content which is indicative of autophagy induction (Ertmer et al., 2007b). Previous studies have shown that SM induced autophagy in H9C2 cells, as demonstrated by increased staining for AOs and GFP-tagged LC3II; however, these images were presumably taken using a 488 nm laser and therefore the GFP-tagged protein could have been SM autofluorescence. Their findings were reinforced with increased expression of LC3 via Western blotting and therefore gives value to their findings even disregarding GFP-tagged data (Y. Zhao et al., 2010). The study also lacks a lysosomal inhibitory control, and therefore a conclusion regarding the impact of SM on the autophagic flux cannot be drawn. Other studies have shown SM to induce non-apoptotic lysosome-dependent cell death, either via the leakage of lysosomal content, which has been shown to activate BAX (this could explain the increased BAX expression seen in our study) or through plasma membrane rupturing (Ellegaard et al., 2013). Further data are therefore required to understand the involvement of autophagy and mitochondrial impairment in SM-induced CPC cytotoxicity.

5.3.4 Store operated calcium entry is unchanged by sunitinib and lowered calcium concentration does not rescue cell recovery

As discussed in chapter 4, calcium is an important s messenger involved in cell survival and cell death. Sunitinib showed no effects on SOCE, suggesting that SM treatment does not increase calcium reuptake after internal stores are depleted. Previous studies in human cardiomyocytes showed that SM reduced sarcomere shortening, accompanied by a reduced calcium transient (Rainer et al., 2012). In our study, results indicate that lowering the calcium concentration over 24 h had no effect on CPC viability after SM treatment, suggesting that calcium is not the main contributor to cell death.

5.3.5 Sunitinib is initiating an alternative death pathway such as necroptotic cell death

Due to the lack of evidence of apoptosis-induced cell death and indications of an alternative pathway, necroptotic cell death was studied. The study of necroptosis is a relatively new and developing field, and there is limited research available, especially regarding SM-induced toxicity. Gene expression analyses for necroptosis-associated genes (RIP1, RIP3 and MLKL) identified no changes, suggesting that SM does not increase necroptosis transcription. Our study also investigated the involvement of MLKL protein activation, with early findings showing increased MLKL activation, which indicates necroptotic cell death. However, our study had limited replicates due to time constraints, hence more experiments are needed to confirm whether SM-induces necroptosis.

5.3.6 Trough concentrations of sunitinib are toxic to cardiac progenitor cells but do not initiate apoptosis

It was important to investigate the long-term effects of SM by assessing the toxicity of 'trough' concentrations applied over 7 d. These data showed that SM significantly reduced CPC viability after 0.5 μM SM exposure for 7 d, reinforced by live-cell staining for ToPro-3. In contrast to the peak concentration data, there was no autofluorescence detected, this could be due to either a) a lower dose of SM being used or b) the retention of SM within the cell has a limited lifespan. The primary focus of this thesis was on the peak concentration, however these data reinforce that even a low dose of SM over a long period can be toxic to CPCs. Future avenues for trough concentration investigation should involve the study of necroptosis protein expression and autophagy.

5.3.7 Conclusions

In summary, these data do not give a categorical identification of the cell death pathway induced by SM in CPCs. Cardiac progenitor cell viability was reduced by both peak and trough concentrations of SM. Sunitinib was sequestered by both autophagosomes and lysosomes within CPCs and reduced $\Delta\psi m$. Sunitinib increased apoptosis-associated genes and protein expression (BAX, FASR, Calpain 1 and downregulation of BCL-2). However, late-stage apoptosis was not induced by SM, as indicated by the lack of CPC recovery from a caspase inhibitor and also negative staining for annexin V. Preliminary findings showed increase in MLKL activity; however, limited data was available to support the conclusion of necroptotic cell death. Therefore, it is

too early in the investigation to suggest possible targets for manipulation and further data are required. Suggestions moving forward would involve the use of wortmannin to inhibit autophagosome formation; to determine whether SM can be removed from the autophagic organelles and assessment of how this would affect viability. Further investigations are required to assess the involvement of necroptosis and how the apoptosis-associated proteins are involved in the alternative cell death pathway.

Chapter 6. Cardiac progenitor cells treated with sorafenib induced calcium-dependent cell death

6.1 Introduction

Sorafenib tosylate has been used to treat patients with RCC, HCC, AML and thyroid carcinoma. Sorafenib has multiple targets including on-target VEGFR1-3, PDGFR-α, PDGFR-β and off-target RAF (serine/threonine kinase), which are involved in cell proliferation and tumour angiogenesis.

Untreated patients with late-stage HCC have an average survival rate of 6-7 months; however, this has been shown to be extended in the TACE trail with a median of 16-20 months with ST treatment (El-Serag et al., 2008; Keating and Santoro, 2009; Llovet and Bruix, 2008). The Asia-Pacific region trial showed the placebo group to have an average survival of 4.2 months, which was prolonged to 6.5 months with ST treatment; this trial was with patients with a more advanced HCC than previous trials such as SHARP (Cheng et al., 2009). The SHARP study showed an average survival of 7.9 months, compared to 10.7 within the sorafenib-treated group. Overall ST is a well-tolerated treatment which can extend patient survival in advanced HCC (Llovet et al., 2008).

Although ST has been deemed tolerable for patients, there are still adverse side effects, including cardiotoxicity. Three trials outline the importance of investigating ST-induced cardiotoxicity, with the SHARP study showing 2.7% of RCC patients treated with ST experienced cardiac ischaemia or infarction, compared to 1.3% in the placebo group. Following this, the DECISION study

showed 0% of placebo-treated patients suffered cardiac ischaemia or infarction, compared to 1.9% in the ST treated group. Finally, this was reaffirmed by the TARGET trial for RCC patients, which again showed 2.9% of patients expressing symptoms of cardiac ischaemia or infarction, as compared to 0.4% in the placebo group ("Mechanism of Action | NEXAVAR® (sorafenib)," n.d.). Other cardiac symptoms have been reported including hypertension, with one phase I trial showing 11-15% of patients developing hypertension after ST treatment; a separate study showed 17% of patients developed signs of hypertension. A study of RCC patients showed 33.8% (of 74 patients) experienced a "cardiac event", defined as the presence of symptomatic arrhythmia that needed treatment, increase in troponin T, CK-MB (if baseline values were normal), change in LVEF, or acute coronary syndrome.

Our group has confirmed similar findings at the cellular level in cardiac progenitor cells. Sorafenib has been shown to be toxic in CPCs at clinically-comparable concentrations demonstrated by reduced cell viability (Smith et al., 2018). In addition, ST reduced CPC proliferation and the expression of both cell survival proteins (AKT and p63) and factors associated with differentiation (Nkx2.5 and PECAM) (Smith, et al., 2018).

The aim of the work described in this chapter was to identify cell death pathways involved in ST-induced toxicity in endogenous human CPCs, with a view to identifying possible targets for pharmacological protection.

6.2. Results

6.2.1. Cardiac progenitor cell viability after sorafenib treatment

Cell viability remained unchanged after 1 µM ST treatment; however, cell viability was reduced by 33.2 ± 8.9% after cells were treated for 24 h with 10 µM ST or by 78.5 ± 6.5% after 100 µM exposure relative to the control (n=8, $p<0.05$. **Figure 6.1A**). There was no significant effect of the solvent DMSO in control cells (n=8, $p<0.05$. **Figure 6.1B**).

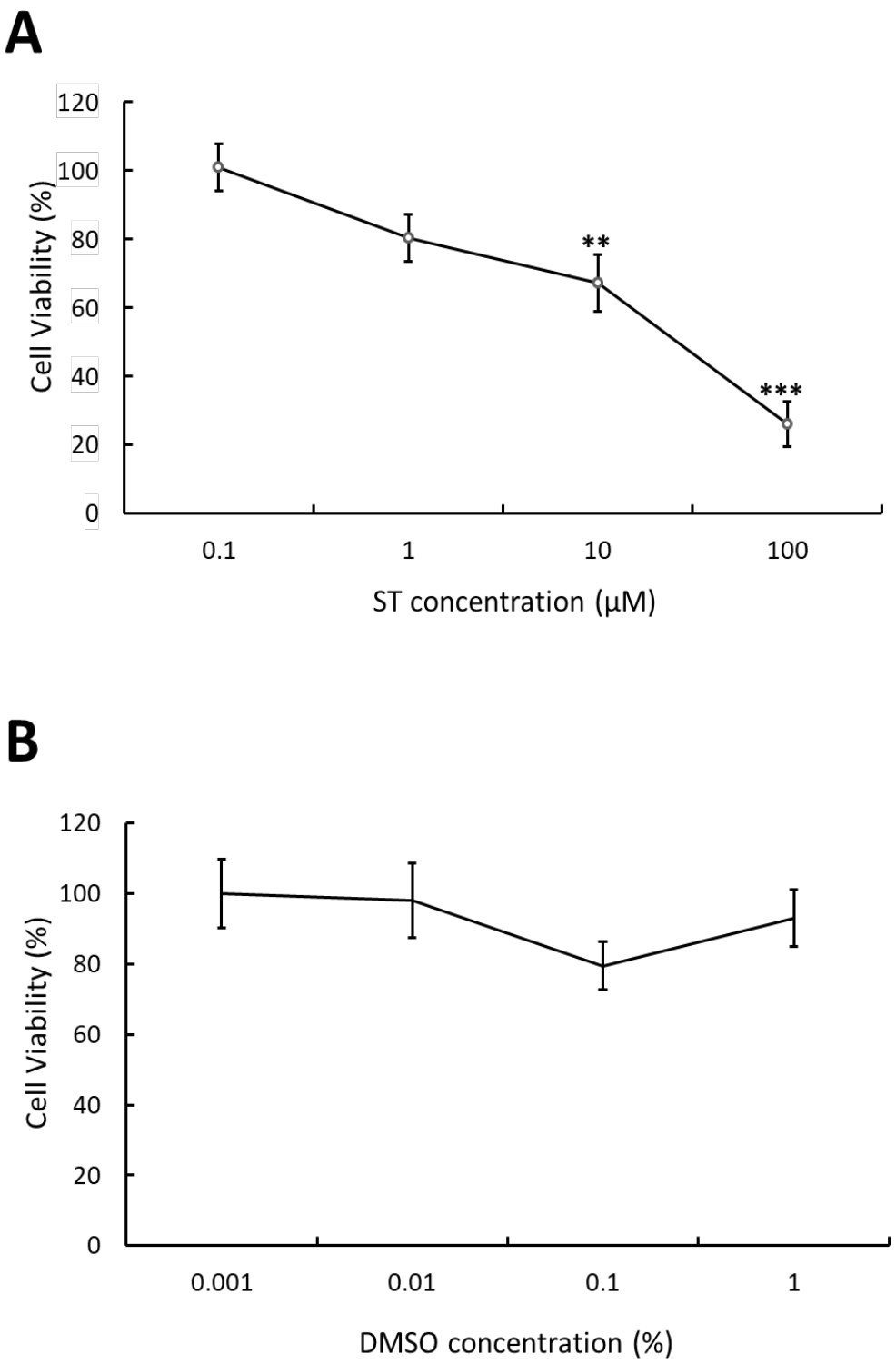

Figure 6.1. CPCs viability after 24 h in response to ST treatment. (A) Cells treated with 0.1, 1, 10 or 100 µM ST for 24 h before assessment of viability **(B)** Cells treated with 0.002-1% DMSO for 24 h. Data are mean ± SEM, n=8; **p*<0.05, ***p*<0.01, ****p*<0.001, ANOVA with *post hoc* Tukey's test.

The same analysis of viability was applied to CPCs exposed to 0.5 μM, 5 μM and 50 μM) ST for 7 d. The results showed that 0.05 μM and 0.5 μM ST did not affect viability. However, 5 μM ST reduced viability by 35.2 ± 5.4% and 50 μM ST by 86.1 ± 7.7% relative to control (100.0 ± 2.5%) (n=5, $p<0.05$. **Figure 6.2A**). Again, DMSO had no significant effect on CPC viability (n=5, $p<0.05$. **Figure 6.2B**).

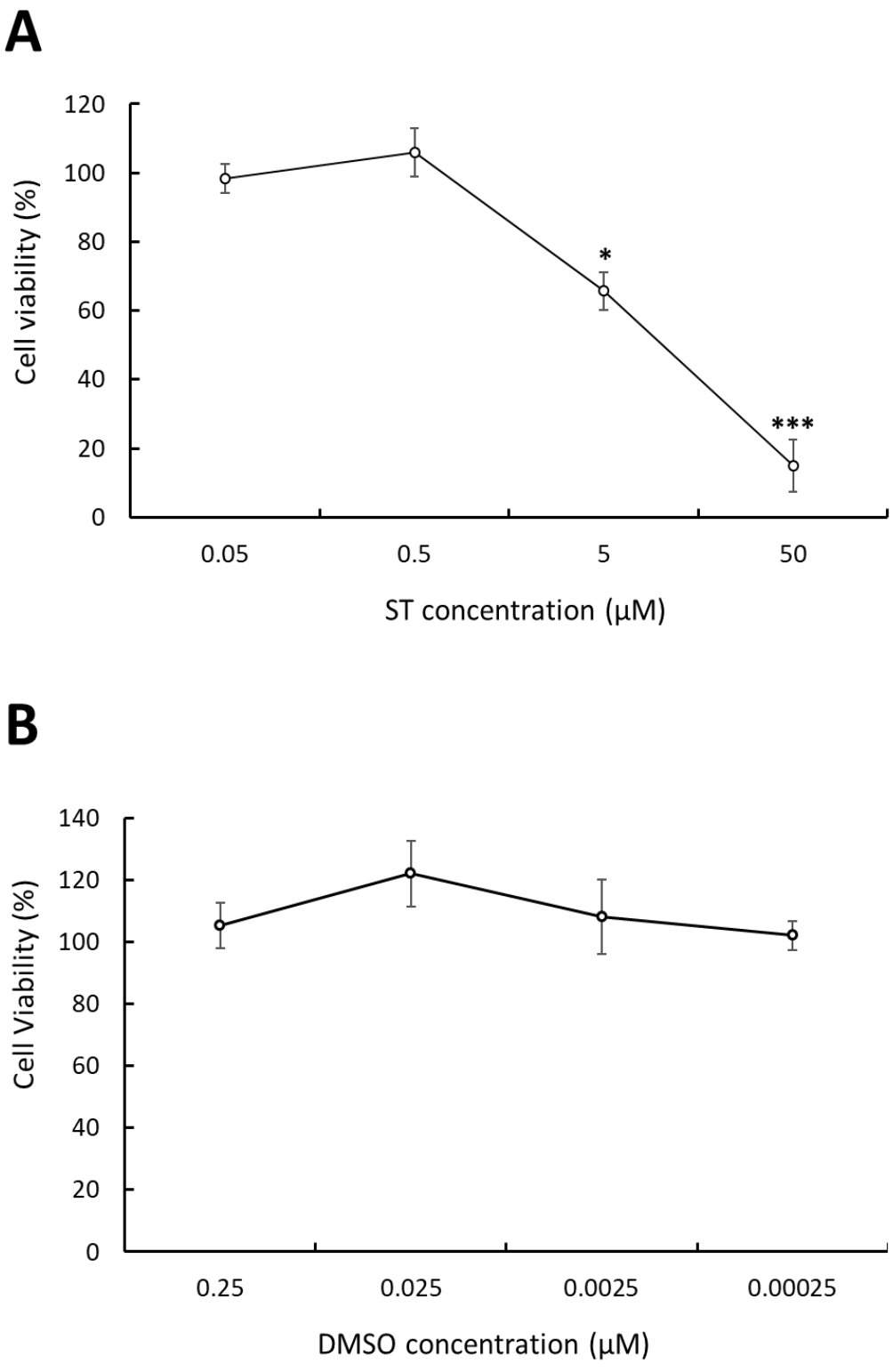

Figure 6. 2. CPC viability over 7 d in response to ST treatment (A) Cells treated with 0.1, 1, 10 or 100 µM ST for 7 d before assessment of viability **(B)** Cells treated with 0.002-1% DMSO for 7 d. Data are mean±SEM, n=8; **p*<0.05, **p<0.01, ****p*<0.001, ANOVA with *post hoc* Tukey's test.

6.2.2 Sorafenib did not induce apoptosis

As described in chapters 4 and 5, live cells were stained after ST treatment for 24 h or 7 d using four dyes: caspase-3/7, TMRM, To-Pro-3, and DAPI (Mioulane et al., 2012). After treatment with 10 μM or 100 μM ST for 24 h, no signs of increased caspase-3/7 activity were seen in either ST-treated or control cells (**Figure 6.3A)**. However, To-Pro-3 was identified within the nuclei of CPCs after treatment with 10 μM or 100 μM ST (**Figure 6.3A**). Quantification of To-Pro-3 staining showed there was no significant change with 1 μM ST, however, a significant increase did occur at 10 μM ST 4.2 ± 0.3% and 100 μM ST caused a significant increase in To-Pro-3 positive cells of 72.1 ± 4.5% *vs.* control 2.6 ± 0.3% (n=4, $p<0.05$. **Figure 6.3B**).

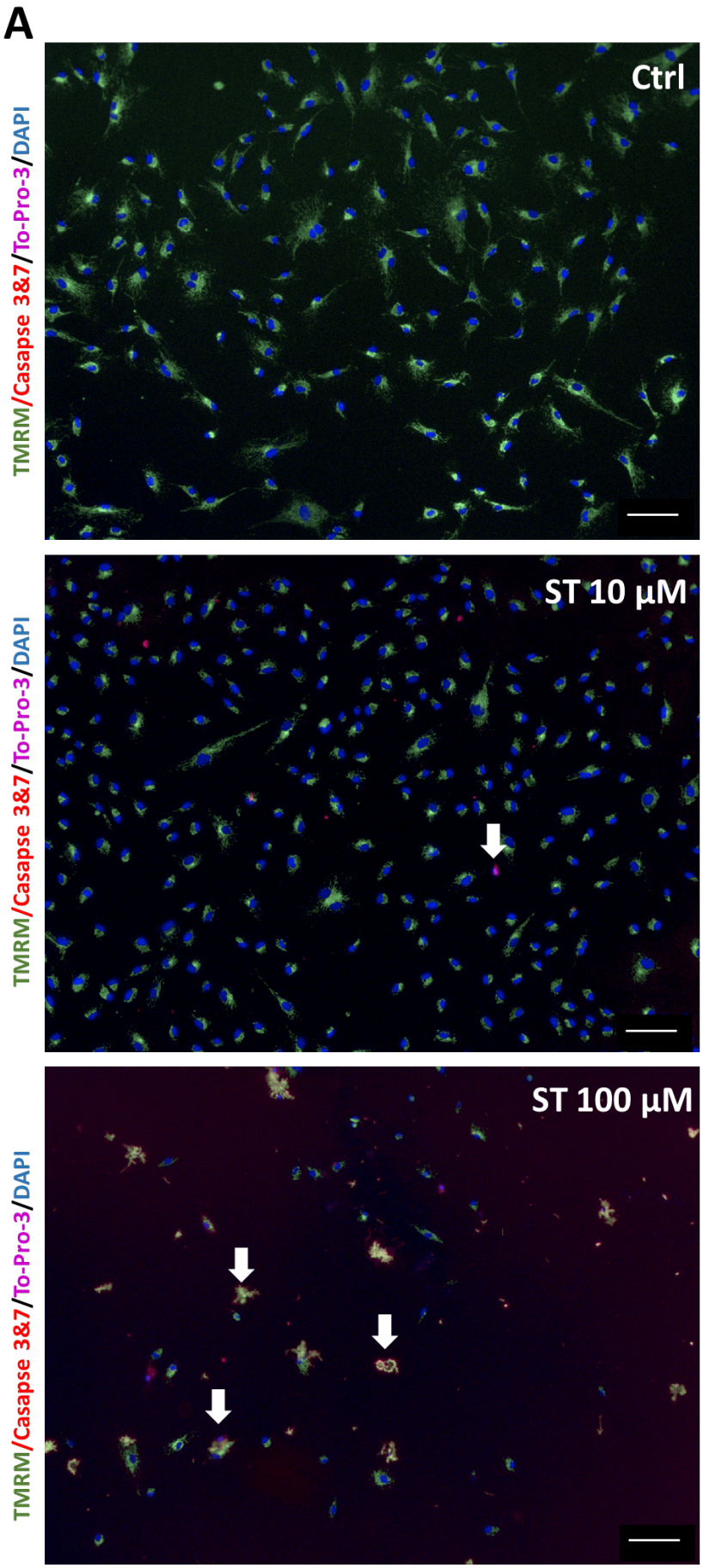
A
TMRM/Casapse 3&7/To-Pro-3/DAPI
Ctrl
TMRM/Casapse 3&7/To-Pro-3/DAPI
ST 10 µM
TMRM/Casapse 3&7/To-Pro-3/DAPI
ST 100 µM

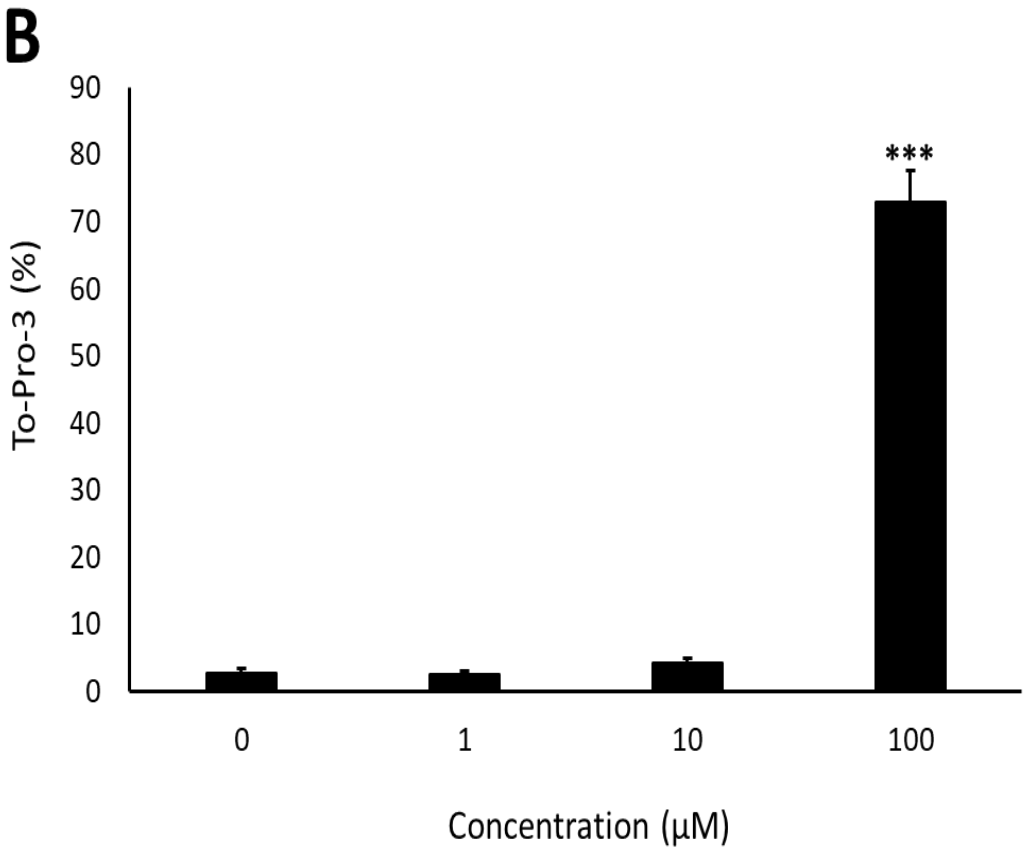

Figure 6. 3. Identifying the activation of executioner caspases and presence of ToPro-3 in CPCs after ST 24 h treatment. (A) Images of untreated cells and cells treated with 10 µM or 100 µM ST and stained for TMRM (dark green), ToPro-3 (magenta), and caspase 3/7 (red). Control cells and ST-treated cells showed no caspase 3 and 7 activation. Sorafenib treated cells showed ToPro-3 staining (arrows). **(B)** Quantification of ToPro-3 positive cells after 0-100 µM ST treatment. Data are mean±SEM, n=4, *p<0.05, ***p<0.001, scale bar=100 µM, Student's ANOVA with *post hoc* Tukey's test.

Further investigation to confirm the cell death pathways involved after ST treatment used RT-qPCR: cells were treated with 10 μM ST for 24 h and an array of apoptosis and necroptosis genes were assessed. There was no significant change in gene expression for TNF-α, BAX, RAF-1, PARP, RIP1, RIP3 and MlKL (n=3, p>0.05, **Figure 6.4**).

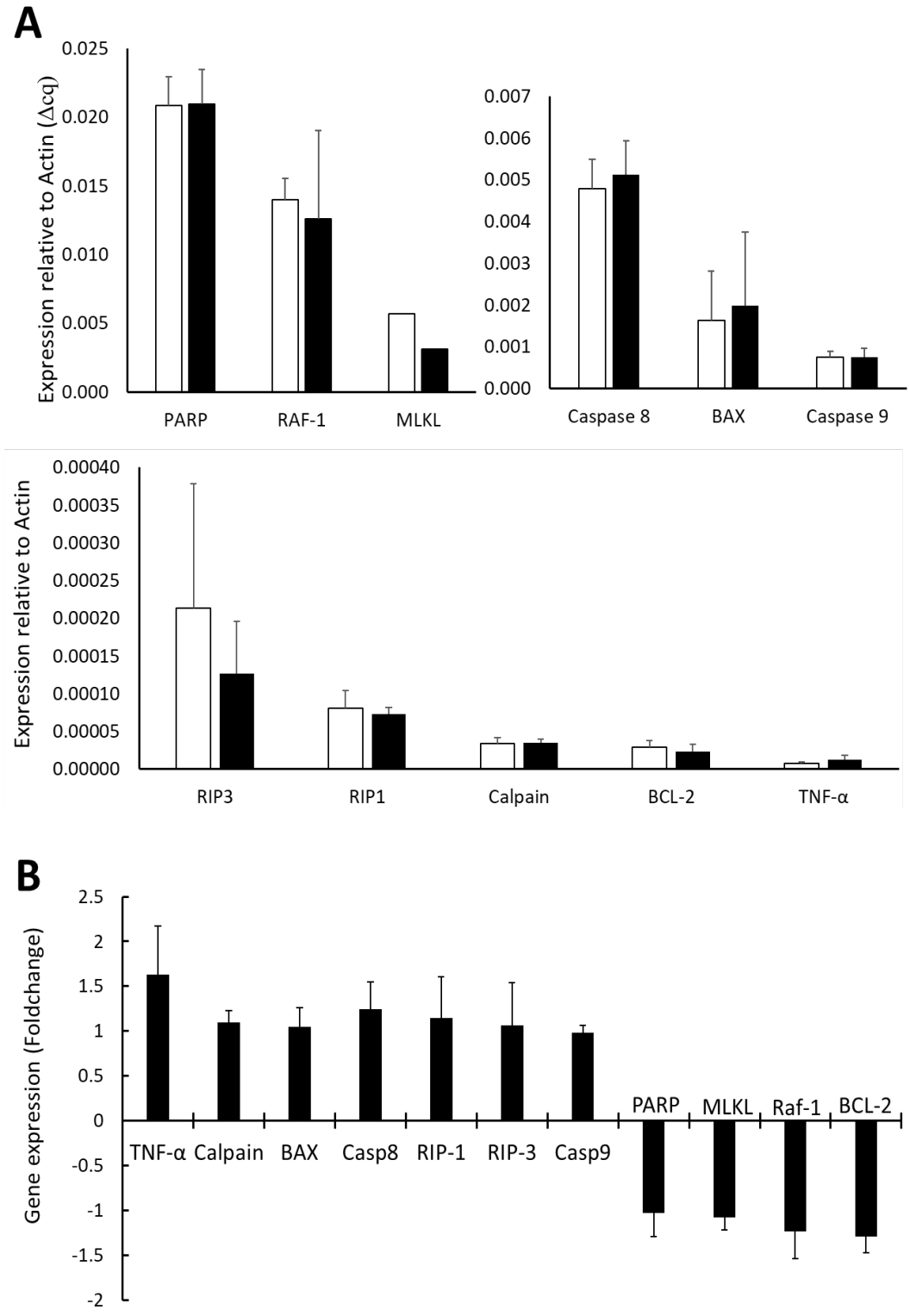

Figure 6. 4. Changes in gene expression in CPCs after exposure to 10μM ST for 24 h. **(A)** Gene expression (relative to β-actin) in control (white) and ST-treated (black) samples, for a range of cell death-associated genes. **(B)** Changes in gene expression over control (1.0); negative values represent reduced gene expression. Data are **(A)** Δcq±SEM or **(B)** ΔΔcq±SEM, n=3, *t*-test, control vs ST.

Cells treated with 5 μM ST for 7 d also showed no signs of caspase 3 or 7 activity. As with 24-h treatments, To-Pro-3 staining was present within CPC nuclei after 5 μM and 50 μM ST treatment (**Figure 6.5A**). Quantification of To-Pro-3 staining showed a significant increase after 5 μM ST with 6.9 ± 0.4% and 50 μM 23.6 ± 5.2% *vs.* control cells with 1.8 ± 0.5% of ToPro-3 staining (n=4, $p<0.05$. **Figure 6.5B**). These data showed upregulation in gene expression of TNF-α 9.94 ± 2.6, RIP1 1.8 ± 0.2 and BAX 1.7 ± 0.2 (n=3, $p>0.05$. **Figure 6.5C**).

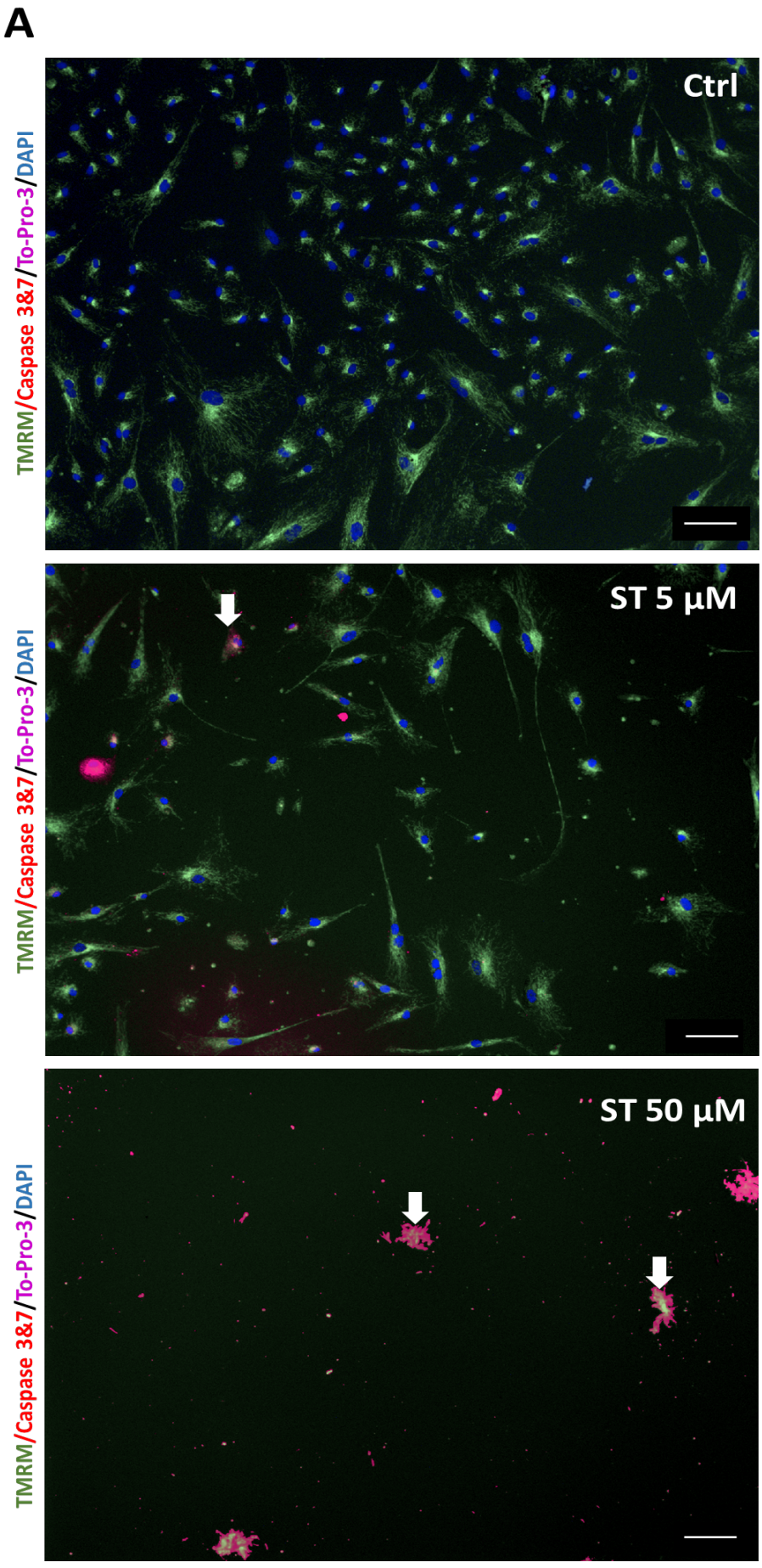
A
TMRM/Caspase 3&7/To-Pro-3/DAPI
Ctrl
TMRM/Caspase 3&7/To-Pro-3/DAPI
ST 5 µM
TMRM/Caspase 3&7/To-Pro-3/DAPI
ST 50 µM

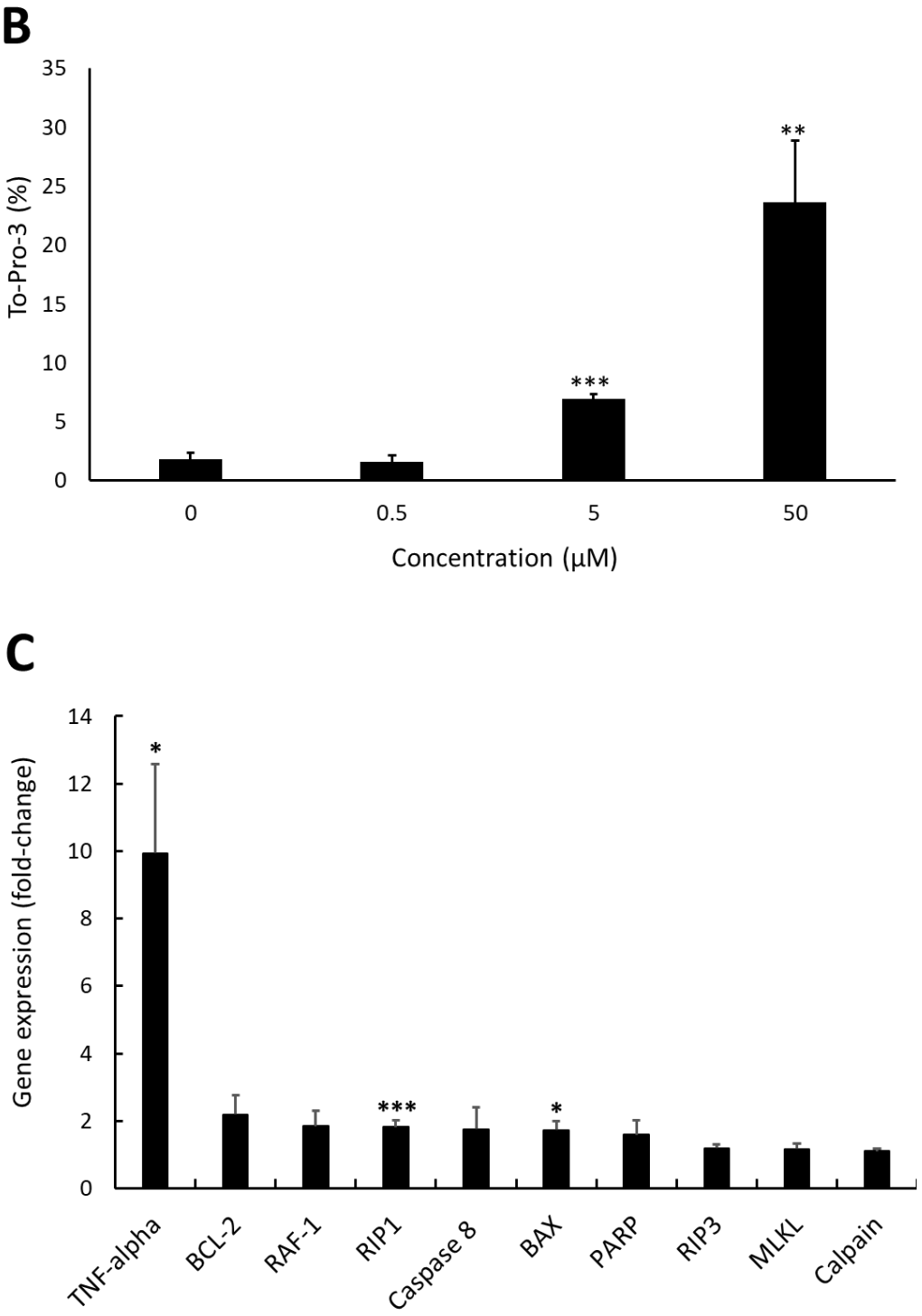

Figure 6. 5. Identifying the activation of executioner caspases, ToPro-3 and changes in gene expression in CPCs after ST 7 d treatment. (A) Cells treated with 0µM, 5 µM or 50 µM ST stained for TMRM (dark green), ToPro-3 (magenta), and caspase 3/7 (red). Control cells and ST-treated cells showed no caspase 3 and 7 activation. Sorafenib treated cells showed ToPro-3 staining (arrows). **(B)** Quantification of ToPro-3 positive cells after 0-100 µM ST treatment. Data are mean±SEM, n=4, $^{**}p<0.01$, $^{***}p<0.001$, ANOVA with *post hoc* Tukey's test. **(C)** Changes in gene expression in CPCs after ST 7 d treatment *vs.* control (1.0). Data are ΔΔcq±SEM, n=3, $^{*}p<0.05$, $^{***}p<0.001$, ANOVA *post hoc* Tukey's test.

6.2.3 Sorafenib did not increase acidic organelle content

To determine whether autophagy contributed to cell death, acridine orange staining was used to identify any increase in acidic content within CPCs. Cells were treated with 10 μM ST for 24-72 h, with no significant change in acridine orange staining seen compared to the control. The staining signal was low in both DMSO control cells and ST-treated cells (**Figure 6.6**).

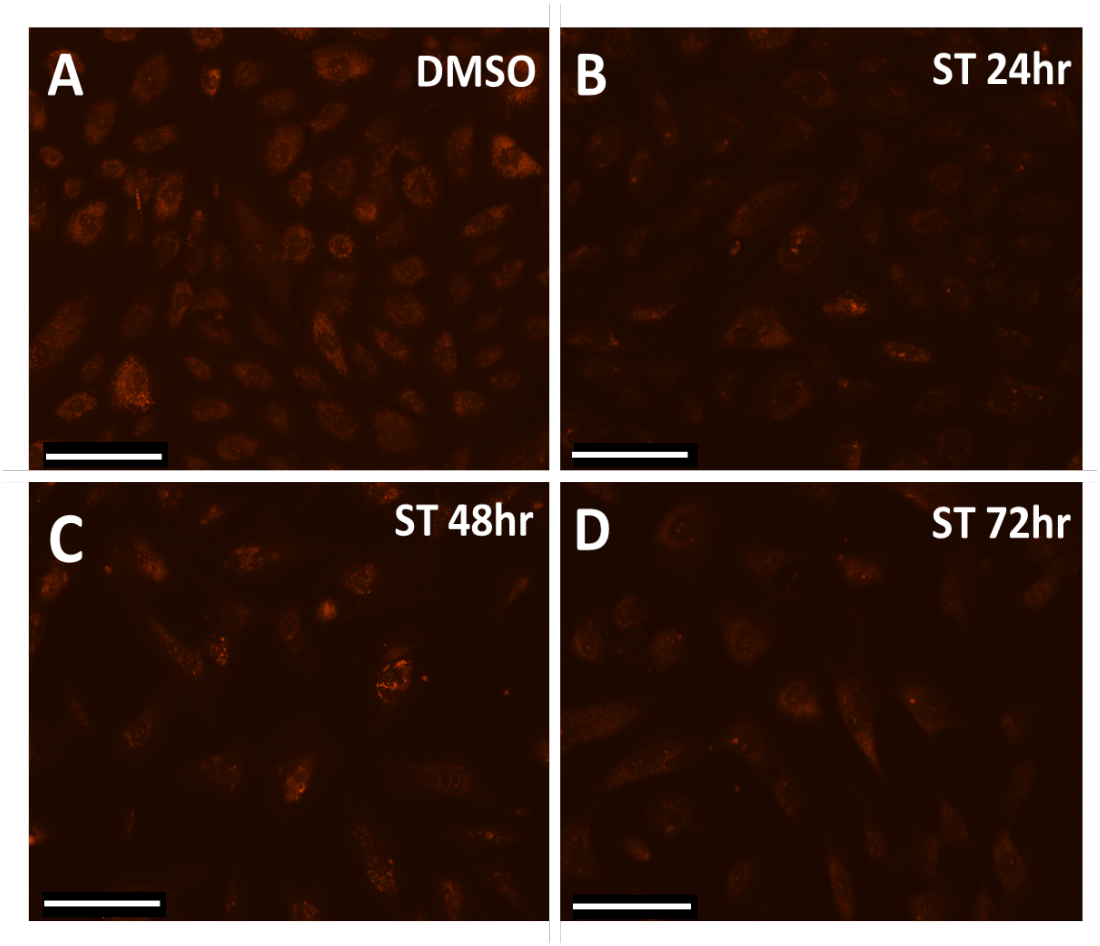

Figure 6. 6. ST did not induce accumulation of acidic vesicle organelles. Representative images of CPCs stained with acridine orange: staining represents acidic organelles in **(A)** DMSO control cells, **(B-D)** 10 μM ST for **(B)** 24 **(C)** 48 and **(D)** 72 h treatment. No acridine orange staining was observed. Scale bar=275 μm.

6.2.4 Sorafenib does not affect the mitochondrial membrane potential of Cardiac progenitor cells

Flow cytometry was used to analyse the effects of ST treatment on CPC mitochondrial membrane potential. Cells were grown *in vitro* and treated with 10 μM, 20 μM or 50 μM ST, then live-stained with TMRM. Application of ST caused no apparent change in TMRM fluorescence relative to control (**Figure 6.7A**). These data were confirmed by assessment of TMRM mean fluorescence intensity (MFI), with no significant difference compared to the DMSO treated control cells (n=6, $p<0.05$. **Figure 6.7B**).

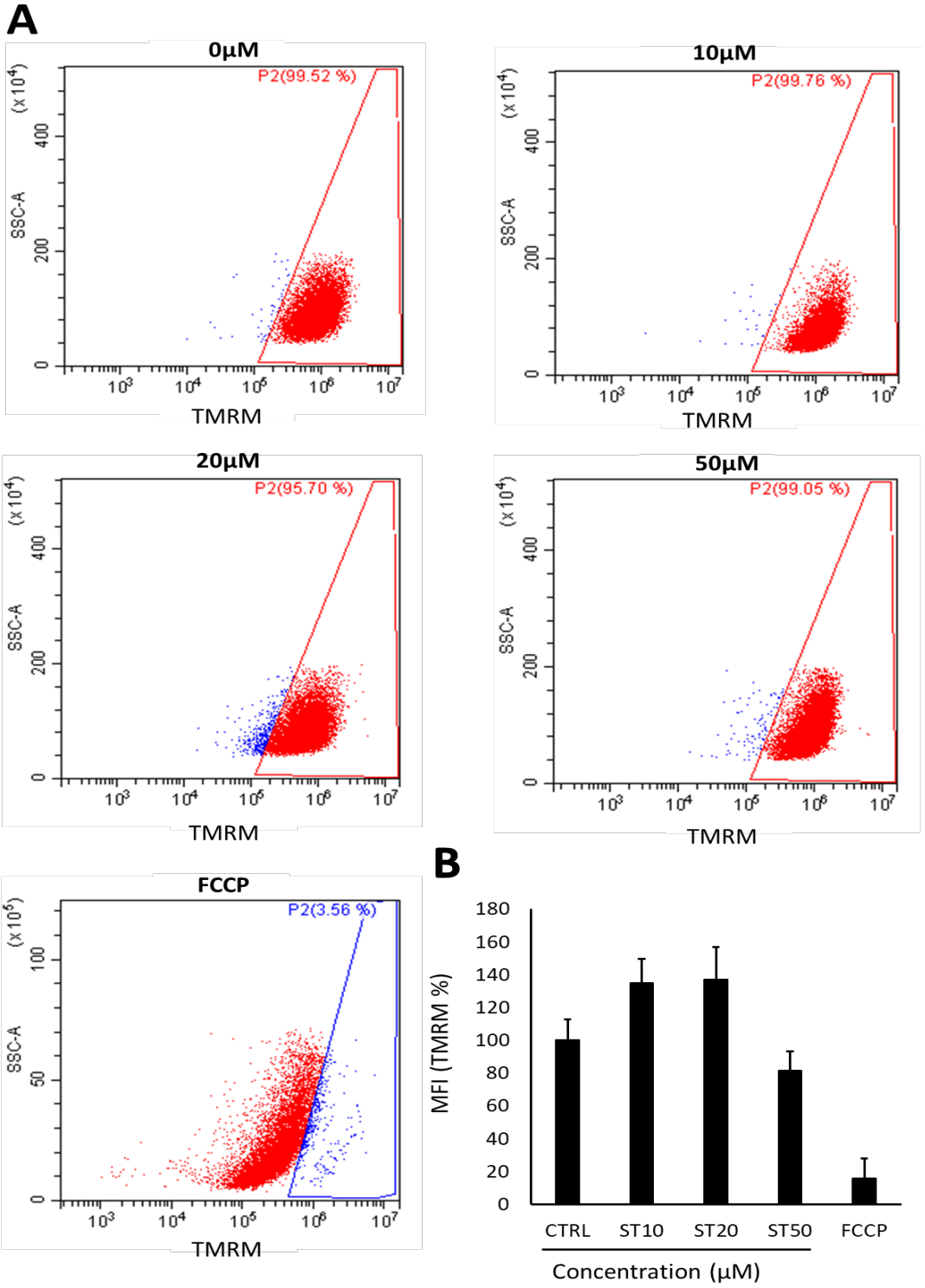

Figure 6. 7. ST did not change mitochondrial ΔΨm in CPCs. **(A)** Intensity of TMRM fluorescence following application of ST or FCCP, untreated control 0 µM, 10 µM, 20 µM and 50 µM ST treatment and 10 µM FCCP. The positive control of 10 µM FCCP showed cells with left shift in intensity (red). **(B)** Quantification of TMRM MFI normalised against control cells (100%). Data are mean±SEM, n=6, $p>0.05$, ANOVA with *post hoc* Tukey's test.

6.2.5 Sorafenib inhibits store operated calcium entry and cardiac progenitor cell toxicity is rescued by reducing calcium concentrations

All basal intracellular calcium levels remained stable, until stimulation with the addition of extracellular calcium, with or without ST (at 30 s); the negative control remained relatively unchanged even after addition of calcium, with peak fluorescence reaching 1.0 ± 0.08-fold. The control cells (ST0) showed a peak fluorescence of 1.5 ± 0.0-fold, 1 μM ST had 1.4 ± 0.0-fold, 10 μM ST, 1.3 ± 0.0-fold and 100 μM ST, 1.2 ± 0.0-fold increase in Fluo-4 staining (**Figure 6.8A**). The maximum change in fluorescence shows 1 μM ST, 0.7 ± 0.0-fold decrease, 10 μM ST, 0.6 ± 0.0 and 100 μM ST, 0.3 ± 0.00-fold decrease in calcium response when normalised against the control (**Figure 6.8B**).

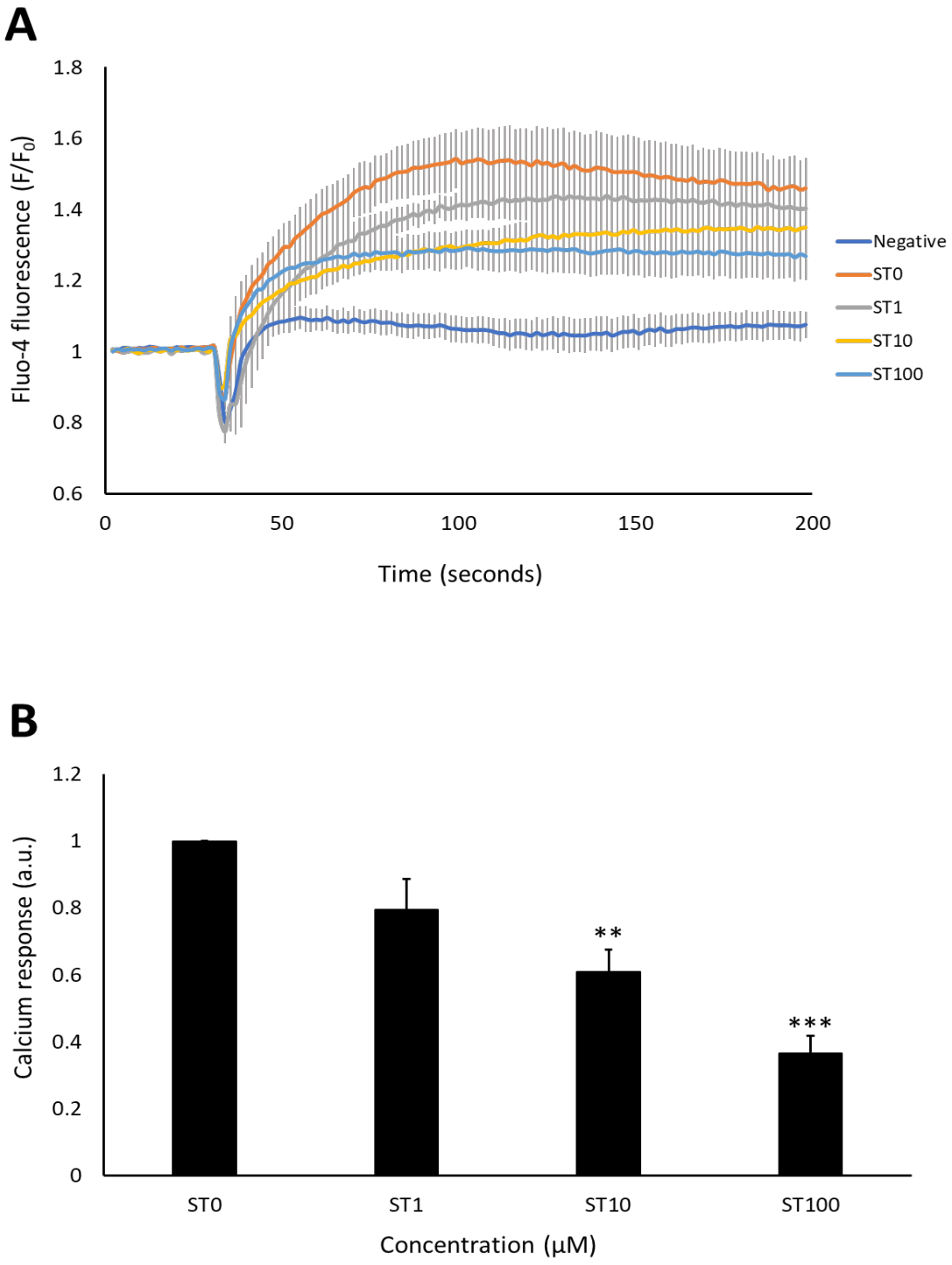

Figure 6. 8. Calcium exchange in CPCs after ST treatment. **(A)** Time course assay of fluo-4 fluorescence signal after thapsigargin pre-treatment, +/-1 µM, 10 µM and 100 µM ST, each data point represents 1.52 s. After 30 s of imaging the different concentrations of ST were injected with calcium. Negative control are cells without thapsigargin pre-treatment. Data are mean ± SEM, n=5. **(B)** Quantification of calcium response (peak signal-mean baseline signal) for 1, 10, 100 µM ST treatment. Data are mean ± SEM, n=5 *p<0.05. ANOVA with *post hoc* Tukey's test.

As there was a small increase in calcium reuptake, it was essential to analyse whether calcium impacted on cell viability. Cells were grown in medium with or without ST and with or without 1 mM of EGTA, for 24-h followed by measurement of viability using the FDA assay. There was a significant reduction in viability to 62.8 ± 5.9% after 10 μM ST treatment; however, there was no significant reduction in viability in cells treated with 10 μM ST and 1 mM EGTA (88.4 ± 8.2%), or in ST untreated cells treated with 1 mM of EGTA (94.8 ± 1.6%) (n=3, $p>0.05$). There was a significant difference between 10 μM ST when compared to 10 μM ST co-treated with 1 mM EGTA (n=3, $p<0.05$, **Figure 6.9**).

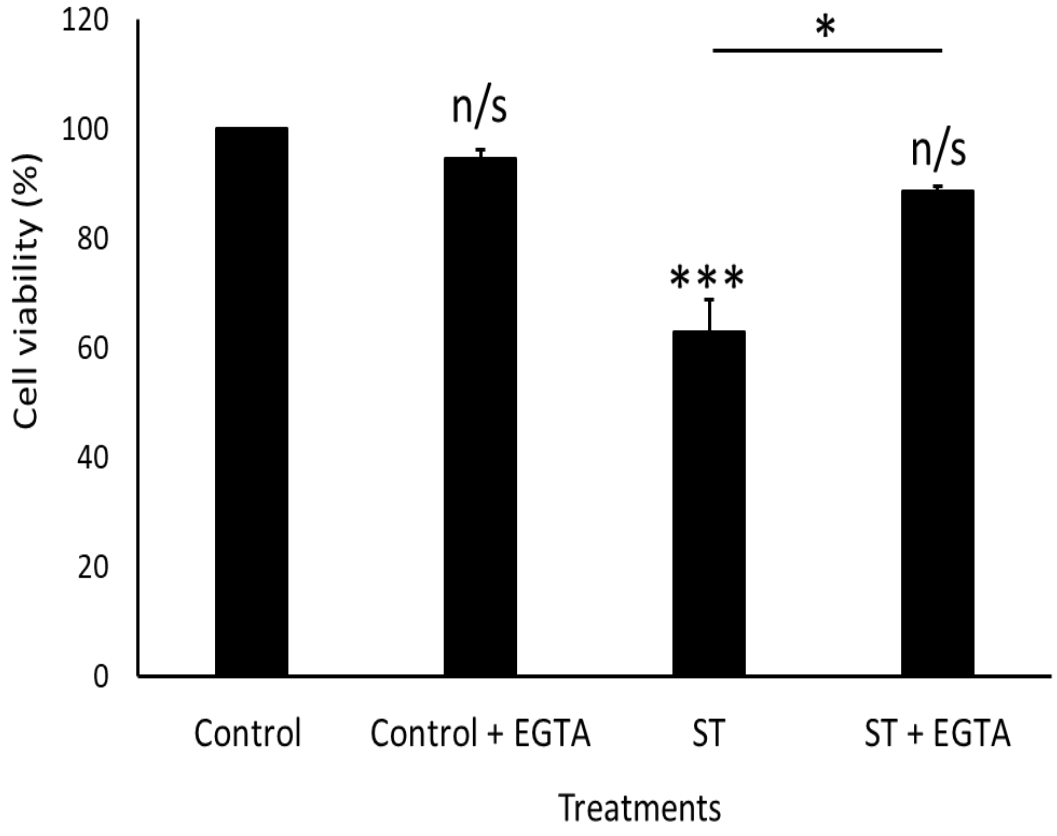

Figure 6. 9. EGTA rescues ST-induced cell death. Cell viability measured using FDA assay, cells were either untreated (control), treated with 1 mM EGTA, 10 µM ST alone or 10 µM ST co-treated with 1 mM EGTA for 24 h followed by detection of viable cells. Data are mean±SEM, n=3, *p<0.05, **p<0.01, ANOVA with *post hoc* Tukey's test.

6.2.6 Voltage-gated ion channel blockers rescue cardiac progenitor cell viability after ST treatment

After confirming that ST caused an acute inhibition of calcium re-entry after store depletion and reducing the external calcium concentration improved CPC viability, we wished to identify the ion channels involved. Similar experimental designs were used as for the SOCE procedure, to confirm that the calcium channel blockers inhibited calcium re-entry after store depletion. Firstly, the t-type calcium channel inhibitor known as NNC 55-0396 (NNC) was used, with cells co-treated by NNC (with or without ST) and calcium detected using fluo-4. These data showed there was no difference in calcium re-entry when NNC was added to control cells (1.3 ± 0.0), ST caused a lowered calcium fluorescence of 1.2 ± 0.0 after 10 μM ST treatment, which was reduced further by addition of NNC **(**1.1 ± 0.0) *vs.* positive control cells (1.3 ± 0.0) (n=5, **Figure 6.10A**). These data were confirmed by analysing the calcium response (peak-base MFI fluorescence), which showed no difference relative to control cells co-treated by NNC (1.0 ± 0.0-fold), a reduced maximum change with ST causing 0.7 ± 0.0-fold change and this was reduced further to 0.3 ± 0.0-fold after ST was co-treated with NNC when compared to control (n=5, $p<0.05$. **Figure 6.10B**).

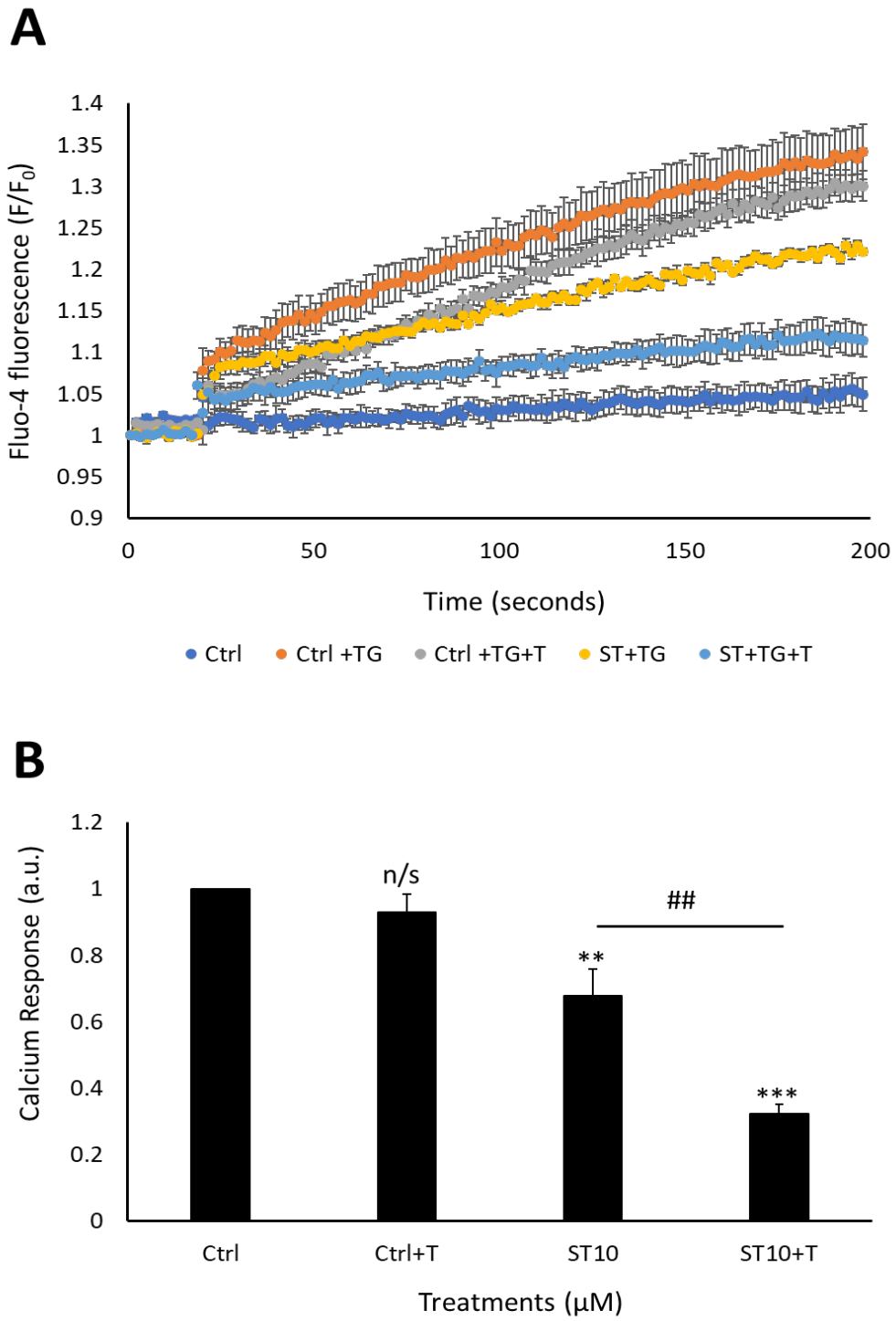

Figure 6. 10. SOCE in CPCs after ST treatment co-treated with NNC. **(A)** Time course assay of calcium signalling after thapsigargin pre-treatment, +/- 10 µM ST +/- 100 nM NNC (T) and each data point represents 1.52 s. After 30 s of imaging, the different concentrations of ST with or without T was injected with calcium. Negative control: cells without thapsigargin pre-treatment. Data are mean±SEM, n=5. **(B)** Quantification of calcium response (peak signal-mean baseline signal) for cells treated with 10 µM ST treatment +/- T. Data are mean±SEM, n=5 ***p*<0.01. ****p*<0.001 *vs.* control and ##*p*<0.01 *vs.* 10 µM ST only. ANOVA with *post hoc* Tukey's test.

Next, the L-type calcium channel was investigated, using nifedipine to block the channel and measure calcium reuptake after store depletion. Peak calcium fluorescence was 1.3 ± 0.0 for control cells treated with nifedipine, 1.2 ± 0.0 in cells treated with ST and 1.2 ± 0.0 in cells treated with nifedipine (n=5, **Figure 6.11A**). These data were confirmed by analysing the calcium response showing no difference with control cells co-treated with nifedipine 0.8 ± 0.0, a reduced maximum change with ST 0.7 ± 0.0 and this was reduced further to 0.5 ± 0.0 after ST was co-treated with NNC when compared to control (n=5, $p<0.05$. **Figure 6.11B**).

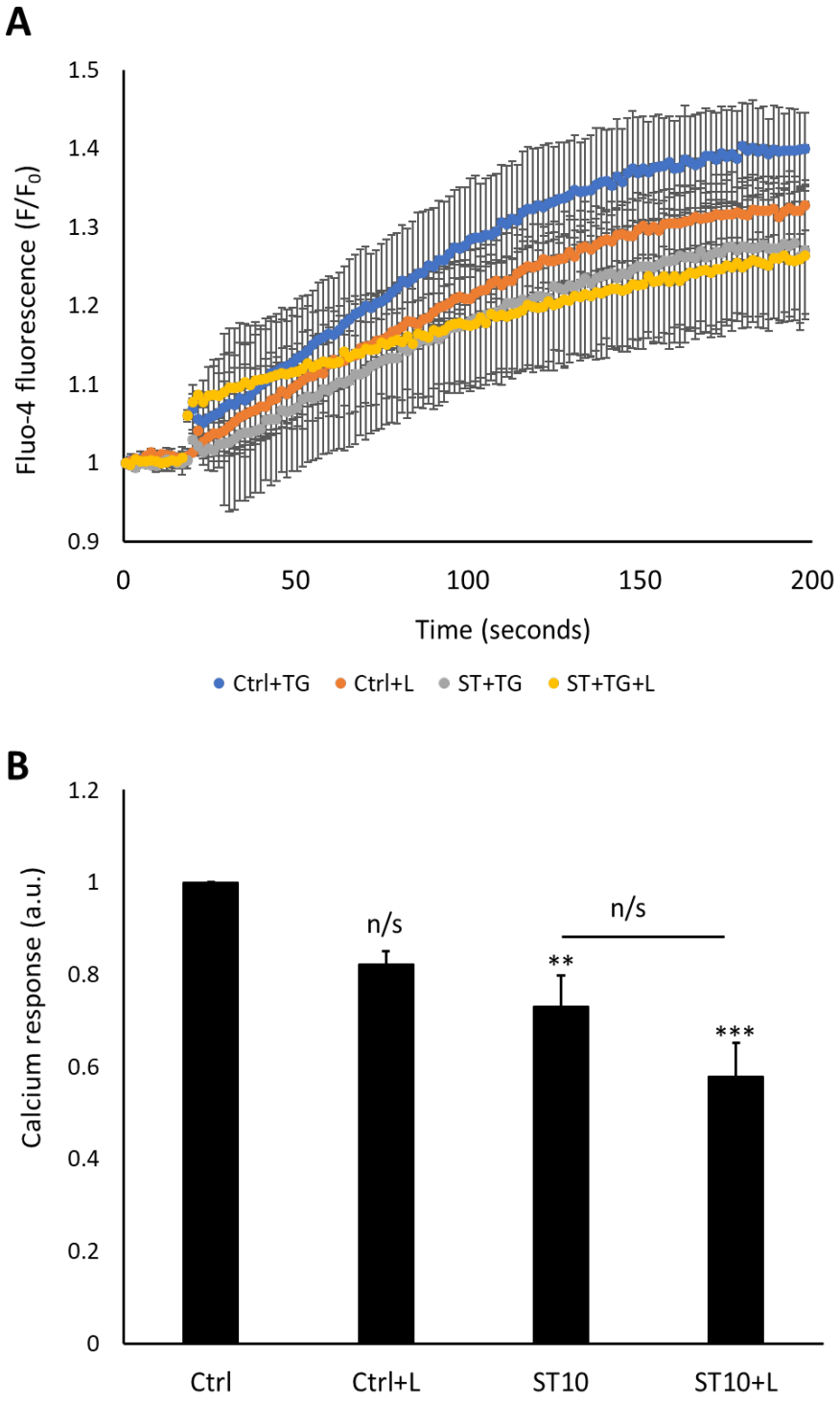

Figure 6. 11. SOCE in CPCs after ST treatment cotreated with nifedipine. **(A)** Time course assay of calcium signalling after thapsigargin pre-treatment, +/- 10 µM ST +/- 100 nM nifedipine (L) and each data point represents 1.52 s. After 30 s of imaging the different concentrations of ST +/- L was injected with calcium. Negative control are cells without thapsigargin pre-treatment. Data are mean±SEM, n=5. **(B)** Quantification of calcium response (peak signal-mean baseline signal) for cells treated with 10 µM ST treatment +/- L. Data are mean±SEM, n=5 **p<0.01. ***p<0.001 *vs.* control and ##p<0.01 *vs.* 10 µM ST only. ANOVA with *post hoc* Tukey's test.

The effects of the non-selective sarcolemmal calcium channel inhibitor gadolinium (Gd^{3+}) were also investigated. Cells were treated as previously described and analysed for calcium changes. Peak calcium fluorescence showed no change when comparing 1.3 ± 0.0 for control cells treated with Gd^{3+}, ST only showed 1.2 ± 0.0 and ST co-treated with Gd^{3+} 1.2 ± 0.0 increase in fluorescence (n=5, **Figure 6.12A**). These data were confirmed by analysing the calcium response showing a significant difference when control cells were co-treated with Gd^{3+} 0.6 ± 0.0-fold change, and ST only showed 0.6 ± 0.0-fold and this unchanged after ST was co-treated with Gd^{3+}, 0.6 ± 0.0-fold when compared to control (n=5, $p<0.05$. **Figure 6.12B**).

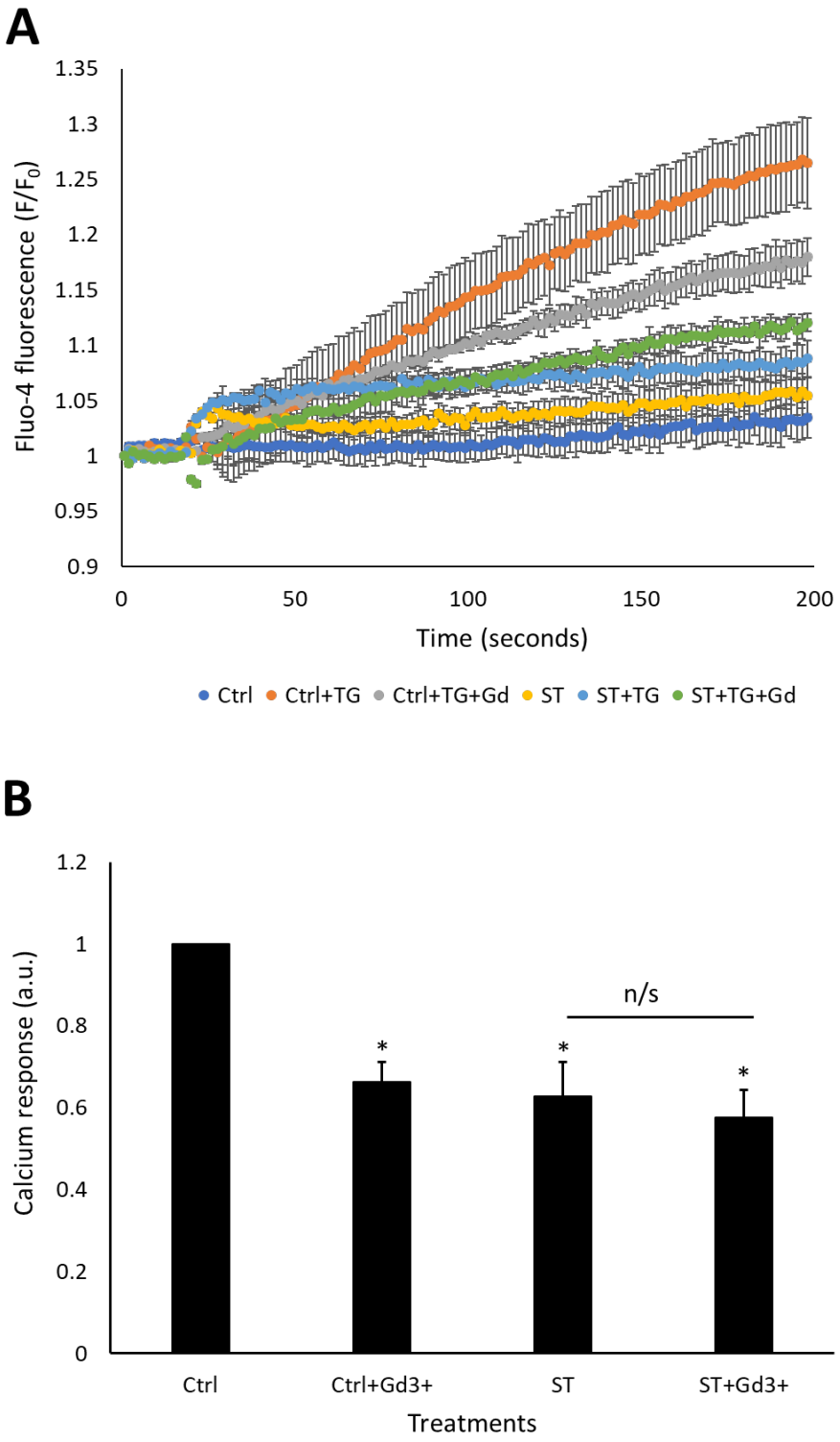

Figure 6. 12. SOCE in CPCs after ST treatment cotreated with gadolinium. **(A)** Time course assay of calcium signalling after thapsigargin pre-treatment, +/- 10 μM ST +/- 100 nM Gd^{3+} and each data point represents 1.52 s. After 30 s of imaging the different concentrations of ST +/- Gd^{3+} was injected with calcium. Negative control are cells without thapsigargin pre-treatment. Data are mean±SEM, n=5. **(B)** Quantification of calcium response (peak signal-mean baseline signal) for cells treated with 10 μM ST treatment +/- Gd^{3+}. Data are mean±SEM, n=5 ***p*<0.01. ****p*<0.001 *vs.* control and ##*p*<0.01 *vs.* 10 μM ST only. ANOVA with *post hoc* Tukey's test.

Having confirmed that the inhibitors were able to block calcium entry into CPCs, it was important to investigate how this might affect CPC viability after treatment with ST after 24 h. Cells were treated with or without ST and co-treated with or without NNC or nifedipine for 24 h, followed by FDA assays. There was no significant change in cell viability with control cells co-treated with different concentrations of nifedipine (10-1000 nM). Cells treated with ST only showed a significant reduction in viability to 85.1 ± 1.8%, ST co-treated with 10 nM nifedipine, 10 91.6 ± 0.9, ST co-treated with 100 nM nifedipine, 92.6 ± 2.2% and cells treated with ST and co-treated with 1000 nM nefipdine showed 89.4 ± 1.6% viability *vs.* control cells 100.0 ± 5.0% ($n=7$, $p<0.05$). There was a significant increase in viability when comparing ST only to ST co-treated with 100 nM nefipdine, although the viability was still significantly less than the control cells ($n=7$, $p<0.05$, **Figure 6.13A**).

There was also no significant change in cell viability with control cells co-treated with different concentrations of NNC (10-1000 nM). Cells treated with ST only showed a significant reduction in viability to 85.7 ± 1.1%, ST co-treated with 10 nM NNC, 91.4 ± 1.3 and co-treated with 1000 nM NNC showed 86.2 ± 2.0% viability ($n=7$, $p<0.05$) *vs.* control cells 100.0 ± 3.5%. However, no change was detected when comparing cells treated with ST and co-treated with 100 nM NNC, 94.9 ± 1.9% to control cells ($n=7$, $p>0.05$). There was a significant increase in viability when comparing ST only to ST co-treated with 100 nM NNC ($n=7$, $p<0.05$, **Figure 6.13B**).

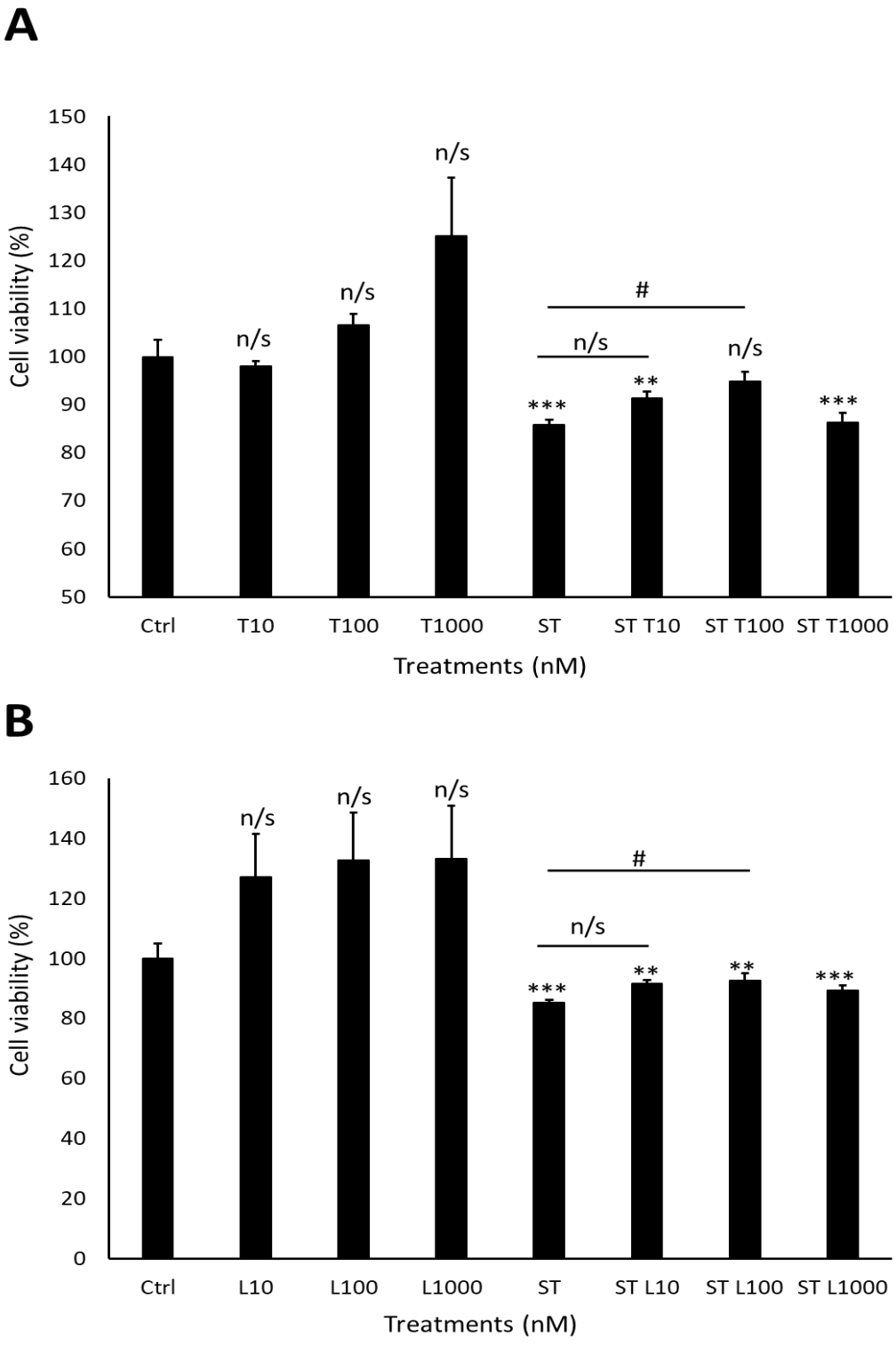

Figure 6. 13. CPC viability is rescued by voltage gated ion channel inhibitors. (A) Cells treated with 10 μM ST +/- 10-1000 nM NNC (T) for 24 h before assessment of viability **(B)** Cells treated with 10 μM ST +/- 10-1000 nm nifedipine (L) . Data are mean±SEM, n=7; *p<0.05, **p<0.01, ***p<0.001 *vs.* control, #p<0.05 *vs.* ST only. ANOVA with *post hoc* Tukey's test.

6.2.7 EPAC agonists protect cells from sorafenib-induced cell death, due to AKT activation

Western blotting was used to determine whether CPCs expressed EPAC proteins 1 and 2. Two distinct bands were detected for both EPAC 1 and EPAC2 (**Figure 6.14A**). Having confirmed EPAC expression in CPCs, an EPAC agonist (8CPT) was used to see if it could protect against calcium-induced cell death. Cell viability was unchanged by 8CPT only (10 and 20 μM), ST significantly reduced cell viability to 85.2 ± 0.9%, ST co-treated 10 μM reduced viability to 93.1 ± 0.6% and ST co-treated with 20 μM reduced viability to 90.5 ± 2.4% *vs.* control (100.0 ± 4.2%) (n=4, $p<0.05$, **Figure 6.14**). However, cells treated with ST and co-treated with 10 μM 8CPT showed significant improvement in cell viability compared to control (n=4, $p<0.05$).

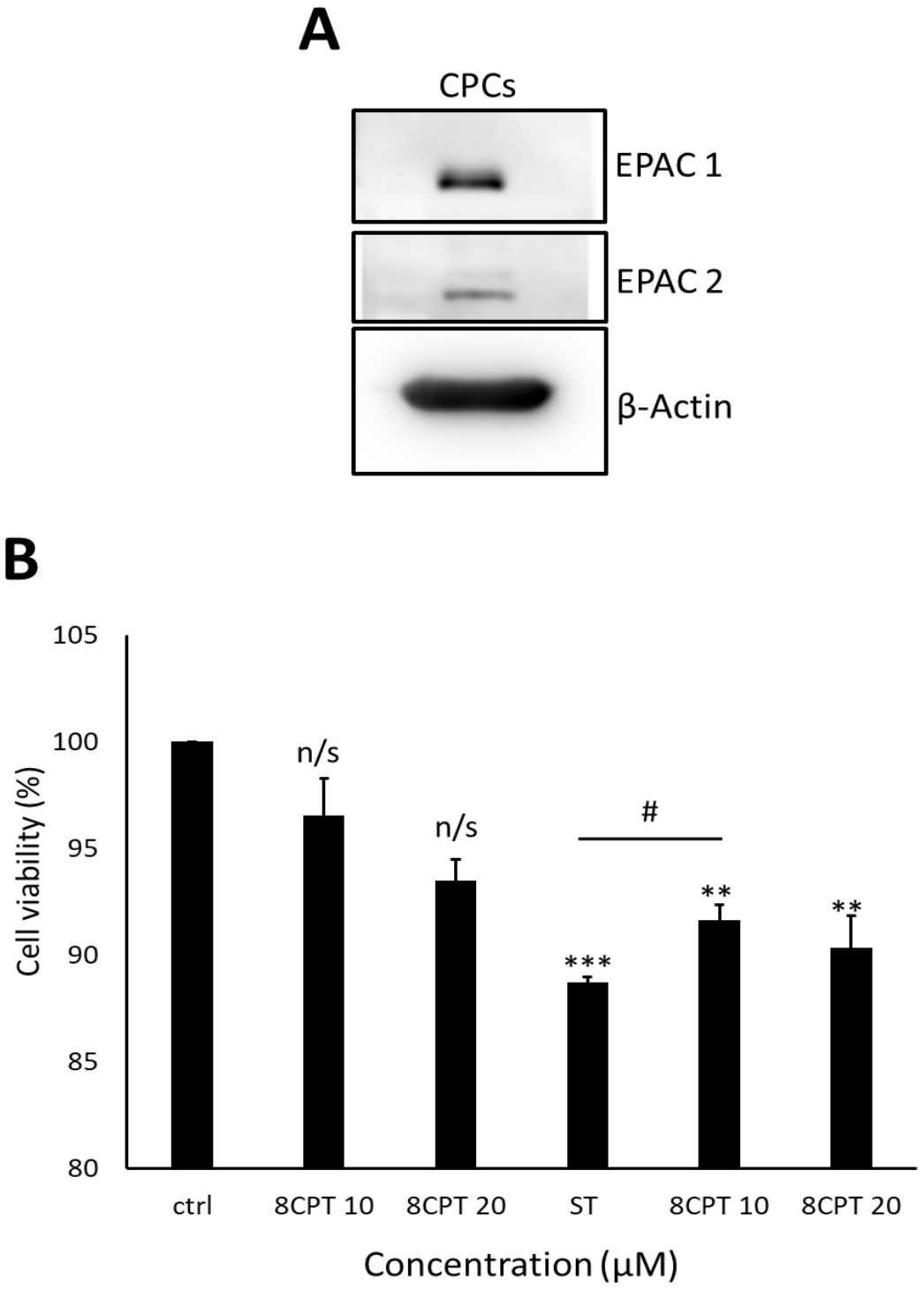

Figure 6. 14. EPAC protects against ST-induced cell death. Western blot representative images showing expression of EPAC 1 and 2 **(B)** Cell viability analysis after cells treated with ST and co-treated with 10 μM or 20 μM 8CPT (EPAC agonist); control cells, control cells treated with 10 μM or 20 μM EPAC, with or without ST. Data are mean±SEM, n=4. **p*<0.05, ****p*<0.001, n/s=not significant *vs.* control, #*p*<0.05 vs. ST 24 h, ANOVA with *post hoc* Tukey's test.

Western blotting was used to determine whether 8CPT-induced recovery in CPCs after ST treatment involved AKT signalling. There was a significant increase in AKT activation when control cells were treated with 8CPT by 2.1 ± 0.1-fold. Cells treated with ST reduced AKT activation by 0.8 ± 0.0-fold; this was increased when cells were treated with ST and co-treated with 8CPT to 2.5 ± 0.2-fold *vs.* control (1.0 ± 0.0) (n=3, $p<0.05$, **Figure 6.15**).

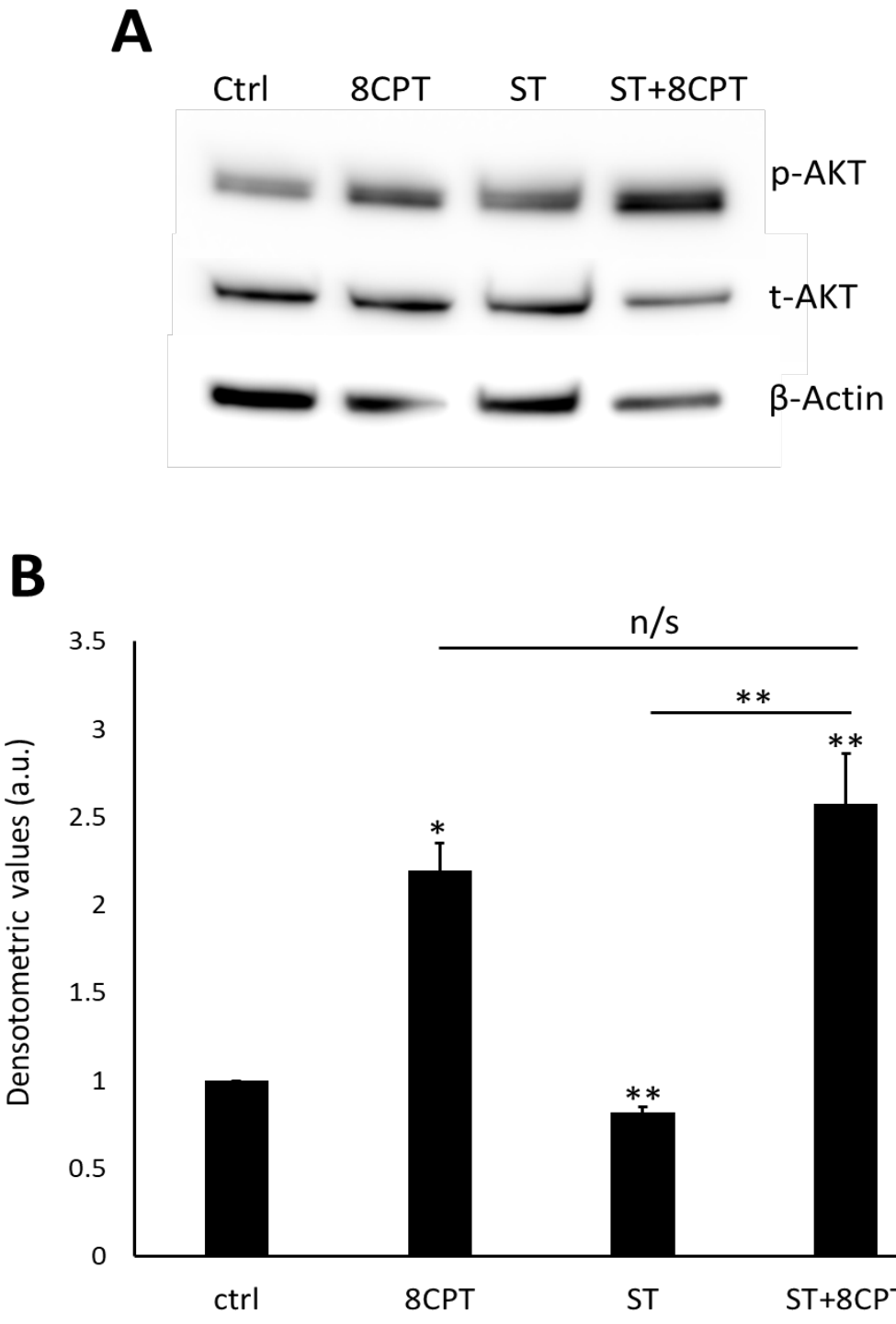

Figure 6. 15. **EPAC agonist increases AKT activation**. Western blot representative image showing expression of total AKT and p-AKT in cell treated with or without 10 μM 8CPT and with or without 10 μM ST (B) Densitometric values showed AKT activation after ST treatment with or without 8CPT. Data are mean±SEM, n=3, ANOVA with *post hoc* Tukey's test.

6.3. Discussion

6.3.1. Sorafenib reduced cell viability but did not induce apoptosis

Cardiac progenitor cell viability was shown to be reduced after 10 μM (24 h) and 5 μM (7 d) of ST treatment. Previously ST has been shown to reduce cell viability in H9C2 cells and myocytes (Hasinoff and Patel, 2010; Will et al., 2008). There was no sign of increased caspase 3 and 7 activity, consistent with previous findings in cardiomyocytes (Duran et al., 2014; Hasinoff and Patel, 2010). However other research has demonstrated caspase activity in a range of cancer cells and also c-kit positive progenitor cells (Ding et al., 2018; Duran et al., 2014; Godin et al., 2015; Sonntag et al., 2014; Zhang et al., 2019). However, limited information was provided on the methods for how the c-kit positive progenitor cells were isolated in the study and therefore, this could be a mixed population. The lack of caspase 3 and 7 activity in our study indicated a cell death independent to apoptosis. These findings were reinforced by no change in apoptotic gene expression after 10 μM ST treatment. There was a limitation with this method as it only assessed the changes in gene expression and not protein levels however, the lack of investigation into these changes was considered justified, due to the absence of both gene changes and caspase activity.

6.3.2 Sorafenib does not increase acidic properties within the cell and does not affect the mitochondrial membrane potential

Acridine orange staining was used to determine if there was any change in AO in the CPCs after ST treatment. No change in cellular acidity indicates

there is no change in lysosomal content, in turn indicative of autophagy. These data show that ST is unlikely to affect autophagy in CPCs. However, previous research has shown that ST does induce autophagy in macrophages, HCC and RCC; these studies suggest a link between autophagy and ST-resistant tumour growth (Lin et al., 2013; Serrano-Oviedo et al., 2018; Sun et al., 2017). Overall, this present study will need to follow up procedures including LC3II Western blots to assess autophagic flux. One study used 3-MA to inhibit the autophagy process, which in turn increased tumour cell surival to ST treatment (Serrano-Oviedo et al., 2018).

After it was determined that AO did not increase with ST treatment, the effects of ST on mitochondrial membrane potential was assessed. Cardiac progenitor cells were treated with ST for 24 h and TMRM used to determine any changes in $\Delta\Psi m$: these data showed no change in TMRM signal with increasing ST dose. These suggest that CPC death is independent of mitochondrial damage, which is in contrast to previous studies using hepatocytes, neuroblastoma cells and rat hepatocholangiocarcinoma cell line (LCSC-2). These studies showed reduced mitochondrial membrane potential and energy production, which was linked to ST inhibition of complex I activity (Bull et al., 2012; Rouleau et al., 2016; Tesori et al., 2015). One study supports our findings, suggesting that overnight applications of ST followed by medium change reversed the effects of ST on the mitochondria (Rouleau et al., 2016). Our study, may have missed this depolarisation of the mitochondria due to media changes. Therefore, future experimental designs should optimise a technique of visualising mitochondrial membrane potential at the point of cell death.

6.3.3 Cardiac progenitor cells calcium entry is inhibited by sorafenib treatment after store depletion

Treatment of cells with ST reduced their ability to replenish internal calcium levels after store depletion with thapsigargin. Previous research has shown ST caused damage to cardiomyocytes and also reduced cytosolic calcium and SR calcium load during systole (Schneider et al., 2018). Although there is limited research on how ST affects the SOCE pathway, there are previous studies on the interaction of SOCE and tumour development. Inhibition of SOCE has been shown to inhibit HCC cell migration (Yang et al., 2013). It has also been shown that progenitor endothelial cells from patients with RCC have a larger amplitude of SOCE. It was also demonstrated that SOCE directly controls endothelial cell proliferation and *in vitro* tubulogenesis. These findings suggest that the ability of ST to inhibit the amplitude of SOCE is a beneficial property for the treatment of HCC and RCC, leaving little room to manipulate the pathway without interfering with the chemotherapeutic action.

Another study which examined the changes in SOCE in RCC cells showed that inhibition of SOCE using gadolinium did not affect RCC cell proliferation. This could mean that either the cells adapted to resist changes in SOCE or that inhibition of SOCE is only an indirect effect of an alternative calcium pathway. As our current study is focused on analysing the acute impact of ST, we therefore designed an experiment that examined how lowering calcium concentrations using a calcium chelator would affect CPC viability over 24 h.

6.3.4 Calcium is the main contributor to cell death after sorafenib treatment

Although ST acutely inhibits SOCE, this does not inform us of how calcium is involved in cell death at the 24 h time point. Typically, in cell death there is a large calcium influx which causes ER overload and induction of apoptosis (Pinton et al., 2008). Therefore, our study used EGTA to chelate calcium which showed that lowering calcium concentrations protected CPCs from ST-induced toxicity, a finding that supports the concept that cell death is linked to an influx of calcium. Previous studies have shown ST to increase intracellular calcium concentrations in leukocyte-depleted erythrocytes (Lupescu et al., 2012). It has also been demonstrated that ST lethality in human leukaemia cells is due to ST-induction of ER stress, which could be due to calcium (Rahmani et al., 2007). As our present study only indicates that a lowered calcium concentration would protect against ST-induced CPC damage, further investigation was needed to establish which specific calcium channels were involved: ion gated or voltage-gated ion channels.

6.3.5 Voltage-gated ion channel inhibitors could provide a therapeutic strategy to prevent cardiotoxicity

Inhibitors for the T type calcium channel have been used for conditions such as noise-induced hearing loss and seizures and have also been shown to be cardioprotective in rat hearts after heart failure and can limit infarct size (Paul Mulder et al., 1997; Mocanu et al., 1999; Shen et al., 2007). One non-specific T type inhibitor (Mibefradil) has been shown to protect neurons post-ischaemic injury and also to reduce cell death in cortical neurons (Nikonenko

et al., 2005; Wildburger et al., 2009). Our study showed that the specific T type inhibitor NNC rescued viability after ST-induced toxicity. This inhibitor is a structural analogue of Mibefradil and has been shown to be more specific for T type calcium channel inhibition (Perez-Reyes, 2003).

The study also investigated the involvement of the L type calcium channel. These channel blockers have also previously been shown to be protective, especially against ischaemic damage, by preventing apoptotic and necrotic cell death. The L type calcium inhibitors have also been shown to be neuroprotective for both hippocampal and cortical neurons (Nikonenko et al., 2005). Our study showed inhibiting the L type channel with nifedipine rescued CPC viability after ST-induced toxicity.

However, other researchers have shown that the inhibition of L or T type calcium channels increases cell death and prevent cell proliferation in NSCs, AML cancer cells and different cancer cell types (Granados et al., 2020; Kim et al., 2018; Huang et al., 2015). These studies used a higher dose of both inhibitors above the 100 nM used in our study and therefore, this could be the reason for the observed toxicity. These findings could be a benefit identified by this project; if the drugs can increase tumour cell death while also protecting CPCs from damage, this would provide a valuable therapeutic target. Our findings indicate that the T-type calcium channel inhibitor (NNC) was more successful at the recovery of CPC viability after ST treatment compared to blocking the L type calcium channel (nifedipine). The reason for this could be that the CPCs rely more on the T type calcium channel for calcium exchange; however, further calcium imaging experiments would be needed to confirm this conclusion.

Moving forward from these findings, the T and L type calcium channel inhibitors should be tested on cancer cell lines to confirm that the blockage of calcium channels does not affect their overall chemotherapeutic action. Caution would be needed if using Mibefradil alongside ST treatment, as it can increase the risk of torsades (Gounder et al., 2018). However, the specific T type calcium inhibitor used in our study might be suitable due to the low concentration and high selectivity for the T type calcium channel compared to its structural analogue.

6.3.6 EPAC protein is protective and acts through AKT signalling

EPAC proteins (EPAC 1 and EPAC 2) are intracellular sensors of prototypic s messenger cAMP (Cheng et al., 2008). Cyclic AMP is one of the most critical s messengers, as it regulates hormones and neurotransmitters in a range of cell types. EPAC 1 and EPAC 2 are activated by cAMP (Borland et al., 2009). The EPAC proteins have been shown to activate important downstream pathways, including the opening of RyR2 and interacting with RAS and therefore increasing activation of AKT and ERK. Therapeutic compounds have been synthesised to activate EPAC proteins; our study used the agonist 8CPT, which activates both EPAC 1 and EPAC 2 (Enserink et al., 2002). However, a study has shown that 8CPT has a greater potency for EPAC 1, with 3 times higher activation than cAMP (Schwede et al., 2015). Our study showed that EPAC activation protects CPCs from ST-induced damage, possible explanations for this could include: opening of RyR channels; causing ER calcium release and thereby protecting the ER from overload/stress (Pereira et al., 2013). However, further experiments involving RyR receptor

manipulation would be needed to confirm this. Our study showed that 8CPT increased AKT activation, which is known to increase cell survival and proliferation: a further experiment inhibiting AKT could solidify this hypothesis. Similar findings have been shown in previous studies, with 8CPT used to protect adult ventricular myocytes from isoproterenol-induced cell death and 8CPT has also protected cortical neurons from β-amyloid-induced cell death (Parvathenani et al., 2000; Yang and Steele, 2013).

6.3.7 Long-term exposure to sorafenib-induces apoptosis independent cell death in cardiac progenitor cells

Similar to the other two RTKIs examined in our study, the long term effects of ST on CPCs were investigated over 7 d. The data showed that ST caused a significant reduction in CPC viability after 5 μM and 50 μM exposure for 7 d, which was reinforced by live-cell staining for ToPro-3. The ToPro-3 staining was significantly increased in CPCs after ST exposure, indicating an increase in end-stage cell death. There was no evidence of apoptosis, shown by the absence of caspase 3 and caspase 7 activity. Analysis of gene expression showed increase in TNF-α. BAX and RIP1 could indicate towards TNF receptor activation of complex IIB or IIC activation.

As with the other RTKIs examined, the trough concentration study was restricted by the available time to limited data, with no experiments assessing the involvement of necroptosis or calcium-dependent cell death. Therefore, the future work suggested would be to investigate necroptosis using protein assays and the contribution of calcium over 7 d. However, these data reinforced that the lower concentrations of ST are toxic to CPCs over 7 d.

6.3.8 Conclusions

In summary, our study showed that ST does not induce apoptosis in CPCs, instead being associated with an alternative cell death pathway, and did not reduce $\Delta\Psi m$. Our study showed that acute CPC exposure to ST reduced calcium reuptake after store depletion. The study also showed that lowering external calcium levels protected CPCs from ST-induced cell death over 24 h, suggesting a calcium-dependent cell death. Further information was provided, which indicated that voltage-gated ion channels are also involved in the cell death process. However, general membrane calcium inhibitors (Gd^{3+}) did not affect calcium exchange in ST-treated samples. Additionally, EPAC agonist 8CPT was shown to protect CPCs from ST-induced cell death, which evidence suggested was through increased AKT signalling. Overall our study offers possible therapeutic actions such as the use of NNC, nifedipine or 8CPT to protect the CPCs from damage.

The main limitation of this study is the lack of evidence for exactly how ST-induces calcium-dependent cell death. Further experiments are required to fully understand whether this calcium-induced cell death is through direct interaction of ST on calcium channels or via indirect mechanism. The study would also benefit from further investigations into calcium membrane ion channels, including TRP channels.

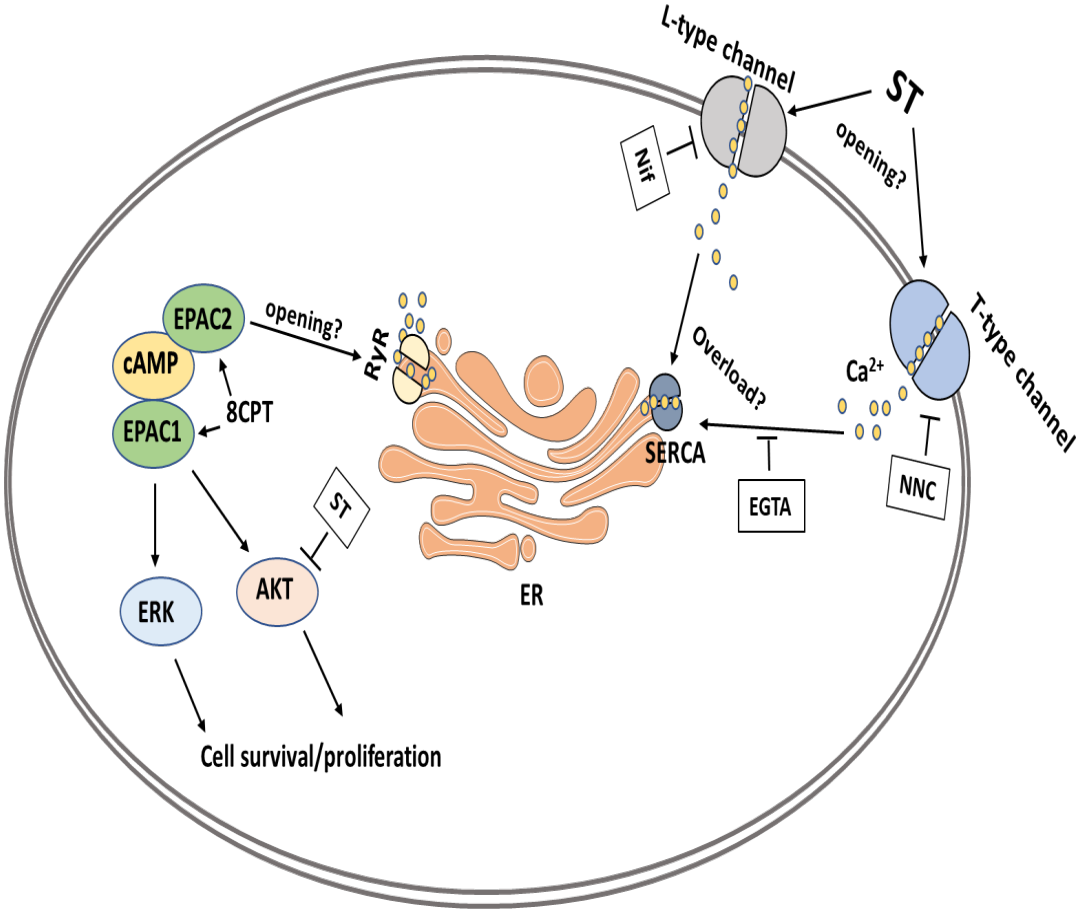

Figure 6. 16. Schematic overview of proposed model for ST-induced cell death in CPCs. The figure shows possible mechanism where ST could induce opening of T and L type calcium channels, causing an influx of calcium into the cytoplasm, this is then up taken by the ER through SERCA protein. Once the calcium uptake exceeds capacity this would cause ER overload/stress and therefore cell death. The diagram shows EGTA reducing calcium uptake into the ER and the use of NNC and nifedipine (Nif) to prevent calcium entry into the cytoplasm, these would limit ER overload. 8CPT activation of EPAC could cause the opening of RyR relieving the ER of calcium overload or EPAC could cause increased activation of ERK and AKT, therefore increasing cell survival and proliferation. AKT activation is reducd by ST-treatment.

Chapter 7. Summary and conclusions

The three drugs examined had similarities, in that they all reduced CPC viability at both peak and trough concentrations. None of the three induced end-stage apoptosis; however, SM appeared to increase expression of apoptosis-linked genes and proteins, including BAX, FASR and calpain, along with downregulation of BCL-2. These findings could be due to the potency of the drug: SM inhibits multiple RTKIs including VEGFRs, c-Kit and PDGFRs, which could cause the induction of early-stage apoptosis. In contrast, IM has fewer targets, meaning it might not be potent enough to induce apoptosis (Iqbal and Iqbal, 2014; Aparicio-Gallego et al., 2011). Sorafenib inhibits a similar range of targets to SM, but can also inhibit downstream signalling proteins such as RAF-1, making it more potent and therefore could induce necrosis rather than apoptosis (Wilhelm et al., 2008). Both IM and SM reduced $\Delta\Psi m$, whereas ST did not, this could be because both IM and SM are known to be sequestered by autophagic organelles. The uptake of these drugs into autophagic organelles has been shown to impair the mitochondria, through the secretion of lysosomal content (e.g. secretion of Zn^{2+}) (Pan et al., 2019).

None of the three drugs changed expression of necroptosis-linked genes when applied for 24 h, however, IM caused an increase in MLKL protein activation and necroptosis. Preliminary results showed SM increased MLKL activation; however, the number of replicates was too small to be conclusive. These findings have not previously been investigated in either CPCs or cancer cells, therefore it is difficult to identify a reason why IM would induce necroptosis. An explanation could be that IM impairs the autophagic flux, causing the release of p62 protein from autophagosomes and lysosomes,

aiding in the initiation of the ripoptosome formation and hence necroptotic cell death (Yan et al., 2017). In contrast, ST did not increase acidic organelle content within the cell and therefore, p62 clearance could be more efficient than IM meaning ST might not induce the formation of the ripoptosome.

Imatinib was shown to increase calcium reuptake after store depletion, however, CPC cell viability did not recover after lowering the calcium concentration. Sunitinib did not affect SOCE in CPCs and chelating calcium failed to recover cell viability. Notably, ST caused a dose-dependent reduction in SOCE and CPC viability was rescued by calcium chelation, suggesting an essential role for calcium in ST-induced cell death. This was investigated further using specific calcium inhibitors, including gadolinium, nifedipine and NNC, which showed that the voltage-gated calcium inhibitors reversed ST-induced cell death.

Our study theorised that calcium was causing an ER-overload response such that lowering the internal calcium concentration would protect the cell. There is no apparent reason that ST-induced cell death would be calcium-dependent while that induced by either IM or SM was not. It is possible that ST directly binds to calcium channels on the membrane or ST manipulates the SOCE pathway (by interacting with STIM or ORAI1). However, further testing using co-immunoprecipitation or super resolution microscopy would be needed to determine the direct relationship between ST and calcium. Finally, the EPAC agonist 8CPT was shown to protect CPCs from calcium-dependent cell death due to the increase in AKT activation leading to increased cell survival and could be another therapeutic strategy.

None of the three RTKIs induced activation of caspase 3 or 7 at trough concentrations. Furthermore neither IM nor SM changed expression of apoptosis-associated genes. However, ST upregulated TNF-α, RIP1 and BAX; although these genes are linked to apoptosis (complex IIB), they are also involved in necroptotic cell death (complex IIC). Limited data were available to determine the role these genes had in CPCs after exposure to trough concentrations of ST. Therefore, conclusions cannot be drawn on the cell death pathways induced by trough concentrations of RTKIs and further experiments are needed to assess the involvement of necroptosis, autophagy and cellular calcium levels.

Overall, this study provides the first indication of IM- and ST-induced cell death mechanisms in CPCs. Our experimental evidence indicates that IM-induced necroptosis and autophagy induced cell death, which was reversible with Nec-1 and partially by wortmannin. Sorafenib-induced cell death was dependent on calcium and was reversible with the T- and L-type calcium channel inhibitors and EPAC agonist (8CPT). Sunitinib did not cause a clearly-defined cell death mechanism and therefore, no suggested target for intervention could be identified.

Building on the findings of this project, it would be of value to test the suggested potential treatments on cancer cell lines to ensure that they do not interfere with the RTKIs' chemotherapy action; if successful, the targeted therapy should be used in rodent models to see if they could reverse the cardiotoxic effects of each RTKI. This study's aim was not to criticise the use of these drugs, as there are findings to show they are of huge benefit to patients suffering from RCC, HCC and CML. The motivation for this study was

to better understand these cardiotoxic effects caused by RTKIs and highlighting the importance of monitoring these adverse side effects, especially in patients with pre-existing conditions. A long-term impact of this study could be in the use of some of the targeted therapies suggested, for example use of nec-1 or wortmannin, to overcome the toxic effects of IM on CPCs and in the longer term protect the cardiomyocytes. The use of T or L type calcium channel inhibitors could also be of benefit to patients being treated with ST. This study also provides benefits to the field of CPC biology, adding valuable information on how these cells function, including calcium signalling, autophagy and cell death signalling. This study has shown that human CPCs across multiple lines are clonogenic and can differentiate (endothelial and smooth muscle cells). The study also highlights the importance of investigating cell death pathways other than apoptosis, especially necroptosis, which has often been overlooked.

List of References

Abram s, T.J., Lee, L.B., Murray, L.J., Pryer, N.K., Cherrington, J.M., 2003. SU11248 Inhibits KIT and Platelet-derived Growth Factor Receptor β in Preclinical Models of Human Small Cell Lung Cancer. Mol Cancer Ther 2, 471–478.

Adigun, R., Basit, H., Murray, J., 2020. Necrosis, Cell (Liquefactive, Coagulative, Caseous, Fat, Fibrinoid, and Gangrenous), in: StatPearls. StatPearls Publishing, Treasure Island (FL).

Aggarwal, S., Pittenger, M.F., 2005. Human mesenchymal stem cells modulate allogeneic immune cell responses. Blood 105, 1815–1822. https://doi.org/10.1182/blood-2004-04-1559

Alcacer-Pitarch, B., Buch, M.H., Gray, J., Denton, C.P., Herrick, A., Navarro-Coy, N., Collier, H., Loughrey, L., Pavitt, S., Siddle, H.J., Wright, J., Helliwell, P.S., Emery, P., Redmond, A.C., 2012. Pressure and pain In Systemic sclerosis/Scleroderma - an evaluation of a simple intervention (PISCES): randomised controlled trial protocol. BMC Musculoskelet Disord 13, 11. https://doi.org/10.1186/1471-2474-13-11

An Introduction to Modern Genetics. By C. H. Waddington, 1939. . Proceedings of the Royal Entomological Society of London. Series A, General Entomology 14, 82–82. https://doi.org/10.1111/j.1365-3032.1939.tb00039.x

Aparicio-Gallego, G., Blanco, M., Figueroa, A., García-Campelo, R., Valladares-Ayerbes, M., Grande-Pulido, E., Antón-Aparicio, L., 2011. New Insights into Molecular Mechanisms of Sunitinib-Associated Side Effects. Mol Cancer Ther 10, 2215–2223. https://doi.org/10.1158/1535-7163.MCT-10-1124

Arora, A., Scholar, E.M., 2005. Role of Tyrosine Kinase Inhibitors in Cancer Therapy. J Pharmacol Exp Ther 315, 971–979. https://doi.org/10.1124/jpet.105.084145

Ashe, P.C., Berry, M.D., 2003. Apoptotic signalling cascades. Progress in Neuro-Psychopharmacology and Biological Psychiatry, Apoptosis and Human Neurodegenerative Diseases 27, 199–214. https://doi.org/10.1016/S0278-5846(03)00016-2

Atallah, E., Kantarjian, H., Cortes, J., 2007a. In reply to “Cardiotoxicity of the cancer therapeutic agent imatinib mesylate.” Nature Medicine 13, 14. https://doi.org/10.1038/nm0107-14

Atallah, E., Kantarjian, H., Cortes, J., 2007b. In reply to “Cardiotoxicity of the cancer therapeutic agent imatinib mesylate.” Nature Medicine 13, 14. https://doi.org/10.1038/nm0107-14

Barr, L.A., Makarewich, C.A., Berretta, R.M., Gao, H., Troupes, C.D., Woitek, F., Recchia, F., Kubo, H., Force, T., Houser, S.R., 2014. Imatinib Activates Pathological Hypertrophy by Altering Myocyte Calcium Regulation. Clin Transl Sci 7, 360–367. https://doi.org/10.1111/cts.12173

Bello, C.L., Mulay, M., Huang, X., Patyna, S., Dinolfo, M., Levine, S., Vugt, A.V., Toh, M., Baum, C., Rosen, L., 2009. Electrocardiographic Characterization of the QTc Interval in Patients with Advanced Solid Tumors: Pharmacokinetic- Pharmacodynamic Evaluation of Sunitinib. Clin Cancer Res 15, 7045–7052. https://doi.org/10.1158/1078-0432.CCR-09-1521

Belloc, F., Moreau-Gaudry, F., Uhalde, M., Cazalis, L., Jeanneteau, M., Lacombe, F., Praloran, V., Mahon, F.-X., 2007. Imatinib and nilotinib induce apoptosis of chronic myeloid leukemia cells through a Bim-dependant pathway modulated by cytokines. Cancer Biol. Ther. 6, 912–919. https://doi.org/10.4161/cbt.6.6.4101

Beltrami, A.P., Barlucchi, L., Torella, D., Baker, M., Limana, F., Chimenti, S., Kasahara, H., Rota, M., Musso, E., Urbanek, K., Leri, A., Kajstura, J., Nadal-Ginard, B., Anversa, P., 2003. Adult Cardiac Stem Cells Are Multipotent and Support Myocardial Regeneration. Cell 114, 763–776. https://doi.org/10.1016/S0092-8674(03)00687-1

Bergmann, O., Bhardwaj, R.D., Bernard, S., Zdunek, S., Barnabé-Heider, F., Walsh, S., Zupicich, J., Alkass, K., Buchholz, B.A., Druid, H., Jovinge, S., Frisén, J., 2009. Evidence for Cardiomyocyte Renewal in Humans. Science 324, 98–102. https://doi.org/10.1126/science.1164680

Bhattacharya, S., Zhang, Q., Andersen, M.E., 2011. A deterministic map of Waddington's epigenetic landscape for cell fate specification. BMC Systems Biology 5, 85. https://doi.org/10.1186/1752-0509-5-85

Bikfalvi, A., 2004. Recent developments in the inhibition of angiogenesis: examples from studies on platelet factor-4 and the VEGF/VEGFR system. Biochemical Pharmacology, Proceedings from the 6th and 7th international conferences, Signal Transduction 2004 and Chromatin 2004 68, 1017–1021. https://doi.org/10.1016/j.bcp.2004.05.030

Blau, H.M., Brazelton, T.R., Weimann, J.M., 2001. The Evolving Concept of a Stem Cell: Entity or Function? Cell 105, 829–841. https://doi.org/10.1016/S0092-8674(01)00409-3

Boehning, D., Patterson, R.L., Sedaghat, L., Glebova, N.O., Kurosaki, T., Snyder, S.H., 2003. Cytochrome c binds to inositol (1,4,5) trisphosphate receptors, amplifying calcium-dependent apoptosis. Nature Cell Biology 5, 1051–1061. https://doi.org/10.1038/ncb1063

Bono, F., De Smet, F., Herbert, C., De Bock, K., Georgiadou, M., Fons, P., Tjwa, M., Alcouffe, C., Ny, A., Bianciotto, M., Jonckx, B., Murakami, M., Lanahan, A.A., Michielsen, C., Sibrac, D., Dol-Gleizes, F., Mazzone, M., Zacchigna, S., Herault, J.-P., Fischer, C., Rigon, P., Ruiz de Almodovar, C., Claes, F., Blanc, I., Poesen, K., Zhang, J., Segura, I., Gueguen, G., Bordes, M.-F., Lambrechts, D., Broussy, R., van de Wouwer, M., Michaux, C., Shimada, T., Jean, I., Blacher, S., Noel, A., Motte, P., Rom, E., Rakic, J.-M., Katsuma, S., Schaeffer, P., Yayon, A., Van Schepdael, A., Schwalbe, H., Gervasio, F.L., Carmeliet, G., Rozensky, J., Dewerchin, M., Simons, M., Christopoulos, A., Herbert, J.-M., Carmeliet, P., 2013. Inhibition of Tumor Angiogenesis and Growth by a Small-Molecule Multi-FGF Receptor Blocker with Allosteric Properties. Cancer Cell 23, 477–488. https://doi.org/10.1016/j.ccr.2013.02.019

Boonen, K.J.M., Post, M.J., 2008. The Muscle Stem Cell Niche: Regulation of Satellite Cells During Regeneration. Tissue Engineering Part B: Reviews 14, 419–431. https://doi.org/10.1089/ten.teb.2008.0045

Borland, G., Smith, B.O., Yarwood, S.J., 2009. EPAC proteins transduce diverse cellular actions of cAMP. Br J Pharmacol 158, 70–86. https://doi.org/10.1111/j.1476-5381.2008.00087.x

Boyer, L.A., Lee, T.I., Cole, M.F., Johnstone, S.E., Levine, S.S., Zucker, J.P., Guenther, M.G., Kumar, R.M., Murray, H.L., Jenner, R.G., Gifford,

D.K., Melton, D.A., Jaenisch, R., Young, R.A., 2005. Core Transcriptional Regulatory Circuitry in Human Embryonic Stem Cells. Cell 122, 947–956. https://doi.org/10.1016/j.cell.2005.08.020

Buchdunger, E., Cioffi, C.L., Law, N., Stover, D., Ohno-Jones, S., Druker, B.J., Lydon, N.B., 2000. Abl Protein-Tyrosine Kinase Inhibitor STI571 Inhibits *In-vitro* Signal Transduction Mediated by c-Kit and Platelet-Derived Growth Factor Receptors. J Pharmacol Exp Ther 295, 139–145.

Bull, V.H., Rajalingam, K., Thiede, B., 2012. Sorafenib-Induced Mitochondrial Complex I Inactivation and Cell Death in Human Neuroblastoma Cells. J. Proteome Res. 11, 1609–1620. https://doi.org/10.1021/pr200790e

Burger, H., Dekker, A.T. den, Segeletz, S., Boersma, A.W.M., Bruijn, P. de, Debiec-Rychter, M., Taguchi, T., Sleijfer, S., Sparreboom, A., Mathijssen, R.H.J., Wiemer, E.A.C., 2015. Lysosomal Sequestration Determines Intracellular Imatinib Levels. Mol Pharmacol 88, 477–487. https://doi.org/10.1124/mol.114.097451

Burke, M.J., Walmsley, R., Munsey, T.S., Smith, A.J., 2019. Receptor tyrosine kinase inhibitors cause dysfunction in adult rat cardiac fibroblasts *in-vitro*. Toxicology *in-vitro* 58, 178–186. https://doi.org/10.1016/j.tiv.2019.03.026

Cai, Z., Jitkaew, S., Zhao, J., Chiang, H.-C., Choksi, S., Liu, J., Ward, Y., Wu, L., Liu, Z.-G., 2014. Plasma membrane translocation of trimerized MLKL protein is required for TNF-induced necroptosis. Nature Cell Biology 16, 55–65. https://doi.org/10.1038/ncb2883

Capdeville, R., Buchdunger, E., Zimmermann, J., Matter, A., 2002. Glivec (STI571, imatinib), a rationally developed, targeted anticancer drug. Nature Reviews Drug Discovery 1, 493–502. https://doi.org/10.1038/nrd839

Carew, J.S., Nawrocki, S.T., Giles, F.J., Cleveland, J.L., 2008. Targeting autophagy: a novel anticancer strategy with therapeutic implications for imatinib resistance. Biologics 2, 201–204.

Carpentier, P.A., Palmer, T.D., 2009. Immune Influence on Adult Neural Stem Cell Regulation and Function. Neuron 64, 79–92. https://doi.org/10.1016/j.neuron.2009.08.038

Cerella, C., Diederich, M., Ghibelli, L., 2010. The Dual Role of Calcium as Messenger and Stressor in Cell Damage, Death, and Survival [WWW Document]. International Journal of Cell Biology. https://doi.org/10.1155/2010/546163

Chaitanya, G.V., Alexander, J.S., Babu, P.P., 2010. PARP-1 cleavage fragments: signatures of cell-death proteases in neurodegeneration. Cell Commun Signal 8, 31. https://doi.org/10.1186/1478-811X-8-31

Chapuy, B., Panse, M., Radunski, U., Koch, R., Wenzel, D., Inagaki, N., Haase, D., Truemper, L., Wulf, G.G., 2009. ABC transporter A3 facilitates lysosomal sequestration of imatinib and modulates susceptibility of chronic myeloid leukemia cell lines to this drug. Haematologica 94, 1528–1536. https://doi.org/10.3324/haematol.2009.008631

Chen, G., Deng, C., Li, Y.-P., 2012. TGF-β and BMP Signalling in Osteoblast Differentiation and Bone Formation. Int J Biol Sci 8, 272–288. https://doi.org/10.7150/ijbs.2929

Chen, L., Pan, Y., Zhang, L., Wang, Y., Weintraub, N., Tang, Y., 2013. Two-Step Protocol for Isolation and Culture of Cardiospheres. Methods Mol Biol 1036, 75–80. https://doi.org/10.1007/978-1-62703-511-8_6

Chen, L., Tredget, E.E., Wu, P.Y.G., Wu, Y., 2008. Paracrine Factors of Mesenchymal Stem Cells Recruit Macrophages and Endothelial Lineage Cells and Enhance Wound Healing. PLoS One 3. https://doi.org/10.1371/journal.pone.0001886

Chen, M.H., Kerkela, R., Force, T., 2008. Mechanisms of cardiomyopathy associated with tyrosine kinase inhibitor cancer therapeutics. Circulation 118, 84–95. https://doi.org/10.1161/CIRCULATIONAHA.108.776831

Chen Ming Hui, Kerkelä Risto, Force Thomas, 2008. Mechanisms of Cardiac Dysfunction Associated With Tyrosine Kinase Inhibitor Cancer Therapeutics. Circulation 118, 84–95. https://doi.org/10.1161/CIRCULATIONAHA.108.776831

Chen, P.-H., Liu, A.-J., Ho, K.-H., Chiu, Y.-T., Anne Lin, Z.-H., Lee, Y.-T., Shih, C.-M., Chen, K.-C., 2018. microRNA-199a/b-5p enhance imatinib efficacy via repressing WNT2 signalling-mediated protective autophagy in imatinib-resistant chronic myeloid leukemia cells. Chemico-Biological Interactions 291, 144–151. https://doi.org/10.1016/j.cbi.2018.06.006

Chen, X., Xu, H., Yuan, P., Fang, F., Huss, M., Vega, V.B., Wong, E., Orlov, Y.L., Zhang, W., Jiang, J., Loh, Y.-H., Yeo, H.C., Yeo, Z.X., Narang, V., Govindarajan, K.R., Leong, B., Shahab, A., Ruan, Y., Bourque, G., Sung, W.-K., Clarke, N.D., Wei, C.-L., Ng, H.-H., 2008. Integration of External Signalling Pathways with the Core Transcriptional Network in Embryonic Stem Cells. Cell 133, 1106–1117. https://doi.org/10.1016/j.cell.2008.04.043

Cheng, A.-L., Kang, Y.-K., Chen, Z., Tsao, C.-J., Qin, S., Kim, J.S., Luo, R., Feng, J., Ye, S., Yang, T.-S., Xu, J., Sun, Y., Liang, H., Liu, J., Wang, J., Tak, W.Y., Pan, H., Burock, K., Zou, J., Voliotis, D., Guan, Z., 2009. Efficacy and safety of sorafenib in patients in the Asia-Pacific region with advanced hepatocellular carcinoma: a phase III randomised, double-blind, placebo-controlled trial. The Lancet Oncology 10, 25–34. https://doi.org/10.1016/S1470-2045(08)70285-7

Cheng, X., Ji, Z., Tsalkova, T., Mei, F., 2008. Epac and PKA: a tale of two intracellular cAMP receptors. Acta Biochim Biophys Sin (Shanghai) 40, 651–662.

Chu, T.F., Rupnick, M.A., Kerkela, R., Dallabrida, S.M., Zurakowski, D., Nguyen, L., Woulfe, K., Pravda, E., Cassiola, F., Desai, J., George, S., Harris, D.M., Ismail, N.S., Chen, J.-H., Schoen, F.J., Van den Abbeele, A.D., Demetri, G.D., Force, T., Chen, M.H., Morgan, J.A., 2007. Cardiotoxicity associated with tyrosine kinase inhibitor sunitinib. The Lancet 370, 2011–2019. https://doi.org/10.1016/S0140-6736(07)61865-0

Chugh, A.R., Beache, G., Loughran, J.H., Mewton, N., Elmore, J.B., Kajstura, J., Pappas, P., Tatooles, A., Stoddard, M.F., Lima, J.A.C., Slaughter, M.S., Anversa, P., Bolli, R., 2012. Administration of Cardiac Stem Cells in Patients with Ischemic Cardiomyopathy (the SCIPIO Trial): Surgical Aspects and Interim Analysis of Myocardial Function and Viability by

Magnetic Resonance. Circulation 126, S54–S64. https://doi.org/10.1161/CIRCULATIONAHA.112.092627

Chung, K.M., Jeong, E.-J., Park, H., An, H.-K., Yu, S.-W., 2016. Mediation of Autophagic Cell Death by Type 3 Ryanodine Receptor (RyR3) in Adult Hippocampal Neural Stem Cells. Front. Cell. Neurosci. 10. https://doi.org/10.3389/fncel.2016.00116

Chung, W.-B., Yi, J.-E., Jin, J.Y., Choi, Y.-S., Park, C.S., Park, W.-C., Song, B.J., Youn, H.-J., 2013. Early Cardiac Function Monitoring for Detection of Subclinical Doxorubicin Cardiotoxicity in Young Adult Patients with Breast Cancer. J Breast Cancer 16, 178–183. https://doi.org/10.4048/jbc.2013.16.2.178

Cianflone, E., Torella, M., Chimenti, C., De Angelis, A., Beltrami, A.P., Urbanek, K., Rota, M., Torella, D., 2019. Adult Cardiac Stem Cell Aging: A Reversible Stochastic Phenomenon? [WWW Document]. Oxidative Medicine and Cellular Longevity. https://doi.org/10.1155/2019/5813147

Clapham, D.E., 2007. Calcium Signalling. Cell 131, 1047–1058. https://doi.org/10.1016/j.cell.2007.11.028

Coppin, C., 2008. Sunitinib for advanced renal cell cancer. Biologics 2, 97–105.

Cottage, C.T., Bailey, B., Fischer, K.M., Avitable, D., Collins, B., Tuck, S., Quijada, P., Gude, N., Alvarez, R., Muraski, J., Sussman, M.A., 2010. Cardiac Progenitor Cell Cycling Stimulated by Pim-1 Kinase. Circ Res 106, 891–901. https://doi.org/10.1161/CIRCRESAHA.109.208629

Csordás, G., Madesh, M., Antonsson, B., Hajnóczky, G., 2002. tcBid promotes Ca2+ signal propagation to the mitochondria: control of Ca2+ permeation through the outer mitochondrial membrane. EMBO J 21, 2198–2206. https://doi.org/10.1093/emboj/21.9.2198

D'Arcy, M.S., 2019. Cell death: a review of the major forms of apoptosis, necrosis and autophagy. Cell Biology International 43, 582–592. https://doi.org/10.1002/cbin.11137

Dasari, V.R., Veeravalli, K.K., Dinh, D.H., 2014. Mesenchymal stem cells in the treatment of spinal cord injuries: A review. World J Stem Cells 6, 120–133. https://doi.org/10.4252/wjsc.v6.i2.120

de Arriba, G., Calvino, M., Benito, S., Parra, T., 2013. Cyclosporine A-induced apoptosis in renal tubular cells is related to oxidative damage and mitochondrial fission. Toxicology Letters 218, 30–38. https://doi.org/10.1016/j.toxlet.2013.01.007

Demetri, G.D., van Oosterom, A.T., Garrett, C.R., Blackstein, M.E., Shah, M.H., Verweij, J., McArthur, G., Judson, I.R., Heinrich, M.C., Morgan, J.A., Desai, J., Fletcher, C.D., George, S., Bello, C.L., Huang, X., Baum, C.M., Casali, P.G., 2006. Efficacy and safety of sunitinib in patients with advanced gastrointestinal stromal tumour after failure of imatinib: a randomised controlled trial. The Lancet 368, 1329–1338. https://doi.org/10.1016/S0140-6736(06)69446-4

Demetri, G.D., Wang, Y., Wehrle, E., Racine, A., Nikolova, Z., Blanke, C.D., Joensuu, H., von Mehren, M., 2009. Imatinib Plasma Levels Are Correlated With Clinical Benefit in Patients With Unresectable/Metastatic Gastrointestinal Stromal Tumors. JCO 27, 3141–3147. https://doi.org/10.1200/JCO.2008.20.4818

Dhuriya, Y.K., Sharma, D., 2018. Necroptosis: a regulated inflammatory mode of cell death. Journal of Neuroinflammation 15, 199. https://doi.org/10.1186/s12974-018-1235-0

Dikic, I., Elazar, Z., 2018. Mechanism and medical implications of mammalian autophagy. Nat Rev Mol Cell Biol 19, 349–364. https://doi.org/10.1038/s41580-018-0003-4

Ding, X., Sun, W., Chen, J., 2018. IL-2 augments the sorafenib-induced apoptosis in liver cancer by promoting mitochondrial fission and activating the JNK/TAZ pathway. Cancer Cell Int 18. https://doi.org/10.1186/s12935-018-0671-3

Dondelinger, Y., Aguileta, M.A., Goossens, V., Dubuisson, C., Grootjans, S., Dejardin, E., Vandenabeele, P., Bertrand, M.J.M., 2013. RIPK3 contributes to TNFR1-mediated RIPK1 kinase-dependent apoptosis in conditions of cIAP1/2 depletion or TAK1 kinase inhibition. Cell Death & Differentiation 20, 1381–1392. https://doi.org/10.1038/cdd.2013.94

Dooner, G.J., Colvin, G.A., Dooner, M.S., Johnson, K.W., Quesenberry, P.J., 2008. Gene Expression Fluctuations in Murine Hematopoietic Stem Cells with Cell Cycle Progression. J Cell Physiol 214, 786–795. https://doi.org/10.1002/jcp.21273

Drug Approval Package: Nexavar (Sorafenib) NDA #021923 [WWW Document], n.d. URL https://www.accessdata.fda.gov/drugsatfda_docs/nda/2005/021923_s000_NexavarTOC.cfm (accessed 12.17.19).

Druker, B.J., Tamura, S., Buchdunger, E., Ohno, S., Segal, G.M., Fanning, S., Zimmermann, J., Lydon, N.B., 1996. Effects of a selective inhibitor of the Abl tyrosine kinase on the growth of Bcr–Abl positive cells. Nature Medicine 2, 561. https://doi.org/10.1038/nm0596-561

Duran, J.M., Makarewich, C.A., Trappanese, D., Gross, P., Husain, S., Dunn, J., Lal, H., Sharp, T.E., Starosta, T., Vagnozzi, R.J., Berretta, R.M., Barbe, M., Yu, D., Gao, E., Kubo, H., Force, T., Houser, S.R., 2014. Sorafenib Cardiotoxicity Increases Mortality after Myocardial Infarction. Circ Res 114, 1700–1712. https://doi.org/10.1161/CIRCRESAHA.114.303200

Echtay, K.S., Roussel, D., St-Pierre, J., Jekabsons, M.B., Cadenas, S., Stuart, J.A., Harper, J.A., Roebuck, S.J., Morrison, A., Pickering, S., Clapham, J.C., Brand, M.D., 2002. Superoxide activates mitochondrial uncoupling proteins. Nature 415, 96–99. https://doi.org/10.1038/415096a

Ellegaard, A.-M., Groth-Pedersen, L., Oorschot, V., Klumperman, J., Kirkegaard, T., Nylandsted, J., Jäättelä, M., 2013. Sunitinib and SU11652 Inhibit Acid Sphingomyelinase, Destabilize Lysosomes, and Inhibit Multidrug Resistance. Mol Cancer Ther 12, 2018–2030. https://doi.org/10.1158/1535-7163.MCT-13-0084

Ellison, G.M., Torella, D., Dellegrottaglie, S., Perez-Martinez, C., Perez de Prado, A., Vicinanza, C., Purushothaman, S., Galuppo, V., Iaconetti, C., Waring, C.D., Smith, A., Torella, M., Cuellas Ramon, C., Gonzalo-Orden, J.M., Agosti, V., Indolfi, C., Galiñanes, M., Fernandez-Vazquez, F., Nadal-Ginard, B., 2011. Endogenous Cardiac Stem Cell Activation by Insulin-Like Growth Factor-1/Hepatocyte Growth Factor Intracoronary Injection Fosters Survival and Regeneration of the

Infarcted Pig Heart. Journal of the American College of Cardiology 58, 977–986. https://doi.org/10.1016/j.jacc.2011.05.013

Ellison, G.M., Torella, D., Karakikes, I., Purushothaman, S., Curcio, A., Gasparri, C., Indolfi, C., Cable, N.T., Goldspink, D.F., Nadal-Ginard, B., 2007. Acute β-Adrenergic Overload Produces Myocyte Damage through Calcium Leakage from the Ryanodine Receptor 2 but Spares Cardiac Stem Cells. J. Biol. Chem. 282, 11397–11409. https://doi.org/10.1074/jbc.M607391200

Ellison, G.M., Vicinanza, C., Smith, A.J., Aquila, I., Leone, A., Waring, C.D., Henning, B.J., Stirparo, G.G., Papait, R., Scarfò, M., Agosti, V., Viglietto, G., Condorelli, G., Indolfi, C., Ottolenghi, S., Torella, D., Nadal-Ginard, B., 2013. Adult c-kitpos Cardiac Stem Cells Are Necessary and Sufficient for Functional Cardiac Regeneration and Repair. Cell 154, 827–842. https://doi.org/10.1016/j.cell.2013.07.039

El-Serag, H.B., Marrero, J.A., Rudolph, L., Reddy, K.R., 2008. Diagnosis and Treatment of Hepatocellular Carcinoma. Gastroenterology 134, 1752–1763. https://doi.org/10.1053/j.gastro.2008.02.090

Enserink, J.M., Christensen, A.E., de Rooij, J., van Triest, M., Schwede, F., Genieser, H.G., Døskeland, S.O., Blank, J.L., Bos, J.L., 2002. A novel Epac-specific cAMP analogue demonstrates independent regulation of Rap1 and ERK. Nature Cell Biology 4, 901–906. https://doi.org/10.1038/ncb874

Ertmer, A., Huber, V., Gilch, S., Yoshimori, T., Erfle, V., Duyster, J., Elsässer, H.-P., Schätzl, H.M., 2007a. The anticancer drug imatinib induces cellular autophagy. Leukemia 21, 936–942. https://doi.org/10.1038/sj.leu.2404606

Ertmer, A., Huber, V., Gilch, S., Yoshimori, T., Erfle, V., Duyster, J., Elsässer, H.-P., Schätzl, H.M., 2007b. The anticancer drug imatinib induces cellular autophagy. Leukemia 21, 936–942. https://doi.org/10.1038/sj.leu.2404606

Escudier, B., Eisen, T., Stadler, W.M., Szczylik, C., Oudard, S., Staehler, M., Negrier, S., Chevreau, C., Desai, A.A., Rolland, F., Demkow, T., Hutson, T.E., Gore, M., Anderson, S., Hofilena, G., Shan, M., Pena, C., Lathia, C., Bukowski, R.M., 2009a. Sorafenib for Treatment of Renal Cell Carcinoma: Final Efficacy and Safety Results of the Phase III Treatment Approaches in Renal Cancer Global Evaluation Trial. JCO 27, 3312–3318. https://doi.org/10.1200/JCO.2008.19.5511

Escudier, B., Szczylik, C., Hutson, T.E., Demkow, T., Staehler, M., Rolland, F., Negrier, S., Laferriere, N., Scheuring, U.J., Cella, D., Shah, S., Bukowski, R.M., 2009b. Randomized Phase II Trial of First-Line Treatment With Sorafenib Versus Interferon Alfa-2a in Patients With Metastatic Renal Cell Carcinoma. JCO 27, 1280–1289. https://doi.org/10.1200/JCO.2008.19.3342

Faissner, A., 2020. Evaluation of Kjell et al.: Defining the Adult Neural Stem Cell Niche Proteome Identifies Key Regulators of Adult Neurogenesis. Cell Stem Cell 26, 127–128. https://doi.org/10.1016/j.stem.2020.01.014

Fernández, A., Sanguino, A., Peng, Z., Ozturk, E., Chen, J., Crespo, A., Wulf, S., Shavrin, A., Qin, C., Ma, J., Trent, J., Lin, Y., Han, H.-D., Mangala, L.S., Bankson, J.A., Gelovani, J., Samarel, A., Bornmann, W., Sood, A.K., Lopez-Berestein, G., 2007. An anticancer C-Kit kinase inhibitor is

reengineered to make it more active and less cardiotoxic. J Clin Invest 117, 4044–4054. https://doi.org/10.1172/JCI32373

Ferreira-Martins João, Rondon-Clavo Carlos, Tugal Derin, Korn Justin A., Rizzi Roberto, Padin-Iruegas Maria Elena, Ottolenghi Sergio, De Angelis Antonella, Urbanek Konrad, Ide-Iwata Noriko, D'Amario Domenico, Hosoda Toru, Leri Annarosa, Kajstura Jan, Anversa Piero, Rota Marcello, 2009. Spontaneous Calcium Oscillations Regulate Human Cardiac Progenitor Cell Growth. Circulation Research 105, 764–774. https://doi.org/10.1161/CIRCRESAHA.109.206698

Force, T., Krause, D.S., Van Etten, R.A., 2007. Molecular mechanisms of cardiotoxicity of tyrosine kinase inhibition. Nature Reviews Cancer 7, 332–344. https://doi.org/10.1038/nrc2106

Foyouzi-Youssefi, R., Arnaudeau, S., Borner, C., Kelley, W.L., Tschopp, J., Lew, D.P., Demaurex, N., Krause, K.-H., 2000. Bcl-2 decreases the free Ca2+ concentration within the endoplasmic reticulum. Proc Natl Acad Sci U S A 97, 5723–5728.

Franco, S.J., Gil-Sanz, C., Martinez-Garay, I., Espinosa, A., Harkins-Perry, S.R., Ramos, C., Müller, U., 2012. Fate-Restricted Neural Progenitors in the Mammalian Cerebral Cortex. Science 337, 746–749. https://doi.org/10.1126/science.1223616

Fuchs, Y., Steller, H., 2011. Programmed Cell Death in Animal Development and Disease. Cell 147, 742–758. https://doi.org/10.1016/j.cell.2011.10.033

Galipeau, J., Sensébé, L., 2018. Mesenchymal stromal cells: clinical challenges and therapeutic opportunities. Cell Stem Cell 22, 824–833. https://doi.org/10.1016/j.stem.2018.05.004

Galluzzi, L., López-Soto, A., Kumar, S., Kroemer, G., 2016. Caspases Connect Cell-Death Signalling to Organismal Homeostasis. Immunity 44, 221–231. https://doi.org/10.1016/j.immuni.2016.01.020

Galluzzi, L., Vitale, I., Aaronson, S.A., Abrams, J.M., Adam, D., Agostinis, P., Alnemri, E.S., Altucci, L., Amelio, I., Andrews, D.W., Annicchiarico-Petruzzelli, M., Antonov, A.V., Arama, E., Baehrecke, E.H., Barlev, N.A., Bazan, N.G., Bernassola, F., Bertrand, M.J.M., Bianchi, K., Blagosklonny, M.V., Blomgren, K., Borner, C., Boya, P., Brenner, C., Campanella, M., Candi, E., Carmona-Gutierrez, D., Cecconi, F., Chan, F.K.-M., Chandel, N.S., Cheng, E.H., Chipuk, J.E., Cidlowski, J.A., Ciechanover, A., Cohen, G.M., Conrad, M., Cubillos-Ruiz, J.R., Czabotar, P.E., D'Angiolella, V., Dawson, T.M., Dawson, V.L., De Laurenzi, V., De Maria, R., Debatin, K.-M., DeBerardinis, R.J., Deshmukh, M., Di Daniele, N., Di Virgilio, F., Dixit, V.M., Dixon, S.J., Duckett, C.S., Dynlacht, B.D., El-Deiry, W.S., Elrod, J.W., Fimia, G.M., Fulda, S., García-Sáez, A.J., Garg, A.D., Garrido, C., Gavathiotis, E., Golstein, P., Gottlieb, E., Green, D.R., Greene, L.A., Gronemeyer, H., Gross, A., Hajnoczky, G., Hardwick, J.M., Harris, I.S., Hengartner, M.O., Hetz, C., Ichijo, H., Jäättelä, M., Joseph, B., Jost, P.J., Juin, P.P., Kaiser, W.J., Karin, M., Kaufmann, T., Kepp, O., Kimchi, A., Kitsis, R.N., Klionsky, D.J., Knight, R.A., Kumar, S., Lee, S.W., Lemasters, J.J., Levine, B., Linkermann, A., Lipton, S.A., Lockshin, R.A., López-Otín, C., Lowe, S.W., Luedde, T., Lugli, E., MacFarlane, M., Madeo, F., Malewicz, M., Malorni, W., Manic, G., Marine, J.-C., Martin, S.J., Martinou, J.-C., Medema, J.P., Mehlen, P., Meier, P., Melino, S., Miao,

E.A., Molkentin, J.D., Moll, U.M., Muñoz-Pinedo, C., Nagata, S., Nuñez, G., Oberst, A., Oren, M., Overholtzer, M., Pagano, M., Panaretakis, T., Pasparakis, M., Penninger, J.M., Pereira, D.M., Pervaiz, S., Peter, M.E., Piacentini, M., Pinton, P., Prehn, J.H.M., Puthalakath, H., Rabinovich, G.A., Rehm, M., Rizzuto, R., Rodrigues, C.M.P., Rubinsztein, D.C., Rudel, T., Ryan, K.M., Sayan, E., Scorrano, L., Shao, F., Shi, Y., Silke, J., Simon, H.-U., Sistigu, A., Stockwell, B.R., Strasser, A., Szabadkai, G., Tait, S.W.G., Tang, D., Tavernarakis, N., Thorburn, A., Tsujimoto, Y., Turk, B., Vanden Berghe, T., Vandenabeele, P., Vander Heiden, M.G., Villunger, A., Virgin, H.W., Vousden, K.H., Vucic, D., Wagner, E.F., Walczak, H., Wallach, D., Wang, Y., Wells, J.A., Wood, W., Yuan, J., Zakeri, Z., Zhivotovsky, B., Zitvogel, L., Melino, G., Kroemer, G., 2018. Molecular mechanisms of cell death: recommendations of the Nomenclature Committee on Cell Death 2018. Cell Death & Differentiation 25, 486–541. https://doi.org/10.1038/s41418-017-0012-4

Gatzemeier, U., Blumenschein, G., Fosella, F., Simantov, R., Elting, J., Bigwood, D., Cihon, F., Reck, M., 2006. Phase II trial of single-agent sorafenib in patients with advanced non-small cell lung carcinoma. JCO 24, 7002–7002. https://doi.org/10.1200/jco.2006.24.18_suppl.7002

Gilbert, S.F., Gilbert, S.F., 2000. Developmental Biology, 6th ed. Sinauer Associates.

GIST | SUTENT® (sunitinib malate) | Safety Info [WWW Document], n.d. URL https://www.sutent.com/GIST/gist_prescribing_information (accessed 11.4.19).

Godin, C., Louandre, C., Bodeau, S., Diouf, M., Saidak, Z., Conte, M.-A., Chauffert, B., Barbare, J.-C., Barget, N., Trinchet, J.-C., Ganne, N., Galmiche, A., 2015. Biomarkers of Apoptosis and Necrosis in Patients with Hepatocellular Carcinoma Treated with Sorafenib. Anticancer Res 35, 1803–1808.

Goldberg, A.D., Allis, C.D., Bernstein, E., 2007. Epigenetics: A Landscape Takes Shape. Cell 128, 635–638. https://doi.org/10.1016/j.cell.2007.02.006

Gonzalez, A.C. de O., Costa, T.F., Andrade, Z. de A., Medrado, A.R.A.P., 2016. Wound healing - A literature review. An Bras Dermatol 91, 614–620. https://doi.org/10.1590/abd1806-4841.20164741

Goodall, M.L., Fitzwalter, B.E., Zahedi, S., Wu, M., Rodriguez, D., Mulcahy-Levy, J.M., Green, D.R., Morgan, M., Cramer, S.D., Thorburn, A., 2016. The Autophagy Machinery Controls Cell Death Switching between Apoptosis and Necroptosis. Developmental Cell 37, 337–349. https://doi.org/10.1016/j.devcel.2016.04.018

Gotink, K.J., Broxterman, H.J., Labots, M., de Haas, R.R., Dekker, H., Honeywell, R.J., Rudek, M.A., Beerepoot, L.V., Musters, R.J., Jansen, G., Griffioen, A.W., Assaraf, Y.G., Pili, R., Peters, G.J., Verheul, H.M.W., 2011. Lysosomal Sequestration of Sunitinib: A Novel Mechanism of Drug Resistance. Clin Cancer Res 17, 7337–7346. https://doi.org/10.1158/1078-0432.CCR-11-1667

Gounder, M.M., Mahoney, M.R., Van Tine, B.A., Ravi, V., Attia, S., Deshpande, H.A., Gupta, A.A., Milhem, M.M., Conry, R.M., Movva, S., Pishvaian, M.J., Riedel, R.F., Sabagh, T., Tap, W.D., Horvat, N., Basch, E., Schwartz, L.H., Maki, R.G., Agaram, N.P., Lefkowitz, R.A.,

Mazaheri, Y., Yamashita, R., Wright, J.J., Dueck, A.C., Schwartz, G.K., 2018. Sorafenib for Advanced and Refractory Desmoid Tumors. N Engl J Med 379, 2417–2428. https://doi.org/10.1056/NEJMoa1805052

Graf, U., Casanova, E.A., Cinelli, P., 2011. The Role of the Leukemia Inhibitory Factor (LIF) — Pathway in Derivation and Maintenance of Murine Pluripotent Stem Cells. Genes (Basel) 2, 280–297. https://doi.org/10.3390/genes2010280

Granados, K., Hüser, L., Federico, A., Sachindra, S., Wolff, G., Hielscher, T., Novak, D., Madrigal-Gamboa, V., Sun, Q., Vierthaler, M., Larribère, L., Umansky, V., Utikal, J., 2020. T-type calcium channel inhibition restores sensitivity to MAPK inhibitors in de-differentiated and adaptive melanoma cells. British Journal of Cancer 1–14. https://doi.org/10.1038/s41416-020-0751-8

Guicciardi, M.E., Leist, M., Gores, G.J., 2004. Lysosomes in cell death. Oncogene 23, 2881. https://doi.org/10.1038/sj.onc.1207512

Gumbiner, B.M., Kim, N.-G., 2014. The Hippo-YAP signalling pathway and contact inhibition of growth. J Cell Sci 127, 709–717. https://doi.org/10.1242/jcs.140103

Hajnóczky, G., Davies, E., Madesh, M., 2003. Calcium signalling and apoptosis. Biochemical and Biophysical Research Communications 304, 445–454. https://doi.org/10.1016/S0006-291X(03)00616-8

Halestrap, A.P., 2009. What is the mitochondrial permeability transition pore? Journal of Molecular and Cellular Cardiology 46, 821–831. https://doi.org/10.1016/j.yjmcc.2009.02.021

Hasinoff, B.B., Patel, D., 2010. Mechanisms of Myocyte Cytotoxicity Induced by the Multikinase Inhibitor Sorafenib. Cardiovasc Toxicol 10, 1–8. https://doi.org/10.1007/s12012-009-9056-0

Heinrich, M.C., Griffith, D.J., Druker, B.J., Wait, C.L., Ott, K.A., Zigler, A.J., 2000. Inhibition of c-kit receptor tyrosine kinase activity by STI 571, a selective tyrosine kinase inhibitor. Blood 96, 925–932.

Herman, E.H., Knapton, A., Rosen, E., Thompson, K., Rosenzweig, B., Estis, J., Agee, S., Lu, Q.-A., Todd, J.A., Lipshultz, S., Hasinoff, B., Zhang, J., 2011. A Multifaceted Evaluation of Imatinib-induced Cardiotoxicity in the Rat. Toxicol Pathol 39, 1091–1106. https://doi.org/10.1177/0192623311419524

Hochhaus, A., Larson, R.A., Guilhot, F., Radich, J.P., Branford, S., Hughes, T.P., Baccarani, M., Deininger, M.W., Cervantes, F., Fujihara, S., Ortmann, C.-E., Menssen, H.D., Kantarjian, H., O'Brien, S.G., Druker, B.J., Investigators, for the I., 2017. Long-Term Outcomes of Imatinib Treatment for Chronic Myeloid Leukemia. The New England journal of medicine 376, 917. https://doi.org/10.1056/NEJMoa1609324

Hoffman, A.M., Dow, S.W., 2016. Concise Review: Stem Cell Trials Using Companion Animal Disease Models. STEM CELLS 34, 1709–1729. https://doi.org/10.1002/stem.2377

Hong, K.U., Guo, Y., Li, Q.-H., Cao, P., Al-Maqtari, T., Vajravelu, B.N., Du, J., Book, M.J., Zhu, X., Nong, Y., Bhatnagar, A., Bolli, R., 2014. c-kit+ Cardiac Stem Cells Alleviate Post-Myocardial Infarction Left Ventricular Dysfunction Despite Poor Engraftment and Negligible Retention in the Recipient Heart. PLoS One 9. https://doi.org/10.1371/journal.pone.0096725

Hotchkiss, A., Feridooni, T., Zhang, F., Pasumarthi, K.B.S., 2014. The effects of calcium channel blockade on proliferation and differentiation of cardiac progenitor cells. Cell Calcium 55, 238–251. https://doi.org/10.1016/j.ceca.2014.02.018

Huang, C.-Y., Kuo, W.-T., Huang, Y.-C., Lee, T.-C., Yu, L.C.H., 2013. Resistance to hypoxia-induced necroptosis is conferred by glycolytic pyruvate scavenging of mitochondrial superoxide in colorectal cancer cells. Cell Death Dis 4, e622. https://doi.org/10.1038/cddis.2013.149

Huang, W., Lu, C., Wu, Y., Ouyang, S., Chen, Y., 2015. T-type calcium channel antagonists, mibefradil and NNC-55-0396 inhibit cell proliferation and induce cell apoptosis in leukemia cell lines. J Exp Clin Cancer Res 34. https://doi.org/10.1186/s13046-015-0171-4

Ichijo, H., Nishida, E., Irie, K., Dijke, P. ten, Saitoh, M., Moriguchi, T., Takagi, M., Matsumoto, K., Miyazono, K., Gotoh, Y., 1997. Induction of Apoptosis by ASK1, a Mammalian MAPKKK That Activates SAPK/JNK and p38 Signalling Pathways. Science 275, 90–94. https://doi.org/10.1126/science.275.5296.90

Iqbal, Nida, Iqbal, Naveed, 2014. Imatinib: A Breakthrough of Targeted Therapy in Cancer [WWW Document]. Chemotherapy Research and Practice. https://doi.org/10.1155/2014/357027

Jesty, S.A., Steffey, M.A., Lee, F.K., Breitbach, M., Hesse, M., Reining, S., Lee, J.C., Doran, R.M., Nikitin, A.Y., Fleischmann, B.K., Kotlikoff, M.I., 2012. c-kit+ precursors support postinfarction myogenesis in the neonatal, but not adult, heart. PNAS 109, 13380–13385. https://doi.org/10.1073/pnas.1208114109

Jiang, L., Xu, Q., 2019. Current status and prospects of cardiovascular stem/progenitor cells in cardiovascular regenerative medicine. Sci. Sin.-Vitae 49, 965–976. https://doi.org/10.1360/SSV-2019-0066

Jopling, C., Boue, S., Belmonte, J.C.I., 2011. Dedifferentiation, transdifferentiation and reprogramming: three routes to regeneration. Nature Reviews Molecular Cell Biology 12, 79–89. https://doi.org/10.1038/nrm3043

Jopling, C., Sleep, E., Raya, M., Martí, M., Raya, A., Belmonte, J.C.I., 2010. Zebrafish heart regeneration occurs by cardiomyocyte dedifferentiation and proliferation. Nature 464, 606–609. https://doi.org/10.1038/nature08899

Jung, Y., Song, J., Shiozawa, Y., Wang, J., Wang, Z., Williams, B., Havens, A., Schneider, A., Ge, C., Franceschi, R.T., McCauley, L.K., Krebsbach, P.H., Taichman, R.S., 2008. Hematopoietic Stem Cells Regulate Mesenchymal Stromal Cell Induction into Osteoblasts Thereby Participating in The Formation of the Stem Cell Niche. Stem Cells 26, 2042–2051. https://doi.org/10.1634/stemcells.2008-0149

Juurikivi, A., Sandler, C., Lindstedt, K.A., Kovanen, P.T., Juutilainen, T., Leskinen, M.J., Mäki, T., Eklund, K.K., 2005. Inhibition of c-kit tyrosine kinase by imatinib mesylate induces apoptosis in mast cells in rheumatoid synovia: a potential approach to the treatment of arthritis. Annals of the Rheumatic Diseases 64, 1126–1131. https://doi.org/10.1136/ard.2004.029835

Kantarjian, H., O'Brien, S., Jabbour, E., Garcia-Manero, G., Quintas-Cardama, A., Shan, J., Rios, M.B., Ravandi, F., Faderl, S., Kadia, T., Borthakur, G., Huang, X., Champlin, R., Talpaz, M., Cortes, J., 2012.

Improved survival in chronic myeloid leukemia since the introduction of imatinib therapy: a single-institution historical experience. Blood 119, 1981–1987. https://doi.org/10.1182/blood-2011-08-358135

Karch, J., Kanisicak, O., Brody, M.J., Sargent, M.A., Michael, D.M., Molkentin, J.D., 2015. Necroptosis Interfaces with MOMP and the MPTP in Mediating Cell Death. PLoS One 10. https://doi.org/10.1371/journal.pone.0130520

Kaufmann, A.M., Krise, J.P., 2007. Lysosomal Sequestration of Amine-Containing Drugs: Analysis and Therapeutic Implications. Journal of Pharmaceutical Sciences 96, 729–746. https://doi.org/10.1002/jps.20792

Kawabata, M., Umemoto, N., Shimada, Y., Nishimura, Y., Zhang, B., Kuroyanagi, J., Miyabe, M., Tanaka, T., 2015. Downregulation of Stanniocalcin 1 Is Responsible for Sorafenib-Induced Cardiotoxicity. Toxicol Sci 143, 374–384. https://doi.org/10.1093/toxsci/kfu235

Kawaguchi, N., Smith, A.J., Waring, C.D., Hasan, M.K., Miyamoto, S., Matsuoka, R., Ellison, G.M., 2010. c-kitpos GATA-4 High Rat Cardiac Stem Cells Foster Adult Cardiomyocyte Survival through IGF-1 Paracrine Signalling. PLoS One 5. https://doi.org/10.1371/journal.pone.0014297

Keating, G.M., Santoro, A., 2009. Sorafenib. Drugs 69, 223–240. https://doi.org/10.2165/00003495-200969020-00006

Kerkelä, R., Grazette, L., Yacobi, R., Iliescu, C., Patten, R., Beahm, C., Walters, B., Shevtsov, S., Pesant, S., Clubb, F.J., Rosenzweig, A., Salomon, R.N., Etten, R.A.V., Alroy, J., Durand, J.-B., Force, T., 2006a. Cardiotoxicity of the cancer therapeutic agent imatinib mesylate. Nat Med 12, 908–916. https://doi.org/10.1038/nm1446

Kerkelä, R., Grazette, L., Yacobi, R., Iliescu, C., Patten, R., Beahm, C., Walters, B., Shevtsov, S., Pesant, S., Clubb, F.J., Rosenzweig, A., Salomon, R.N., Van Etten, R.A., Alroy, J., Durand, J.-B., Force, T., 2006b. Cardiotoxicity of the cancer therapeutic agent imatinib mesylate. 12, 908–916.

Kerkela, R., Woulfe, K.C., Durand, J., Vagnozzi, R., Kramer, D., Chu, T.F., Beahm, C., Chen, M.H., Force, T., 2009a. Sunitinib-Induced Cardiotoxicity Is Mediated by Off-Target Inhibition of AMP-Activated Protein Kinase. Clin Transl Sci 2, 15–25. https://doi.org/10.1111/j.1752-8062.2008.00090.x

Kerkela, R., Woulfe, K.C., Durand, J.-B., Vagnozzi, R., Kramer, D., Chu, T.F., Beahm, C., Chen, M.H., Force, T., 2009b. Sunitinib-Induced Cardiotoxicity Is Mediated by Off-Target Inhibition of AMP-Activated Protein Kinase. Clinical and Translational Science 2, 15–25. https://doi.org/10.1111/j.1752-8062.2008.00090.x

Khan, M.A., 1995. Effects of myotoxins on skeletal muscle fibers. Progress in Neurobiology 46, 541–560. https://doi.org/10.1016/0301-0082(95)00015-N

Kim, J.S., Jeung, H.K., Cheong, J.-W., Maeng, H., Lee, S.T., Hahn, J.S., Ko, Y.W., Min, Y.H., 2004. Apicidin potentiates the imatinib-induced apoptosis of Bcr–Abl-positive human leukaemia cells by enhancing the activation of mitochondria-dependent caspase cascades. British Journal of Haematology 124, 166–178. https://doi.org/10.1046/j.1365-2141.2003.04759.x

Kim, J.-W., Oh, H.A., Lee, S.H., Kim, K.C., Eun, P.H., Ko, M.J., Gonzales, E.L.T., Seung, H., Kim, S., Bahn, G.H., Shin, C.Y., 2018. T-Type Calcium Channels Are Required to Maintain Viability of Neural Progenitor Cells. Biomol Ther (Seoul) 26, 439–445. https://doi.org/10.4062/biomolther.2017.223

Kim, Y.-S., Morgan, M.J., Choksi, S., Liu, Z., 2007. TNF-Induced Activation of the Nox1 NADPH Oxidase and Its Role in the Induction of Necrotic Cell Death. Molecular Cell 26, 675–687. https://doi.org/10.1016/j.molcel.2007.04.021

Kong, H., Jones, P.P., Koop, A., Zhang, L., Duff, H.J., Wayne Chen, S.R., 2008. Caffeine Induces Ca2+ Release by Reducing The Threshold for Luminal Ca2+ Activation of the Ryanodine Receptor. Biochem J 414, 441–452. https://doi.org/10.1042/BJ20080489

Kroemer, G., Jäättelä, M., 2005. Lysosomes and autophagy in cell death control. Nature Reviews Cancer 5, 886. https://doi.org/10.1038/nrc1738

Krysko, D.V., Berghe, T.V., Parthoens, E., D'Herde, K., Vandenabeele, P., 2008. Chapter 16 Methods for Distinguishing Apoptotic from Necrotic Cells and Measuring Their Clearance, in: Methods in Enzymology, Programmed Cell Death,General Principles ForStudying Cell Death, Part A. Academic Press, pp. 307–341. https://doi.org/10.1016/S0076-6879(08)01416-X

Kyrylkova, K., Kyryachenko, S., Leid, M., Kioussi, C., 2012. Detection of Apoptosis by TUNEL Assay, in: Kioussi, C. (Ed.), Odontogenesis: Methods and Protocols, Methods in Molecular Biology. Humana Press, Totowa, NJ, pp. 41–47. https://doi.org/10.1007/978-1-61779-860-3_5

Lai, E.C., 2004. Notch signalling: control of cell communication and cell fate. Development 131, 965–973. https://doi.org/10.1242/dev.01074

Lecoeur, H., Ledru, E., Prévost, M.-C., Gougeon, M.-L., 1997. Strategies for phenotyping apoptotic peripheral human lymphocytes comparing ISNT, annexin-V and 7-AAD cytofluorometric staining methods. Journal of Immunological Methods 209, 111–123. https://doi.org/10.1016/S0022-1759(97)00138-5

Lee, W.-S., Kim, J., 2018. Cardiotoxicity associated with tyrosine kinase-targeted anticancer therapy. Mol. Cell. Toxicol. 14, 247–254. https://doi.org/10.1007/s13273-018-0027-z

Lennartsson, J., Rönnstrand, L., 2012. Stem Cell Factor Receptor/c-Kit: From Basic Science to Clinical Implications. Physiological Reviews 92, 1619–1649. https://doi.org/10.1152/physrev.00046.2011

Leveque, D., Maloisel, F., 2005. Clinical Pharmacokinetics of Imatinib Mesylate. *In-vivo* 19, 77–84.

Lewis-McDougall, F.C., Ruchaya, P.J., Domenjo-Vila, E., Shin Teoh, T., Prata, L., Cottle, B.J., Clark, J.E., Punjabi, P.P., Awad, W., Torella, D., Tchkonia, T., Kirkland, J.L., Ellison-Hughes, G.M., 2019. Aged-senescent cells contribute to impaired heart regeneration. Aging Cell 18. https://doi.org/10.1111/acel.12931

Li, F., Munsey, T.S., Sivaprasadarao, A., 2017a. TRPM2-mediated rise in mitochondrial Zn2+ promotes palmitate-induced mitochondrial fission and pancreatic β-cell death in rodents. Cell Death Differ 24, 1999–2012. https://doi.org/10.1038/cdd.2017.118

Li, F., Munsey, T.S., Sivaprasadarao, A., 2017b. TRPM2-mediated rise in mitochondrial Zn2+ promotes palmitate-induced mitochondrial fission and pancreatic β-cell death in rodents. Cell Death Differ 24, 1999–2012. https://doi.org/10.1038/cdd.2017.118

Li, X., Tamama, K., Xie, X., Guan, J., 2016. Improving Cell Engraftment in Cardiac Stem Cell Therapy. Stem Cells Int 2016. https://doi.org/10.1155/2016/7168797

Lian, J., Lv, S., Liu, C., Liu, Y., Wang, S., Guo, X., Nan, F., Yu, H., He, X., Sun, G., Ma, X., 2016. Effects of Serial Passage on the Characteristics and Cardiac and Neural Differentiation of Human Umbilical Cord Wharton's Jelly-Derived Mesenchymal Stem Cells. Stem Cells Int 2016. https://doi.org/10.1155/2016/9291013

Lin, J.-C., Liu, C.-L., Lee, J.-J., Liu, T.-P., Ko, W.-C., Huang, Y.-C., Wu, C.-H., Chen, Y.-J., 2013. Sorafenib induces autophagy and suppresses activation of human macrophage. International Immunopharmacology 15, 333–339. https://doi.org/10.1016/j.intimp.2013.01.006

Linask, K.L., Linask, K.K., 2010. Calcium Channel Blockade in Embryonic Cardiac Progenitor Cells Disrupts Normal Cardiac Cell Differentiation. Stem Cells and Development 19, 1959–1965. https://doi.org/10.1089/scd.2010.0192

Linke, A., Müller, P., Nurzynska, D., Casarsa, C., Torella, D., Nascimbene, A., Castaldo, C., Cascapera, S., Böhm, M., Quaini, F., Urbanek, K., Leri, A., Hintze, T.H., Kajstura, J., Anversa, P., 2005. Stem cells in the dog heart are self-renewing, clonogenic, and multipotent and regenerate infarcted myocardium, improving cardiac function. PNAS 102, 8966–8971. https://doi.org/10.1073/pnas.0502678102

Linkermann, A., Green, D.R., 2014. Necroptosis. New England Journal of Medicine 370, 455–465. https://doi.org/10.1056/NEJMra1310050

Liu, D., Huang, L., Wang, Y., Wang, W., Wehrens, X.H.T., Belousova, T., Abdelrahim, M., DiMattia, G., Sheikh-Hamad, D., 2012. Human Stanniocalcin-1 Suppresses Angiotensin II-Induced Superoxide Generation in Cardiomyocytes through UCP3-Mediated Anti-Oxidant Pathway. PLOS ONE 7, e36994. https://doi.org/10.1371/journal.pone.0036994

Liu, J., Saul, D., Böker, K.O., Ernst, J., Lehman, W., Schilling, A.F., 2018. Current Methods for Skeletal Muscle Tissue Repair and Regeneration. Biomed Res Int 2018. https://doi.org/10.1155/2018/1984879

Liu, J., Wu, X., Mitchell, B., Kintner, C., Ding, S., Schultz, P.G., 2005. A Small-Molecule Agonist of the Wnt Signalling Pathway. Angewandte Chemie International Edition 44, 1987–1990. https://doi.org/10.1002/anie.200462552

Liu, Y., Liu, T., Lei, T., Zhang, D., Du, S., Girani, L., Qi, D., Lin, C., Tong, R., Wang, Y., 2019. RIP1/RIP3-regulated necroptosis as a target for multifaceted disease therapy (Review). International Journal of Molecular Medicine 44, 771–786. https://doi.org/10.3892/ijmm.2019.4244

Llovet, J.M., Bruix, J., 2008. Novel advancements in the management of hepatocellular carcinoma in 2008. Journal of Hepatology, Management of Liver Diseases 2008 48, S20–S37. https://doi.org/10.1016/j.jhep.2008.01.022

Llovet, J.M., Ricci, S., Mazzaferro, V., Hilgard, P., Gane, E., Blanc, J.-F., de Oliveira, A.C., Santoro, A., Raoul, J.-L., Forner, A., Schwartz, M., Porta, C., Zeuzem, S., Bolondi, L., Greten, T.F., Galle, P.R., Seitz, J.-F., Borbath, I., Häussinger, D., Giannaris, T., Shan, M., Moscovici, M., Voliotis, D., Bruix, J., 2008. Sorafenib in Advanced Hepatocellular Carcinoma. New England Journal of Medicine 359, 378–390. https://doi.org/10.1056/NEJMoa0708857

Lupescu, A., Shaik, N., Jilani, K., Zelenak, C., Lang, E., Pasham, V., Zbidah, M., Plate, A., Bitzer, M., Föller, M., Qadri, S.M., Lang, F., 2012. Enhanced Erythrocyte Membrane Exposure of Phosphatidylserine Following Sorafenib Treatment: An *in-vivo* and *in-vitro* Study. CPB 30, 876–888. https://doi.org/10.1159/000341465

MacFarlane, M., 2009. Cell death pathways – potential therapeutic targets. Xenobiotica 39, 616–624. https://doi.org/10.1080/00498250903137990

Maddams, J., Utley, M., Møller, H., 2012. Projections of cancer prevalence in the United Kingdom, 2010–2040. Br J Cancer 107, 1195–1202. https://doi.org/10.1038/bjc.2012.366

Makkar, R.R., Smith, R.R., Cheng, K., Malliaras, K., Thomson, L.E.J., Berman, D., Czer, L.S.C., Marbán, L., Mendizabal, A., Johnston, P.V., Russell, S.D., Schuleri, K.H., Lardo, A.C., Gerstenblith, G., Marbán, E., 2012. Intracoronary cardiosphere-derived cells for heart regeneration after myocardial infarction (CADUCEUS): a prospective, randomised phase 1 trial. Lancet 379, 895–904. https://doi.org/10.1016/S0140-6736(12)60195-0

Malliaras, K., Makkar, R.R., Smith, R.R., Cheng, K., Wu, E., Bonow, R.O., Marbán, L., Mendizabal, A., Cingolani, E., Johnston, P.V., Gerstenblith, G., Schuleri, K.H., Lardo, A.C., Marbán, E., 2014. Intracoronary Cardiosphere-Derived Cells After Myocardial Infarction. J Am Coll Cardiol 63, 110–122. https://doi.org/10.1016/j.jacc.2013.08.724

Mancini, M., Leo, E., Campi, V., Castagnetti, F., Zazzeroni, L., Gugliotta, G., Santucci, M.A., Martinelli, G., 2014. A calpain-cleaved fragment of β-catenin promotes BCRABL1+ cell survival evoked by autophagy induction in response to imatinib. Cellular Signalling 26, 1690–1697. https://doi.org/10.1016/j.cellsig.2014.04.010

Mazure, N.M., Pouysségur, J., 2010. Hypoxia-induced autophagy: cell death or cell survival? Current Opinion in Cell Biology, Cell regulation 22, 177–180. https://doi.org/10.1016/j.ceb.2009.11.015

McMullen, C.J., McCluskey, C., Kim, S.J., Laovitthayanggoon, S., MacDonald, M., Safar, M., Wood, R., Cunningham, M.R., Currie, S., 2018. Anti-cancer tyrosine kinase inhibitors increase oxidative stress in primary cardiac fibroblasts, in: Heart. Presented at the The Scottish Cardiovascular Forum 2018. https://doi.org/10.1136/heartintjnl-2018-SCF22

McMullen, C.J., Wood, R.A., Cunningham, M.R., Currie, S., 2019. P5 Assessment of adult rat cardiac fibroblast viability following chronic sunitinib treatment. Heart 105, A6–A7. https://doi.org/10.1136/heartjnl-2019-SCF.13

Mechanism of Action | NEXAVAR® (sorafenib) [WWW Document], n.d. URL http://hcp.nexavar-us.com/mechanism-of-action/ (accessed 12.5.19).

Meisel, R., Brockers, S., Heseler, K., Degistirici, Ö., Bülle, H., Woite, C., Stuhlsatz, S., Schwippert, W., Jäger, M., Sorg, R., Henschler, R., Seissler, J., Dilloo, D., Däubener, W., 2011. Human but not murine multipotent mesenchymal stromal cells exhibit broad-spectrum antimicrobial effector function mediated by indoleamine 2,3-dioxygenase. Leukemia 25, 648–654. https://doi.org/10.1038/leu.2010.310

Mellor, H.R., Bell, A.R., Valentin, J.-P., Roberts, R.R.A., 2011. Cardiotoxicity Associated with Targeting Kinase Pathways in Cancer. Toxicol Sci 120, 14–32. https://doi.org/10.1093/toxsci/kfq378

Messina Elisa, De Angelis Luciana, Frati Giacomo, Morrone Stefania, Chimenti Stefano, Fiordaliso Fabio, Salio Monica, Battaglia Massimo, Latronico Michael V.G., Coletta Marcello, Vivarelli Elisabetta, Frati Luigi, Cossu Giulio, Giacomello Alessandro, 2004. Isolation and Expansion of Adult Cardiac Stem Cells From Human and Murine Heart. Circulation Research 95, 911–921. https://doi.org/10.1161/01.RES.0000147315.71699.51

Micheau, O., Tschopp, J., 2003. Induction of TNF Receptor I-Mediated Apoptosis via Two Sequential Signalling Complexes. Cell 114, 181–190. https://doi.org/10.1016/S0092-8674(03)00521-X

Mioulane, M., Foldes, G., Ali, N.N., Schneider, M.D., Harding, S.E., 2012. Development of High Content Imaging Methods for Cell Death Detection in Human Pluripotent Stem Cell-Derived Cardiomyocytes. J. of Cardiovasc. Trans. Res. 5, 593–604. https://doi.org/10.1007/s12265-012-9396-1

Mitchell, N., Fong, P.C., Broom, R.J., 2015. Clinical experience with sunitinib dose escalation in metastatic renal cell carcinoma. Asia-Pacific Journal of Clinical Oncology 11, e1–e5. https://doi.org/10.1111/ajco.12296

Mocanu, M.M., Gadgil, S., Yellon, D.M., Baxter, G.F., 1999. Mibefradil, a T-Type and L-Type Calcium Channel Blocker, Limits Infarct Size through a Glibenclamide-Sensitive Mechanism. Cardiovasc Drugs Ther 13, 115–122. https://doi.org/10.1023/A:1007732025184

Moehring, A., Wohlbold, L., Aulitzky, W.E., Kuip, H. van der, 2005. Role of poly(ADP-ribose) polymerase activity in imatinib mesylate-induced cell death. Cell Death Differ 12, 627–636. https://doi.org/10.1038/sj.cdd.4401608

Mohyeldin, A., Garzón-Muvdi, T., Quiñones-Hinojosa, A., 2010. Oxygen in Stem Cell Biology: A Critical Component of the Stem Cell Niche. Cell Stem Cell 7, 150–161. https://doi.org/10.1016/j.stem.2010.07.007

Momeni, H.R., 2011. Role of Calpain in Apoptosis. Cell J 13, 65–72.

Morrison, S.J., Shah, N.M., Anderson, D.J., 1997. Regulatory Mechanisms in Stem Cell Biology. Cell 88, 287–298. https://doi.org/10.1016/S0092-8674(00)81867-X

Motzer, R.J., Hutson, T.E., Tomczak, P., Michaelson, M.D., Bukowski, R.M., Oudard, S., Negrier, S., Szczylik, C., Pili, R., Bjarnason, G.A., Garcia-del-Muro, X., Sosman, J.A., Solska, E., Wilding, G., Thompson, J.A., Kim, S.T., Chen, I., Huang, X., Figlin, R.A., 2009a. Overall Survival and Updated Results for Sunitinib Compared With Interferon Alfa in Patients With Metastatic Renal Cell Carcinoma. J Clin Oncol 27, 3584–3590. https://doi.org/10.1200/JCO.2008.20.1293

Motzer, R.J., Hutson, T.E., Tomczak, P., Michaelson, M.D., Bukowski, R.M., Rixe, O., Oudard, S., Negrier, S., Szczylik, C., Kim, S.T., Chen, I., Bycott, P.W., Baum, C.M., Figlin, R.A., 2009b. Sunitinib versus Interferon Alfa in Metastatic Renal-Cell Carcinoma [WWW Document]. http://dx.doi.org/10.1056/NEJMoa065044. https://doi.org/10.1056/NEJMoa065044

Motzer, R.J., Hutson, T.E., Tomczak, P., Michaelson, M.D., Bukowski, R.M., Rixe, O., Oudard, S., Negrier, S., Szczylik, C., Kim, S.T., Chen, I., Bycott, P.W., Baum, C.M., Figlin, R.A., 2007. Sunitinib versus Interferon Alfa in Metastatic Renal-Cell Carcinoma. N Engl J Med 356, 115–124. https://doi.org/10.1056/NEJMoa065044

Mouquet Frédéric, Pfister Otmar, Jain Mohit, Oikonomopoulos Angelos, Ngoy Soeun, Summer Ross, Fine Alan, Liao Ronglih, 2005. Restoration of Cardiac Progenitor Cells After Myocardial Infarction by Self-Proliferation and Selective Homing of Bone Marrow–Derived Stem Cells. Circulation Research 97, 1090–1092. https://doi.org/10.1161/01.RES.0000194330.66545.f5

Muir, K.W., Bulters, D., Willmot, M., Sprigg, N., Dixit, A., Ward, N., Tyrrell, P., Majid, A., Dunn, L., Bath, P., Howell, J., Stroemer, P., Pollock, K., Sinden, J., 2020. Intracerebral implantation of human neural stem cells and motor recovery after stroke: multicentre prospective single-arm study (PISCES-2). J Neurol Neurosurg Psychiatry. https://doi.org/10.1136/jnnp-2019-322515

Murphy, J.M., Czabotar, P.E., Hildebrand, J.M., Lucet, I.S., Zhang, J.-G., Alvarez-Diaz, S., Lewis, R., Lalaoui, N., Metcalf, D., Webb, A.I., Young, S.N., Varghese, L.N., Tannahill, G.M., Hatchell, E.C., Majewski, I.J., Okamoto, T., Dobson, R.C.J., Hilton, D.J., Babon, J.J., Nicola, N.A., Strasser, A., Silke, J., Alexander, W.S., 2013. The Pseudokinase MLKL Mediates Necroptosis via a Molecular Switch Mechanism. Immunity 39, 443–453. https://doi.org/10.1016/j.immuni.2013.06.018

Nagata, S., 2018. Apoptosis and Clearance of Apoptotic Cells. Annual Review of Immunology 36, 489–517. https://doi.org/10.1146/annurev-immunol-042617-053010

Nagata, S., Tanaka, M., 2017. Programmed cell death and the immune system. Nature Reviews Immunology 17, 333–340. https://doi.org/10.1038/nri.2016.153

Nathan, C., 2003. Specificity of a third kind: reactive oxygen and nitrogen intermediates in cell signalling. J Clin Invest 111, 769–778. https://doi.org/10.1172/JCI18174

Nikonenko, I., Bancila, M., Bloc, A., Muller, D., Bijlenga, P., 2005. Inhibition of T-Type Calcium Channels Protects Neurons from Delayed Ischemia-Induced Damage. Mol Pharmacol 68, 84–89. https://doi.org/10.1124/mol.104.010066

Nomura, M., Ueno, A., Saga, K., Fukuzawa, M., Kaneda, Y., 2014. Accumulation of Cytosolic Calcium Induces Necroptotic Cell Death in Human Neuroblastoma. Cancer Res 74, 1056–1066. https://doi.org/10.1158/0008-5472.CAN-13-1283

Nowak-Sliwinska, P., Weiss, A., van Beijnum, J.R., Wong, T.J., Kilarski, W.W., Szewczyk, G., Verheul, H.M.W., Sarna, T., van den Bergh, H., Griffioen, A.W., 2015. Photoactivation of lysosomally sequestered sunitinib after angiostatic treatment causes vascular occlusion and

enhances tumor growth inhibition. Cell Death Dis 6, e1641. https://doi.org/10.1038/cddis.2015.4

Okada, M., Adachi, S., Imai, T., Watanabe, K., Toyokuni, S., Ueno, M., Zervos, A.S., Kroemer, G., Nakahata, T., 2004. A novel mechanism for imatinib mesylate–induced cell death of BCR-ABL–positive human leukemic cells: caspase-independent, necrosis-like programmed cell death mediated by serine protease activity. Blood 103, 2299–2307. https://doi.org/10.1182/blood-2003-05-1605

Orphanos, G.S., Ioannidis, G.N., Ardavanis, A.G., 2009. Cardiotoxicity induced by tyrosine kinase inhibitors. Acta Oncologica 48, 964–970. https://doi.org/10.1080/02841860903229124

Orrenius, S., Zhivotovsky, B., Nicotera, P., 2003. Regulation of cell death: the calcium–apoptosis link. Nature Reviews Molecular Cell Biology 4, 552–565. https://doi.org/10.1038/nrm1150

O'Sullivan, S., Naot, D., Callon, K., Porteous, F., Horne, A., Wattie, D., Watson, M., Cornish, J., Browett, P., Grey, A., 2007. Imatinib Promotes Osteoblast Differentiation by Inhibiting PDGFR Signalling and Inhibits Osteoclastogenesis by Both Direct and Stromal Cell-Dependent Mechanisms. Journal of Bone and Mineral Research 22, 1679–1689. https://doi.org/10.1359/jbmr.070719

Ott, H.C., Matthiesen, T.S., Brechtken, J., Grindle, S., Goh, S.-K., Nelson, W., Taylor, D.A., 2007. The adult human heart as a source for stem cells: repair strategies with embryonic-like progenitor cells. Nature Clinical Practice Cardiovascular Medicine 4, S27–S39. https://doi.org/10.1038/ncpcardio0771

Palmer, T.D., Markakis, E.A., Willhoite, A.R., Safar, F., Gage, F.H., 1999. Fibroblast Growth Factor-2 Activates a Latent Neurogenic Program in Neural Stem Cells from Diverse Regions of the Adult CNS. J. Neurosci. 19, 8487–8497. https://doi.org/10.1523/JNEUROSCI.19-19-08487.1999

Pan, R., Liu, K.J., Qi, Z., 2019. Zinc causes the death of hypoxic astrocytes by inducing ROS production through mitochondria dysfunction. Biophys Rep 5, 209–217. https://doi.org/10.1007/s41048-019-00098-3

Papaetis, G.S., Syrigos, K.N., 2009. Sunitinib. BioDrugs 23, 377–389. https://doi.org/10.2165/11318860-000000000-00000

Pardanani, A., Tefferi, A., 2004. Imatinib targets other than bcr/abl and their clinical relevance in myeloid disorders. Blood 104, 1931–1939. https://doi.org/10.1182/blood-2004-01-0246

Park, Y.H., Park, H.J., Kim, B.-S., Ha, E., Jung, K.H., Yoon, S.H., Yim, S.V., Chung, J.-H., 2006. BNP as a marker of the heart failure in the treatment of imatinib mesylate. Cancer Letters 243, 16–22. https://doi.org/10.1016/j.canlet.2005.11.014

Parvathenani, L.K., Calandra, V., Roberts, S.B., Posmantur, R., 2000. cAMP delays beta-amyloid (25-35) induced cell death in rat cortical neurons. NeuroReport 11, 2293–2297.

Paul, M.K., Mukhopadhyay, A.K., 2004. Tyrosine kinase – Role and significance in Cancer. Int J Med Sci 1, 101–115.

Paul Mulder, P., Vincent Richard, P., Compagnon, P., Henry, J.-P., Lallemand, F., Clozel, J.-P., Koen, R., Macé, B., Thuillez, C., 1997. Increased Survival After Long-Term Treatment With Mibefradil, a

Selective T-Channel Calcium Antagonist, in Heart Failure. J Am Coll Cardiol 29, 416–421. https://doi.org/10.1016/S0735-1097(96)00491-3

Pearce, A., Haas, M., Viney, R., Pearson, S.-A., Haywood, P., Brown, C., Ward, R., 2017. Incidence and severity of self-reported chemotherapy side effects in routine care: A prospective cohort study. PLoS One 12. https://doi.org/10.1371/journal.pone.0184360

Peng, B., Lloyd, P., Schran, H., 2005. Clinical Pharmacokinetics of Imatinib. Clin Pharmacokinet 44, 879–894. https://doi.org/10.2165/00003088-200544090-00001

Pennings, S., Liu, K.J., Qian, H., 2018. The Stem Cell Niche: Interactions between Stem Cells and Their Environment. Stem Cells Int 2018. https://doi.org/10.1155/2018/4879379

Pereira, L., Cheng, H., Lao, D.H., Na, L., van Oort, R.J., Brown, J.H., Wehrens, X.H.T., Chen, J., Bers, D.M., 2013. Epac2 Mediates Cardiac β1-Adrenergic Dependent SR Ca2+ Leak and Arrhythmia. Circulation 127, 913–922. https://doi.org/10.1161/CIRCULATIONAHA.12.148619

Perez-Reyes, E., 2003. Molecular Physiology of Low-Voltage-Activated T-type Calcium Channels. Physiological Reviews 83, 117–161. https://doi.org/10.1152/physrev.00018.2002

Pfister Otmar, Mouquet Frédéric, Jain Mohit, Summer Ross, Helmes Michiel, Fine Alan, Colucci Wilson S., Liao Ronglih, 2005. CD31− but Not CD31+ Cardiac Side Population Cells Exhibit Functional Cardiomyogenic Differentiation. Circulation Research 97, 52–61. https://doi.org/10.1161/01.RES.0000173297.53793.fa

Phinney, D.G., Pittenger, M.F., 2017. Concise Review: MSC-Derived Exosomes for Cell-Free Therapy. STEM CELLS 35, 851–858. https://doi.org/10.1002/stem.2575

Pietras, E.M., Warr, M.R., Passegué, E., 2011. Cell cycle regulation in hematopoietic stem cells. J Cell Biol 195, 709–720. https://doi.org/10.1083/jcb.201102131

Pinton, P., Ferrari, D., Magalhães, P., Schulze-Osthoff, K., Di Virgilio, F., Pozzan, T., Rizzuto, R., 2000. Reduced Loading of Intracellular Ca2+ Stores and Downregulation of Capacitative Ca2+Influx in Bcl-2–Overexpressing Cells. J Cell Biol 148, 857–862.

Pinton, P., Giorgi, C., Siviero, R., Zecchini, E., Rizzuto, R., 2008. Calcium and apoptosis: ER-mitochondria Ca2+ transfer in the control of apoptosis. Oncogene 27, 6407–6418. https://doi.org/10.1038/onc.2008.308

Poss, K.D., Wilson, L.G., Keating, M.T., 2002. Heart Regeneration in Zebrafish. Science 298, 2188–2190. https://doi.org/10.1126/science.1077857

Quaini, F., Urbanek, K., Beltrami, A.P., Finato, N., Beltrami, C.A., Nadal-Ginard, B., Kajstura, J., Leri, A., Anversa, P., 2002. Chimerism of the Transplanted Heart. New England Journal of Medicine 346, 5–15. https://doi.org/10.1056/NEJMoa012081

Rahmani, M., Davis, E.M., Crabtree, T.R., Habibi, J.R., Nguyen, T.K., Dent, P., Grant, S., 2007. The Kinase Inhibitor Sorafenib Induces Cell Death through a Process Involving Induction of Endoplasmic Reticulum Stress. Mol Cell Biol 27, 5499–5513. https://doi.org/10.1128/MCB.01080-06

Rainer, P.P., Doleschal, B., Kirk, J.A., Sivakumaran, V., Saad, Z., Groschner, K., Maechler, H., Hoefler, G., Bauernhofer, T., Samonigg, H., Hutterer,

G., Kass, D.A., Pieske, B., Lewinski, D. von, Pichler, M., 2012. Sunitinib causes dose-dependent negative functional effects on myocardium and cardiomyocytes. BJU International 110, 1455–1462. https://doi.org/10.1111/j.1464-410X.2012.11134.x

Rammensee, S., Kang, M.S., Georgiou, K., Kumar, S., Schaffer, D.V., 2017. Dynamics of Mechanosensitive Neural Stem Cell Differentiation. STEM CELLS 35, 497–506. https://doi.org/10.1002/stem.2489

Ran, H.-H., Zhang, R., Lu, X.-C., Yang, B., Fan, H., Zhu, H.-L., 2012. Imatinib-induced decompensated heart failure in an elderly patient with chronic myeloid leukemia: case report and literature review. J Geriatr Cardiol 9, 411–414. https://doi.org/10.3724/SP.J.1263.2012.05251

Reya, T., Duncan, A.W., Ailles, L., Domen, J., Scherer, D.C., Willert, K., Hintz, L., Nusse, R., Weissman, I.L., 2003. A role for Wnt signalling in self-renewal of haematopoietic stem cells. Nature 423, 409–414. https://doi.org/10.1038/nature01593

Richards, C.J., Je, Y., Schutz, F.A.B., Heng, D.Y.C., Dallabrida, S.M., Moslehi, J.J., Choueiri, T.K., 2011. Incidence and Risk of Congestive Heart Failure in Patients With Renal and Nonrenal Cell Carcinoma Treated With Sunitinib. JCO 29, 3450–3456. https://doi.org/10.1200/JCO.2010.34.4309

Rossi, D., Simeoni, I., Micheli, M., Bootman, M., Lipp, P., Allen, P.D., Sorrentino, V., 2002. RyR1 and RyR3 isoforms provide distinct intracellular Ca2+ signals in HEK 293 cells. Journal of Cell Science 115, 2497–2504.

Rouleau, L., Antony, A.N., Bisetto, S., Newberg, A., Doria, C., Levine, M., Monti, D.A., Hoek, J.B., 2016. Synergistic effects of ascorbate and sorafenib in hepatocellular carcinoma: New insights into ascorbate cytotoxicity. Free Radic Biol Med 95, 308–322. https://doi.org/10.1016/j.freeradbiomed.2016.03.031

Roy, M.J., Vom, A., Czabotar, P.E., Lessene, G., 2014. Cell death and the mitochondria: therapeutic targeting of the BCL-2 family-driven pathway. Br J Pharmacol 171, 1973–1987. https://doi.org/10.1111/bph.12431

Sacha, T., 2014. Imatinib in Chronic Myeloid Leukemia: an Overview. Mediterr J Hematol Infect Dis 6. https://doi.org/10.4084/MJHID.2014.007

Savi, M., Frati, C., Cavalli, S., Graiani, G., Galati, S., Buschini, A., Madeddu, D., Falco, A., Prezioso, L., Mazzaschi, G., Galaverna, F., Lagrasta, C.A.M., Corradini, E., De Angelis, A., Cappetta, D., Berrino, L., Aversa, F., Quaini, F., Urbanek, K., 2018. Imatinib mesylate-induced cardiomyopathy involves resident cardiac progenitors. Pharmacological Research, Pharmacology of Adult Cardiac Regeneration 127, 15–25. https://doi.org/10.1016/j.phrs.2017.09.020

Scheinfeld, N., Schienfeld, N., 2006. A comprehensive review of imatinib mesylate (Gleevec) for dermatological diseases. Journal of drugs in dermatology : JDD 5, 117–22.

Schenk, B., Fulda, S., 2015. Reactive oxygen species regulate Smac mimetic/TNFα-induced necroptotic signalling and cell death. Oncogene 34, 5796–5806. https://doi.org/10.1038/onc.2015.35

Schlessinger, J., 2000. Cell Signalling by Receptor Tyrosine Kinases. Cell 103, 211–225. https://doi.org/10.1016/S0092-8674(00)00114-8

Schmidinger, M., Zielinski, C.C., Vogl, U.M., Bojic, A., Bojic, M., Schukro, C., Ruhsam, M., Hejna, M., Schmidinger, H., 2008. Cardiac Toxicity of Sunitinib and Sorafenib in Patients With Metastatic Renal Cell Carcinoma. JCO 26, 5204–5212. https://doi.org/10.1200/JCO.2007.15.6331

Schneider, C., Wallner, M., Kolesnik, E., Herbst, V., Mächler, H., Pichler, M., von Lewinski, D., Sedej, S., Rainer, P.P., 2018. The Anti-Cancer Multikinase Inhibitor Sorafenib Impairs Cardiac Contractility by Reducing Phospholamban Phosphorylation and Sarcoplasmic Calcium Transients. Scientific Reports 8, 1–8. https://doi.org/10.1038/s41598-018-23630-w

Schwede, F., Bertinetti, D., Langerijs, C.N., Hadders, M.A., Wienk, H., Ellenbroek, J.H., Koning, E.J.P. de, Bos, J.L., Herberg, F.W., Genieser, H.-G., Janssen, R.A.J., Rehmann, H., 2015. Structure-Guided Design of Selective Epac1 and Epac2 Agonists. PLOS Biology 13, e1002038. https://doi.org/10.1371/journal.pbio.1002038

Scorrano, L., Oakes, S.A., Opferman, J.T., Cheng, E.H., Sorcinelli, M.D., Pozzan, T., Korsmeyer, S.J., 2003. BAX and BAK Regulation of Endoplasmic Reticulum Ca2+: A Control Point for Apoptosis. Science 300, 135–139. https://doi.org/10.1126/science.1081208

Serrano-Oviedo, L., Ortega-Muelas, M., García-Cano, J., Valero, M.L., Cimas, F.J., Pascual-Serra, R., Fernandez-Aroca, D.M., Roche, O., Ruiz-Hidalgo, M.J., Belandia, B., Giménez-Bachs, J.M., Salinas, A.S., Sanchez-Prieto, R., 2018. Autophagic cell death associated to Sorafenib in renal cell carcinoma is mediated through Akt inhibition in an ERK1/2 independent fashion. PLOS ONE 13, e0200878. https://doi.org/10.1371/journal.pone.0200878

Sheikh, M.S., Huang, Y., 2003. Death Receptor Activation Complexes: It Takes Two to Activate TNF Receptor 1. Cell Cycle 2, 549–551. https://doi.org/10.4161/cc.2.6.566

Shen, H., Zhang, B., Shin, J.-H., Lei, D., Du, Y., Gao, X., Wang, Q., Ohlemiller, K.K., Piccirillo, J., Bao, J., 2007. Prophylactic and therapeutic functions of T-type calcium blockers against noise-induced hearing loss. Hearing Research, Pharmacological Strategies for Prevention and Treatment of Hearing Loss and Tinnitus 226, 52–60. https://doi.org/10.1016/j.heares.2006.12.011

Shi, C.-S., Kehrl, J.H., 2019. Bcl-2 regulates pyroptosis and necroptosis by targeting BH3-like domains in GSDMD and MLKL. Cell Death Discovery 5, 1–13. https://doi.org/10.1038/s41420-019-0230-2

Shi, H., Drummond, C.A., Fan, X., Haller, S.T., Liu, J., Malhotra, D., Tian, J., 2016. Hiding inside? Intracellular Expression of Non-Glycosylated c-Kit Protein in Cardiac Progenitor Cells. Stem Cell Res 16, 795–806. https://doi.org/10.1016/j.scr.2016.04.017

Shi, X., Sousa, L.P., Mandel-Bausch, E.M., Tome, F., Reshetnyak, A.V., Hadari, Y., Schlessinger, J., Lax, I., 2016. Distinct cellular properties of oncogenic KIT receptor tyrosine kinase mutants enable alternative courses of cancer cell inhibition. Proc Natl Acad Sci U S A 113, E4784–E4793. https://doi.org/10.1073/pnas.1610179113

Shindo, R., Kakehashi, H., Okumura, K., Kumagai, Y., Nakano, H., 2013. Critical contribution of oxidative stress to TNFα-induced necroptosis downstream of RIPK1 activation. Biochemical and Biophysical

Research Communications 436, 212–216. https://doi.org/10.1016/j.bbrc.2013.05.075

Shingu, T., Fujiwara, K., Bögler, O., Akiyama, Y., Moritake, K., Shinojima, N., Tamada, Y., Yokoyama, T., Kondo, S., 2009. Inhibition of autophagy at a late stage enhances imatinib-induced cytotoxicity in human malignant glioma cells. International Journal of Cancer 124, 1060–1071. https://doi.org/10.1002/ijc.24030

Shiraishi, N., Akiyama, S.-I., Kobayashi, M., Kuwano, M., 1986. Lysosomotropic agents reverse multiple drug resistance in human cancer cells. Cancer Letters 30, 251–259. https://doi.org/10.1016/0304-3835(86)90049-2

Shojaei, F., Rahmati, S., Dehkordi, M.B., 2019. A review on different methods to increase the efficiency of mesenchymal stem cell-based wound therapy. Wound Repair and Regeneration 27, 661–671. https://doi.org/10.1111/wrr.12749

Simpson, D.L., Mishra, R., Sharma, S., Goh, S.K., Deshmukh, S., Kaushal, S., 2012. A Strong Regenerative Ability of Cardiac Stem Cells Derived From Neonatal Hearts. Circulation 126, S46–S53. https://doi.org/10.1161/CIRCULATIONAHA.111.084699

Singh, R., Letai, A., Sarosiek, K., 2019. Regulation of apoptosis in health and disease: the balancing act of BCL-2 family proteins. Nature Reviews Molecular Cell Biology 20, 175–193. https://doi.org/10.1038/s41580-018-0089-8

Skulachev, V.P., 1996. Why are mitochondria involved in apoptosis? Permeability transition pores and apoptosis as selective mechanisms to eliminate superoxide-producing mitochondria and cell. FEBS Letters 397, 7–10. https://doi.org/10.1016/0014-5793(96)00989-1

Slee, E.A., Adrain, C., Martin, S.J., 2001. Executioner Caspase-3, -6, and -7 Perform Distinct, Non-redundant Roles during the Demolition Phase of Apoptosis. J. Biol. Chem. 276, 7320–7326. https://doi.org/10.1074/jbc.M008363200

Smith, A.J., Lewis, F.C., Aquila, I., Waring, C.D., Nocera, A., Agosti, V., Nadal-Ginard, B., Torella, D., Ellison, G.M., 2014. Isolation and characterization of resident endogenous c-Kit + cardiac stem cells from the adult mouse and rat heart. Nature Protocols 9, 1662–1681. https://doi.org/10.1038/nprot.2014.113

Smith, A.J., Tauskela, J.S., Stone, T.W., Smith, R.A., 2009. Preconditioning with 4-aminopyridine protects cerebellar granule neurons against excitotoxicity. Brain Research 1294, 165–175. https://doi.org/10.1016/j.brainres.2009.07.061

Smith Andrew J, Ruchaya Prashant, Walmsley Robert, Wright Kathleen E, Nadal-Ginard Bernardo, Ellison-Hughes Georgina M, 2018. Abstract 15537: Poor Recovery From Receptor Tyrosine Kinase Inhibitor Cardiotoxicity is Linked to Toxic Effects on Cardiac Stem Cells. Circulation 138, A15537–A15537. https://doi.org/10.1161/circ.138.suppl_1.15537

Söderberg, O., Gullberg, M., Jarvius, M., Ridderstråle, K., Leuchowius, K.-J., Jarvius, J., Wester, K., Hydbring, P., Bahram, F., Larsson, L.-G., Landegren, U., 2006. Direct observation of individual endogenous protein complexes in situ by proximity ligation. Nat Methods 3, 995–1000. https://doi.org/10.1038/nmeth947

Song, H., Stevens, C.F., Gage, F.H., 2002. Astroglia induce neurogenesis from adult neural stem cells. Nature 417, 39–44. https://doi.org/10.1038/417039a

Sonntag, R., Gassler, N., Bangen, J.-M., Trautwein, C., Liedtke, C., 2014. Pro-apoptotic Sorafenib signalling in murine hepatocytes depends on malignancy and is associated with PUMA expression *in-vitro* and *in-vivo*. Cell Death & Disease 5, e1030–e1030. https://doi.org/10.1038/cddis.2013.557

Sun, T., Liu, H., Ming, L., 2017. Multiple Roles of Autophagy in the Sorafenib Resistance of Hepatocellular Carcinoma. CPB 44, 716–727. https://doi.org/10.1159/000485285

Sun, X., Lee, J., Navas, T., Baldwin, D.T., Stewart, T.A., Dixit, V.M., 1999. RIP3, a Novel Apoptosis-inducing Kinase. J. Biol. Chem. 274, 16871–16875. https://doi.org/10.1074/jbc.274.24.16871

Takahashi, K., 2012. Cellular reprogramming – lowering gravity on Waddington's epigenetic landscape. J Cell Sci 125, 2553–2560. https://doi.org/10.1242/jcs.084822

Takahashi, K., Yamanaka, S., 2015. A developmental framework for induced pluripotency. Development 142, 3274–3285. https://doi.org/10.1242/dev.114249

Takamiya, M., Haider, K.H., Ashraf, M., 2011. Identification and Characterization of a Novel Multipotent Sub-Population of Sca-1+ Cardiac Progenitor Cells for Myocardial Regeneration. PLOS ONE 6, e25265. https://doi.org/10.1371/journal.pone.0025265

Tang, J.-M., Luo, B., Xiao, J., Lv, Y., Li, X., Zhao, J., Zheng, F., Zhang, L., Chen, L., Yang, J.-Y., Guo, L.-Y., Wang, L., Yan, Y.-W., Pan, Y.-M., Wang, J.-N., Li, D., Wan, Y., Chen, S.-Y., 2015. VEGF-A promotes cardiac stem cell engraftment and myocardial repair in the infarcted heart. International Journal of Cardiology 183, 221–231. https://doi.org/10.1016/j.ijcard.2015.01.050

Taylor, R.C., Cullen, S.P., Martin, S.J., 2008. Apoptosis: controlled demolition at the cellular level. Nature Reviews Molecular Cell Biology 9, 231–241. https://doi.org/10.1038/nrm2312

Tesori, V., Piscaglia, A.C., Samengo, D., Barba, M., Bernardini, C., Scatena, R., Pontoglio, A., Castellini, L., Spelbrink, J.N., Maulucci, G., Puglisi, M.A., Pani, G., Gasbarrini, A., 2015. The multikinase inhibitor Sorafenib enhances glycolysis and synergizes with glycolysis blockade for cancer cell killing. Scientific Reports 5, 1–9. https://doi.org/10.1038/srep09149

Vajravelu, B.N., Hong, K.U., Al-Maqtari, T., Cao, P., Keith, M.C.L., Wysoczynski, M., Zhao, J., Iv, J.B.M., Bolli, R., 2015. C-Kit Promotes Growth and Migration of Human Cardiac Progenitor Cells via the PI3K-AKT and MEK-ERK Pathways. PLOS ONE 10, e0140798. https://doi.org/10.1371/journal.pone.0140798

van Heerde, W.L., Robert-Offerman, S., Dumont, E., Hofstra, L., Doevendans, P.A., Smits, J.F.M., Daemen, M.J.A.P., Reutelingsperger, C.P.M., 2000. Markers of apoptosis in cardiovascular tissuesfocus on Annexin V. Cardiovasc Res 45, 549–559. https://doi.org/10.1016/S0008-6363(99)00396-X

Vanlangenakker, N., Berghe, T.V., Bogaert, P., Laukens, B., Zobel, K., Deshayes, K., Vucic, D., Fulda, S., Vandenabeele, P., Bertrand, M.J.M., 2011. cIAP1 and TAK1 protect cells from TNF-induced

necrosis by preventing RIP1/RIP3-dependent reactive oxygen species production. Cell Death Differ 18, 656–665. https://doi.org/10.1038/cdd.2010.138

Vicinanza, C., Aquila, I., Scalise, M., Cristiano, F., Marino, F., Cianflone, E., Mancuso, T., Marotta, P., Sacco, W., Lewis, F.C., Couch, L., Shone, V., Gritti, G., Torella, A., Smith, A.J., Terracciano, C.M., Britti, D., Veltri, P., Indolfi, C., Nadal-Ginard, B., Ellison-Hughes, G.M., Torella, D., 2017. Adult cardiac stem cells are multipotent and robustly myogenic: c-kit expression is necessary but not sufficient for their identification. Cell Death & Differentiation 24, 2101–2116. https://doi.org/10.1038/cdd.2017.130

Walsh, J.G., Cullen, S.P., Sheridan, C., Lüthi, A.U., Gerner, C., Martin, S.J., 2008. Executioner caspase-3 and caspase-7 are functionally distinct proteases. PNAS 105, 12815–12819. https://doi.org/10.1073/pnas.0707715105

Wang, J.F., Olson, M.E., Ma, L., Brigstock, D.R., Hart, D.A., 2004. Connective tissue growth factor siRNA modulates mRNA levels for a subset of molecules in normal and TGF-β1–stimulated porcine skin fibroblasts. Wound Repair and Regeneration 12, 205–216. https://doi.org/10.1111/j.1067-1927.2004.012113.x

Wang, S., Sdrulla, A.D., diSibio, G., Bush, G., Nofziger, D., Hicks, C., Weinmaster, G., Barres, B.A., 1998. Notch Receptor Activation Inhibits Oligodendrocyte Differentiation. Neuron 21, 63–75. https://doi.org/10.1016/S0896-6273(00)80515-2

Wid, P., 2000. The DFF40/CAD endonuclease and its role in apoptosis. 47, 8.

Wildburger, N.C., Lin-Ye, A., Baird, M.A., Lei, D., Bao, J., 2009. Neuroprotective effects of blockers for T-type calcium channels. Molecular Neurodegeneration 4, 44. https://doi.org/10.1186/1750-1326-4-44

Wilhelm, S.M., Adnane, L., Newell, P., Villanueva, A., Llovet, J.M., Lynch, M., 2008. Preclinical overview of sorafenib, a multikinase inhibitor that targets both Raf and VEGF and PDGF receptor tyrosine kinase signalling. Mol Cancer Ther 7, 3129–3140. https://doi.org/10.1158/1535-7163.MCT-08-0013

Will, Y., Dykens, J.A., Nadanaciva, S., Hirakawa, B., Jamieson, J., Marroquin, L.D., Hynes, J., Patyna, S., Jessen, B.A., 2008. Effect of the Multitargeted Tyrosine Kinase Inhibitors Imatinib, Dasatinib, Sunitinib, and Sorafenib on Mitochondrial Function in Isolated Rat Heart Mitochondria and H9c2 Cells. Toxicol Sci 106, 153–161. https://doi.org/10.1093/toxsci/kfn157

Willert, K., Brown, J.D., Danenberg, E., Duncan, A.W., Weissman, I.L., Reya, T., Yates, J.R., Nusse, R., 2003. Wnt proteins are lipid-modified and can act as stem cell growth factors. Nature 423, 448–452. https://doi.org/10.1038/nature01611

Wolf, A., Couttet, P., Dong, M., Grenet, O., Heron, M., Junker, U., Laengle, U., Ledieu, D., Marrer, E., Nussher, A., Persohn, E., Pognan, F., Rivière, G.-J., Roth, D.R., Trendelenburg, C., Tsao, J., Roman, D., 2010. Imatinib does not induce cardiotoxicity at clinically relevant concentrations in preclinical studies. Leukemia Research 34, 1180–1188. https://doi.org/10.1016/j.leukres.2010.01.004

Wolf, B.B., Schuler, M., Echeverri, F., Green, D.R., 1999. Caspase-3 Is the Primary Activator of Apoptotic DNA Fragmentation via DNA Fragmentation Factor-45/Inhibitor of Caspase-activated DNase Inactivation. J. Biol. Chem. 274, 30651–30656. https://doi.org/10.1074/jbc.274.43.30651

Woodcock, E.A., Matkovich, S.J., 2005. Cardiomyocytes structure, function and associated pathologies. The International Journal of Biochemistry & Cell Biology 37, 1746–1751. https://doi.org/10.1016/j.biocel.2005.04.011

Wright, L.S., Li, J., Caldwell, M.A., Wallace, K., Johnson, J.A., Svendsen, C.N., 2003. Gene expression in human neural stem cells: effects of leukemia inhibitory factor. Journal of Neurochemistry 86, 179–195. https://doi.org/10.1046/j.1471-4159.2003.01826.x

Wu, H., Sun, Y.E., 2006. Epigenetic Regulation of Stem Cell Differentiation. Pediatric Research 59, 21–25. https://doi.org/10.1203/01.pdr.0000203565.76028.2a

Xie, B., Stammes, M.A., van Driel, P.B.A.A., Cruz, L.J., Knol-Blankevoort, V.T., Löwik, M.A.M., Mezzanotte, L., Que, I., Chan, A., van den Wijngaard, J.P.H.M., Siebes, M., Gottschalk, S., Razansky, D., Ntziachristos, V., Keereweer, S., Horobin, R.W., Hoehn, M., Kaijzel, E.L., van Beek, E.R., Snoeks, T.J.A., Löwik, C.W.G.M., 2015. Necrosis avid near infrared fluorescent cyanines for imaging cell death and their use to monitor therapeutic efficacy in mouse tumor models. Oncotarget 6, 39036–39049.

Xie, T., Peng, W., Yan, C., Wu, J., Gong, X., Shi, Y., 2013. Structural Insights into RIP3-Mediated Necroptotic Signalling. Cell Reports 5, 70–78. https://doi.org/10.1016/j.celrep.2013.08.044

Xin, H., Zhang, C., Herrmann, A., Du, Y., Figlin, R., Yu, H., 2009. Sunitinib Inhibition of Stat3 Induces Renal Cell Carcinoma Tumor Cell Apoptosis and Reduces Immunosuppressive Cells. Cancer Res 69, 2506–2513. https://doi.org/10.1158/0008-5472.CAN-08-4323

Xu, Z., Cang, S., Yang, T., Liu, D., 2009. Cardiotoxicity of tyrosine kinase inhibitors in chronic myelogenous leukemia therapy. Hematol Rev 1. https://doi.org/10.4081/hr.2009.e4

Yan, X., Zhang, Y., Zhang, J., Zhang, L., Liu, Y., Wu, Y., Xue, Y., Lu, S., Su, J., Sun, L., 2017. p62/SQSTM1 as an oncotarget mediates cisplatin resistance through activating RIP1-NF-κB pathway in human ovarian cancer cells. Cancer Sci 108, 1405–1413. https://doi.org/10.1111/cas.13276

Yang, D., Pan, Z., Takeshima, H., Wu, C., Nagaraj, R.Y., Ma, J., Cheng, H., 2001. RyR3 Amplifies RyR1-mediated Ca2+-induced Ca2+ Release in Neonatal Mammalian Skeletal Muscle. J. Biol. Chem. 276, 40210–40214. https://doi.org/10.1074/jbc.M106944200

Yang, N., Tang, Y., Wang, F., Zhang, H., Xu, D., Shen, Y., Sun, S., Yang, G., 2013. Blockade of store-operated Ca2+ entry inhibits hepatocarcinoma cell migration and invasion by regulating focal adhesion turnover. Cancer Letters 330, 163–169. https://doi.org/10.1016/j.canlet.2012.11.040

Yang, Z., Steele, D.S., 2013. The EPAC Activator 8-CPT Protects against Isoproterenol-Induced Cell Death in Adult Ventricular Myocytes.

Biophysical Journal 104, 315a. https://doi.org/10.1016/j.bpj.2012.11.1747

Yap, Y.G., Camm, A.J., 2003. Drug induced QT prolongation and torsades de pointes. Heart 89, 1363–1372.

Yıldırım, R., Sincan, G., Pala, C.Y., Düdükçü, M., Kaynar, L., Urlu, S.M., Kiki, İ., Erdem, F., Çetin, M.K., Gundogdu, M.N., Topdağı, Ö., 2016. Effects of Imatinib, Nilotinib, Dasatinib on VEGF and VEGFR-1 Levels in Patients with Chronic Myelogenous Leukemia. https://doi.org/10.15197/ejgm.1527

Yoo, Y.D., Kwon, Y.T., 2015. Molecular mechanisms controlling asymmetric and symmetric self-renewal of cancer stem cells. J Anal Sci Technol 6, 28. https://doi.org/10.1186/s40543-015-0071-4

Yu, J., Moon, A., Kim, H.-R.C., 2001. Both Platelet-Derived Growth Factor Receptor (PDGFR)-α and PDGFR-β Promote Murine Fibroblast Cell Migration. Biochemical and Biophysical Research Communications 282, 697–700. https://doi.org/10.1006/bbrc.2001.4622

Yu, Y., Yang, L., Zhao, M., Zhu, S., Kang, R., Vernon, P., Tang, D., Cao, L., 2012. Targeting microRNA-30a-mediated autophagy enhances imatinib activity against human chronic myeloid leukemia cells. Leukemia 26, 1752–1760. https://doi.org/10.1038/leu.2012.65

Zakrzewski, W., Dobrzyński, M., Szymonowicz, M., Rybak, Z., 2019. Stem cells: past, present, and future. Stem Cell Research & Therapy 10, 68. https://doi.org/10.1186/s13287-019-1165-5

Zamzami, N., Marchetti, P., Castedo, M., Decaudin, D., Macho, A., Hirsch, T., Susin, S.A., Petit, P.X., Mignotte, B., Kroemer, G., 1995. Sequential reduction of mitochondrial transmembrane potential and generation of reactive oxygen species in early programmed cell death. J Exp Med 182, 367–377. https://doi.org/10.1084/jem.182.2.367

Zaruba, M.-M., Soonpaa, M., Reuter, S., Field, L.J., 2010. Cardiomyogenic potential of c-kit+ expressing cells derived from neonatal and adult mouse hearts. Circulation 121, 1992–2000. https://doi.org/10.1161/CIRCULATIONAHA.109.909093

Zhang, J., Jiao, J., 2015. Molecular Biomarkers for Embryonic and Adult Neural Stem Cell and Neurogenesis. Biomed Res Int 2015. https://doi.org/10.1155/2015/727542

Zhang, L., Li, S., Wang, R., Chen, C., Ma, W., Cai, H., 2019. Cytokine augments the sorafenib-induced apoptosis in Huh7 liver cancer cell by inducing mitochondrial fragmentation and activating MAPK-JNK signalling pathway. Biomedicine & Pharmacotherapy 110, 213–223. https://doi.org/10.1016/j.biopha.2018.11.037

Zhao, F., Mancuso, A., Bui, T.V., Tong, X., Gruber, J.J., Swider, C.R., Sanchez, P.V., Lum, J.J., Sayed, N., Melo, J.V., Perl, A.E., Carroll, M., Tuttle, S.W., Thompson, C.B., 2010. Imatinib-resistance associated with BCR-ABL upregulation is dependent on HIF-1α-induced metabolic reprogramming. Oncogene 29, 2962–2972. https://doi.org/10.1038/onc.2010.67

Zhao, Y., Xue, T., Yang, X., Zhu, H., Ding, X., Lou, L., Lu, W., Yang, B., He, Q., 2010. Autophagy plays an important role in Sunitinib-mediated cell death in H9c2 cardiac muscle cells. Toxicology and Applied Pharmacology 248, 20–27. https://doi.org/10.1016/j.taap.2010.07.007

Zhu, P., Hu, S., Jin, Q., Li, D., Tian, F., Toan, S., Li, Y., Zhou, H., Chen, Y., 2018. Ripk3 promotes ER stress-induced necroptosis in cardiac IR injury: A mechanism involving calcium overload/XO/ROS/mPTP pathway. Redox Biology 16, 157–168. https://doi.org/10.1016/j.redox.2018.02.019

Ziegler, U., Groscurth, P., 2004. Morphological Features of Cell Death. Physiology 19, 124–128. https://doi.org/10.1152/nips.01519.2004

Appendix

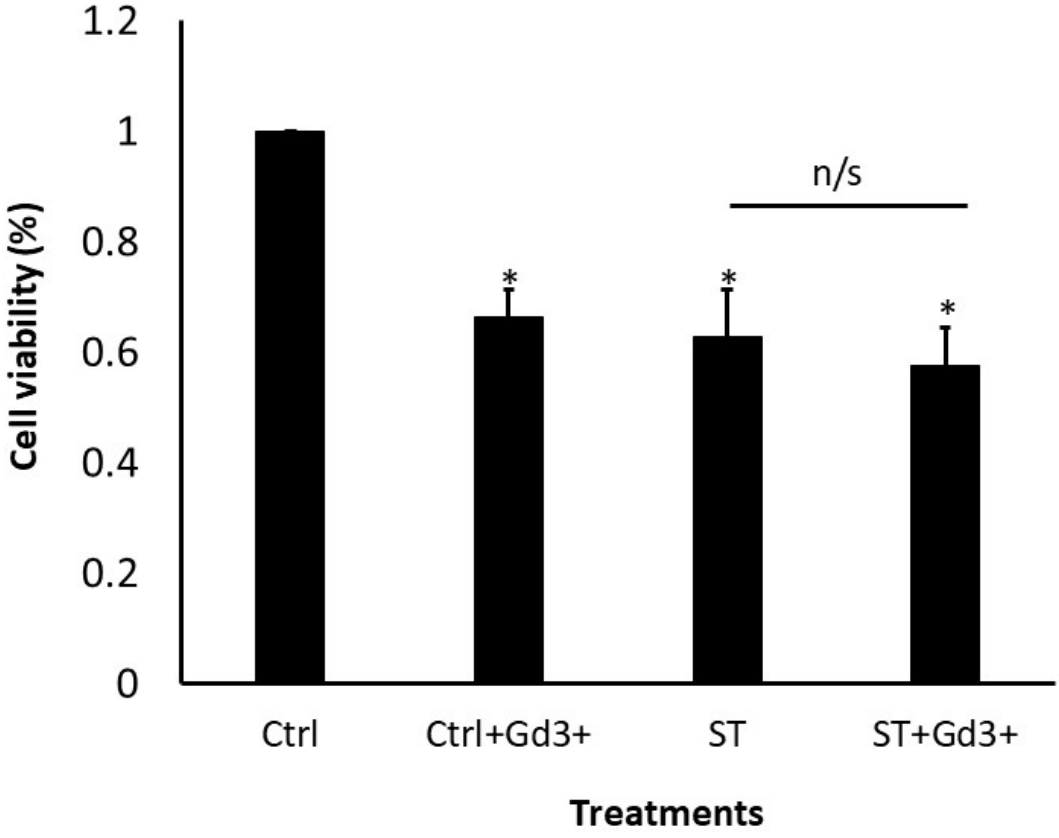

Appendix 1. CPC viability is not rescued by Gd^{3+}. Cells treated with 10 µM ST +/- 100 nM **Gd^{3+}** for 24 h before assessment of viability. Data are mean ± SEM, n=5 *p<0.05 *vs.* control. n/s=not signficiant, ST *vs.* ST+Gd^{3+} ANOVA with *post hoc* Tukey's test.